UNIVERSITÀ DEGLI STUDI DI PADOVA

Sede Amministrativa: Università degli Studi di Padova

Dipartimento di Scienze Chimiche

SCUOLA DI DOTTORATO DI RICERCA IN SCIENZE MOLECOLARI
INDIRIZZO: SCIENZE CHIMICHE
CICLO XXVIII

METODI ELETTROCHIMICI PER LA POLIMERIZZAZIONE RADICALICA A TRASFERIMENTO D'ATOMO DI SISTEMI ACQUOSI E "METAL-FREE"

ELECTROCHEMICAL METHODS FOR ATOM TRANSFER RADICAL POLYMERIZATION OF AQUEOUS AND METAL FREE SYSTEMS

Direttore della Scuola: Ch.mo Prof. Antonino Polimeno
Coordinatore d'indirizzo: Ch.mo Prof. Antonino Polimeno
Supervisore: Prof. Abdirisak Ahmed Isse

Dottorando: Marco Fantin

Contents

Glossary of Acronyms

AA	Acrylic acid
ARGET	Activator regenerated by electron transfer
ATRP	Atom transfer radical polymerization
BAN	Bromoacetonitrile
BB	Benzyl bromide
BC	Benzyl chloride
BiBA	2-bromoisobutyric acid
BPAA	Bromophenylacetic acid
BMIm	1-butyl-3-methylimidazolium
CAN	Chloroacetonitrile
CBZ	Carbazole
CiBA	2-chloroisobutyric acid
CPAA	Chlorophenylacetic acid
CPN	Chloroproprionitrile
CRP	Controlled radical polymerization
CTA	Chain transfer agent
CV	Cyclic voltammetry
$Đ$	Molecular weight dispersity (M_w/M_n)
DCPA	2,2-dichloropropionic acid
DET	Dissociative electron transfer
DMF	Dimethylformamide
DMSO	Dimethyl sulfoxide
DP	Degree of polymerization
DT	Degenerative transfer
***e*ATRP**	Electrochemically mediated atom transfer radical polymerization
EBiB	Ethyl α-bromoisobutyrate
EBPA	α-bromophenylacetate
ECPA	α-chlorophenylacetate
ET	Electron transfer
EBA	Ethyl bromoacetate
ECA	Ethyl chloroacetate
FRP	Free radical polymerization
HEBiB	2-hydroyethyl 2-bromoisobutyrate
HRC	Homogeneous redox catalysis
ICAR	Initiators for continuous activator regeneration
ISET	Inner-sphere electron transfer
M	Monomer
MA	Methyl acrylate
MAA	Methacrylic acid

MBP	Methyl 2-bromopropionate
MCP	Methyl 2-chloropropionate
Me_6TREN	Tris(2-(dimethylamino)ethyl)amine
MMA	Methyl methacrylate
M_n	Number average molecular weight
M_w	Weight average molecular weight
MW	Molecular weight
NMP	Nitroxide mediated polymerization
NiPAM	*N*-isopropyl acrylamide
NiPBPA	*N*-isopropyl 2-bromopropanammide
OEOA	Oligo(ethyleneoxide) methyl ether acrylate, average M_n = 480
OEOBP	Oligo(ethyleneoxide) methyl ether 2-bromopropionate
OEOMA	Oligo(ethyleneoxide) methyl ether methacrylate, average M_n = 500
OMRP	Organometallic mediated radical polymerization
OSET	Outer-sphere electron transfer
OTf	Trifluoromethanesulfonate
PEB	1-phenylethyl bromide
PEC	1-phenylethyl chloride
PMDETA	N,N,N',N',N''-Pentamethyldiethylenetriamine
PMMA	Poly(methyl methacrylate)
ppy	2-phenylpiridine
PRE	Persistent radical effect
PTZ	Phenothiazine
RAFT	Reversible addition fragmentation chain transfer polymerization
RDRP	Reversible deactivation radical polymerization
RDE	Rotating disk electrode
RP	Radical polymerization
RX	Organic halide (ATRP initiator)
SARA	Supplemental activator and reducing agent
SCE	Saturated calomel electrode
SFRP	Stable free-radical polymerization
SRP	Standard reduction potential
TCAA	Trichloroacetic acid
TEMPO	2,2,6,6-tetramethylpiperidinyl-1-oxy
terpy	2,2′:6′,2″-Terpyridine
TPMA	Tris-[(2-pyridyl)methyl]amine
Th	Thiathrene
TS	Transition state
Vis-NIR	Visible – Near-infrared
UV-Vis	Ultraviolet - Visible

Riassunto

Le polimerizzazioni radicaliche controllate (*Controlled Radical Polymerization*, CRP) sono tra le più potenti ed efficaci metodologie per ottenere materiali polimerici avanzati con proprietà ben definite ed alto valore aggiunto.

La polimerizzazione radicalica a trasferimento di atomo (*Atom Transfer Radical Polymerization*, ATRP) è la tecnica più utilizzata in ambito accademico e industriale nel campo delle CRP, grazie alla sua versatilità e facilità di applicazione. In ATRP, un complesso metallico a basso stato di ossidazione Mt^zL_m (tipicamente, un complesso rame-ammina, $[Cu^IL]^+$) reagisce con una catena polimerica dormiente $P_n{-}X$ (dove X = Cl, Br) per produrre i radicali $P_n^\bullet$. Questi accrescono la catena per addizione al monomero nel *bulk* della soluzione. Nel processo, il complesso di rame si ossida e coordina lo ione alogenuro X^-, generando la specie disattivante $[X\text{-}Cu^{II}L]^+$, in grado di catturare i radicali propaganti. Normalmente, l'equilibrio ATRP è fortemente spostato verso lo stato dormiente $P_n{-}X$, cosicché la concentrazione di $P_n^\bullet$ è molto bassa e la probabilità di terminazione radicalica bimolecolare è minima. Si tratta quindi, per molti aspetti, di una polimerizzazione "vivente". La crescita di tutte le macromolecole inizia circa contemporaneamente grazie all'utilizzo di efficienti alogenuri alchilici (RX) come iniziatori polimerici. In queste condizioni, la crescita delle catene è omogenea e permette di ottenere polimeri con pesi molecolari predeterminati, stretta distribuzione delle lunghezze di catena e alta conservazione della funzionalità C-X terminale. Con questa tecnica è quindi possibile generare macromolecole con specifiche composizioni, architettura e posizione dei gruppi funzionali.

Lo scopo di questa tesi è contribuire alla comprensione e allo sviluppo di ATRP catalizzata da complessi di rame, utilizzando metodologie elettrochimiche sia come strumenti di indagine, sia come strumenti di controllo della polimerizzazione. Per molti aspetti, i sistemi ATRP indagati posso essere definiti sistemi "green": (*i*) la maggior parte del lavoro ha riguardato lo studio e lo sviluppo della reazione in acqua, un solvente dove i complessi sono molto attivi ma il controllo sulla polimerizzazione risulta particolarmente difficile; (*ii*) metodologie elettrochimiche per la rigenerazione del catalizzatore hanno permesso di condurre la polimerizzazione riducendo drasticamente la concentrazione di rame; (*iii*) sono state esplorate le potenzialità dei liquidi ionici, materiali non

infiammabili e facilmente riciclabili, come potenziali solventi per ATRP mediata elettrochimicamente; (*iv*) è stato indagato il meccanismo della catalisi ATRP in assenza di catalizzatori metallici, "metal-free" ATRP.

Una caratteristica fondamentale dei catalizzatori di rame(I) è la loro reattività nel rompere il legame P_n-X e generare i radicali propaganti $P_n^{\bullet}$. Lo studio dettagliato dell'attività dei catalizzatori di rame in acqua è risultato finora impossibile a causa dell'estrema attività degli stessi. É stato quindi necessario sviluppare un set di metodologie elettrochimiche transienti, che sfruttano la generazione e l'analisi del complesso attivo di rame nell'immediato intorno dell'elettrodo. Queste tecniche hanno permesso di ampliare l'intervallo di k_{act}(costante di attivazione ATRP) analizzabili di ben 5 ordini di grandezza, rendendo quindi possibile lo studio della reattività dei più recenti e attivi catalizzatori e iniziatori utilizzati, in comuni solventi polari molto attivi (come acqua e DMSO). I risultati permettono di correlare la costante di velocità di attivazione con la costante di equilibrio ATRP, K_{ATRP}. Inoltre, è possibile prevedere la reattività dei sistemi catalitici da semplici dati di energia di legame (di P_n-X), e progettare in modo razionale le ottimali condizioni di polimerizzazione.

Le proprietà dei catalizzatori di rame sono state studiate nel liquido ionico 1-butyl-3-methylimadazolium triflate. Speciazione e reattività dei complessi sono risultate compatibili con un efficiente reazione ATRP. Questo particolare solvente risulta simili ad un comune solvente organico (*e.g.* acetonitrile, DMF) sia per quanto riguarda gli aspetti termodinamici che cinetici dei catalizzatori ATRP.

In acqua, i catalizzatori di rame non sono solo caratterizzati da una estrema reattività, ma anche dalla propensione ad essere coinvolti in reazioni collaterali all'equilibrio ATRP. Queste comprendono la decomposizione del complesso, sia in ambiente acido che basico, e la dissociazione dello ione alogenuro dal complesso disattivante $[X\text{-}Cu^{II}L]^+$. La quantificazione di tali reazioni ha permesso di stabilire con precisione gli intervalli di stabilità dei più comuni catalizzatori utilizzati. I limiti di controllo dell'ATRP acquosa sono quindi stati testati tramite un'estesa serie di polimerizzazioni del monomero "modello" oligo(ethyleneoxide) methylether methacrylate (OEOMA). Le sintesi sono state condotte tramite rigenerazione elettrochimica del catalizzatore attivo, $[Cu^{I}L]^+$ (*e*ATRP). Il range di catalizzatori Cu/L disponibili è stato esteso, includendo catalizzatori estremamente attivi come Cu/Me_6TREN (Me_6TREN = tris[2-(dimethylamino)ethyl]amine), o sistemi molto economici ed interessanti dal punto di vista industriale come Cu/PMDETA

(PMDETA = N,N,N',N'',N''-pentamethyl diethylenetetramine). Inoltre, è stata confermata la particolare stabilità dei leganti piridinici come Cu/TPMA (TPMA = tris(2-pyridylmethyl)amine) fino a pH estremamene acidi (*ca.* 1). Quest'ultimo risultato ha aperto la strada per la polimerizzazione di monomeri acidi (acido acrilico, AA, e metacrilico, MAA).

La polimerizzazione dei monomeri acidi è da sempre considerata uno dei maggiori limiti dell'ATRP. I risultati hanno mostrato la presenza di una ciclizzazione a carico della terminazione di catena, con l'alogeno terminale come gruppo uscente (e quindi perdita della funzionalità attiva C-X). Tre strategie sono state applicate con successo per ridurre l'impatto negativo di questa reazione e ottenere la polimerizzazione controllata di MAA: (*i*) utilizzare la funzionalità C-Cl come terminazione di catena, un gruppo più stabile di C-Br; (*ii*) abbassare ulteriormente il pH per convertire completamente gli ioni carbossilato in acidi carbossilici, nucleofili più deboli; (*iii*) accelerare la velocità di polimerizzazione per diminuire il contributo relativo della ciclizzazione (reazione parassita). Una volta trovate le condizioni ottimali, è stata esplorata la sintesi di acido polimetacrilico ad alto peso molecolare (grado di polimerizzazione > 1000) e con architetture controllate (polimeri lineari, telechelici e stelle a tre braccia).

La polimerizzazione radicalica a trasferimento d'atomo mediata elettrochimicamente permette eccellente controllo sulle condizioni di reazione. Uno dei suoi limiti è però quello di utilizzare sia elettrodo lavorante, sia controelettrodo in platino, un metallo estremamente costoso e raro. Per superare questa limitazione, diversi materiali sono stati testati come catodi per *e*ATRP. Sono state individuate le condizioni ottimali per poter utilizzare sia materiali carboniosi (glassy carbon), sia metalli o leghe di metalli non-nobili (acciaio, nichel-cromo, titanio). Inoltre, la reazione è stata ulteriormente semplificata usando un sistema a due elettrodi in condizioni galvanostatiche (corrente fissata), in presenza di un controelettrodo sacrificale in alluminio, direttamente immerso nell'ambiente di reazione. Quest'ultima soluzione permette di evitare la separazione tra compartimento anodico e catodico.

Un altro importante obiettivo di questo progetto di dottorato riguarda la definizione del meccanismo della polimerizzazione radicalica a trasferimento d'atomo catalizzata da molecole organiche (derivati della fenotiazina, PTZ), quindi effettuata in assenza di metalli (*metal-free* ATRP). In questo caso, una fenotiazina in stato eccitato (per assorbimento di radiazione UV, PTZ*) attiva il legame P_n-X generando i radicali propaganti ($P_n^{\bullet}$)

e il radicale catione $PTZ^{\bullet+}$. La costante di velocità di attivazione sperimentale di P_n-X da parte di PTZ* (7×10^9 M^{-1} s^{-1}) è stata confrontata con quella calcolata utilizzando la teoria di Marcus per il trasferimento elettronico e i suoi successivi sviluppi (2×10^{10} M^{-1} s^{-1}). Il buon accordo tra i due dati ha dimostrato che questa reazione coinvolge un trasferimento elettronico a sfera esterna tra PTZ* e P_n-X, con simultanea rottura del legame C-X. Si tratta quindi di un sistema chiaramente diverso da ATRP mediata da complessi di rame, che prevede un trasferimento elettronico a sfera interna. Differenti sono anche i parametri che regolano l'attività del catalizzatore (frequenza di eccitazione, tempi di vita ed efficienza quantica di fluorescenza, *etc.*). In particolare, la veloce attivazione del legame C-X è impedita dal breve tempo di vita di PTZ*. Per quanto riguarda la disattivazione dei radicali propaganti, in primo luogo, tramite voltammetria ciclica è stata trovata un'ottima correlazione tra la stabilità del radicale catione $PTZ^{\bullet+}$ e l'efficienza di disattivazione. Successivamente, è stata confrontata la velocità relativa di un'ampia gamma di possibili reazioni di disattivazione. Da questo studio cinetico è emerso che la reazione favorita riguarda l'incontro termolecolare di $P_n^{\bullet}$, $PTZ^{\bullet+}$ e X^-. L'efficienza di disattivazione è bassa a causa della bassa probabilità dell'incontro a tre centri. Nel complesso, ATRP mediata in assenza di metalli è catalizzata da un lento processo di attivazione/disattivazione, che correntemente limita il controllo della crescita polimerica. Questi risultati sono necessari per il design di condizioni di reazione ottimali e per la sintesi di catalizzatori più efficaci.

Abstract

Controlled radical polymerizations (CRPs) are among the most powerful methods to obtain polymers with well-defined properties and high value.

Atom transfer radical polymerization (ATRP) is the most used technique in both academia and industry in the field of CRP, thanks to its versatility and simple setup. In ATRP, a metal complex in a low oxidation state, Mt^zL_m (typically a copper-amine system, $[Cu^IL]^+$) reacts with a dormant polymeric chain P_n–X (where X = Cl, Br) to produce radicals $P_n^\bullet$. Such radicals can propagate the polymeric chain by addition to a monomer in the bulk of the solution. In this process, the copper complex is oxidized and binds to X^-, generating the deactivating species $[X\text{-}Cu^{II}L]^+$, which can trap the propagating radicals. ATRP equilibrium is well shifted towards the dormant species P_n-X, so that $P_n^\bullet$ concentration is very low and the probability of bimolecular radical-radical termination is minimized. Macromolecular growth begins essentially at once for all chains thanks to the utilization of very efficient alkyl halides (RX) as polymerization initiators. In such conditions, chain growth is homogenous and it is possible to obtain polymers with predetermined molecular weight, narrow molecular-weight distribution, and high C-X chain end fidelity. ATRP allows constructing macromolecules with specific composition, architecture and position of functional groups.

The aim of this thesis is to contribute to both the understanding and development of ATRP catalyzed by copper complexes, using electrochemical methods as both analytical tools and instruments to carry out and control the polymerization. The work focused on both thermodynamic and kinetic properties of ATRP catalytic systems, and the use of such systems to efficiently control macromolecular growth. The investigated ATRP systems can be considered "green" for several reasons: (*i*) most of the work regarded the study and development of the reaction in water, a solvent generally characterized by high catalytic activity but poor polymerization control; (*ii*) electrochemical methods for catalyst regeneration (electrochemically mediated ATRP, *e*ATRP) allowed carrying out the polymerization with low amounts of copper complexes; (*iii*) ionic liquids, a new class of non-flammable and easily recyclable solvents, were explored as potential media for

*e*ATRP; (*iv*) the mechanism of ATRP mediated by organic catalysts (metal-free ATRP) was investigated and defined.

A fundamental characteristic of Cu^I catalysts is their reactivity towards the P_n-X (or initiator RX) bond cleavage, with generation of propagating radicals $P_n^{\bullet}$. Any detailed investigation of catalyst reactivity in water was impossible up to now, because of their extremely high reactivity in this solvent. For this purpose, it was necessary to develop a set of electrochemical transient methods, which involve active $[Cu^IL]^+$ complex generation, and analysis, in the proximity of the electrode surface. Such techniques allowed measuring k_{act} (ATRP activation rate constant) values spanning a broad interval covering 5 orders of magnitude. This permitted the study of the most active and latest developed catalysts and initiators, in common polar and active solvents such as water and DMSO. k_{act} correlates linearly with both ATRP equilibrium constant (K_{ATRP}) and RX bond dissociation free energy. Such correlations help to predict the reactivity of new catalyst/initiators and to select rationally polymerization conditions.

ATRP catalysts were investigated in the ionic liquid 1-butyl-3-methylimidazolium triflate. Both Cu/L speciation and reactivity were found to be suitable with a well-controlled polymerization process. Overall, thermodynamic and kinetics aspects of ATRP catalysts in ionic liquids appear to be similar to that observed in common organic solvents (*e.g.* CH_3CN, DMF).

In water, copper catalysts are not only characterized by an extreme reactivity, but also by their involvement in side reactions that can undermine efficiency of ATRP equilibrium (*e.g.* complex decomposition in both acid and basic environment and dissociation of the halide ion from the deactivating complex $[X\text{-}Cu^{II}L]^+$). Quantification of such reactions allowed defining stability intervals of most used ATRP catalysts in water. Defined limits of control were tested by carrying out an extensive series of polymerizations of the monomer oligo(ethyleneoxide) methylether methacrylate (OEOMA). Polymerizations were conducted with electrochemical (re)generation of the active $[Cu^IL]^+$ complex (*e*ATRP). Exceptionally active catalysts such as Cu/Me_6TREN (Me_6TREN = tris[2-(dimethylamino)ethyl]amine) provided fast and controlled polymerizations with slow Cu^I regeneration; inexpensive systems such as Cu/PMDETA (PMDETA = N,N,N',N'',N''-pentamethyl diethylenetetramine) needed a large X^- excess in order to prevent $[X\text{-}Cu^{II}L]^+$ dissociation. Pyridinic complexes, such as Cu/TPMA (TPMA = tris(2-pyridylmethyl)amine),

were stable down to extremely acidic pH (*ca.* 1). Overall, these results allowed unprecedented control over conditions of macromolecular growth in water. In addition, they opened a new avenue for the polymerization of acidic monomers, a class of building blocks currently considered to be problematic, or even impossible, to be polymerized by ATRP.

The main reason preventing ATRP of methacrylic acid was a cyclization reaction involving the chain end, with the terminal halogen as leaving group. Three strategies allowed dramatically improving conversion and control over MAA polymerization: (*i*) using C-Cl chain end functionality, which is much more stable than C-Br; (*ii*) lowering further the pH to completely convert carboxylate ions to carboxylic acid, which is a much weaker nucleophile; (*iii*) enhancing the polymerization rate in order to avoid the negative contribution of the cyclization side reaction. Such conditions allowed synthesis of well-controlled high molecular weight poly(methacrylic acid), PMAA, with degree of polymerization > 1000. Simple (poly)halogenated organic initiators such as 2-bromoisobutyric acid, 2,2-dichloropropionic acid, and trichloroacetic acid were used to produce linear, telechelic, and three-arm star PMAA, respectively. An electrochemical switch, used to repeatedly stop and reactivate the growing chains, confirmed the "livingness" of the process.

Electrochemically mediated atom transfer radical polymerization allowed exceptional control over Cu^{I} (re)generation. Its main limitations are the relatively complicated reaction setup and the requirement of both working and counter electrodes made of platinum, an expensive and rare metal. To overcome these limits, first several alternative noble and non-noble metals were tested as cathode materials. Carbon materials (*e.g.* glassy carbon), noble metals (Au, Ag) and non-noble metals and alloys (stainless steel, nickel-chromium, titanium) could efficiently control aqueous *e*ATRP of OEOMA. The system setup was simplified by switching from potentiostatic conditions (three-electrode setup under fixed potential) to galvanostatic conditions (two-electrode setup with fixed current). Moreover, reaction setup was further simplified with the use of a sacrificial counter electrode directly immersed in the polymerization media. This solution allowed avoiding separation of anodic and cathodic compartments. These results can allow easier implementation and scale-up of electrochemically mediated ATRP.

Catalysis in the absence of transition metals is important in fine electronics and biomedical applications. It has recently been shown that some derivatives of phenothiazine

(PTZ) could mediate well-controlled metal-free ATRP of methacrylates, with generation of controlled polymers with living characteristics. In this case, a phenothiazine derivative in the excited state (PTZ*, obtained through UV light absorption) can activate the P_n-X bond generating the propagating radicals ($Pn^{\bullet}$) and the radical cation $PTZ^{\bullet+}$. Experimental rate constant of P_n-X activation by PTZ* (7×10^9 M^{-1} s^{-1}) was compared to the value calculated using Marcus theory for electron transfer and its successive developments (2×10^{10} M^{-1} s^{-1}). The good agreement between the two values proved that the reaction between PTZ* and P_n-X involves an outer sphere electron transfer with simultaneous C-X bond breaking. This system is radically different from traditional Cu-mediated ATRP, which involves an inner sphere electron transfer. In addition, reactivity in metal-free ATRP is regulated by completely different parameters (excitation wavelength, lifetime and quantum efficiency of excited states). In particular, in metal-free ATRP fast activation of the C-X bond is hindered by low lifetime of PTZ* excited state. Regarding deactivation of propagating radicals, cyclic voltammetry evidenced excellent correlation between stability of the radical cation $PTZ^{\bullet+}$ and efficiency of deactivation. The favored pathway for radical deactivation is the termolecular encounter of $P_n^{\bullet}$, $PTZ^{\bullet+}$ and X^{-}, which is severely hampered by the low likelihood of three-center reactions. As a result, metal-free ATRP is mediated by a slow activation-deactivation process, which currently limits control over macromolecular growth. Such results are fundamental for the design of optimal reaction conditions and for the development of more effective catalysts.

Chapter 1
Controlled Reversible-Deactivation Radical Polymerizations

Most of the plastic commodities used worldwide are produced by free radical polymerization (FRP), a chain polymerization in which the chain carriers are radicals (*i.e.* the growing chain end bears an unpaired electron). The commercial success of FRP can be attributed to the large variety of polymerizable monomers and their facile copolymerization. The range of monomers is larger for FRP than for any other chain polymerization because radicals are tolerant to many functionalities, including acidic, hydroxyl, and amino groups. FRP is not affected by water and other protic impurities, and can be carried out in various media, *e.g.*, bulk, solution, aqueous suspension, emulsion, dispersion, *etc*. Moreover, reaction conditions are mild (typically room temperature to 100 °C, atmospheric pressure) and requirements for purification of solvents, monomers and products are minimal, making FRP a straightforward and effective synthetic technique. On the other hand, radicals are extremely reactive species; therefore, unavoidable chain transfer and radical termination reactions dominate FRP, prohibiting precise tailoring of molecular structures. The inadequate level of control over chain growth has limited the application of materials prepared by FRP as commodity plastics, rubbers and fibers.

In contrast, living polymerization processes (*e.g.* cationic and anionic polymerization) allow finely designing macromolecular architectures. In 1956, Swarzc defined a "living polymerization" as one that proceeds "without chain transfer or termination".[1] In contrast to ionic reactions, in which cations or anions do not react via bimolecular termination, organic radicals are short-lived species that terminate with a diffusion-controlled rate through disproportionation and coupling reactions. To form regular, high molecular weight polymers, the relative probability of such termination must be minimized. In other words, in order to obtain a well-defined polymeric growth, the rate of radical generation

must be controlled. For this scope, from the 1990s several controlled reversible-deactivation radical polymerizations (RDRPs) have been developed, which allowed engineering polymers with unprecedented regular, complex and predetermined design and composition. Since RDRPs allow controlling chain growth, they are often called controlled radical polymerizations (CRPs).

In this chapter, first the characteristics of RDRPs (and polymers produced by RDRPs) are discussed. Then, the three approaches to obtain a RDRP are described, namely stable-free-radical mediated polymerization (SFRP),[2] atom transfer radical polymerization (ATRP) and degenerate-transfer radical polymerization (DTRP). For each of the three methods, examples regarding the most used polymerizations are discussed. Lastly, the most relevant RDRP methods are compared.

1.1 Characteristics of a RDRP

Traditional FRP is dominated by the kinetics of very fast and difficult to control reactions, such as radical chain transfer and termination. In contrast, RDRP is propagated by radicals that are deactivated reversibly, bringing them into an active-dormant equilibrium (Scheme 1.1). The existence of a well-defined equilibrium shifted to the left ($k_{act}/k_{deact} << 1$) is the key difference between RDRP and FRP, since it drastically reduces the concentration of active species, reducing the likelihood of radical-radical termination reactions. Ideally, a growing radical should react with few monomer units before it returns to the dormant state (in other words, it should be quickly deactivated before the possible encounter with another radical). The equilibrium should be fast enough (both high k_{act} and k_{deact}) in order to share growth probability equally between all growing chains.

The lifetime of radicals in FRP is in the order of magnitude of one second; it is impossible to execute control over macromolecular structure during such a short time. By inserting periods of *ca.* 1 min dormancy after each *ca.* 1 ms of activity, the overall life of

Scheme 1.1. Equilibrium between dormant and active species in RDRP.

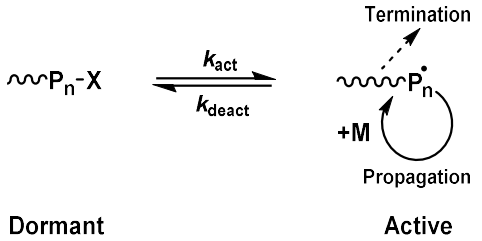

propagating chains can be extended from *ca.* 1 s to more than 1 day. Extension of growing chain lifetime from 1 s to over several hours was accomplished by insertion of multiple reversible radical deactivation steps. This has enabled synthesis of well-defined, essentially tailor-made polymers, via macromolecular engineering.

In RDRP, the proportion of terminated chains is drastically reduced from ~100% to well below 10% (essentially, in FRP all chains are dead at any time). As termination cannot be entirely avoided in RDRP, these systems cannot be defined "living" as, for example, anionic polymerizations. Nevertheless, the degree of control is often sufficient to attain many desirable material properties, and controlled radical polymerizations usually take on much of the character of a living polymerization, *i.e.*, a reaction from which chain termination and irreversible chain transfer are absent.

Controlled radical polymerizations can often be distinguished from kinetically-controlled FRP by analyzing the evolution of the polymer's molecular weight as a function of time and/or monomer conversion. Kinetically controlled FRP provides high molecular weights polymer at relatively early stages. In contrast, molecular weight is directly proportional to monomer conversion in living polymerizations since all chain ends are growing at essentially the same rate. In fact, Gold demonstrated that even when the rate of propagation is orders of magnitude greater than the rate of initiation, a living polymerization can lead to polymers with very narrow molecular weight distributions.[3] These distributions are usually quantified through determination of the sample's molecular-weight dispersity, which is defined as $Đ = M_w/M_n$, where M_w is the weight-averaged molecular weight and M_n is the number-averaged molecular weight. In systems where the rate of initiation is faster than or similar to the rate of propagation, control over the polymerization is obtained at an early stage. Under these conditions, access to well-defined, monodispersed materials of low molecular weight is possible. Thus, in addition to Swarzc's original constraint, a RDRP reaction should exhibit the following characteristics in order to be considered controlled: (*i*) fast and complete initiation, (*ii*) linear relationship between M_n and monomer consumption, and (*iii*) $Đ < 1.5$. This enables the synthesis of well-defined polymers with narrow distributions and predictable molecular weights specified by the initial monomer to initiator ratio (C_M/C_I).

Chain functionality is another important peculiarity of controlled radical polymerizations. Most RDRPs can be initiated by a functional initiator (*e.g.* organic molecule, nanoparticle, or biomolecule), which is covalently attached to the polymer chain. All

RDRPs contain a functional chain end (carbon halide bond, alkoxyamine, thiocarbonylthio, *etc*, depending on the RDRP technique).

It has to be noted that propagation of radicals in RDRP and FRP is mechanistically indistinguishable: radicals show high regioselectivities and add to the less substituted carbon in alkenes, but they present low stereoselectivities due to their sp^2 hybridized nature. Thus, polymers have head-to-tail structures and are usually atactic.

The three approaches used to obtain a RDRP are described in the next sections.

1.1.1 Stable-free-radical polymerization (SFRP)

Stable-free-radical polymerization (SFRP) is a controlled reversible-deactivation radical polymerization in which the deactivation involves reversible coupling with stable (persistent) radicals (Scheme 1.2). Newly generated radicals are rapidly trapped in the deactivation process (with a deactivation rate constant k_{deact}) by a radical scavenger T, which is typically a stable radical such as a nitroxide (as in nitroxide-mediated radical polymerization, NMP, Section 1.2.1) or an organometallic species such as a cobalt complex (as in organometallic-mediated radical polymerization, OMRP, Section 1.2.3). In each of these cases, a direct covalent bond is formed between the propagating radical and the radical scavenger. The dormant species are activated (with a rate constant k_{act}) through homolytic cleavage of the bond between the propagating and the trapping agent (P_n–T). This can occur either spontaneously/thermally, in the presence of light, or with an appropriate catalyst to reform the growing centers. The equilibrium is well-shifted toward the left, in order to suppress radical concentration and avoid termination reactions.

The approach of SFRP is based on the persistent radical effect (PRE).[4] Whereas the newly generated radicals can propagate or undergo bimolecular termination, the so-called persistent radicals, T, cannot terminate with each other but can only reversibly cross-couple with the growing species. Thus, every act of radical termination is accompanied by the irreversible accumulation of T, whose concentration progressively increases with

Scheme 1.2. Reversible radical trapping in SFRP

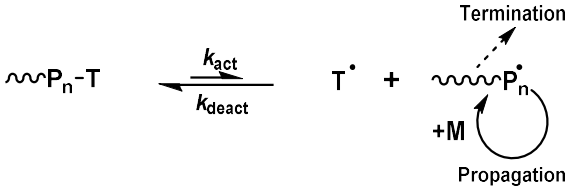

time. As the concentration of T increases with time, the concentration of radicals decreases in virtue of the equilibrium in Scheme 1.2, which becomes shifted toward the dormant species. The growing radicals predominantly react with T rather than with themselves, which results in a decrease of termination probability. In systems based on the PRE, a steady state of growing radicals is therefore established through the activation-deactivation process but not through initiation-termination like in conventional FRP. If initiation is much faster than termination, simultaneous growth of all chains is essentially achieved.

It is worth noting that a stoichiometric amount of the mediating species is required in these systems because all of the propagating chains require an end-group.

1.1.2 Atom transfer radical polymerization (ATRP)

In 1995, Matyjaszewki[5] and Sawamoto[6] independently reported the atom transfer radical polymerization (ATRP) of methyl methacrylate (MMA), giving rise to the most used technique in the field of the RDRP. In ATRP, the deactivation of radicals involves reversible atom transfer (or reversible group transfer) catalyzed usually, though not exclusively, by redox active transition-metal complexes (Scheme 1.3). A metal complex in a low oxidation state reacts with a dormant species bearing a C−X bond (either the macromolecular chain P_n−X or an alkyl halide initiator R−X) to produce the propagating radicals and the oxidized metal complex coordinated by the halogen atom. As in SFRP, the equilibrium between dormant and active states is shifted toward the left, allowing a low concentration of $P_n^{\bullet}$ and the consequent suppression of the termination reactions. This mechanism also relies on the persistent radical effect, but in this case, the deactivating complex $Mt^{n+1}X_{m+1}/L$ is accumulated (L = ligand). Since the dormant species are capped by halogen atoms transferred by the metal catalyst, sub-stoichiometric amounts of metal complex can be used.

Scheme 1.3. General mechanism of ATRP

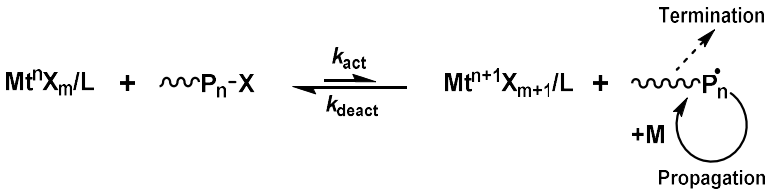

A fundamental requirement of the catalyst is the reversible activation of a dormant species with a terminal carbon-halogen bond, which involves one electron oxidation of the metal associated with an abstraction of a halogen atom. Thus, the metal catalyst should allow formation of at least two oxidation states separated by a single electron transfer. Moreover, the complex should have good halogen affinity. The activation step formally corresponds to a dissociative "one electron transfer" from the catalyst to a dormant chain end, with the formation of a radical and a X^- fragment, which is coordinated by the oxidized metal. Thus, a good activator bears a high electron density on the metal center. For these aspects, late transition metals in a lower valence state are generally favorable, although some early transition metals have also been employed. Examples include Ru, Cu, Fe, Ni, Mo, Mn, Os, Co, *etc*. The most used catalyst is undoubtedly the Cu^I/Cu^{II} redox couple. Copper ATRP, the topic of this thesis, is thoroughly discussed in Chapter 2.

1.1.3 Degenerative transfer radical polymerization (DTRP)

The process in Scheme 1.4 is known as degenerative transfer radical polymerization (DTRP) and is based on a thermodynamically neutral bimolecular exchange between a low concentration of growing radical chains ($P^\bullet$) and a dormant species (P-X).[7] The exchange occurs via the chain transfer agent (X), which may be an atom or a group in quantitative amount with respect to the number of growing species. In degenerative transfer (DT) processes, control is obtained because growth probability is shared among all polymer chains, through the fast and neutral ($K_{DTRP} \approx 1$) equilibrium in Scheme 1.4. Relevant examples of chain transfer agent (X) include alkyl iodides, organotelluriums, organostibines and organobismuthines. Addition-fragmentation chemistry also utilizes the degenerative transfer process, the most relevant example being reversible addition-fragmentation chain transfer (RAFT), which is discussed in Section 1.2.2. RAFT polymerization is also termed macromolecular architecture design by interchange of xanthates (MADIX), when these are used as chain transfer agents.[8]

Scheme 1.4. General mechanism of degenerative transfer radical polymerization

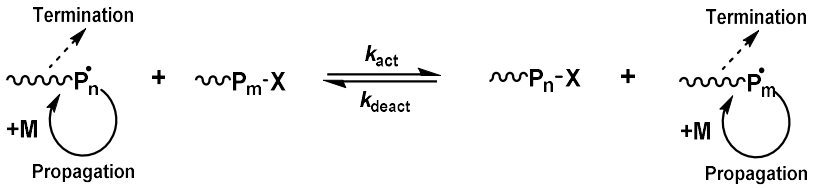

DTRP exchange system is different from the first two processes shown in Scheme 1.2 and 1.3, because DT does not involve a persistent radical and the kinetics and rate of polymerization are therefore similar to a conventional radical polymerization. The polymerization rate is proportional to the square root of the concentration of the radical initiator, rather than the concentration of the transfer agent, and the exchange process usually takes place through short-lived intermediate species.[9]

1.2 Relevant RDRPs

1.2.1 Nitroxide mediated polymerization (NMP)

The most relevant example of SFRP (Scheme 1.2) is nitroxide mediated radical polymerization (NMP), one of the first reported controlled radical polymerizations.[10] Polystyrene was prepared with a narrow molecular weight distribution by using a nitroxide stable radical (TEMPO, 2,2,6,6-Tetramethyl-1-piperidinyloxy) as trapping agent and dibenzoyl peroxide as initiator.[11] NMP is based on the reversible homolytic cleavage of a C−O bond to generate a growing radical and a non-reactive species (the persistent nitroxide radical). This species should not react with radicals of the same kind, or with monomers to initiate the growth of new chains, or with any other species in side reactions such as the abstraction of β-H atoms; it should react reversibly only with the growing radical. In particular, electron transfer between T and $P_n^{\bullet}$ should be negligible.

Three parameters of the nitroxide radical are critical for a successful NMP: (*i*) the activation/deactivation ratio with the propagating radical; (*ii*) the intrinsic stability of the nitroxide radical in the polymerization conditions; (*iii*) solubility in the reaction environment. For these reasons, several new nitroxide mediators have been reported, providing a range of C−O bond strengths, better control over the side reactions and solubility extended also to aqueous environment (Scheme 1.5).

Scheme 1.5. Structures of common nitroxide compounds used as trapping agents (T$^{\bullet}$) in NMP

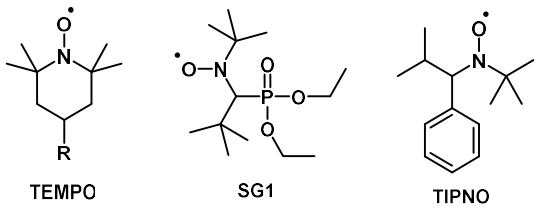

TEMPO and its derivatives form alkoxyamines with relatively strong covalent bonds, resulting in very low equilibrium constants ($K_{NMP} = k_{act}/k_{deact} = 2.0\times10^{-11}$ at 120 °C for polystyrene, PS),[12] and therefore require high polymerization temperatures. Alkoxyamines derived from nitroxide radicals containing a H atom in the α-C, such as SG1 and TIPNO, are much more labile than those of TEMPO, undergoing fast decomposition to alkyl and nitroxide radicals ($K_{NMP} = 6\times10^{-9}$ at 120 °C for PS). Also, compounds like SG1 have good solubility in aqueous media, and were used for the polymerization of acrylamide[13] and 2-(diethylamino)ethyl methacrylate[14] in water.

Typically, nitroxide radicals in NMP are employed together with common radical initiators, used at nearly stoichiometric amounts. Alternatively, alkoxyamines can be used as both initiators and control agents.

The range of monomers polymerizable by NMP includes styrene, various acrylates, acrylamides, dienes, and acrylonitrile. Monomers forming less stable radicals such as vinyl acetate have not yet been successfully polymerized via NMP because of too low equilibrium constant. In addition, disubstituted alkenes such as methacrylates that form more sterically hindered tertiary radicals show difficulties in control by NMP owing to very slow deactivation and/or a tendency to heterolytic dissociation.[15]

1.2.2 Reversible-addition-fragmentation chain-transfer polymerization (RAFT)

In 1998, Rizzardo *et al.* patented reversible addition-fragmentation chain transfer polymerization (RAFT).[16] An unsaturated compound acts as a chain transfer agent (CTA) through a two-step addition-fragmentation mechanism (Scheme 1.6). A traditional radical initiator (*e.g.* azobisisobutyronitrile) provides radicals. In the RAFT pre-equilibrium, an exchange reaction between a propagating radical chain and a chain transfer agent releases a second radical R•, which continues the propagation reaction. During the main RAFT equilibrium, two different polymer chains, P_n and P_m, undergo exchange.

RAFT polymerization, carried out by thiocarbonylthio (or similar) chain transfer agents is one of the most versatile methods of controlled radical polymerization, because it is tolerant of a very wide range of functionalities in the monomer and solvent, including aqueous solutions. Monomers include (meth)acrylates, (meth)acrylamides, meth(acrylic) acids, acid chlorides, acrylonitrile, styrene and derivatives, butadiene, vinyl acetate and N-vinylpyrrolidone.

Scheme 1.6. Pre-equilibrium in reversible addition-fragmentation chain transfer polymerization (in the main equilibrium, R = P_m).

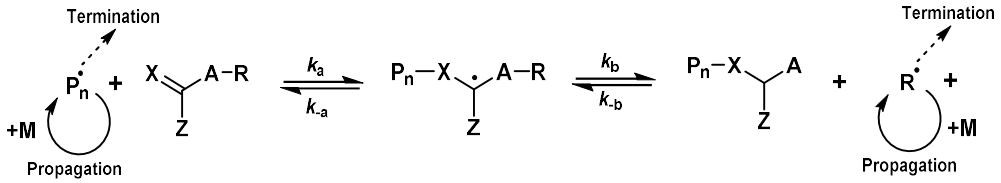

Generally, a CTA molecule is characterized by the presence of three groups: X, A and Z. Usually, both X and A are sulfur atoms. The Z group affects the stability of the S=C bond and the radical adduct (P_n-S-C•(Z)-S-R). This in turn affects equilibrium position and rates of the elementary reactions in the pre- and main-equilibrium. R• should be more stable than P_n•, so that it can be readily formed from the radical intermediate and efficiently initiate the polymerization (pre-equilibrium should be shifted toward the right, in order to ensure a fast activation). However, R• should be unstable enough to effectively add monomers and initiate growth of a new polymer chain (ideally faster than P_n•). As such, a RAFT agent must be designed with consideration of the monomer and temperature, since both these parameters strongly influence the kinetics and thermodynamics of the equilibrium. For example, strongly stabilizing Z groups such as Ph are efficient for the polymerization of styrene and methacrylates, whereas they retard polymerization of acrylates and inhibit reaction of vinyl esters. On the other hand, very weakly stabilizing groups, such as $–NR_2$ in dithiocarbamates or –OR in xanthates, are good for vinyl esters but less efficient for styrene. Thus, the proper choice of the Z substituent can dramatically enhance the reactivity of the CTA compounds.

1.2.3 Organometallic-mediated radical polymerization (OMRP)

Organometallic-mediated radical polymerization (OMRP) is the most recent of the RDRP techniques here discussed. In OMRP, the deactivation of the radicals involves reversible homolytic cleavage of a weak bond between an alkyl group and a transition metal. OMRP can proceed either via radical trapping, RT, or via degenerative transfer, DT (Scheme 1.7).

RT OMRP is initiated by using conventional radical initiators (*e.g.* peroxides or azobenzenes) with a redox-active metal compound, or by utilizing a complex containing a pre-formed metal–carbon bond. The growing radical-terminated chain exists in equilibrium with the dormant species, which in the case of RT OMRP is metal-terminated. A

Scheme 1.7. Radical trapping and Degenerative transfer in OMRP.

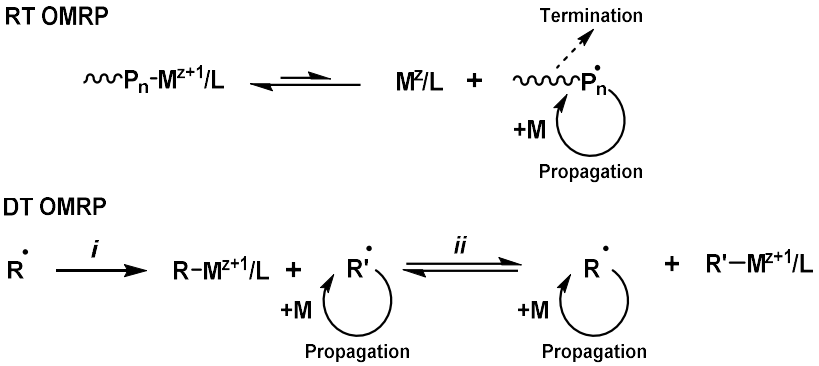

low concentration of radical species present at any one time allows control over the molecular weight and molecular-weight dispersity. The free radical initiator decomposes homolytically to release carbon-based radicals, which can either enter the propagation stage or react reversibly with the transition metal complex to form new dormant species with a weak metal–carbon bond.

OMRP may also proceed through a degenerative transfer process. In this case, the rate of polymerization is negligible until the amount of produced radicals exceeds the concentration of the initial metal species, because radicals formed from the initiation process firstly react with the metal complex to form the dormant organometallic species, (*i,* Scheme 1.7). For this reason, DT OMRP reactions are often characterized by long induction periods. An associative exchange then takes place, with an active radical, R′•, replacing the metal-bound radical of the dormant species, starting the main reaction equilibrium, (*ii*). Reactions are often quenched by the addition of a protic solvent such as methanol, which can hydrolyze the metal–carbon bonds and yield polymer chains with saturated end-groups.

With judicious choice of metal center and careful ligand design, metal–carbon bond strengths possess great tunability. By exploiting the steric effects of the ligand coordination sphere, it should be possible to adjust the metal–carbon bond strengths to suit any monomer. This will allow the controlled polymerization of a wide variety of monomers and promote the production of copolymers and advanced polymer architectures.

1.3 Comparison of the most relevant RDRPs

ATRP, RAFT and NMP are the most widely used techniques in the field of CRP. As qualitatively outlined in Figure 1.1, each technique has advantages and drawbacks in comparison to the others, as applied to the synthesis of low molecular weight (LMW) and high molecular weight polymers (HMW), range of polymerizable monomers (Mon. Range), preparation of block copolymers (Blocks), end-functional polymers (End Funct.), Hybrids, aqueous systems (Water) and some environmental issues (Env.).[17]

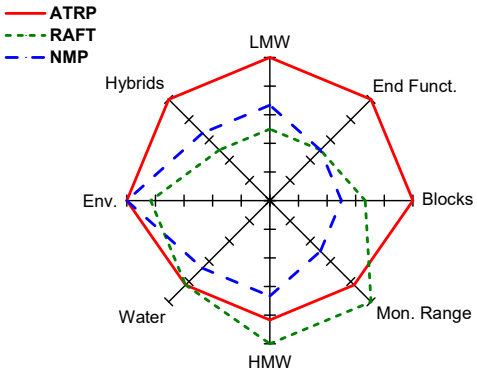

Figure 1.1. Comparative advantages of ATRP, RAFT and NMP.

ATRP is a catalytic process, whereas NMP and RAFT require stoichiometric amounts of the mediator to the macromolecular chains. All three methods require purification of the final polymer; however, ATRP and RAFT are more sensitive to this issue due to toxicity and colors of the mediators, and even unpleasant odor in the case of dithioesters. RAFT and NMP agents are often time consuming to synthetize, and each agent is typically useful only for a limited number of monomers. On the other hand, most of ATRP catalysts and initiators are commercially available.

Contrary to ATRP, RAFT and NMP do not require use of transition metals. Recently, the development of metal-free ATRP catalysis opened a new avenue to reduce environmental impact of this technique, especially for applications in fine electronic or biomedical systems. The definition of the mechanism of metal-free ATRP is a topic of this thesis, and this technique is presented in the next chapter.

Chain end functionality is a key feature of controlled radical polymerizations. The possibility to introduce specific functionality through post-polymerization reactions depends on the chemistry of the macromolecular chain end, *i.e.* the alkoxyamine function for NMP, the C−X bond for ATRP and the C−S bond for RAFT. From this standpoint,

ATRP has undoubtedly many advantages due to the well-known C−X chemistry, providing several routes for the halogen displacement like electrophilic or nucleophilic substitutions, and radical reactions.

Regarding the capability to polymerize various types of monomers, RAFT seems to be the best methodology. Indeed, NMP has some limitations with disubstituted alkenes such as methacrylates, whereas ATRP currently cannot polymerize non-activated monomers such as vinyl acetate and N-vinylpyrrolidone, because of poor reactivity of the corresponding dormant species. Coordinating monomers would require the development of new catalysts that can strongly bond halide ions. In addition, ATRP has some problems in the polymerization of acidic monomers (*e.g.* protonation of the ligand). The first successful atom transfer radical polymerization of both acrylic and methacrylic acid was obtain during this thesis work, and is described in chapter 5.

RDRP in water has traditionally been a challenge. Relatively few examples exist of NMP in water or protic media. In water, solubility and hydrolysis of RAFT dithiocarbonyl agents are a concern. Chain transfer agents are also incompatible with primary and secondary amines, thiols and reducing agents. ATRP in water typically requires high concentration of catalyst (ca. 10,000 ppm). Up to now, a general lack of understanding of the detailed ATRP mechanism in water prevented precise and rational optimization of reaction conditions. This is an important topic of this thesis and is discussed in more depth in Chapter 2 (Section 2.1.2).

References

(1) Szwarc M. *Nature* **1956**, *178*, 1168–1169.

(2) The IUPAC recommended term for "stable-free-radical polymerization (SFRP) is "stable-radical-mediated polymerization" (SRMP). Similarly, the recommended term for "nitroxide-mediated polymerization" (NMP) is "aminoxyl-mediated radical polymerization" (AMRP). However, for better comprehension, the terminology in current use is adopted throughout this chapter.

(3) Gold, L. J. *J. Chem. Phys.* **1958**, *28*, 91–99.

(4) H. Fischer, *Chem. Rev.* **2001**, *101*, 3581-3610.

(5) Wang, J.-S., Matyjaszewski, K. *J. Am. Chem. Soc.* **1995**, *117*, pp. 5614-5615.

(6) Kato, M.; Kamigaito, M.; Sawamoto, M.; Higashimura, T. *Macromolecules*, **1995**, *28*, 1721-1723.

(7) Poli R. *Eur. J. Inorg. Chem.* **2011**, *2011*, 1513–1530.

(8) Taton, D.; Wilczewska, A.-Z.; Destarac, M. *Macromol. Rapid Commun*. **2001**, *22*, 1497-1503.

(9) Barner-Kowollik, Ed. *Handbook of RAFT Polymerization* **2008**, Wiley, New York, NY.

(10) Salomon, D. H.; Rizzardo, E.; Cacioli, P. *Polymerization Process and Polymers Produced Thereby*, CSIRO, US4581429, 1986.

(11) M.K. Georges, R.P.N. Veregin, P.M. Kazmaier, G.K. Hamer, *Macromolecules* **1993**, *26*, 2987-2988.

(12) A. Goto, T. Fukuda, *Prog. Pol. Sci.* **2004**, *29*, 329-385.

(13) Grassl, B.; Clisson, G.; Khoukh, A.; Billon, L. *Eur. Pol. J.* **2008**, *44*, 50-58.

(14) Darabi, A.; Shirin-Abadi, A. R.; Jessop, P. G.; Cunningham, M. F. *Macromolecules* **2015**, *48*, 72-80.

(15) Y. Guillaneuf, D. Gigmes, S.R.A. Marque, P. Astolfi, L. Greci, P. Tordo, D. Bertin, *Macromolecules* **2007**, *40*, 3108-3114.

(16) Chiefari, J.; Mayadunne, R. T.; Moad, G.; Rizzardo, E.; Thang, S. H. US patent US6642318, **1998**.

(17) Controlled Radical Polymerization consortium objectives. http://www.chem.cmu.edu/groups/maty/ crp/objectives.html (accessed Dec 28, 2015).

Chapter 2

Atom Transfer Radical Polymerization

Atom transfer radical polymerization (ATRP) is the most often used technique in the field of controlled radical polymerization. This method is used in both academia and industry to design complex and rationally engineered macromolecules. Synthetic polymers can be prepared with chains displaying unrivaled uniformity ($Đ$ < 1.5), predefined molecular weight, controlled topology, and precisely selected end groups (Figure 2.1). Individual macromolecules can be prepared in the shapes of stars, combs, bottlebrushes, and rings or as networks with well-defined mesh size. The composition of individual copolymer chains can follow certain statistics, or change periodically, in a smooth gradient fashion or abruptly, as in block copolymers that can spontaneously phase-separate into various predefined nanostructured morphologies. Useful functionalities can be precisely incorporated into macromolecules by modifying either the end group, or reactive moieties at the center, or other specifically selected positions, to provide targeted properties. The recent improvements in the ATRP catalysts system, summarized in this chapter, helped moving

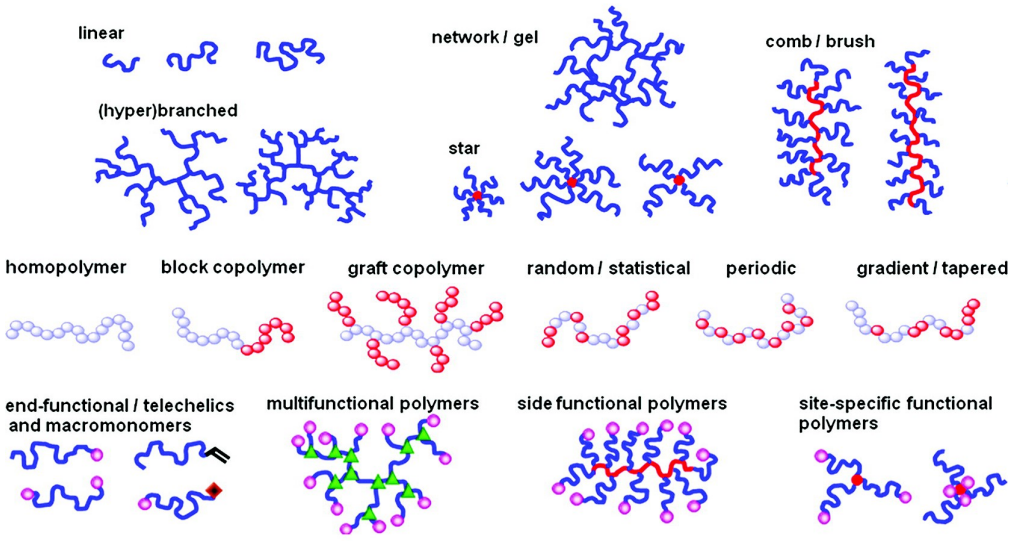

Figure 2.1. From top to bottom, examples of polymers with controlled topology, composition and position of the functional groups.

this polymerization technique to commercialization, as several polymers produced by this technique found applications in fields as diverse as coatings and adhesives, electronics, medicine and cosmetics, environment, and countless others.

2.1 The mechanism of copper-based ATRP

ATRP is usually catalyzed by a copper-amine complex, through a reversible equilibrium that involves the activator complex $[Cu^{I}L]^{+}$ (L = amine ligand) and the deactivator $[X\text{-}Cu^{II}L]^{+}$ (X = Cl, Br; Scheme 2.1).[1] Usually, $K_{ATRP} << 1$, so that the concentration of propagating species in the dormant state (P_n–X) is significantly higher than the concentration of active radicals ($C_{P_n^{\bullet}}$ between 10^{-9} and 10^{-7} M), in order to minimize the occurrence of termination reactions and promote concurrent growth of all polymer chains. Once a radical is generated, it typically adds only few monomer units before being quickly deactivated.

Scheme 2.1. General Mechanism of ATRP

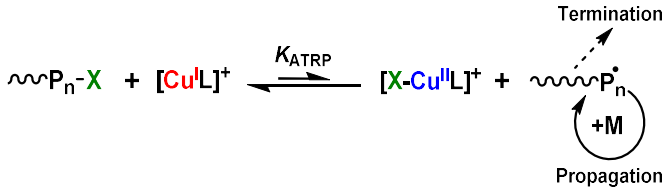

The rate of an ATRP depends on the rate constant of radical propagation (k_p) and on the concentrations of monomer and growing radicals. The radical concentration depends on the ATRP equilibrium constant and the concentration of dormant species, activators, and deactivators, as shown in eq. 2.1.

$$R_p = k_p C_M C_{R^{\bullet}} = k_p \frac{k_{act}}{k_{deact}} C_M C_{RX} \frac{C_{[Cu^{I}L]^{+}}}{C_{[X\text{-}Cu^{II}L]^{+}}} \quad (2.1)$$

The structure of the ligand and monomer/dormant species as well as reaction conditions (solvent, temperature, and pressure) can strongly influence the values of the rate constants, k_{act} and k_{deact}, and their ratio, K_{ATRP} (see Section 2.1.2).[2] Generally, the overall rate of ATRP increases with catalyst activity (K_{ATRP}), although under certain conditions it may decrease because of radical termination leading to a decrease of the $[Cu^{I}L]^{+}/[X{-}Cu^{II}/L]^{+}$ ratio as a consequence of a buildup of the concentration of deactivator via the persistent radical effect.[3]

2.1.1 ISET vs. OSET

ATRP is a radical-based process and radicals can be formed from dormant species by several pathways. Mechanistically, halogen atom transfer from an alkyl halide to a Cu^{I} complex can occur via either outer-sphere electron transfer (OSET) or inner-sphere electron transfer (ISET), *i.e.*, atom transfer passing through a Cu−X−C transition state, which is formally also a single electron transfer process. According to Marcus analysis of electron transfer processes, OSET has an energy barrier ∼15 kcal/mol higher than what is experimentally measured, *i.e.*, OSET is $\sim 10^{10}$ times slower than ISET.[4] The differences are much greater than any computational or experimental errors, and consequently, it must be concluded that a copper-catalyzed ATRP occurs via concerted homolytic dissociation of the alkyl halide via ISET, *i.e.*, an atom transfer process.

2.1.2 ATRP catalytic system

Equilibrium constants in ATRP depend on the structure of the catalysts and alkyl halides (*i.e.*, initiators and monomer) and on the reaction medium. Generally, ATRP equilibrium (K_{ATRP}) and activation (k_{act}) constants increase strongly with solvent polarity, by stabilization of more polar Cu^{II} species, and with temperature. Deactivation rate constants are usually very high and may approach diffusion-controlled limits ($k_{deact} > 10^6\ M^{-1}\ s^{-1}$). They are less influenced by the structure of the involved reagents than the activation rate constants.[2b] Figure 2.2 illustrates variation of the values of k_{act} with the ligand and alkyl halide structure, and variation of K_{ATRP} with solvent.

Cu/L Complexes. The range of activity of ATRP catalyst complexes covers over 6 orders of magnitude. The general order of Cu complex activity in ATRP for ligands is tetradentate (cyclic-bridged) > tetradentate (branched) > tetradentate (cyclic) > tridentate > tetradentate (linear) > bidentate ligands; *i.e.*, complexes with tris(2-dimethylaminoethyl)-amine (Me_6TREN), and tris(2-pyridylmethyl)amine (TPMA) are among the most active, whereas 2,2′-bipyridine (bpy) forms the least active catalyst. The nature of nitrogen atoms in the ligands also plays a role in the activity of the Cu complexes and follows the order pyridine ≈ aliphatic amine > imine < aromatic amine. A two-carbon bridge between N atoms generates the most active complexes. The least active Cu complexes (especially those based on bpy) show excellent control for the polymerization of highly reactive monomers that form stabilized propagating radicals. Instead, ligands that give more active complexes are suitable for less reactive monomers, or for ATRP with

low catalyst loadings[5] (see Section 2.2). In ATRP, the dynamics of the exchange reactions may be even more important than the overall values of the equilibrium constants: radicals must be very quickly deactivated, and values of k_{deact} should be as large as possible.

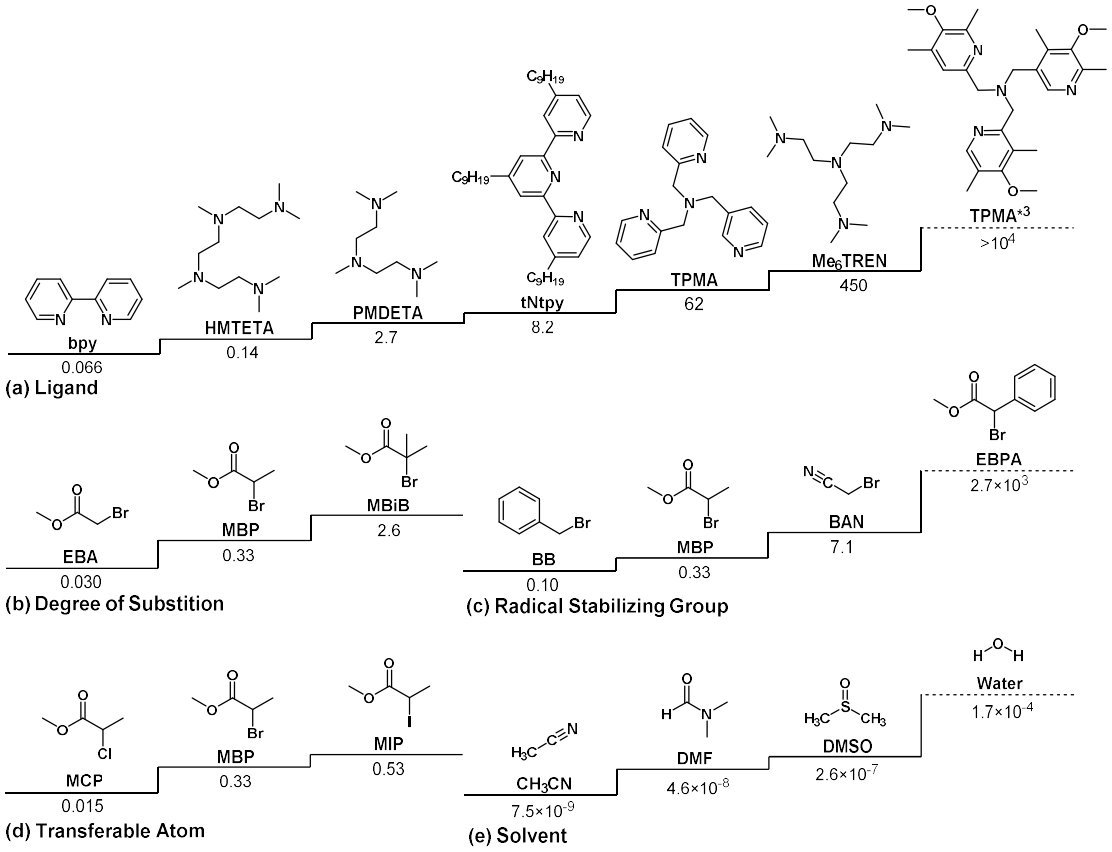

Figure 2.2. ATRP activation rate constants in CH_3CN at 35 °C: (a) for ethyl 2-bromoisobutyrate with Cu^IBr in the presence of various ligands;[2a] (b-d) for various initiators with Cu^IX/PMDETA (X = Br or Cl).[6] (e) ATRP equilibrium constants for the reaction between methyl 2-bromopropionate and $[Cu^IHMTETA]^+$.[7] Values underlined by a dashed line were extrapolated.

Alkyl Halides. Reactivities of alkyl halides in ATRP depend on the structure of the alkyl group and transferable halogen. It is important to select a sufficiently reactive species for an efficient ATRP initiation for polymerization of the selected monomer. Reactivity of alkyl halides follows the order of 3° > 2° > 1°, in agreement with bond dissociation energy needed for homolytic bond cleavage. In addition, the values of K_{ATRP} increase with the addition of strong radical-stabilizing groups (aryl, carbonyl, ester, cyano) attached to the carbon forming the C−X bond (Figure 2.2c). This is related to resonance stabilization as well as to polar and steric effects. The most active initiator is ethyl α-bromophenylacetate, with combined activation effect of both benzyl and ester species. Alkyl halide reactivities follow the order I > Br > Cl.

Solvents. ATRP has been successfully carried out in a broad range of solvents, including both common organic solvents and "greener" ones such as protic solvents (alcohols, water), supercritical CO_2, ionic liquids. The properties of copper complexes in ionic liquids are discussed in Chapter 3 (Section 3.4). Solvents have much smaller effects on radical polymerization than on ionic polymerization. Nevertheless, ATRP equilibrium and rate constants are strongly influenced by the choice of the polymerization medium. The main reason is the less polar character of Cu^{I} complexes (which can be considered neutral if weakly coordinated by a halide ion) with respect to the cationic Cu^{II} complexes, which are strongly stabilized in more polar solvents. The difference is exacerbated in water, which is characterized by very large equilibrium constants, 10,000 times larger than in CH_3CN. Too high K_{ATRP} can lead to excessive radical concentration and difficulties in controlling the polymerization. Consequently, Cu mediated polymerizations in water and protic media have traditionally been a challenge. Controlling ATRP in water is highly desirable because water is an inexpensive and environmentally friendly solvent, with high thermal capacity. In particular, any relevant polymerization involving a biocompatible moiety, such as formation of protein−polymer conjugates[1] or other biohybrids,[2] requires conducting the polymerization in an aqueous environment with a very limited monomer content. The design of optimized reaction conditions requires the knowledge of thermodynamic and kinetic information on the catalytic system, which currently are impossible to obtain for the most frequently used systems (very active Cu/L-RX couples, or common polar solvents like water and DMSO; for example, all values underlined by a dashed line in Figure 2.2 were not directly measured). Chapter 3 describes a set of electrochemical methods for the determination of fast and very fast ATRP activation rate constants in water.

Conditions should be adjusted from those applied in traditional organic solvents to account for higher k_{act} and K_{ATRP}, lower complex stability that may lead to disproportionation and potential hydrolysis of Cu^{II}–X and Pn–X bonds. The detailed mechanism of aqueous ATRP and the relative importance of potential side reactions are still unknown. For this reason, extensive application of ATRP in water is so far limited and, as a consequence, no relevant commercial applications of aqueous ATRP are available. Detailed investigation of the catalytic system in water and the strategies implemented to overcome some of the challenges of aqueous ATRP are described in Chapter 4.

2.2 ATRP with low catalyst loadings

In traditional ATRP, relatively large amounts of catalyst were used, often comparable to the amount of the initiator. Although very active ATRP catalysts were developed, they could not be used at very low concentrations because in ATRP, as in any other radical polymerization, radical termination occurs, leading to irreversible accumulation of the deactivator, $[X\text{-}Cu^{II}L]^+$, at the expense of the activating complex, $[Cu^{I}L]^+$, due to the persistent radical effect. Consequently, when all the activator is irreversibly transformed to deactivator, which can happen at low monomer conversion, the reaction stops. However, the rate of ATRP depends only upon the ratio of activator and deactivator concentrations but not upon their absolute concentrations (eq. 2.1). If that ratio could be kept constant throughout the polymerization, the ATRP rate should remain high. To reach this goal, an additional redox cycle was employed that converted the higher-oxidation-state deactivator complex, formed during termination events, to the lower-oxidation-state activator (Scheme 2.2). In the presence of reducing agents (or of a reduction process), ATRP could be successfully conducted to high monomer conversion at very low (often single-digit ppm) amounts of catalyst.

Scheme 2.2. ATRP with low catalyst loadings.

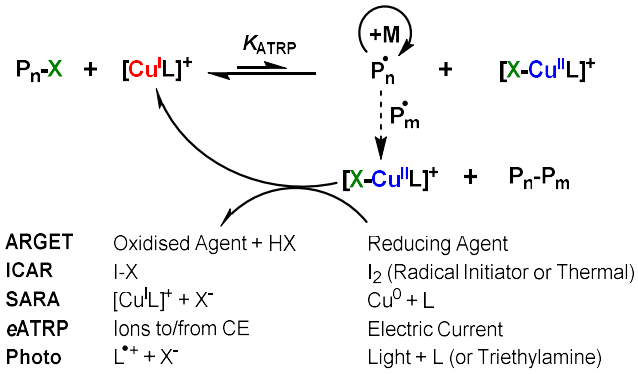

2.2.1 ARGET, SARA and ICAR ATRP systems

In activator regenerated by electron transfer (ARGET) ATRP, a small amount of catalyst is continuously regenerated by a reducing agent. ARGET is a "green" procedure that uses ppm amounts of the catalyst in the presence of appropriate reducing agents such as tin(II) 2-ethylhexanoate ($Sn(EH)_2$), glucose, ascorbic acid, phenol, hydrazine, phenylhydrazine, excess inexpensive ligands, nitrogen-containing monomers, or zerovalent metals. Typically, highly active copper complexes are employed to account for the lower amount of catalyst. To provide the required reduction rate and appropriate concentration of radicals,

mild reducing agents or controlled continuous dosing of more active agents are used. Since the reducing agents allow starting an ATRP with the oxidatively stable Cu^{II} species, the reducing/reactivating cycle can be also employed to eliminate air, or other radical traps, from the system. For example, styrene was polymerized with only 5 ppm of $CuCl_2$/Me_6TREN catalyst, and by adding 500 ppm of $Sn(EH)_2$ to the reaction mixture, resulting in preparation of a polystyrene with M_n = 12 500 ($M_{n,th}$ = 12 600) and M_w/M_n = 1.28 without removal of inhibitors or deoxygenation.[8] An additional advantage of AR-GET ATRP is that catalyst induced side reactions are reduced (as for example catalytic termination).[9] Therefore, it is possible to prepare copolymers with higher molecular weight while retaining chain end functionality.

Metals such as Cu, Fe, Mg, or Zn can also be used as the reducing agent for $[X\text{-}Cu^{II}L]^+$ species.[10] In addition to acting as a reducing agent, they can act as supplemental activators by a direct reaction with alkyl halides, therefore in this case the process is termed SARA ATRP (supplemental activators and reducing agent ATRP). However, transition metal complexes other than Cu or Fe are generally relatively poor deactivators. ATRP with Cu^0 can be considered as a special case because, in the presence of ligand, it produces in situ the efficient activating/deactivating species (Cu^I/Cu^{II}).

In ICAR ATRP, a source of organic free radicals is employed to continuously regenerate the Cu^I activator, which would otherwise be consumed in termination reactions, when catalysts are used at very low concentrations. Therefore, the reaction is driven to completion with addition of low concentrations of standard free radical initiators (*e.g.* azobisisobutyronitrile). ICAR can be seen as ARGET ATRP with reducing agents that are radicals. With this technique, controlled synthesis of polystyrene and poly(meth)acrylates ($M_w/M_n < 1.2$) can be conducted with catalyst concentrations between 5 and 50 ppm, levels at which removal or recycling of the catalyst complex could be avoided for some applications. The rate of ICAR ATRP is governed by the rate of decomposition of the added free radical initiator, as in RAFT, while the degree of control and the rate of deactivation are controlled by K_{ATRP}, as in ATRP. Since the radical initiator could potentially lead to the initiation of new polymer chains, some applications of this technique are limited.

A discussed in the next two sections, active catalyst regeneration can be also accomplished by physical means such as electrical current or light. The advantage of both of

these systems is that they can be fine-tuned by external stimuli (changing electrical potential/current or light intensity/wavelength) and they usually produce less undesired side products.

2.2.2 Electrochemically mediated ATRP

In all ARGET, SARA and ICAR processes, reducing agents are oxidized, generating some side products: new chains in ICAR, metal halides in SARA, dehydroascorbic acid, and tin(IV) species, *etc.*, in ARGET. These oxidized species might be more harmful than the original reducing agents. Therefore, it would be of interest to avoid using chemicals as reducing agents and replace them by electrons, specifically electrical current. This is the concept of the latest developed low-ppm technique, electrochemically mediated ATRP (*e*ATRP), in which the ratio of the concentrations of activator and deactivator is controlled by the potential applied at the working electrode (E_{app}).[11]

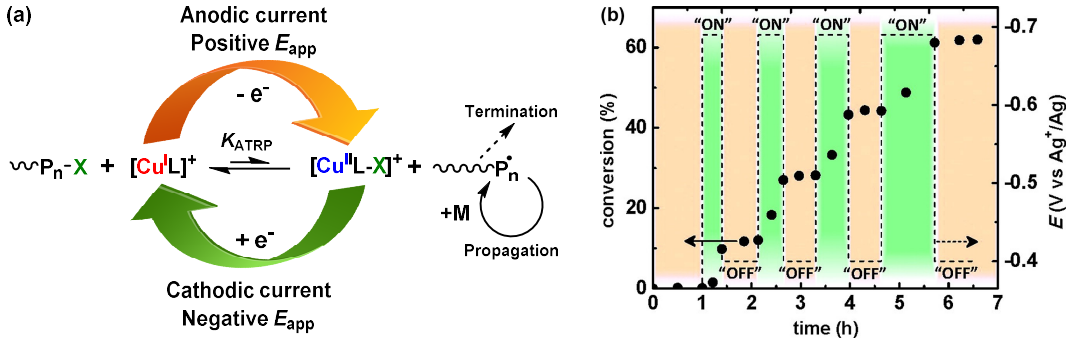

Figure 2.3. (a) Mechanism of electrochemically mediated ATRP. (b) Conversion (solid circles) and applied potential (dashed line) with respect to time, in methyl acrylate polymerization.

Several parameters, such as applied current, potential, and total charge passed, can be controlled in *e*ATRP to allow selection of the desired concentration of the redox-active catalytic species. The mechanism of ATRP mediated through electrochemical control over the ratio of Cu^I/Cu^{II} and (re)generation of activator is shown in Figure 2.3a. A targeted amount of the air-stable Cu^{II}/L catalyst complex can be electrochemically reduced to Cu^I/L activator to start a controlled polymerization. The rate of *e*ATRP can be controlled by changing the applied potential (E_{app}). In proximity of the electrode surface, the Nernst equation is usually considered valid:

$$E_{app} = E_{1/2} + \frac{RT}{nF} \ln \frac{C_{Cu^{II}}}{C_{Cu^{I}}} \qquad (2.2)$$

where $E_{1/2}$ is the half-wave potential of the copper catalyst. In the absence of mass transport limitations, the rate of reduction is directly dictated by the applied potential (E_{app}), enabling fine-tuning the polymerization rate by the generated ratio of $C_{Cu^I}/C_{Cu^{II}}$ (a more negative potential induces an increase in the $C_{Cu^I}/C_{Cu^{II}}$ ratio, resulting in a faster rate of polymerization).

Exploiting the same principle, electrochemistry also permits a lower oxidation state catalyst (Cu^I/L) to be reverted back to its original higher oxidation state by simply shifting E_{app} to more positive values. Therefore, the procedure provides a means to rapidly deactivate an ongoing polymerization, essentially quickly changing between "on" and "off" polymerization states (Figure 2.3b). Monomer conversion quickly stops when an appropriate positive potential is applied. The polymerization is started again when E_{app} is shifted to more negative values. Usually, no change in the "livingness" of the formed polymer is observed during the enforced dormant state.

One of the limits of *e*ATRP is that it usually requires working electrodes made of Pt, an expensive, rare and non-functionalizable metal. The use of alternative cathodic materials (based on carbon or non-noble metals and alloys) in *e*ATRP was investigated as presented in Chapter 6.

2.2.3 Photochemically mediated ATRP

Cu-based systems. Light has been used to mediate copper ATRP under various conditions, in the presence of radical photoinitiators, by direct breaking of the alkyl-halogen bond and also by photoreduction of the Cu^{II}/L species. This latter case is of special interest. In Cu-based ATRP, several species can absorb in the UV-visible region. Such species can participate in a photoreduction process (with generation of radicals) alone or in a combination with other reagents.[12] The dominant mode of Cu^I/L activator (re)generation (>90%) is the photochemically mediated reduction of Cu^{II} complexes by electron donors. Simple addition of triethylamine or an excess of Me_6TREN or TPMA ligand provides free amines that can serve as electron donors. Cu^{II}/L species absorb strongly in UV/VIS and the excited species are reduced to Cu^I/L species and, concurrently, free amines are oxidized to the corresponding radical cation, which can initiate a new chain after proton transfer (Scheme 2.2).

Photoredox systems. In 2012, Hawker *et al*. reported an ATRP process mediated by photoredox catalysts[13] (Scheme 2.3), not requiring traditional Cu-based catalysts. In this

case, the excited Cat* would reduce an alkyl bromide initiator to give the desired alkyl radical, which could initiate polymerization of the monomer. In particular, the use of the photocatalyst 10-phenylphenothiazine (Cat = Ph-PTZ) allowed overcoming the challenge of metal contamination in traditional ATRP systems, which was limiting some applications in microelectronics or biomaterials.[14] The process retained many characteristics of traditional ATRP procedures, including accurate control over molecular weight, low dispersity, and high retention of C–X chain end functionality. This allowed a variety of block copolymers to be prepared in a sequential manner as well as in combination with other ATRP processes.

Scheme 2.3. Proposed simplified mechanism of photo-mediated ATRP with *fac*-[Ir(ppy)$_3$] or 10-phenylphenothiazine as catalyst.

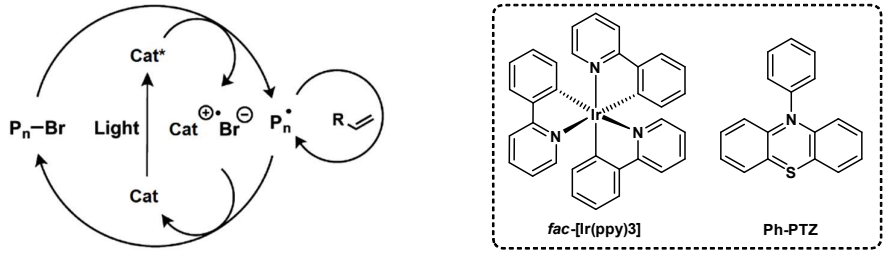

The most advantageous aspect of these systems, which also distinguishes them from traditional Cu-mediated ATRP methods, is the ability to reversibly activate or deactivate the polymerization with visible light. Specifically, when light is removed from this reaction no Cat* will be present, and the polymerization will rest at the dormant, and stable, bromine chain-terminated species. Nevertheless, the detailed mechanism of this process is still unknown, especially regarding the deactivation of the growing radicals, and studies about these aspects are explained in Chapter 7.

2.3 Scope and organization of the Ph.D. thesis

The aim of this Ph.D. project is to investigate some of the current most important issues of ATRP, with the purpose of expanding the limits of control. Electrochemical methods are the principal tools used. They are well suitable for the investigation of the ATRP catalytic system, which involves an electron transfer between copper species (or organic photocatalysts) and alkyl halides. Fundamental kinetic and thermodynamic aspects were investigated, with particular attention paid to the reaction in water. The obtained results

had some important implications from both mechanistic and synthetic standpoints, and overall allowed to expand the scope of ATRP polymerization.

The Ph.D. project is presented as follows:

- *Chapter 3* introduces a set of electrochemical methods developed to determine ATRP activation rate constants of fast reactions in water (and organic solvents). In addition, the effect of the presence of monomer on the kinetics is analyzed. Correlations between ATRP kinetics (k_{act}) and thermodynamics (K_{ATRP}) are presented.
- In *Chapter 4*, the effect of pH on the redox properties of Cu/L complexes and the stability of the Cu-X bond are investigated in water. The obtained results allowed defining the limits of control of aqueous ATRP. Several well-controlled *e*ATRPs were conducted, with the model monomer oligo(ethyleneoxide) methylether methacrylate (OEOMA). Conditions were optimized for the use of inexpensive PMDETA or very active Me_6TREN ligands. The effect of the concentration and of the type (Cl^-, Br^-) of added halide ion is discussed.
- *Chapter 5* describes the ATRP of (meth)acrylic acid in water. First, the reason preventing the polymerization was investigated. The principle cause was found in cyclization of the chain end with the active halogen atom as leaving group. This allowed to introduce several simple but innovative approaches that led to successfully controlled polymerization of acid monomers by both *e*ATRP and SARA ATRP.
- In *Chapter 6,* the use of a set of different working electrodes in aqueous *e*ATRP is described (carbon material and non-noble metals). Several challenges had to be faced, especially regarding the reactivity of the metals in water (*e.g.* corrosion, side reaction with initiator RX).
- In *Chapter 7*, several metal-free ATRP catalysts were investigated by cyclic voltammetry, which proved to be a reliable technique for the screening of organic molecules as potential useful photoredox catalysts. Moreover, a detailed kinetic investigation by means of Marcus theory for electron transfer (and its successive developments) allowed to understand the mechanism of both metal-free ATRP activation and deactivation processes.

References

(1) De Paoli, P.; Isse, A. A.; Bortolamei, N.; Gennaro, A. *Chem. Commun.* **2011**, *47*, 3580–3582.

(2) (a) Tang, W.; Matyjaszewski, K. *Macromolecules* **2006**, *39*, 4953− 4959. (b) Tang, W.; Kwak, Y.; Braunecker, W.; Tsarevsky, N. V.; Coote, M. L.; Matyjaszewski, K. *J. Am. Chem. Soc.* **2008**, *130*, 10702− 10713. (c) Matyjaszewski, K.; Paik, H.-j.; Zhou, P.; Diamanti, S. J. *Macromolecules* **2001**, *34*, 5125−5131.

(3) Fischer, H. *Chem. Rev*. **2001**, *101*, 3581−3610.

(4) (a) Lin, C. Y.; Coote, M. L.; Gennaro, A.; Matyjaszewski, K. *J. Am. Chem. Soc.* **2008**, *130*, 12762−12774. (b) Isse, A. A.; Bortolamei, N.; De Paoli, P.; Gennaro, A. *Electrochim. Acta* **2013**, *110*, 655–662.

(5) Woodruff, S. R.; Davis, B. J.; Tsarevsky, N. V. *ACS Symp. Ser.* **2012**, *1100*, 99–113.

(6) Tang, W.; Matyjaszewski, K. *Macromolecules* **2007**, *40*, 1858–1863.

(7) Braunecker, W. A.; Tsarevsky, N. V.; Gennaro, A.; Matyjaszewski, K. *Macromolecules* **2009**, *42*, 6348−6360.

(8) Jakubowski, W.; Min, K.; Matyjaszewski, K. *Macromolecules* **2006**, *39*, 39−45.

(9) Wang, Y.; Soerensen, N.; Zhong, M.; Schroeder, H.; Buback, M.; Matyjaszewski, K. *Macromolecules* **2013**, *46* (3), 683–691.

(10) Zhang, Y.; Wang, Y.; Matyjaszewski, K. *Macromolecules* **2011**, *44*, 683−685.

(11) (a) Magenau, A. J. D.; Strandwitz, N. C.; Gennaro,A.; Matyjaszewski, K. *Science* **2011**, *332*, 81−84. (b) Bortolamei, N.; Isse, A. A.; Magenau, A. J. D.; Gennaro, A.; Matyjaszewski, K. *Angew Chem. Int. Ed.* **2011**, *50*, 11391-11394.

(12) Ribelli, T. G.; Konkolewicz, D.; Bernhard, S.; Matyjaszewski, K. *J. Am. Chem. Soc.* **2014**, *136*, 13303–13312.

(13) Fors, B. P.; Hawker, C. J. *Angew. Chemie - Int. Ed.* **2012**, *51* (35), 8850–8853.

(14) Treat, N. J.; Sprafke, H.; Kramer, J. W.; Clark, P. G.; Barton, B. E.; Read de Alaniz, J.; Fors, B. P.; Hawker, C. J. *J. Am. Chem. Soc.* **2014**, *136*, 16096−16101.

Chapter 3

Electrochemical Determination of ATRP Activation Rate Constants

Considering the ATRP equilibrium constant, defined as $K_{ATRP} = k_{act}/k_{deact}$, it has been shown that the deactivation rate constant, k_{deact}, is much less sensitive to the molecular structures of both catalyst and initiator (RX) than the activation rate constant, k_{act}.[1] Consequently, k_{act} is the main indicator of the activity of the catalyst/initiator couple and can be used alone to obtain a rough estimate of the order of magnitude of K_{ATRP}. The equilibrium constant can be used to relate the rate of polymerization, R_p, to the concentration of the propagating radicals:

$$R_p = k_p C_M C_{R\bullet} = k_p K_{ATRP} C_M C_{RX} \frac{C_{Cu^I}}{C_{Cu^{II}}} \tag{3.1}$$

Therefore, information on k_{act} values is important to understand the ATRP process and for easy choice of the most appropriate experimental conditions. For example, knowledge of k_{act} values permits the construction of structure-reactivity relationships allowing a rational choice of the best catalyst/initiator couple for a specific polymerization system. Indeed, since some initiators mimic the dormant chain ends (e.g. $PhCH_2X$ for polystyrene, $CH_3CH(X)CO_2CH_3$ for methyl acrylate, $CH_3CH(X)CN$ for acrylonitrile, etc.), these data are relevant for the characterization of the activation step during the whole course of the polymerization. In this context, the effect of the chain length is considered to be rather weak as previously shown by Fukuda and Goto.[2]

Recently, several efficient methods have been developed for the generation and regeneration of the active Cu^I catalyst. Knowledge of k_{act} allows the choice of the best methodology for any polymerization system. Catalytic systems with low to moderate activity are suitable for the direct ATRP method, where Cu^I is directly injected in the reaction mixture. More active systems can be employed at a low catalyst concentration, provided that the active Cu^I species are efficiently generated (and regenerated).[3]

It has to be noted that a considerable number of activation rate constants have been already reported in the literature. However, the employed methodologies (GC or LC chromatography,[4] spectrophotometry,[5] NMR[6]) were suitable only for the characterization of slow reactions. Therefore, most of the published data for the most active and successful catalysts (namely, $[Cu^{I}PMDETA]^{+}$, $[Cu^{I}TPMA]^{+}$ and $[Cu^{I}Me_6TREN]^{+}$) were estimated with predictive correlations that have never been verified. More precisely, these correlations are based on the assumption that the k_{act} ratio of two different alkyl halides (*e.g.* $k_{act,RX_1} / k_{act,RX_2}$) is maintained by changing the nature of the Cu^{I} complex, which is hardly sustainable considering the inner-sphere nature of the ATRP mechanism.[7] Current available methodologies are not suitable for kinetic investigations on reactions involving the most used and/or newly developed active catalysts such as copper ligated by Me_6TREN, TPMA* and analogues[8], Me_4Cyclam and bridged Cyclam[9], *etc*., and several very reactive initiators. Moreover, polar solvents, such as DMSO and water, which are recently drawing a feverish interest in the field of ATRP, present extremely high activation rate constants[10] that cannot be measured by the traditional techniques.

Scheme 3.1. Structures of the investigated copper ligands, initiators and monomers.

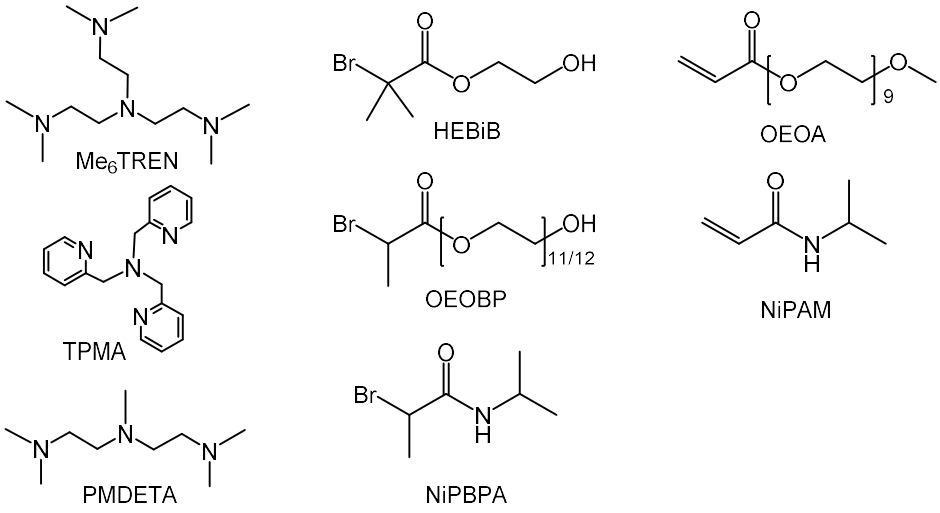

A collection of electrochemical methods suitable for the determination of a wide range of k_{act} values, including rate constants of extremely fast reactions with k_{act} even approaching the diffusion-controlled limit is described in this chapter. Although application of some of these methods to kinetic analysis of ATRP systems has already appeared in the literature,[10,11] we provide here a brief description of all methods and show their application for the determination of k_{act} of an extensive set of reactions involving three

$[Cu^IL]^+$ complexes (L = Me_6TREN, TPMA and PMDETA, Scheme 3.1) and three initiators in aqueous solutions (Scheme 2c). Moreover, the effect of the presence of monomer in water was investigated. The data collected for each catalyst/initiators were then used to build structure-reactivity correlations.

3.1 Electrochemical techniques for k_{act} determination

3.1.1 Hydrodynamic chronoamperometry at a rotating disk electrode

Determination of k_{act} by monitoring the rate of disappearance of Cu^I by applying a fixed potential at a rotating disc electrode has already been described.[12,13] Therefore, for the sake of completeness, we include in this section only a brief description of the method.

Scheme 3.2 Mechanism of activation of RX by Cu^I in the presence of a nitroxyl radical, R′NO.

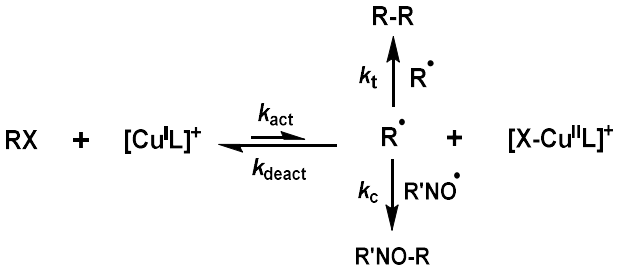

To extract kinetic information from the ATRP equilibrium, the reaction must be made irreversible by conducting all experiments in the presence of a good radical scavenger such as 2,2,6,6-tetramethyl-1-piperidinyloxy (TEMPO), in a large excess with respect to $[Cu^IL]^+$.[14] The overall reaction is shown in Scheme 3.2. It is known that nitroxyl free radicals such as TEMPO rapidly react with alkyl radicals ($k_c \approx 10^9$ $M^{-1}s^{-1}$)[15,16,17] to give relatively stable alkoxyamines.[18] Since in these conditions reaction of the radical $R^\bullet$ with TEMPO is much faster than deactivation, the whole reaction becomes irreversible with the initial radical generation as rate-determining step. It is therefore possible to measure k_{act} by monitoring the decrease of $[Cu^IL]^+$ concentration with time.

Since $[Cu^IL]^+$ exhibits a well-defined anodic wave at the RDE (Figure 3.1a), the limiting current, I_L, due to oxidation of Cu^I can be used to monitor $C_{[Cu^IL]^+}$ during the reaction of an initiator RX with a Cu^I complex. The limiting current is related to $C_{[Cu^IL]^+}$ by the Levich equation:[19]

$$I_L = 0.62nFAD^{2/3}\omega^{1/2}\nu^{-1/6}C_{[Cu^IL]^+} \quad (3.2)$$

where n is the number of exchanged electrons, F is the faraday constant, D is the diffusion coefficient of $[Cu^IL]^+$, A is the area of the electrode and ν is the kinematic viscosity.

If equimolar quantities of Cu^I and RX are used, *i.e.*, $C^0_{[Cu^IL]^+} = C^0_{RX}$, the kinetic analysis of the system under second-order conditions leads to:

$$\frac{1}{C_{[Cu^IL]^+}} - \frac{1}{C^0_{[Cu^IL]^+}} = k_{act}t \quad (3.3)$$

If on the other hand $C^o_{RX} >> C^o_{[Cu^IL]^+}$, pseudo-first order conditions are established and the rate law becomes:

$$\ln C_{[Cu^IL]^+} = \ln C^0_{[Cu^IL]^+} - k't \quad (3.4)$$

where $k' = k_{act}C^0_{RX}$.

From the experimental point of view, a solution of $[Cu^IL]^+$ is prepared in an electrochemical cell complete with all electrodes, background electrolyte and a radical scavenger, *e.g.*, TEMPO. Then a constant potential in the plateau region of the oxidation wave of Cu^I is applied with recording of I_L and immediately the initiator is injected. The output of the experiment is a decay curve for the oxidation current of Cu^I, but since I_L is proportional to $C_{[Cu^IL]^+}$, the curve represents the rate of disappearance of $[Cu^IL]^+$. Elaboration of the data according to eq. 3.3 or eq. 3.4, depending on the experimental conditions, provides the rate constant, k_{act}. Examples of linear plots based on eqs. 3.3 and 3.4 are reported in Figure 3.1.

This technique is applicable in both water and organic solvents as long as E_{app} is significantly more positive than $E_{1/2}$ of all the relevant copper complexes present in solution. The application of hydrodynamic voltammetry is limited to the measurement of k_{act} values below 5×10^3 M^{-1} s^{-1}. If $k_{act} = 5\times10^3$ M^{-1} s^{-1} and $C^0_{[Cu^IL]^+} = C^0_{RX} = 5\times10^{-4}$ M, the half-life time of $[Cu^IL]^+$ is 0.4 s, which is comparable with the mixing time under the best conditions, therefore preventing the possibility of obtaining reliable results. Thus, the upper limit of the RDE technique is typically $k_{act} < 2\times10^3 - 5\times10^3$ M^{-1} s^{-1}, depending on the particular conditions chosen or imposed by the system (*e.g.* Cu^I concentration, angular velocity ω, diffusion coefficients, solvent, viscosity, etc.).

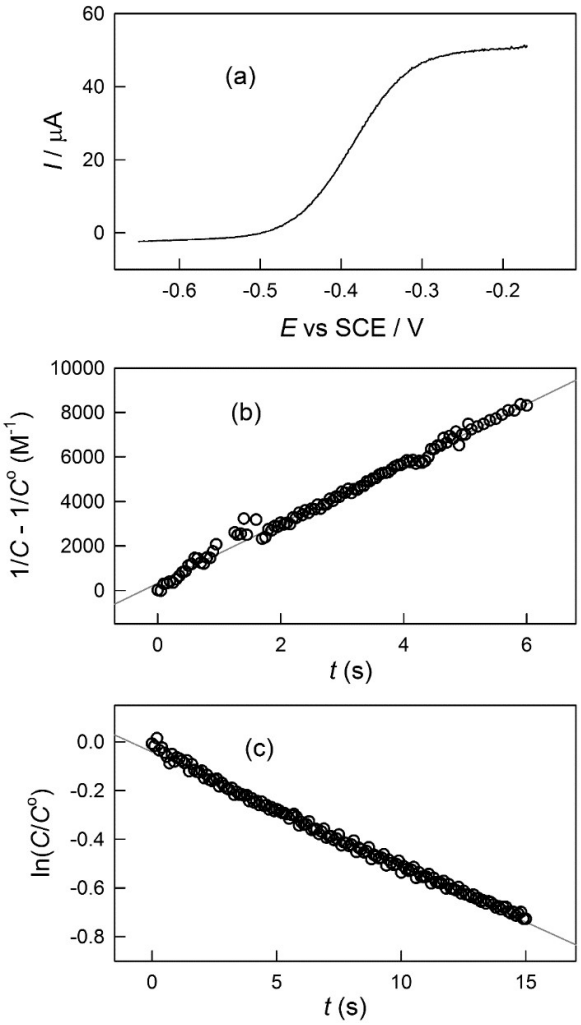

Figure 3.1. a) Linear sweep voltammogram of 10^{-3} M $[Cu^{I}TPMA]^{+}$ in H_2O + 0.1 M Et_4NBF_4 at RDE (ω = 2500 rpm). b) Variation of I_L with time recorded at E = -0.2 V on RDE (ω = 2500 rpm) for the oxidation of 2.5×10^{-4} M $[Cu^{I}L]^{+}$ in the presence of 2.5×10^{-4} M and 5×10^{-3} M TEMPO; inset: kinetic analysis according to a second-order rate law.

3.1.2 Homogeneous redox catalysis in water

Activation rate constants in aqueous media are very high with values well beyond the limit of the RDE technique. Fast reactions can be studied by transient voltammetric techniques. The possibility of employing electrogenerated Cu^{I} species is easily achievable and allows to study fast reactions with rate constants even approaching the diffusion-controlled limit. In homogeneous redox catalysis (HRC)[20,21] the active form of a catalyst (*e.g.* Cu^{I}) is generated at the electrode. This species then reacts with the substrate (*e.g.* alkyl halide initiator) in a thin reaction layer adjacent to the electrode surface, whereby the

starting inactive form of the catalyst is regenerated. Diffusion of the latter back to the electrode and electron transfer to regenerate the active form of the catalyst start a new catalytic cycle, which produces a catalytic current in cyclic voltammetry. This catalytic current enhancement is a source of kinetic information on the reaction between the catalyst and substrate (*e.g.* activation of RX by Cu^{I}).

It has been recently shown that voltammetric reduction of Cu^{II} complexes in water, under ATRP conditions, triggers a catalytic process with remarkable current enhancements for the reduction peak of Cu^{II},[10,22] suggesting that these systems are amenable to kinetic analysis according to the HRC approach. The reason for the establishment of redox catalysis with peak current enhancement in aqueous ATRP is that all Cu^{II} species generated in the system are reducible at the reduction potential of the starting $[Cu^{II}L]^{2+}$ complex. In other words, $E^{\ominus}_{[X\text{-}Cu^{II}L]^{+}/[X\text{-}Cu^{I}L]} \geq E^{\ominus}_{[Cu^{II}L]^{2+}/[Cu^{I}L]^{+}}$ so that the deactivator is reduced to Cu^{I} as soon as it reaches the electrode. During the voltammetric reduction of $[Cu^{II}L]^{2+}$ to $[Cu^{I}L]^{+}$ in water in the presence of RX, a series of reactions including activation of the alkyl halide and regeneration of $[Cu^{I}L]^{+}$ by reduction of the ensuing deactivator, $[X\text{-}Cu^{II}L]^{+}$, should be considered. The following reactions occur:

$$[Cu^{II}L]^{2+} + e^{-} \rightleftharpoons [Cu^{I}L]^{+} \tag{3.5}$$

$$[Cu^{I}L]^{+} + RX \rightleftharpoons [X\text{-}Cu^{II}L]^{+} + R^{\bullet} \tag{3.6}$$

$$[X\text{-}Cu^{II}L]^{+} \rightleftharpoons [Cu^{II}L]^{2+} + X^{-} \tag{3.7}$$

$$[X\text{-}Cu^{II}L]^{+} + e^{-} \rightleftharpoons [X\text{-}Cu^{I}L] \tag{3.8}$$

$$[X\text{-}Cu^{II}L]^{+} + [Cu^{I}L]^{+} \rightleftharpoons [X\text{-}Cu^{I}L] + [Cu^{II}L]^{2+} \tag{3.9}$$

$$[X\text{-}Cu^{I}L] \rightleftharpoons [Cu^{I}L]^{+} + X^{-} \tag{3.10}$$

$$R^{\bullet} + R^{\bullet} \rightarrow R\text{–}R \tag{3.11}$$

$$R^{\bullet} + R'NO \rightarrow R\text{–}ONR' \tag{3.12}$$

These reactions represent a catalytic cycle where $[Cu^{I}L]^{+}$, the only species capable of activating RX,[12] is continuously regenerated at the electrode. This catalytic cycle is better illustrated in Scheme 3.3 for electrochemically mediated activation of RBr by $[Cu^{I}L]^{+}$. The $[Br\text{-}Cu^{II}L]^{+}$ species arising from the activation reaction between RBr and $[Cu^{I}L]^{+}$ has two possibilities. Since in water $E^{\ominus}_{[Cu^{II}L]^{2+}/[Cu^{I}L]^{+}} < E^{\ominus}_{[Br\text{-}Cu^{II}L]^{+}/[Br\text{-}Cu^{I}L]}$,[22b] one possibility is fast reduction at the electrode (lower cycle in Scheme 3.3) or in solution by $[Cu^{I}L]^{+}$ (for simplicity, not shown in Scheme 3.3). This will generate $[Br\text{-}Cu^{I}L]$ in equi-

librium with $[Cu^{I}L]^{+}$, which readily starts another cycle. The second possibility is dissociation of $[Br\text{-}Cu^{II}L]^{+}$ to $[Cu^{II}L]^{2+}$ and Br^{-}. The binding constant of Br^{-} to $[Cu^{II}L]^{2+}$ is quite low ($K_{Br} \approx 10$),[22b] therefore only a small fraction of Cu^{II} is present in solution as $[Br\text{-}Cu^{II}L]^{+}$, unless a large excess of Br^{-} is used.

Scheme 3.3. Mechanism of electrocatalytic activation of alkyl bromide by $[Cu^{I}L]^{+}$ in aqueous media.

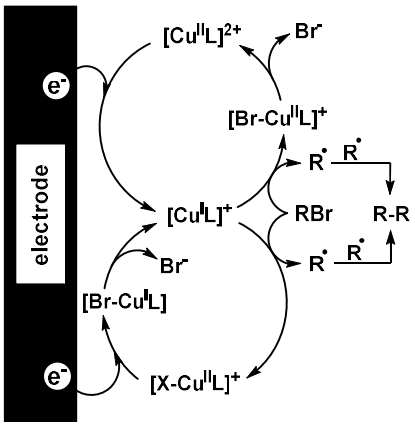

Figure 3.2 shows cyclic voltammetry of $[Cu^{II}TPMA]^{2+}$ in H_2O + 0.1 M Et_4NBF_4, recorded in the absence and presence of oligoethyleneoxide bromopropionate (OEOBP). In the absence of RBr, the voltammetric response shows a peak couple at $E_{1/2}$ = -0.348 V vs. SCE corresponding to a reversible $1e^{-}$ reduction of $[Cu^{II}TPMA]^{2+}$ to $[Cu^{I}TPMA]^{+}$ (eq. 3.5). As RBr is added, a remarkable enhancement of the cathodic peak and a decrease up to disappearance of the anodic peak are observed, as expected for a catalytic system.[23] The effects of C_{RBr} and scan rate (υ) on the cyclic voltammetry of $[Cu^{II}TPMA]^{2+}$ are shown in Figure 3.2. The peak current for the reduction of $[Cu^{II}L]^{2+}$ is enhanced by the homogenous catalytic cycle, therefore increasing C_{RBr} enhances the catalytic effect, whereas increasing υ has the opposite effect. Faster scan rates tend to suppress the contribution of catalysis as the amount of catalyst regenerated through reactions in Scheme 3.3 during the CV decreases with increasing υ. As shown in Figure 3.2b, an increase of υ leads to a decrease of the degree of catalysis, defined as I_p/I_p^0, where I_p^0 and I_p stand for the peak current of $[Cu^{II}L]^{2+}$ reduction measured in the absence and presence of initiator, respectively.

The degree of catalysis I_p/I_p^0 is related to the ratio between the concentrations of initiator and catalyst, $\gamma = C_{RX}/C_{[Cu^{II}L]^{2+}}$, and to a dimensionless kinetic parameter λ, defined as:

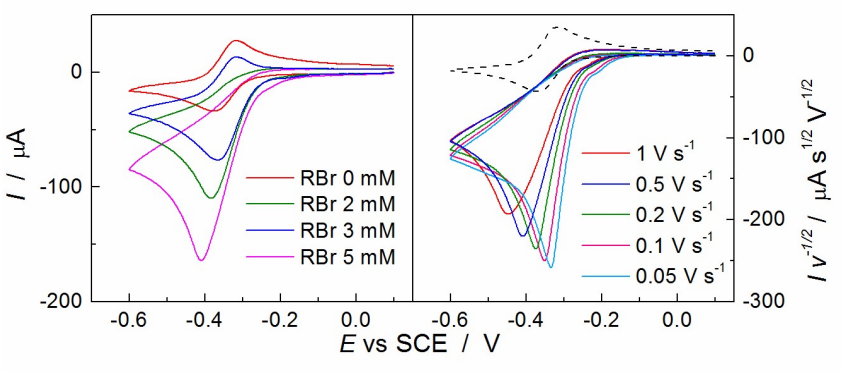

Figure 3.2. Background subtracted CVs of 10^{-3} M $[Cu^{II}TPMA]^{2+}$ in H_2O + 0.1 M Et_4NBF_4, recorded at a glassy carbon electrode: (a) in the absence and presence of OEOBP at different concentrations at v = 0.5 V s^{-1}; (b) in the absence (dotted line) and presence (solid lines) of 5×10^{-3} M OEOBP at different scan rates.

$$\lambda = \frac{RTk_{act}C_{[Cu^{II}L]^{2+}}}{Fv} \tag{3.13}$$

Theoretical working curves relating the degree of catalysis with λ can be constructed by digital simulation of the reaction sequence shown in eqs. 3.5-3.12. Digital simulation requires various thermodynamic and kinetic parameters, such as K_{ATRP}, association constants of $[Cu^{II}L]^{2+}$ and $[Cu^{I}L]^{+}$ with Br^-, standard reduction potentials of copper catalysts, standard electron transfer rate constants, $k°$, and diffusion coefficients, D. Some of these parameters were measured during the Ph.D. work, whereas others were taken from the literature or estimated on the basis of literature data. For all radicals, coupling reactions (eqs 3.11 and 3.12) were considered to be very fast with rate constants $k_{3.11} = 2.7\times10^8$ $M^{-1}s^{-1}$ and $k_{3.12} = 10^8$ M^{-1} s^{-1}.[15,16,17,22b] The equilibrium constants of Br^- association with $[Cu^{II}L]^{2+}$ and $[Cu^{I}L]^{+}$ in water have recently been reported.[22b] We used these values for both pure water and aqueous solutions containing 18% monomer (w/w). Additionally, we assumed that the association/dissociation equilibria are fast so that they constitute conditions of pre-equilibrium for the activation step. Therefore, we used a rate constant, k_{Br}, of 10^4 $M^{-1}s^{-1}$ for the reaction of Br^- with both $[Cu^{II}L]^{2+}$ and $[Cu^{I}L]^{+}$. Higher values of k_{Br} did not affect the degree of catalysis. K_{ATRP} for the reaction between Cu^I complexes and HEBiB in water is in the range 0.05 – 0.80.[22b] K_{ATRP} values in water/monomer mixtures are not known, but are expected to be smaller than in pure water. The role of K_{ATRP} on the simulation was investigated and it was found that simulated CV responses are unaffected provided that $K_{ATRP} > 10^{-4}$. Since this limit is much smaller than the typical K_{ATRP}

values in aqueous media,[22b] the values reported for pure water were used in all aqueous solutions.

E^{e} and k° of the complexes $[Cu^{II}L]^{2+}$ as well as the diffusion coefficients of all species were determined by cyclic voltammetry. E^{e} was measured as the half-sum of the anodic and cathodic peak potentials. The standard reduction potentials of the ternary complexes $[X\text{-}Cu^{II}L]^{+}$ could not be measured, but since $E^{e}_{[X\text{-}Cu^{II}L]^{+}/[X\text{-}Cu^{I}L]} \geq E^{e}_{[Cu^{II}L]^{2+}/[Cu^{I}L]^{+}}$ the same values have been used for $[Cu^{II}L]^{2+}$ and $[X\text{-}Cu^{II}L]^{+}$. Diffusion coefficients of the complexes were obtained from the cathodic peak current, I_{pc}, according to the following equation valid for a reversible electrode process:

$$I_{pc} = (2.69\times10^{5})n^{3/2}AD^{1/2}C\upsilon^{1/2} \tag{3.14}$$

where n is the number of exchanged electrons, A is the area of the electrode and C is the bulk concentration of the Cu^{II} complex. The initiators HEBiB, OEOBP and NiPBPA give a single irreversible reduction peak in cyclic voltammetry (Figure 3) corresponding to $2e^{-}$ reduction of the carbon-bromine bond to RH and Br^{-}. The peak current can be used also in this case to calculate D from the following equation:

$$I_{pc} = (2.99\times10^{5})\alpha^{1/2}nAD^{1/2}C\upsilon^{1/2} \tag{3.15}$$

where C is the bulk concentration of RX and α is the transfer coefficient, which also was determined from the peak characteristics according to known procedures.[24] Table 3.1 summarizes all thermodynamic and kinetic data determined from cyclic voltammetry for Cu complexes and initiators.

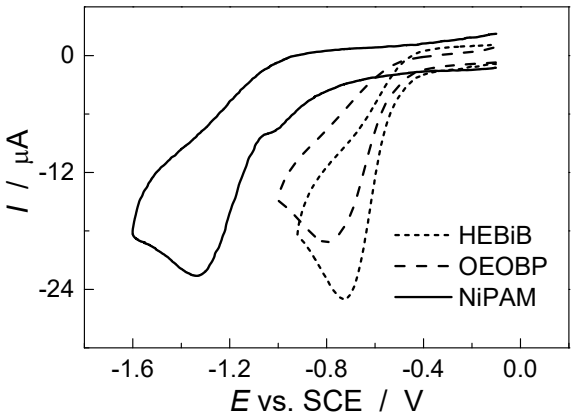

Figure 3.3. CVs of 10^{-3} M RX in H_2O + 0.1 M Et_4NBF_4, recorded at a glassy carbon electrode at υ = 0.2 V s^{-1}.

Table 3.1. Data from cyclic voltammetry of $[Cu^{II}L]^{2+}$ and RX in H_2O and in H_2O + 18 wt% monomer (OEOA or NiPAM). [a]

Species	Water			Water/OEOA			Water/NiPAM		
	$E^{\ominus}$ [b] (V)	10^6D (cm^2/s)	10^3k^0 (cm/s)	$E^{\ominus}$ [b] (V)	10^6D (cm^2/s)	10^3k^0 (cm/s)	$E^{\ominus}$ [b] (V)	10^6D (cm^2/s)	10^3k^0 (cm/s)
$[Cu^{II}TPMA]^{2+}$	-0.35	4.6	18	-0.18	0.98	3.1	-0.17	1.1	2.0
$[Cu^{II}Me_6TREN]^{2+}$	-0.40	2.0	10	-0.34	0.58	1.5	-0.33	0.91	1.0
$[Cu^{II}PMDETA]^{2+}$	-0.37	2.0	10	-0.34	0.58	1.5	-0.33	0.91	1.0
HEBiB	-0.73[c]	6.0		-1.23	2.0				
OEOBP	-0.81[c]	3.1		-1.11	0.58				
NiPBPA	-1.34[c]	8.3					-1.57	3.2	

[a]Data obtained at 25 °C, using 0.1 M Et_4NBF_4 as supporting electrolyte. [b]Versus saturated calomel electrode (SCE). [c]Cathodic peak potential at $\upsilon = 0.2$ Vs^{-1}.

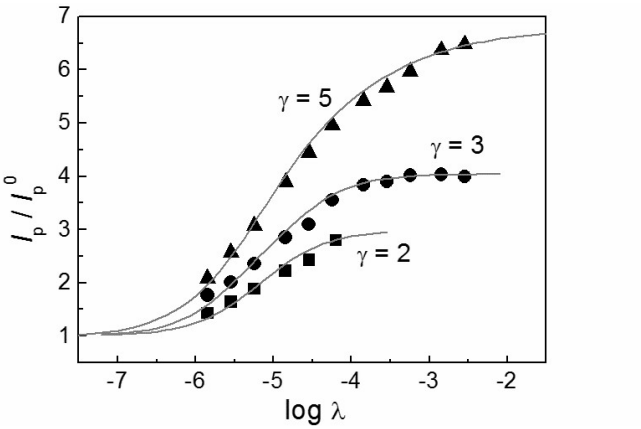

Figure 3.4. Fitting of the experimental values of I_p/I_p^0 (black dots) on the theoretical curves (red lines), for the system $[Cu^{II}TPMA]^{2+}$/OEOBP in water at various $C_{RX} / C_{[Cu^{II}L]^{2+}}$ ratios.

Theoretical curves were built specifically for every $[Cu^{I}L]^{+}$/RX system at fixed initiator to catalyst ratios (γ), each γ value providing a single working curve relating the degree of catalysis to a kinetic parameter λ. An example for the system $[Cu^{II}TPMA]^{2+}$/OEOBP is presented in Figure 3.4, where experimental data obtained at different γ values are compared with the corresponding theoretical curves to determine k_{act}.

The above described method, based on the occurrence of a homogeneous redox catalysis in the presence of electrogenerated $[Cu^{I}L]^{+}$, is applicable to a wide range of systems, including moderately fast to very fast reactions. Moreover, only one parameter, I_{pc}, is utilized from the CV. This technique is not very demanding in terms of quality of the

voltammetric response: systems characterized by noisy or not perfectly reversible CV give reproducible results, with k_{act} values in good agreement with values determined by other techniques (within the experimental error, see later). On the other hand, this method is quite time-demanding as precise determination of k_{act} requires the independent determination or estimation of a large number of thermodynamic and kinetic parameters necessary for the digital simulation of cyclic voltammetry. The presence of a scavenger, such as TEMPO, is not necessary for very fast kinetics, where radical-radical termination is sufficient to obtain an irreversible activation reaction.

3.1.3 CV under total catalysis

In cyclic voltammetry, systems with homogenous catalysis sometimes exhibit unusual voltammetric pattern with splitting of the cathodic peak of the catalyst into two peaks. This occurs under particular conditions of extremely fast reaction between catalyst and substrate, combined with low substrate to catalyst ratio (low γ) and low to moderate υ, and is known as "total catalysis".[23] An example of a catalytic system with this peculiar behavior is $[Cu^{II}TPMA]^{2+}$/HEBiB and its voltammetric pattern is shown in Figure 3.5. Peak splitting occurs because the reaction is very fast and since $C_{RBr} < C_{[Cu^{II}L]^{2+}}$, only a small fraction of the catalyst suffices for the complete catalytic reduction of RBr, giving a first irreversible peak at $E > E^{e}_{[Cu^{II}L]^{2+}/[Cu^{I}L]^{+}}$ due to the extremely fast catalytic reduction of HEBiB. Since only a small fraction of the copper complex is involved in the catalytic process at the pre-peak, the remaining $[Cu^{II}L]^{2+}$ gives its reversible peak couple at its usual redox potential. Note that no radical scavenger was added to the system. The overall catalytic reduction of RX by Cu^{I} is made irreversible by radical-radical coupling (eq. 3.11), which is very fast because all RX is converted to $R^{\bullet}$ in a thin reaction layer adjacent to the electrode.

When a catalytic process is so efficient as to present a peak splitting, the position of the pre-peak can be used to determine the rate constant of the chemical reaction, according to the following equation relating the potential of the pre-peak, E_p, to a kinetic parameter:[25]

$$E_p = E^{e}_{[Cu^{II}L]^{2+}/[Cu^{I}L]^{+}} - 0.409\frac{RT}{F} + \frac{RT}{2F}\ln\left(\frac{RTk_{act}C^{2}_{[Cu^{II}L]^{2+}}}{C_{RBr}\upsilon}\right) \qquad (3.16)$$

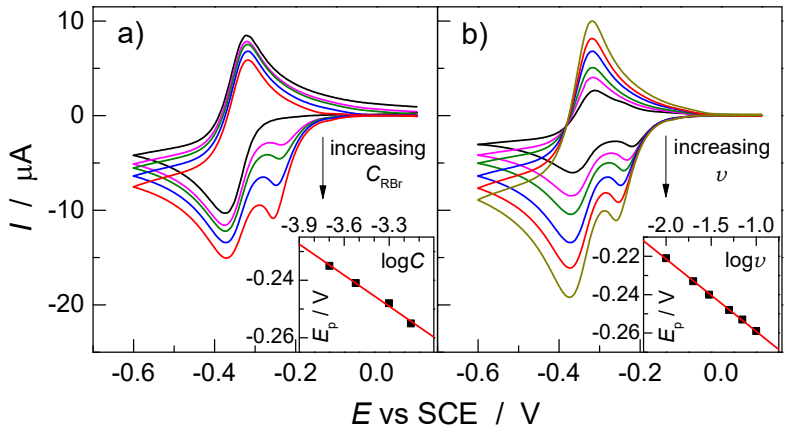

Figure 3.5. Cyclic voltammetry of 10^{-3} M $[Cu^{II}TPMA]^{2+}$ recorded in H_2O + 0.1 M Et_4NBF_4 at: (a) 0.05 V s^{-1} in the absence and presence of HEBiB with C_{HEBiB} from 2×10^{-4} to 7×10^{-4} M; (b) different scan rates from 0.01 V s^{-1} to 0.1 V s^{-1} in the presence of 5×10^{-4} M HEBiB. Insets: variation of pre-peak potential, E_p, with logC_{HEBiB} or logυ.

This equation allows to determine k_{act} directly by cyclic voltammetry using E_p values measured at different initiator concentrations, C_{RBr}, and/or different scan rates. The effects of C_{RBr} and υ on the voltammetric response of $[Cu^{II}TPMA]^{2+}$ in the presence of HEBiB are illustrated in Figure 3.5. An increase of either C_{RBr} or υ results in an increase of the pre-peak, which also shifts to more negative potentials. As long as the total catalysis conditions are maintained, a plot of E_p vs log C_{RBr} or log υ should give a straight line with a slope of -30 mV $decade^{-1}$. Straight lines with slopes -34 to -37 mV $decade^{-1}$, which are only slightly more negative than the theoretical values predicted for a reversible electron transfer involved in a fast catalytic system, were found for the $[Cu^{II}L]^{2+}$/HEBiB system. Considering that the experimental $\partial E_p/\partial \log C_{RBr}$ and $\partial E_p/\partial \log \upsilon$ slopes reasonably agree with the theoretical values, we used equation 3.16 to calculate k_{act}, working at conditions that keep the system under the kinetic regime of total catalysis, that is, very low scan rates and low $C_{RBr} / C_{[Cu^{II}L]^{2+}}$. This yielded $k_{act} = 5.4\times10^6$ M^{-1} s^{-1}.

This voltammetric method is easy and fast to apply, but is quite stringent in that it demands quite clear and stable voltammetric responses of the complex. In addition, the aqueous system should be under the kinetic regime of total catalysis, which is the case only for $k_{act} > 10^6$ and slow scan rates. On the other hand, this procedure can be straightforwardly applied to measure extremely high k_{act} values, up to the diffusion controlled limit (~10^8–10^9 M^{-1} s^{-1}).

3.1.4 Cyclic voltammetry with digital simulation

Equation 3.16 is valid for a catalytic system involving a fast or nernstian electron transfer, followed by an irreversible chemical reaction. Strictly speaking neither of these conditions apparently holds for the system discussed above, which involves a quasi-reversible electron transfer (k^0 = 0.018 cm s^{-1}) and a reversible activation reaction (K_{ATRP} = 0.18).[22b] Therefore, we decided to confirm the results by analyzing the whole voltammetric response of the catalytic system $[Cu^{II}TPMA]^{2+}$/HEBiB through digital simulation. Comparing experimental CVs with voltammograms obtained by digital simulation is a more rigorous method that allows to extract the kinetic parameter of interest (k_{act}) without assumptions on electron transfer kinetics and irreversibility of the activation step. The reaction mechanism was set in agreement with equations 3.5-3.11 and CV was simulated using the previously defined thermodynamic and kinetic parameters. A comparison of some simulated cyclic voltammograms with experimental CVs is shown in Figure 3.6.

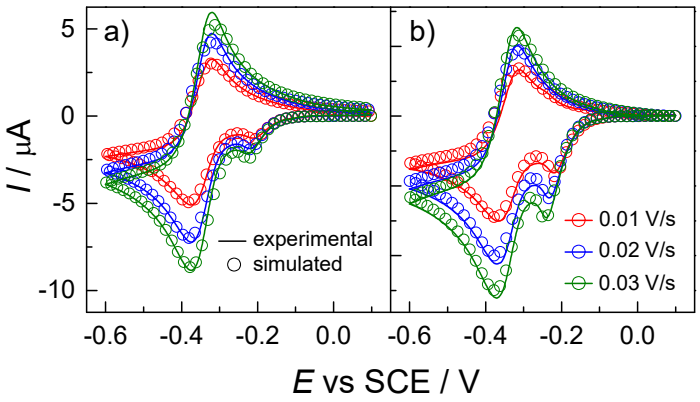

Figure 3.6. Comparison between experimental (lines) and simulated (circles) CVs of 10^{-3} M $[Cu^{II}TPMA]^{2+}$ in H_2O + 0.1 M Et_4NBF_4 in the presence of HEBiB (a) 2×10^{-4} M or (b) 5×10^{-4} M.

The best agreement between simulation and experiment for the system $[Cu^{II}TPMA]^{2+}$/HEBiB in water was obtained using the value 5.4×10^6 M^{-1} s^{-1}, previously determined from the potential of the pre-peak under total catalysis conditions. This is a very interesting result showing that kinetic data can be easily obtained from voltammetric peak potential measurements even for ATRP systems, which, unlike many irreversible chemical reactions triggered by electron transfer, are characterized by a reversible activation step. In this case, the overall sequence of reactions following electrochemical reduction of Cu^{II} to Cu^{I} behaves as an irreversible chemical reaction by virtue of the fast ATRP activation step and the successive diffusion-controlled radical-radical coupling step (eq.

3.11). Simulation of the CV to measure k_{act} was also applied to the reaction between OE-OBP and $[Cu^{I}TPMA]^{+}$ in water. Again a good agreement between simulated and experimental CVs allowed to determine $k_{act} = 1.3\times10^{5}$ $M^{-1}s^{-1}$.

3.2 Activation rate constants, structure-reactivity correlations and effect of monomer in water

The series of methods described in the previous sections allowed the determination of a vast range of k_{act} values in water and water/monomer mixtures. In particular, extremely high k_{act} values that are hardly accessible via other techniques were determined. The whole set of data are reported in Table 3.2. To check the reliability of the different methods, most of the systems were investigated with two different techniques, which in each case gave the same k_{act} value within experimental error.

Table 3.2. Activation rate constants, k_{act}, measured at 25 °C in aqueous solutions containing 0.1 M Et_4NBF_4 as supporting electrolyte.

Entry	L	RBr	Solvent	k_{act} (M^{-1} s^{-1})	Method[a]
1	Me_6TREN	HEBiB	water	$(2.6\pm0.5)\times10^{7}$	total catalysis
2	Me_6TREN	HEBiB	water	$(2.6\pm0.7)\times10^{7}$ [b]	HRC
3	TPMA	HEBiB	water	$(5.4\pm1.5)\times10^{6}$	total catalysis
4	TPMA	HEBiB	water	$(5.4\pm1.5)\times10^{6}$	CV simulation
5	PMDETA	HEBiB	water	$(3.2\pm0.8)\times10^{5}$	HRC
6	Me_6TREN	OEOBP	water	$(3.2\pm0.6)\times10^{5}$ [b]	HRC
7	TPMA	OEOBP	water	$(1.2\pm0.2)\times10^{5}$	HRC
8	TPMA	OEOBP	water	$(1.3\pm0.3)\times10^{5}$	CV simulation
9	Me_6TREN	NiPBPA	water	$(2.9\pm0.6)\times10^{5}$	HRC
10	TPMA	NiPBPA	water	$(1.2\pm0.1)\times10^{4}$	HRC
11	Me_6TREN	HEBiB	water/OEOA (82:18)	$(2.9\pm0.6)\times10^{6}$ [b]	HRC
12	Me_6TREN	OEOBP	water/OEOA (82:18)	$(2.5\pm0.6)\times10^{4}$ [b]	HRC
13	TPMA	OEOBP	water/OEOA (82:18)	$(1.2\pm0.2)\times10^{3}$	HRC
14	TPMA	OEOBP	water/OEOA (82:18)	$(1.3\pm0.1)\times10^{3}$	RDE
15	Me_6TREN	NiPBPA	water/NiPAM (82:18)	$(7.7\pm0.5)\times10^{2}$	HRC
16	TPMA	NiPBPA	water/NiPAM (82:18)	10.1±2.3	HRC
17	TPMA	NiPBPA	water/NiPAM (82:18)	9.3±0.9	RDE

[a]HRC: comparison of experimental data with a theoretical working curve in conditions of homogeneous redox catalysis; RDE: kinetics followed by monitoring the decay of Cu^{I} on a rotating disk electrode. [b]From reference 10.

The order of reactivity (k_{act}) of the catalyst is $[Cu^{I}Me_6TREN]^+$ > $[Cu^{I}TPMA]^+$ > $[Cu^{I}PMDETA]^+$, which matches the order of ATRP equilibrium constant, K_{ATRP}. The activation rate constant is also affected by the structure of RX, which shows the following order of reactivity: tertiary ester > secondary ester > secondary amide. Both these trends have already been observed for the activation of ATRP initiators by copper-amine complexes.[26] Interestingly, in water activity of the catalyst does not follow the trend of $E^{o}_{[Cu^{II}L]^{2+}/[Cu^{I}L]^+}$. This result has two important implications: (*i*) it is not possible to directly correlate the catalyst activity to its reduction potential, instead K_{ATRP} should be used; (*ii*) k_{act} is largely influenced by the molecular structure of Cu complex and initiator, while the redox potential of the catalyst appears to play a subordinate role. This is a clear demonstration that the activation-driving force relationship of the process differs from that of an outer-sphere electron transfer; it is considerably affected by inner-sphere, specific interactions between RX and Cu^{I}.

The investigation of ATRP catalytic systems was carried out also in the presence of the monomer, which is always present in considerable quantities in typical ATRP reaction media, thus extending the kinetic analysis to an environment that matches the polymerization conditions as closely as possible. The vastly used oligo(ethyleneoxide) acrylate (OEOA) and N-isopropylacrylamide (NiPAM) were investigated. The effect of the presence of a monomer is a general suppression of catalytic activity from both kinetic and thermodynamic points of view. Table 3.2 shows that $[Cu^{I}TPMA]^+$ and $[Cu^{I}Me_6TREN]^+$ activation rates are reduced by a factor of at least 10^2 and 10, respectively. This is in agreement with data reported in Table 3.1, which shows that $[Cu^{I}L]^+$ becomes a weaker (less active) reducing agent in water/monomer mixtures. On the other hand, the reduction potential of RBr becomes more negative in passing from pure water to water/monomer mixtures (Table 1). Therefore, the presence of a monomer in the reaction medium makes reduction of RBr by Cu^{I} or by any other means less favorable than in water. The huge effect of monomer in $[Cu^{I}L]^+$ activity may be explained by invoking significant interactions between monomer and copper.[27] The incomplete reversibility observed in the voltammetric response of $[Cu^{II}L]^{2+}$ in the presence of monomer supports this assumption.

The measured k_{act} values can be used together with K_{ATRP} to calculate the deactivation rate constant, $k_{deact} = k_{act}/ K_{ATRP}$. K_{ATRP} data are available for the reaction of HEBiB and OEOBP with $[Cu^{I}L]^+$ only in pure water and the calculated values of k_{deact} are reported in Table 3.3. K_{ATRP} and k_{act} values, recently reported by Smolne and Buback,[28] for the acti-

Table 3.3. ATRP equilibrium constants (K_{ATRP}), activation rate constant (k_{act}) and deactivation rate constant (k_{deact}).

Entry	Catalyst	Initiator	K_{ATRP}	k_{act} (M^{-1} s^{-1})	k_{deact} (M^{-1} s^{-1})
1	$[Cu^{I}Me_6TREN]^+$	HEBiB	8.0×10^{-1}	2.6×10^{7}	3.2×10^{7}
2	$[Cu^{I}TPMA]^+$	HEBiB	1.8×10^{-1}	5.4×10^{6}	2.9×10^{7}
3	$[Cu^{I}PMDETA]^+$	HEBiB	4.6×10^{-2}	3.2×10^{5}	7.0×10^{6}
4[a]	$[Cu^{I}(bpy)_2]^+$	HEBiB	2.5×10^{-5}	6.6×10^{1}	2.6×10^{6}
5	$[Cu^{I}Me_6TREN]^+$	OEOBP	2.4×10^{-2}	3.2×10^{5}	1.3×10^{7}
6	$[Cu^{I}TPMA]^+$	OEOBP	5.5×10^{-3}	1.2×10^{5}	2.2×10^{7}

[a]From ref. 28.

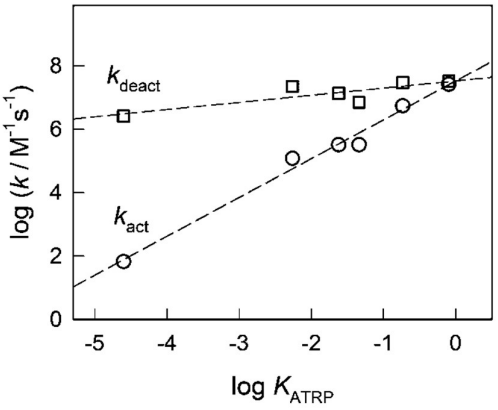

Figure 3.7. Correlation of k_{act} and k_{deact} with K_{ATRP} for various $[Cu^{I}L]^+$ catalysts with HEBiB and OEOBP in water at 25°C.

vation of HEBiB by $[Cu^{I}(bpy)_2]^+$ in water are also reported in the table (entry 4). It is interesting to note that while both K_{ATRP} and k_{act} vary by about 5 orders of magnitude, k_{deact} values are scattered in a very narrow range from 2.6×10^{6} to 3.2×10^{7}. This suggests that, unlike the activation reaction, deactivation is little affected by the chemical structure of RX and copper catalyst. This is better evidenced by Figure 3.7, which shows plots of log k_{act} and log k_{deact} as a function log K_{ATRP}. Both k_{act} and k_{deact} show good linear correlations with K_{ATRP}. However, while k_{act} shows a remarkable dependence on K_{ATRP}, k_{deact} only slightly increases with K_{ATRP}, A similar strong dependence of k_{act} on K_{ATRP} was observed in acetonitrile (ref. 1a and next section). On the other hand, in acetonitrile k_{deact} is less affected by, or only slightly decreases with, K_{ATRP}. The high deactivation efficiency observed in water, especially for the more active solvents, suggests that controlled polymerization is possible with low catalyst loading. On the other hand, the high k_{act} necessitates methods to slowly regenerate Cu^{I} species in order to keep Cu^{I}/Cu^{II} ratio as low as possible.

3.3 Structure-reactivity correlations in acetonitrile

The good correlations observed for k_{act} and k_{deact} in water with K_{ATRP} prompted us to analyze literature data on the activation of RX by Cu^I complexes in other solvents. A large set of rate constants of the reaction between $[Cu^IL]^+$ (L= PMDETA, TPMA and Me_6TREN) and an extended series of alkyl halides (Scheme 3.4), commonly used as initiators in ATRP, have recently been determined by electrochemical techniques in CH_3CN.[29] These values together with deactivation rate constants, calculated as $k_{deact} = k_{act}/K_{ATRP}$ using previously reported K_{ATRP} values,[26] are summarized in Table 3.4.

Scheme 3.4. Molecular structures of ATRP initiators investigated in CH_3CN.

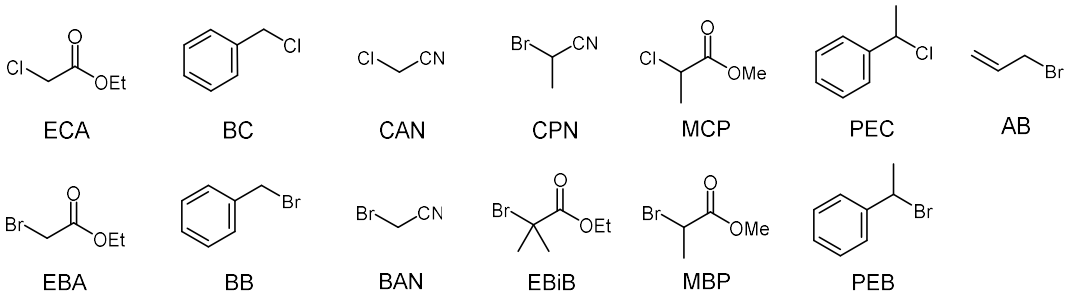

Table 3.4. Activation and deactivation rate constants of the reaction between alkyl halides and Cu^I complexes in CH_3CN + 0.1 M Et_4NBF_4 at 25 °C.

RX	L = Me_6TREN		L = TPMA		L = PMDETA	
	k_{act} (M^{-1} s^{-1})	k_{deact} (M^{-1} s^{-1})[a]	k_{act} (M^{-1} s^{-1})	k_{deact} (M^{-1} s^{-1})[a]	k_{act} (M^{-1} s^{-1})	k_{deact} (M^{-1} s^{-1})[a]
MCP	1.7×10^{1}	5.6×10^{5}	1.4	3.4×10^{7}	6.8×10^{-2}	2.1×10^{8}
BC	1.9	1.4×10^{5}	7.8×10^{-1}	1.7×10^{6}	7.3×10^{-3}	2.1×10^{6}
PEC	7.7		3.5	4.0×10^{6}	1.0×10^{-2}	1.5×10^{6}
ECA	0.47	8.5×10^{6}	5.5×10^{-2}	1.3×10^{5}	4.3×10^{-4}	1.3×10^{5}
CAN	2.3×10^{2}	5.1×10^{5}	3.8×10^{1}	1.2×10^{6}	4.0×10^{-2}	1.7×10^{5}
CPN	8.1×10^{2}		1.1×10^{2}	4.9×10^{6}	9.0×10^{-2}	5.3×10^{5}
MBP	2.1×10^{3}	7.2×10^{8}	2.2×10^{2}	6.9×10^{8}	1.7×10^{-1}	4.3×10^{7}
BB	4.1×10^{2}	4.9×10^{8}	1.6×10^{2}	2.4×10^{8}	3.4×10^{-2}	6.4×10^{6}
PEB	1.9×10^{3}	7.3×10^{6}	7.7×10^{2}	1.7×10^{8}	1.4×10^{-1}	4.2×10^{6}
EBA	2.2×10^{1}	1.0×10^{6}	2.0	6.3×10^{6}	3.2×10^{-3}	1.3×10^{6}
BAN	2.1×10^{4}	2.4×10^{7}	2.7×10^{3}	4.8×10^{7}	3.4	3.9×10^{5}
EBiB	1.2×10^{4}	8.0×10^{7}	4.5×10^{3}	4.7×10^{8}	2.0	2.7×10^{7}
AB	3.3×10^{2}	1.2×10^{6}	1.2×10^{2}	7.1×10^{6}	3.7×10^{-2}	2.9×10^{5}

[a]Determined as k_{act}/K_{ATRP}. K_{ATRP} values at T = 22°C from reference 4a.

The standard reduction potentials of $[Cu^{II}L]^{2+}$ complexes are -0.120, -0.015 and 0.063 V vs SCE for L = Me_6TREN, TPMA and PMDETA, respectively.[30] The reactivity of the Cu^I complexes for a given RX roughly follows their reducing power. For example, $[Cu^IPMDETA]^+$ is ca. 180 mV less reducing than $[Cu^IMe_6TREN]^+$ and this is reflected in its reactivity, which is some orders of magnitude lower than that of $[Cu^IMe_6TREN]^+$. The difference of reactivity between the complexes strongly depends on the structure of RX and on the type of halogen atom. The rate constants measured with $[Cu^IMe_6TREN]^+$ and $[Cu^ITPMA]^+$ were normalized with respect to k_{act} values obtained with $[Cu^IPMDETA]^+$ and this ratio, denoted as $k_{act}/k_{act,CuPMDETA}$, is reported in Figure 3.8. In the chloride series, $k_{act}/k_{act,CuPMDETA}$ varies from 2.5×10^2 to 9.0×10^3 for $[Cu^IMe_6TREN]^+$ and 2.1×10^1 to 1.2×10^3 for $[Cu^ITPMA]^+$. A similar trend is observed for the bromide series. Again both $[Cu^IMe_6TREN]^+$ and $[Cu^ITPMA]^+$ are much more reactive than $[Cu^IPMDETA]^+$.

It is important to note that while the observed reactivity trend $[Cu^IPMDETA]^+ << [Cu^ITPMA]^+ < [Cu^IMe_6TREN]^+$ does not disagree with the $E^\ominus$ of the complexes, which decreases in the order $[Cu^IPMDETA]^+ > [Cu^ITPMA]^+ > [Cu^IMe_6TREN]^+$, the two trends do not perfectly match. Comparing $[Cu^ITPMA]^+$ and $[Cu^IPMDETA]^+$, a difference of 78 mV in their standard potentials produces k_{act} enhancement of *ca.* 10^1–10^3 for chlorides and *ca.* 6×10^2–3×10^3 for bromides. In contrast, a comparison between $[Cu^ITPMA]^+$ and $[Cu^IMe_6TREN]^+$ shows that although the difference between their standard potentials (105 mV) is significantly higher than that between $[Cu^IPMDETA]^+$ and $[Cu^ITPMA]^+$, k_{act}

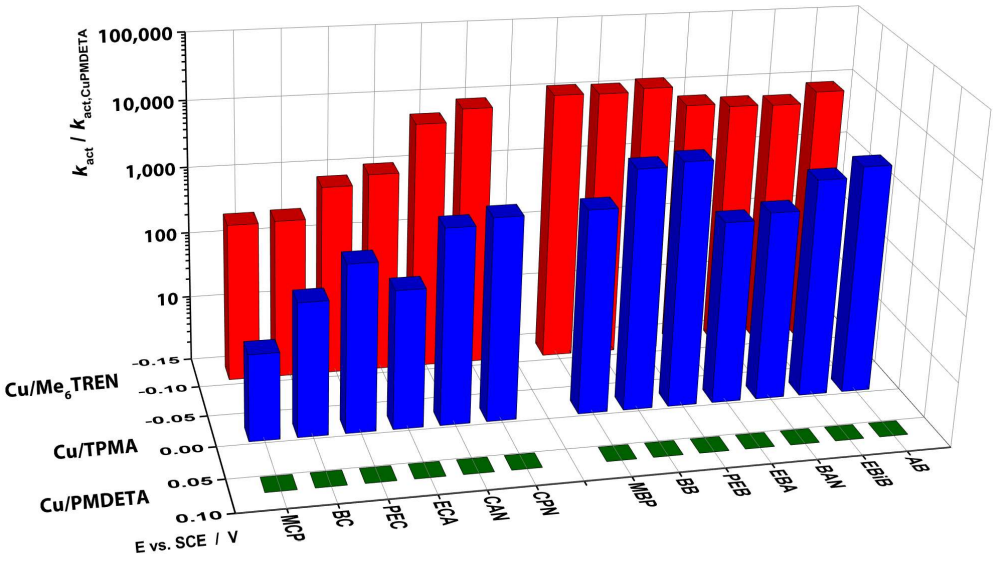

Figure 3.8. Comparison between rate constants of RX activation by different Cu^I complexes in CH_3CN + 0.1 M Et_4NBF_4 at 25 °C.

increases less than 10 times for both alkyl halide series when passing from $[Cu^{I}TPMA]^{+}$ to $[Cu^{I}Me_6TREN]^{+}$. Similarly to what was observed for copper complexes in water, the strong dependence of k_{act} ratio on both molecular structure, Cu complex and halogen atom is a clear demonstration that the activation-driving force relationship of the process is not compatible with outer-sphere electron transfer, as it is considerably affected by specific interactions between RX and Cu^{I}.

Other interesting observations come from the analysis of the reactivity order of RX for any given catalyst. As expected, alkyl chlorides are always less reactive than the corresponding bromides, k_{act} of RCl being more than 10 times smaller than that of RBr. As previously reported,[31] k_{act} values for tertiary, secondary, and primary ester initiators follow the order 3° > 2° > 1° (e.g. EBiB > MBP > EBA). Furthermore, within a fixed set of tertiary, secondary and primary chlorides or bromides, the order of reactivity follows the ability of the substituent to stabilize the radical. Thus, the general order is -CN > -Ph > -COOR (e.g. CAN > BC > ECA and BAN > BB > EBA).

In a well-controlled ATRP the overall propagation rate depends on K_{ATRP} (eq. 3.1). On the other hand, the control on ATRP, in terms of molecular weight distribution (M_w/M_n), is strongly dependent on the deactivation constant (k_{deact}). In the ideal case of fast activation and no termination M_w/M_n is expressed as:[32]

$$\frac{M_w}{M_n} = 1 + \frac{1}{DP} + \frac{k_p C_{P_nX}}{k_{deact} C_{[XCu^{II}L]^+}} \left(\frac{2}{p} - 1 \right) \tag{3.17}$$

where DP is the average degree of polymerization, C_{P_nX} is the concentration of dormant species, k_p is the rate constant of propagation and p is monomer conversion. Therefore, a good control in ATRP requires very fast deactivation of radicals, which means k_{deact} should be as high as possible. Figure 3.9 shows correlations of k_{act} and k_{deact} with K_{ATRP}. Both k_{act} and K_{ATRP} depend on the structure of RX and amine ligand and particularly on the nature of the halogen atom. Two separate plots were therefore constructed for the chloride and bromide series. As shown for each series, log k_{act} increases with log K_{ATRP} and the whole set of data obtained on different complexes can be roughly fit to a straight line. In contrast, k_{deact} is very high for all investigated systems, as required by ATRP, and is little affected by the molecular structure of RX or amine ligand. Although k_{deact} of the chloride series shows a slight tendency to decrease with increasing K_{ATRP}, on average k_{deact} of each series can be fairly considered to be constant with log k_{deact} = 6.2±0.9 for

RCl and log k_{deact} = 7.3±1.1 for RBr. It is important to stress that each set of data covers a wide range of k_{act} (4.3×10^{-4}–8.1×10^{2} $M^{-1}s^{-1}$ for RCl and 3.2×10^{-3}–2.1×10^{4} $M^{-1}s^{-1}$ for RBr) and K_{ATRP} (*ca.* 6 orders of magnitude) values, which makes particularly significant the observed trends.

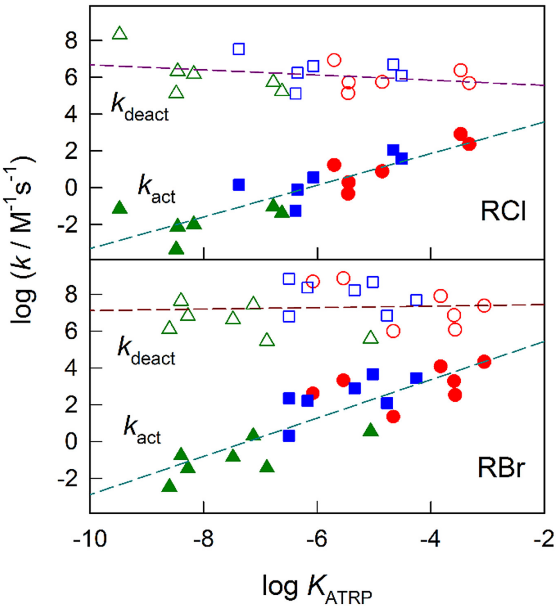

Figure 3.9. Correlation of k_{act} and k_{deact} with K_{ATRP} for the reaction of various alkyl chlorides (RCl) and bromides (RBr) with $[Cu^{I}L]^{+}$ complexes in CH_3CN: L = Me_6TREN (circles), TPMA (squares) and PMDETA (triangles). K_{ATRP} values were taken from ref. 4a. The broken lines were drawn to show the trends.

Scheme 3.5. Splitting the activation equilibrium into separate reactions.

$$[Cu^{I}L]^{+} \rightleftharpoons [Cu^{II}L]^{2+} + e^{-} \quad (3.18)$$

$$RX \rightleftharpoons R^{\bullet} + X^{\bullet} \quad (3.19)$$

$$X^{\bullet} + e^{-} \rightleftharpoons X^{-} \quad (3.20)$$

$$X^{-} + [Cu^{II}L]^{+} \rightleftharpoons [X\text{-}Cu^{II}L]^{+} \quad (3.21)$$

$$[Cu^{I}L]^{+} + RX \rightleftharpoons [X\text{-}Cu^{II}L]^{+} + R^{\bullet} \quad (3.6)$$

The log k_{act} vs log K_{ATRP} plots shown inFigure 3.9 represent an important result enabling the estimation of k_{act} from experimental K_{ATRP} and vice versa. Since the mechanism of ATRP activation involves the transfer of a halogen atom from RX to a Cu^{I} complex, it is likely that the reaction kinetics are related to the bond energy. Indeed, the overall activation reaction (eq. 3.6) can be split into four steps as shown in Scheme 3.5. The sum of

the free energies of reactions 3.18-3.21 corresponds to the Gibbs free energy of reaction 3.6, $\Delta_r G^e$. If one considers a particular copper complex and a series of chlorides or bromides, reactions 3.18, 3.20 and 3.21 will be the same for the whole series with a fixed contribution to $\Delta_r G^e$. Therefore, k_{act} is expected to correlate with the bond dissociation free energy, BDFE, of RX. Experimental data on BDFE of alkyl halides used as initiators of ATRP are not available. However, reliable BDFE values can be obtained by computational methods and indeed, data for a large set of initiators have recently been reported in CH_3CN.[33] Fairly linear correlations were found for all three investigated complexes (Figure 3.10). In each data set, k_{act} decreases with increasing BDFE. Activation of allyl bromide is a clear exception to this trend: with all three Cu complexes k_{act} for this halide is *ca.* 2 orders of magnitude lower than the value predicted on the basis of the correlations. The lowered reactivity of Cu^I with allyl bromide might be due to stabilization of the metal by complexation with the initiator thorough π-interaction of the C=C double bond. It has been shown that olefins can form complexes with $[Cu^IPMDETA]^+$.[27]

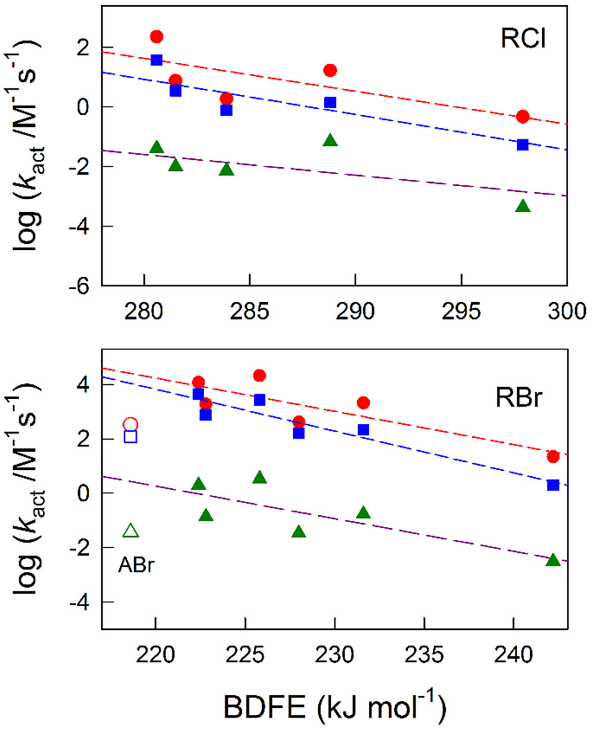

Figure 3.10. Correlation of k_{act} with bond dissociation free energy of RX for the reaction of various alkyl chlorides (RCl) and bromides (RBr) with $[Cu^IL]^+$ complexes in CH_3CN: L = Me_6TREN (circles), TPMA (squares) and PMDETA (triangles). BDFE values were taken from ref. 33.

3.4 Activation rate constants and structure-reactivity correlations in an ionic liquid

Ionic liquids are gaining great importance as green solvents for many polymerization processes. These materials are salts with melting point below 100°C, low toxicity and good conductivity. They are non-volatile, generally non-flammable, and easily recyclable.[34] Room temperature ionic liquids, RTILs, are liquid at ambient temperature. Despite being quite viscous solvents, conductivity of RTILs is high enough to avoid the need of a supporting electrolyte in an electrochemical cell. A great advantage of RTILs is their wide electrochemical stability window (from 4,5 to 7 V).[35] Indeed, the electrochemical stability of traditional solvents is often limited by the presence of supporting electrolyte. Purity of ionic liquids is often an issue. For this purpose, a careful purification procedure was developed, as described in Appendix A.

RTILs, especially based on the 1-butyl-3-methylimidazolium cation, have been extensively used in ATRP.[36] Despite the presence of a large number of reports in the literature, properties and reactivity of the ATRP catalytic system in an ionic liquid have never been studied. Such information is fundamental to compare RTILs to water and traditional organic solvents.

3.4.1 Electrochemical characterization of the catalytic system

Addition of an equimolar amount of ligand and $Cu^{II}(OTf)_2$ in 1-butyl-3-methylimidazolium triflate ([BMIm][OTf]) generates the binary complex $[Cu^{II}L]^+$ (L = Me_6TREN, TPMA, or PMDETA). Cyclic voltammetry in Figure 3.11a shows the reversible signal of the $[Cu^{II}L]^{2+}/[Cu^{I}L]^+$ redox couple and a less intense irreversible peak at a more negative potential. This is a different behavior with respect to what is typically observed in both water and traditional organic solvents, where only one reversible peak couple is observed (Figure 3.2). The irreversible peak was assigned to the irreversible reduction of a Cu^{II} complex with different stoichiometry, indicated as $[Cu^{II}L_n]^{2+}$, with n > 1. As expected, intensity of the peak associated with $[Cu^{II}L_n]^{2+}$ increased with increasing C_L (Figure 3.11b). In the reverse scan, oxidation of $[Cu^{I}L]^+$ was predominant, regardless of the $C_L/C_{Cu^{II}(OTf)_2}$ ratio.

Cu^{II} generally has 5 coordination sites, whereas Cu^{I} has only 4 coordination sites, which are completely saturated by tetradentate amine ligands such as Me_6TREN and TPMA. Therefore, only Cu^{II} may accommodate more than one ligand molecule in its coordination sphere. The higher affinity of Cu^{II} for L with respect to Cu^{I} was already reported.[37]

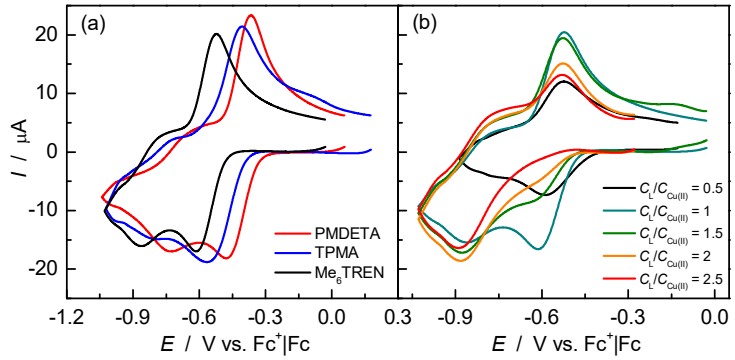

Figure 3.11. Cyclic voltammetry of Cu^{II} complexes in [BMIm][OTf], recorded on a glassy carbon electrode at $\upsilon = 0.2$ Vs^{-1} and $T = 50$ °C: (a) 10^{-2} M $Cu^{II}(OTf)_2$ + 10^{-2} M L; (b) 10^{-2} M $Cu^{II}(OTf)_2$ + Me_6TREN with $C_{Me_6TREN}/C_{Cu^{II}(OTf)_2}$ = 0.5 – 2.5.

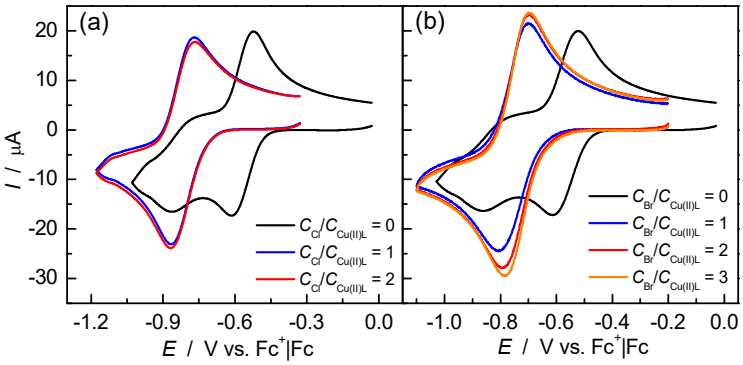

Figure 3.12. CVs of $Cu^{II}(OTf)_2$/Me_6TREN = 1/1, C_{Cu} = 10 mM, registered on GC disk in [BMIm][OTf], T = 50 °C, with the addiction of different concentrations of (a) Et_4NCl and (b) Et_4NBr.

Ternary Cu^{I} complexes, $[X\text{-}Cu^{II}L]^+$, were formed in situ by mixing $Cu^{II}(OTf)_2$, a ligand, and Et_4NCl or Et_4NBr. When equimolar amounts of $Cu^{II}(OTf)_2$, L and X^- were mixed, a reversible peak couple was observed at potentials more negative than E^e of the $[Cu^{II}L]^{2+}/[Cu^{I}L]^+$ redox couple (Figure 3.12). This signal was associated to the well-defined $1e^-$ reduction of $[X\text{-}Cu^{II}L]^+$. In this case, the coordination sites of Cu^{II} were filled by the tetradentate amine and by the halide ion, preventing formation of species with different stoichiometry. Varying the $C_{X^-}/C_{Cu^{II}}$ ratio showed that an equimolar amount of Cl^- was necessary for the quantitative formation of $[Cl\text{-}Cu^{II}L]^+$ (the signal did not change with further Et_4NCl additions, Figure 3.12a). Conversely, a $C_{Br^-}/C_{Cu^{II}}$ ratio of 2 was necessary to obtain a stable $[Br\text{-}Cu^{II}L]^+$ signal (Figure 3.12b). The presence of a well-defined $[X\text{-}Cu^{II}L]^+$ species allowed studying the kinetics of RX activation, as explained in the next section.

3.4.2 Determination of activation rate constants in [BMIm][OTf]

In the presence of $[X\text{-}Cu^{II}L]^+$ and RX, homogenous redox catalysis was observed, as evidenced from the catalytic current in Figure 3.13. k_{act} determination was carried out using the ratio between the reduction current in the presence and absence of RX (I_p/I_p^0), as explained in Section 3.1.2. Experimental I_p/I_p^0 values were compared to theoretical working curves obtained through simulation of the cyclic voltammetry response. Construction of reliable working curves requires knowledge of several chemico-physical parameters of the system. Relevant parameters regarding the binary $[Cu^{II}L]^+$ and ternary $[X\text{-}Cu^{II}L]^+$ complexes, determined as explained in the previous sections, are presented in Table 3.5. Moreover, both stability and formation rate constants of the $[X\text{-}Cu^{II}L]^+$ must be known. The values reported for $[Br\text{-}Cu^{II}Me_6TREN]^+$ in CH_3CN were used (K_X = 1000 and k_X = 10^4 M^{-1} s^{-1}). This approximation might introduce a non-negligible error in k_{act} determination.

Diffusion coefficients of alkyl bromides were calculated from cyclic voltammetry experiments according to eq. 3.15. This requires knowledge of the transfer coefficients, α, which was measured by cyclic voltammetry according to two different equations (the two results were averaged to obtain a more reliable value):

$$\frac{\partial E_p}{\partial \log \upsilon} = -1.15\frac{RT}{\alpha F} \tag{3.22}$$

$$\left|E_{p/2} - E_p\right| = \frac{\partial E_p}{\partial \log \upsilon} = 1.857\frac{RT}{\alpha F} \tag{3.23}$$

where E_p is the reduction peak potential and $E_{p/2}$ is the half-peak potential (*i.e.* the potential when reduction current is half of the peak value).

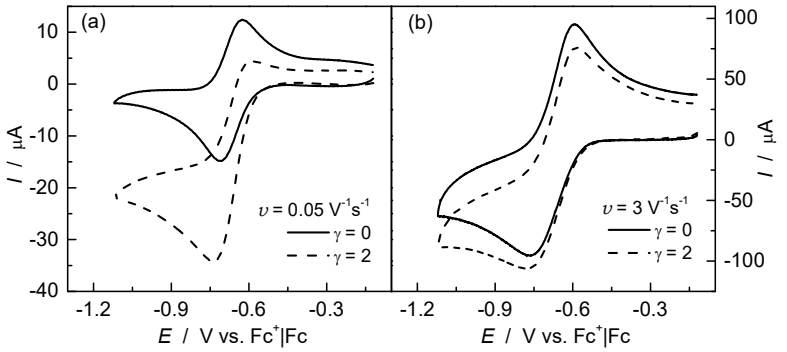

Figure 3.13. Cyclic voltammetry of 10 mM $[Br\text{-}Cu^{II}TPMA]^+$, in the absence (black lines) and presence (red lines) of MBrP, registered on GC disk, in [BMIm][OTf], T = 50 °C. $\gamma = C_{RX}/C_{Cu}$.

Table 3.5. Redox properties of copper binary and ternary complexes in [BMIm][OTf], T = 50 °C.

Entry	Complex	$D\times10^8$ ($cm^2\ s^{-1}$)	$k^0\times10^3$ ($cm\ s^{-1}$)	E^{eq} (V vs. Fc^+/Fc)
1	$[Cu^{II}Me_6TREN]^{2+}$	4.63	1.0	-0.57
2	$[Cl\text{-}Cu^{II}Me_6TREN]^{+}$	12.9	1.3	-0.82
3	$[Br\text{-}Cu^{II}Me_6TREN]^{+}$	10.2	0.88	-0.76
4	$[Cu^{II}TPMA]^{2+}$	4.5	0.44	-0.42
5	$[Cl\text{-}Cu^{II}TPMA]^{+}$	15.0	1.8	-0.71
6	$[Br\text{-}Cu^{II}TPMA]^{+}$	10.7	0.94	-0.66
7	$[Cu^{II}PMDETA]^{2+}$	5.8	0.18	-0.48
8	$[Cl\text{-}Cu^{II}PMDETA]^{+}$	10.9	1.1	-0.71
9	$[Br\text{-}Cu^{II}PMDETA]^{+}$	10.8	1.8	-0.66

Table 3.6. Redox and physical parameters of alkyl halides in [BMIm][OTf], T = 50 °C.

En-try	RX	E_p (V vs. Fc^+/Fc)[a]	r (nm)	$D\times10^8$ (cm^2s^{-1})	α[b]	α[c]	α_m[d]
1	EBA	-1.84	0.302	5.4	0.40	0.32	0.36
2	MBP	-1.81	0.353	7.0	0.41	0.31	0.36
3	EBiB	-1.79	0.378	4.7	0.38	0.30	0.34
4	BB	-1.94	0.361	4.9	0.26	0.32	0.29
5	PEB	-1.86	0.354	4.3	0.23	0.30	0.27
6	BAN	-1.66	0.388	12.1	0.27	0.32	0.30
7	CAN	-2.26	0.375	12.8 [e]	0.24	0.31	0.28
8	CPN	-2.30	0.293	8.9 [e]	0.23	0.32	0.28
9	PEC	-2.39	0.327	4.7 [e]	0.36	0.28	0.32
10	MCP	-2.38	0.356	6.2 [e]	0.27	0.29	0.28

[a] Measured whit υ = 0.2 Vs^{-1}. [b] Calculated according eq. 3.22. [c] Calculated according eq. 3.23. [d] Average α value. [e] Estimated on the basis of D vs $1/r$ correlation (eq. 3.24).

This procedure could not be applied to alkyl chlorides, because their reduction potential was too close to the reduction of [BMIm][OTf] and this prevented reliable determination of peak currents. Therefore, D was estimated on the basis of its linear dependence on the inverse molecular hydrodynamic radius, r^{-1}. First, the dependence of D on r was determined for the investigated set of alkyl bromides, which showed a fairly linear correlation of D with r^{-1} (Figure 3.14). The linear regression gave the following equation:

$$D(\mathrm{cm^2 s^{-1}}) = \frac{1.09\times10^{-6}}{r} - 2.46\times10^{-6} \tag{3.24}$$

where r in nm is the hard-sphere molecular radius obtained from the density (ρ) and molecular mass (M) of each alkyl halide , according to the equation:

$$r = \left(\frac{3M}{4\pi\rho N_A}\right)^{1/3} \tag{3.25}$$

Values of D measured for alkyl bromides as well as those estimated for the chloride series are summarized in Table 3.6. As expected, the diffusion coefficients of both copper complexes and alkyl halide initiators were more than one order of magnitude lower than the values determined in traditional organic solvents. This is due to the high viscosity of the ionic liquid. From a viewpoint of synthesis, a low D value may be convenient as it reduces the probability of undesired termination processes, which are essentially under diffusion control.

Figure 3.15 and 3.16 show the best fit of experimental I_p/I_p^0 data on working curves calculated for two different alkyl halides. Good fittings of the experimental data on appropriate working curves were found for all investigated systems and the measured k_{act} values are reported in Table 3.7. In addition, the dependence of the degree of catalysis on K_{ATRP} was investigated in [BMIm][OTf]. When K_{ATRP} was set below a certain limit, experimental I_p/I_p^0 values did not fit any theoretical working curves. On the other hand, K_{ATRP} did not affect the theoretical working curves if it was set > 10^{-5} (Figure 3.16). This allowed estimation of a lower limit for K_{ATRP}, which reported in Table 3.7 for each system.

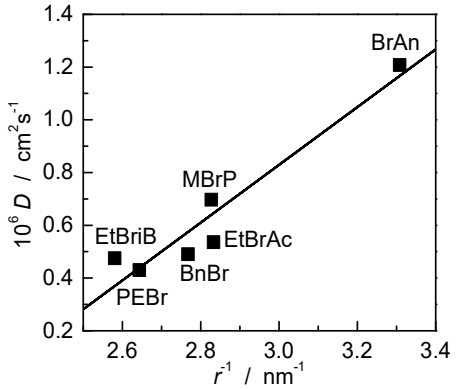

Figure 3.14. Correlation between diffusion coefficients and molecular radii of analyzed alkyl bromides, in [BMIm][OTf], T = 50 °C.

Table 3.7. Kinetic and thermodynamic parameters for the activation reactions of RX by Cu^{I}/TPMA in [BMIm][OTf], T = 50 °C.[a]

	RX	γ	K_{ATRP}	k_{act} ($M^{-1}s^{-1}$)	k_{deact} ($M^{-1}s^{-1}$)	k_{act} ($M^{-1}s^{-1}$)[b]	BDE (kJ mol^{-1})[c]
1	EBiB	1/2	$\geq 10^{-5}$	2.4×10^{4}	$\leq2.4\times10^{9}$	4.5×10^{3}	258.4
2	BAN	1/2	$\geq 10^{-5}$	7.5×10^{3}	$\leq7.5\times10^{8}$	2.7×10^{3}	246.3
3	PEB	1/2	$\geq 10^{-6}$	4.4×10^{3}	$\leq4.4\times10^{9}$	7.7×10^{2}	240.1
4	BB	1/2	$\geq 10^{-6}$	9.1×10^{2}	$\leq9.1\times10^{8}$	1.6×10^{2}	239.3
5	MBP	2/5	$\geq 10^{-6}$	7.1×10^{2}	$\leq7.1\times10^{8}$	2.2×10^{2}	262.9
6	EBA	20	-	6	-	2.0	267.6
7	CAN	1/2	$\geq 10^{-6}$	2.1×10^{3}	$\leq2.1\times10^{9}$	3.8×10^{1}	299.5
8	CPN	1/2	$\geq 10^{-5}$	6.0×10^{3}	$\leq6.0\times10^{8}$	1.1×10^{2}	301.9
9	PEC	5/20	$\geq 10^{-6}$	1.8×10^{2}	$\leq1.8\times10^{8}$	3.5	292.4
10	MCP	5/20	$\geq 10^{-6}$	1.2×10^{2}	$\leq1.2\times10^{8}$	1.4	316.7

[a] In the presence of a twofold amount of Et_4NX with respect to C_{Cu}. [b] From ref. 29, in CH_3CN, T = 25 °C. [c] Literature data.

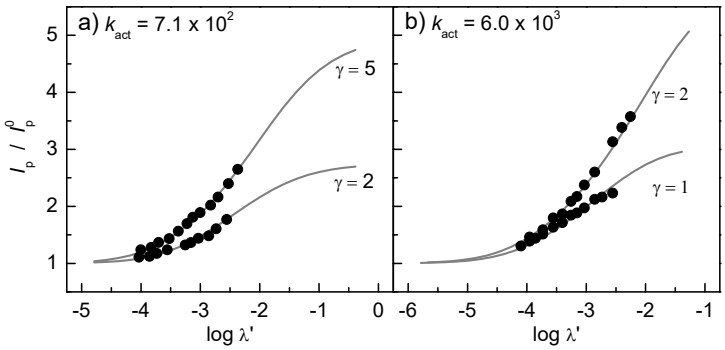

Figure 3.15. Fitting of experimental data on theoretical working curves for the determination of k_{act} of (a) MBrP and (b) ClPn by $[Cu^{I}TPMA]^{+}$ in [BMIm][OTf] at 50 °C. The experimental were data obtained through cyclic voltammetry on a GC disk for 10^{-2} M $CuBr_2$ + 10^{-2} M TPMA + RX with $\gamma = C_{RX}/C_{cat}$ = 1, 2 or 5. Working curves were calculated using $K_{ATRP} = 10^{-6}$ for MBrP and $K_{ATRP} = 10^{-5}$ for ClPn.

k_{act} values increased with decreasing bond dissociation energy, thanks to the easier C-X bond cleavage. Consequently, alkyl bromides are more active than chlorides. Moreover, for the same halogen, k_{act} increased by switching from primary to tertiary compounds. For comparison with data obtained in the ionic liquid, Table 3.7 also reports the activation rate constants determined in CH_3CN for the same RX. However, there are some significant experimental differences between the two systems. While k_{act} values in CH_3CN were

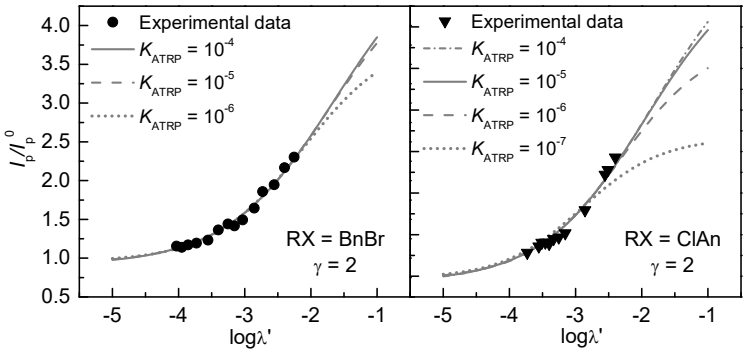

Figure 3.16. Experimental data fitted on theoretical working curves for CuX_2/TPMA/RX; experimental data obtained by cyclic voltammetry on a GC disk for 10^{-2} M $CuBr_2$ + 10^{-2} M TPMA + 2×10^{-2} M RX.

measured at 25 °C, all kinetic analysis in [BMIm][OTf] were carried out at50°C. In addition, the catalyst prepared in situ was $[Cu^{II}L]^{2+}$ in CH_3CN, whereas $[X\text{-}Cu^{II}L]^{+}$ was used in [BMIm][OTf]. It is known that halide anions are able to reduce the concentration of the active catalyst species $[Cu^{I}L]^{+}$, thus diminishing k_{act} by about 70% in CH_3CN.[12] Increasing the temperature, on the other hand, enhances the rate constant. These two opposite effects tend to cancel each other. Therefore, it can be concluded that ATRP catalytic systems in [BMIm][OTf] are around one order of magnitude more active than in CH_3CN.

3.5 Conclusions

Electrochemical techniques based on direct monitoring of Cu^{I} species (RDE) or on the generation of transient reactive species near the electrode, can be used to accurately determine ATRP rate constant in the range $10^{-4} < k_{act} < 10^{8}$ M^{-1} s^{-1}. Figure 3.17 displays the applied techniques together with their respective k_{act} range. In every case, adequate accuracy and reliability were observed. These methodologies greatly enhance the possibility to study and predict the behavior of the newly developed, most active ATRP systems.

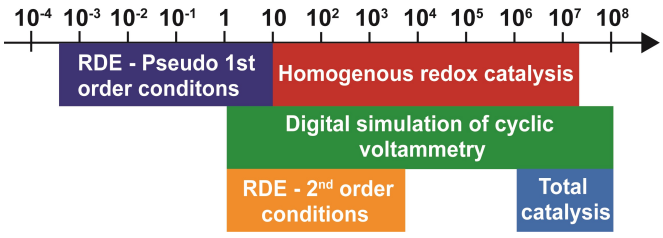

Figure 3.17. Summary of the electrochemical techniques used to determine activation rate constants.

Cyclic voltammetry under kinetic regime of "total catalysis" was applied for the first time to determine extremely high ATRP activation rate constants. Although this is a very simple method based on the easy measurement of a peak potential, care should be exercised in its application because the validity of the equation relating E_p with k_{act} is limited to the conditions of "total catalysis". Another powerful method exploits the so-called homogeneous redox catalysis involving generation of Cu^I at the electrode combined with RX activation in the homogeneous phase: the comparison of current enhancements in CV with theoretical working curves allows extraction of the kinetic constant k_{act}. This technique, however, is more demanding as it requires knowledge of kinetic and thermodynamic parameters pertaining to all reactions as well as some physical properties of reagents and products. k_{act} can also be obtained by digital simulation of the entire CV, which requires both perfectly reproducible CV responses and the complete chemico-physical characterization of the catalyst-initiator system.

The measured values of k_{act} for the aqueous $[Cu^IL]^+$/RX systems are several orders of magnitude greater than k_{act} values reported in acetonitrile.[26,29] The extremely high activity of Cu^I in water contributes to the very fast ATRP reactions and the difficulty of control in aqueous media. k_{act} steeply decreases upon addition of the monomer, reducing the reactivity difference observed between water and organic solvent.

Analysis of the data in both water and acetonitrile shows that k_{act} strongly depends on K_{ATRP}, whereas k_{deact} is roughly constant in CH_3CN and slightly increases with increasing K_{ATRP} in water. Additionally, k_{deact} is very high ($> 10^5$ $M^{-1}s^{-1}$) in both solvents, indicating that deactivation limitations observed in aqueous media are not due to low reactivity of Cu^{II} deactivator complexes but rather to their limited stabilities. In both solvents k_{act} gives satisfactory correlations with K_{ATRP}. This makes possible prediction of k_{act} provided that K_{ATRP} is known and vice versa. Estimation of k_{act} in CH_3CN is also possible with knowledge of bond dissociation free energy (BDFE) of RX, which can be reliably obtained by computational methods.

[BMIm][OTf] proved to be a suitable solvent for ATRP catalyzed with copper complexes. Cyclic voltammetry showed the signal of the active $[Cu^IL]^+$ binary complex. A stable $[X\text{-}Cu^{II}L]^+$ deactivator was formed by addition of a small amount of halide ions. Activity of the catalyst was found to be slightly higher than that in acetonitrile. Overall, ATRP catalytic systems in [BMIm][OTf] behaves similarly to common organic solvents.

References

(1) (a) Tang, W.; Kwak, Y.; Braunecker, W.; Tsarevsky, N. V; Coote, M. L.; Matyjaszewski, K. *J. Am. Chem. Soc.* **2008**, *130*, 10702–10713. (b) Braunecker, W. A.; Tsarevsky, N. V.; Gennaro, A.; Matyjaszewski, K. *Macromolecules*, **2009**, *42*, 6348–6360.

(2) A. Goto, T. Fukuda, *Macromol. Rapid Commun.* **1999**, 20, 633–636.

(3) Woodruff, S. R.; Davis, B. J.; Tsarevsky, N. V. *ACS Symp. Ser.* **2012**, *1100*, 99–113.

(4) (a) Chambard, G.; Klumperman, B.; German, A. L. *Macromolecules* **2000**, *33*, 4417–4421. (b) Matyjaszewski, K.; Göbelt, B.; Paik, H.; Horwitz, C. P. *Macromolecules* **2001**, *34*, 430–440. (c) Matyjaszewski, K.; Paik, H.; Zhou, P.; Diamanti, S. J. *Macromolecules* **2001**, *34*, 5125–5131. (d) Schellekens, M. A. J.; de Wit, F.; Klumperman, B. *Macromolecules* **2001**, *34*, 7961–7966. (e) Pintauer, T.; Zhou, P.; Matyjaszewski, K. *J. Am. Chem. Soc.* **2002**, *124*, 8196–8197. (f) Nanda, A. K.; Matyjaszewski, K. *Macromolecules* **2003**, *36*, 599–604. (g) Nanda, A. K.; Matyjaszewski, K. *Macromolecules* **2003**, *36*, 1487–1493. (h) Tang, W.; Matyjaszewski, K. *Macromolecules* **2006**, *39*, 4953–4959.

(5) (a) Seeliger, F.; Matyjaszewski, K. *Macromolecules* **2009**, *42*, 6050–6055. (b) Buback, M.; Morick, J. *Macromol. Chem. Phys.* **2010**, *211*, 2154–2161.

(6) Goto, A.; Fukuda, T. *Macromol. Rapid Commun.* **1999**, *20*, 633–636.

(7) Lin, C. Y.; Coote, M. L.; Gennaro, A. *J. Am. Chem. Soc.* **2008**, *12*, 12762–12774.

(8) Der, K. S.; Mathers, R. T.; Buback, J.; Konkolewicz, D.; Magenau, A. J. D.; Matyjaszewski, K. *Macro Lett.* **2012**, *1*, 1037−1040

(9) (a) di Lena, F.; Chai, C. L. L. *Polym. Chem.* **2010**, *1*, 922–930.

(10) Konkolewicz, D.; Krys, P.; Góis, J. R.; Mendonça, V.; Zhong, M.; Wang, Y.; Gennaro, A.; Isse, A. A.; Fantin, M.; Matyjaszewski, K. *Macromolecules* **2014**, *47*, 560–570.

(11) (a) Bell, C. A.; Bernhardt, P. V.;Monteiro, M. J. *J. Am. Chem. Soc.* **2011**, *133*, 11944-11947. (b) Zerk, T. J.; Bernhardt, P. V. *Dalton Trans.* **2013**, *42*, 11683-11694. (c) Zerk, T. J.; Bernhardt, P. V. *Inorg. Chem.* **2014**, *53*, 11531-11533.

(12) De Paoli, P.; Bortolamei, N.; Isse, A.A.; Gennaro, A. *Chem. Commun.* **2011,** *47*, 3580-3582.

(13) Lorandi, F.; Fantin, M.; Isse, A. A.; Gennaro, A. *Polymer* **2015***, 72*, 238-245.

(14) Matyjaszewski K.; Paik H.; Zhou P.; Diamanti S. J. *Macromolecules* **2001**, *34*, 5125–5131.

(15) V. W. Bowry, K. U. Ingold, *J. Am. Chem. Soc.* **1992**, *114*, 4992–4996.

(16) W. G. Skene, J. C. Scaiano, N. A. Listigovers, P. M. Kazmaier, M. K. Georges, *Macromolecules* **2000**, *33*, 5065–5072.

(17) N. V. Lebedeva, D. P. Zubenko, E. G. Bagryanskaya, R. Z. Sagdeev, G. S. Ananchenko, S. Marque, D. Bertin, P. Tordo, *Phys. Chem. Chem. Phys.* **2004**, *6*, 2254–2259.

(18) K. Matyjaszewski, H. Piak, P. Zhou, S. Diamanti, *Macromolecules* **2001**, *34*, 5125–5131.

(19) Bard A. J.; Faulkner R. L. *Electrochemical methods*, 2nd ed., John Wiley & Sons, New York, **2001**.

(20) (a) Andrieux, C. P.; Dumas-Bouchiat, J.-M.; Savéant, J.-M. *J. Electroanal. Chem.* **1978**, *87*, 39-53. (c) Andrieux, C. P.; Blocman, C.; Dumas-Bouchiat, J.-M.; M'Halla, F.; Savéant, J.-M. *J. Electroanal. Chem.* **1980**, *113*, 19-40.

(21) Isse, A. A.; Gennaro, A. *J. Phys. Chem. A* **2004**, *108*, 4180-4186.

(22) (a) Bortolamei, N.; Isse, A. A.; Magenau, A. J. D.; Gennaro, A.; Matyjaszewski, K. *Angew Chem. Int. Ed.* **2011**, *50*, 11391-11394. (b) Fantin, M.; Isse, A. A.; Gennaro, A. Matyjaszewski, K. *Macromolecules*, 2015, 48, 6862-6875.

(23) Savéant, J.-M. *Elements of Molecular and Biomolecular Electrochemistry*, Wiley-Interscience, New York, **2006**.

(24) The equation $\frac{\partial E_p}{\partial \log v} = -1.15\frac{RT}{\alpha F}$ was used, which relates the shift in the reduction peak potential, E_p, with $\log v$, to the transfer coefficient, α. Isse, A. A.; Berzi, G.; Falciola, L.; Rossi, M.; Mussini, P. R.; Gennaro, A. *J. Appl. Electrochem.* **2009**, *39*, 2217-2225.

(25) Savéant, J.-M.; Su, K. B. *J. Electroanal. Chem.* **1984**, *171*, 341–349.

(26) Tang, W.; Matyjaszewski, K. *Macromolecules* **2007**, *40*, 1858–1863.

(27) Braunecker, W. A.; Pintauer, T.; Tsarevsky, N. V.; Kickelbick, G.; Matyjaszewski, K. *J. Organomet. Chem.* **2005**, *690*, 916-924.

(28) Smolne, S.; Buback, M. *Macromol. Chem Phys.* **2015**, *216*, 894-902.

(29) Bortolamei, N. PhD Thesis, University of Padova, 2012.

(30) Isse, A. A.; Bortolamei, N.; De Paoli, P.; Gennaro, A. *Electrochim. Acta* **2013**, *110*, 655–662.

(31) Pintauer, T.; Braunecker, W.; Collange, E.; Poli, R.; Matyjaszewski, K. *Macromolecules* **2004**, *37*, 2679-2782.

(32) (a) Matyjaszewski, K. *Macromol. Symp.* **1996**, *111*, 47−61. (b) Litvinenko, G.; Mueller, A. H. E. *Macromolecules* **1997**, *30*, 1253− 1266.

(33) Lin, C. Y.; Marque, S. R. A.; Matyjaszewski, K.; Coote, M. L. *Macromolecules* **2011**, *44*, 7568-7583.

(34) Walden, P. *Bull. Acad. Imp. Sci. St. Petersbourg* **1914**, *8*, 405.

(35) Suarez, P.A.Z.; Consorti, C.S.; de Souza, R.F.; Dupont, J.; Gonçalves, R.S. *J. Braz. Chem. Soc.* **2002**, *13*, 106.

(36) (a) Carmichael, A.C.; Haddleton, D.M.; Bon, S.A.F.; Seddon, K.R. *Chem. Commun.* **2000**, *22*, 1237. (b) Maria, S.; Biedron, T.; Poli, R.; Kubisa, P. *J Appl Polym Sci* **2007**, *105*, 278–281. (c) Xie, M.; Kong, Y.; Han, H.; Shi, J.; Ding, L.; Song, C.; Zhang, Y. *React Funct Polym* **2008**, *68*, 1601–1608. (d) Zhao Y-L, Zhang J-M, Jiang J, Chen C-F, Xi F. *J Polym Sci Part A: Polym Chem* **2002**, *40*, 3360–3366. (e) Biedron, T; Kubisa, P. *Macromol. Rapid Commun.*

2001, *22*, 1237-1242. (f) Biedron, T.; Kubisa, P. *J Polym Sci Part A: Polym Chem* **2002**, *40*, 2799–2809.

(37) Bortolamei, N.; Isse, A. a.; Di Marco, V. B.; Gennaro, A.; Matyjaszewski, K. *Macromolecules* **2010**, *43* (22), 9257–9267.

Chapter 4

From Mechanism to Better Control of Aqueous ATRP

Aqueous controlled radical polymerization is a powerful technique for the preparation of water-soluble polymers for biomedical and pharmaceutical applications. In particular, any relevant polymerization involving a biocompatible moiety, such as formation of protein-polymer conjugates[1] or other biohybrids,[2] requires conducting the polymerization in an aqueous environment with a very limited monomer content. Presently however, full application of atom transfer radical polymerization (ATRP) in water has not been achieved because of a limited level of control over polymer growth.[3] Conducting an ATRP in water provides several intriguing challenges. In order to attain a deeper understanding of the mechanism of aqueous ATRP, with particular attention to the reasons for the potential loss of control, a systematic investigation was carried out with three copper-amine catalysts ($[Cu^{II}L]^{2+}$, L = PMDETA, TPMA and Me_6TREN). In particular, we set out to determine as accurately as possible all relevant kinetic and thermodynamic parameters that contribute to the process. Once this goal was achieved, the next step was to explore the limits of control of aqueous ATRP with different catalyst complexes and define a set of guidelines for conducting efficient, controlled polymerizations in water.

4.1 Characterization of the Cu/L complexes in water

4.1.1 Effect of pH and monomer concentration on the redox properties of copper

In water, pH is an important variable that may drastically affect the properties of the catalyst system and the polymerization process in general. Both the copper complexes and their amine ligands can be involved in proton transfer reactions. Before we discuss the effect of pH on copper complexes, it is instructive to recall that, in copper-amine complexes, the preferred coordination numbers of Cu^{II} and Cu^{I} are 5 and 4, respectively.[1] Considering that the examined amines are tetradentate (Me_6TREN, TPMA) or tridentate (PMDETA) ligands, at least one molecule of H_2O is required to complete the coordination

sphere of $[Cu^{II}L]^{2+}$ in water. On the other hand, these ligands can complete the coordination sphere of Cu^{I}, except in the case of $[Cu^{I}PMDETA]^{+}$, which requires one molecule of H_2O. Indeed, similar situations prevail in all coordinating solvents, but in general solvent molecules are omitted and the complexes are simply written as $[Cu^{II}L]^{2+}$ and $[Cu^{I}L]^{+}$. This formalism will be adopted in this and in the following chapters with the tacit understanding that any coordination site remaining after amine coordination is occupied by H_2O.

The main direct effect of increasing pH is the formation of a new complex $[HO\text{-}Cu^{II}L]^{+}$ with an OH^{-} ligand, which is a much stronger ligand than H_2O and any of the halide ions. A decrease of pH, on the other hand, favors protonation of the amine ligand, decreasing its ability to coordinate the metal center, resulting in a dissociation of the complex. These considerations are valid also for Cu^{I}, which easily undergoes disproportionation in the absence of stabilizing ligands. The following acid-base reactions may occur at high and low pH, eqs. 4.1 and 4.2 respectively:

$$[Cu^{II}L]^{2+} + OH^{-} \rightleftharpoons [HO\text{-}Cu^{II}L]^{+} \tag{4.1}$$

$$L + H_3O^{+} \rightleftharpoons LH^{+} + H_2O \tag{4.2}$$

Side reactions involving acidic or basic species are also represented in Scheme 4.1 (bottom).

Scheme 4.1. ATRP equilibrium and relevant side reactions in water.

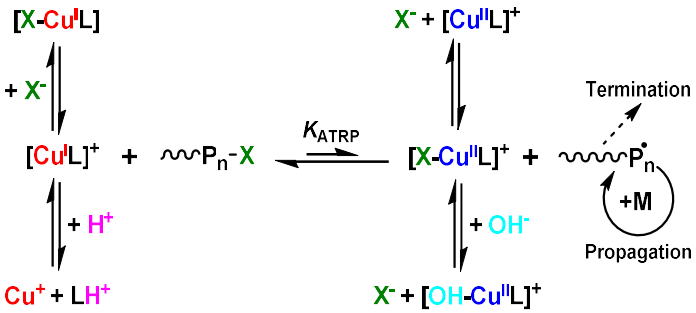

The effect of both reaction 4.1 and 4.2 can be observed by cyclic voltammetry (CV) of $[Cu^{II}L]^{2+}$ at different pHs. In general, Cu^{II} in these complexes undergoes a quasi-reversible one electron transfer to the corresponding Cu^{I} complex, but the voltammetric pattern is strongly affected by pH. Examples of voltammograms recorded at a scan rate (v) of 0.2 V s^{-1} for all complexes are reported in Figure 4.1. Except in the case of TPMA, which shows two closely separated peak couples at pH 7-9, a single peak couple is observed in the range of pH from 5 to 10. This voltammetric pattern remains substantially

unaffected by changing the scan rate. The redox potentials of the Cu^{II}/Cu^{I} redox couples were obtained as the midpoint between the cathodic, E_{pc}, and anodic, E_{pa}, peak potentials, $(E_{pc} + E_{pa})/2 = E_{1/2} \approx E^{o}$. Values of $E_{1/2}$ measured at pH 5-6 and pH > 9.5 are reported in Table 4.1, while the dependence of $E_{1/2}$ on pH is illustrated in Figure 4.2 for complexes with Me_6TREN and PMDETA.

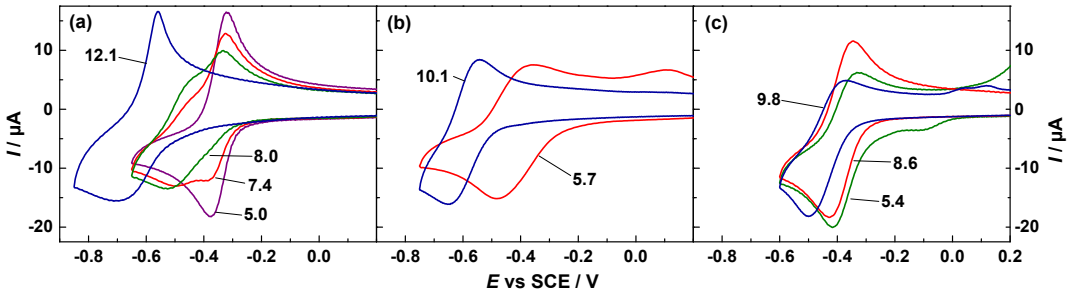

Figure 4.1. CV curves of (a) 1 mM $[Cu^{II}TPMA]^{2+}$, (b) 1 mM $[Cu^{II}Me_6TREN]^{2+}$ and (c) 1 mM $[Cu^{II}PMDETA]^{2+}$, recorded at 0.2 V s^{-1} in H_2O + 0.1 M Et_4NBF_4 at different pHs (values labelled on the curves).

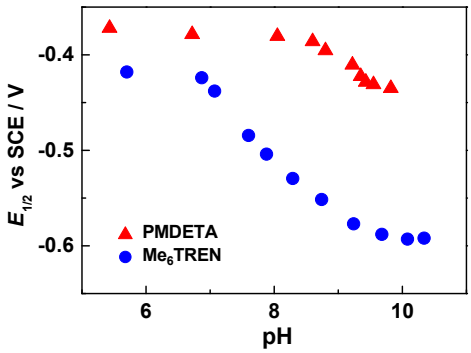

Figure 4.2. Dependence of $E_{1/2}$ of $[Cu^{II}Me_6TREN]^{2+}$ and $[Cu^{II}PMDETA]^{2+}$ on pH.

$E_{1/2}$ strongly depends on pH, shifting to more negative potentials upon increasing pH. A similar trend was already observed for other amine ligands in water.[2] This variation indicates that Cu^{II} becomes relatively more stable than Cu^{I} as the pH becomes higher.

All three Cu^{II} complexes behave as very weak acids, with pK_a values in the range of 7.4 to 8.6 (Table 4.1). Consequently, the protonated and dissociated forms dominate at pH < 7 and pH > 8.6, respectively. Both species are important at intermediate pH, with $E_{1/2}$ depending on pH because of the dynamic equilibrium relating the two species, eq. 4.1. As shown by Figure 4.2, $E_{1/2}$ tends to a constant value both at low and high pH. These two limiting values can be assigned to the standard reduction potentials of the two forms of Cu^{II}, *i.e.*, $[Cu^{II}L]^{2+}$ at low pH and $[HO\text{-}Cu^{II}L]^{+}$ at high pH.

$$[Cu^{II}L]^{2+} + e^- \rightleftharpoons [Cu^{I}L]^{+} \quad (4.3)$$

$$[HO\text{-}Cu^{II}L]^{+} + e^- \rightleftharpoons [HO\text{-}Cu^{I}L] \quad (4.4)$$

The measured standard potentials of the redox reactions 4.3 (pH 5-6) and 4.4 (pH > 9.5) are reported in Table 4.1. These values were obtained in the two limiting pH domains when the voltammetric response does not vary with continued change in pH. A situation of this type could not be realized in the case of TPMA in the region of high pH, as $E_{1/2}$ continued to shift with increasing pH. For this reason the E^e value of [HO-Cu^{II}T-PMA]$^+$/[HO-Cu^{I}TPMA] redox couple was not measured.

Table 4.1. Standard reduction potentials and stability constants of binary complexes $[Cu^{II}L]^{2+}$.

L	pK_a ($Cu^{II}L$)[a]	pK_a (L)[a]	E^e [b] (pH 5-6)[d]	E^e [b] (pH >9.5)[d]	E^e [b] (H_2O/OEOMA)[e]	logβ^{II} [c]	logβ^{I} [c]
TPMA	7.4[f]	6.2[g]	-0.348	-	-0.260	17.59[g]	13.6
Me_6TREN	8.1[f]	10.1[f]	-0.400	-0.600	-0.420	15.7[f]	10.7
PMDETA	8.6[h]	9.2[i]	-0.370	-0.440	-0.290	12.2[i]	7.8

[a] $K_{a\,(Cu^{II}L)}$ and $K_{a\,(L)}$ refer to the acid dissociation reactions of $[Cu^{II}L(H_2O)]^{2+}$ ($[Cu^{II}L(H_2O)_2]^{2+}$ in the case L = PMDETA) and LH^+, respectively. [b] In V vs. SCE; E^e obtained as the average of values measured at different scan rates and/or different experiments, with estimated uncertainty of 0.005 V. [c] β^I and β^{II} are the stability constants of $[Cu^{I}L]^+$ and $[Cu^{II}L]^{2+}$, respectively: $Cu^{z+} + L = [CuL]^{z+}$; estimated uncertainty < 10%. [d] In H_2O + 0.1 M Et_4NBF_4. [e] In unbuffered H_2O/oligoethyleneoxide methylether methacrylate (OEOMA) 10%, v/v + 0.1 M Et_4NBr. [f] From reference 3. [g] From reference 4. [h] From reference 5. [i] From reference 6.

Some deformations of the typical quasi-reversible voltammetric pattern, such as presence of a shoulder, peak broadening, and loss of reversibility, appear at both high and low pH (Figure 4.1). Decreasing the pH below a certain value causes protonation of the ligand, and hence modification, or even dissociation, of the original complex. Some data on pK_a of the ligands are reported in Table 4.1. Although polydentate amine ligands can undergo several proton transfer reactions, for simplicity we only consider the first acid dissociation constant, pK_{a1}. Cyclic voltammetry at low pH shows symptoms that can be attributed to instability of the complexes. First, the anodic peak (due to the re-oxidation of Cu^I to Cu^{II}) decreases indicating decreased stability of $[Cu^{I}L]^+$. Second, a new oxidation peak at-

tributed to anodic stripping of Cu^0 was observed at ca 0.1 V. Metallic copper on the electrode surface was probably generated by the reduction of free Cu^{2+} and/or by fast disproportionation of free Cu^+. Both possibilities point to the dissociation of copper complexes with release of free solvated copper ions. Protonation of the ligand occurs earlier for the more basic tertiary amines, Me_6TREN and PMDETA, whose complexes already show some instability at about pH 6.5, as compared to the less basic aromatic amine, TPMA, whose copper complex continues to provide a stable redox pattern below pH 4.

Even though $[HO\text{-}Cu^{I}L]$ is a stronger reducing agent than $[Cu^{I}L]^+$ (see Table 4.1), the presence of OH^- is expected to decrease the catalytic efficiency of the controlled polymerization system, since both the activation and deactivation reactions will be hampered. The real catalyst in the reversible activation/deactivation of ATRP is the $[Cu^{I}L]^+/[X\text{-}Cu^{II}L]^+$ couple, with a "free" coordination site on the metal center for the incoming halide ion in the case of the activator. In general, the presence of a strong ligand in solution decreases the rate of the activation reaction, and if the ligand is different and much stronger than X^-, it tends to suppress the deactivation reaction as Cu^{II} will be mainly present as $[HO\text{-}Cu^{II}L]^+$ instead of $[X\text{-}Cu^{II}L]^+$ (eqs. 4.5-4.7). Indeed, a trend confirming the difficulty of retaining control with an increase of pH was experimentally observed.[7]

$$[HO\text{-}Cu^{I}L] \rightleftharpoons [Cu^{I}L]^+ + OH^- \quad (4.5)$$

$$[Cu^{I}L]^+ + RX \rightleftharpoons [X\text{-}Cu^{II}L]^+ + R^\bullet \quad (4.6)$$

$$[X\text{-}Cu^{II}L] + OH^- \rightleftharpoons [HO\text{-}Cu^{II}L]^+ + X^- \quad (4.7)$$

An acid environment would also not be expected to be favorable for the polymerization process as the catalyst is prone to ligand protonation, complex dissociation and Cu^{I} disproportionation, all leading to inefficient ATRP catalysis. This behavior may well account for some problems reported for ATRP reactions conducted with acidic monomers and/or in unbuffered solutions.[8]

The redox properties of the Cu^{II}/Cu^{I} couple were also investigated under typical conditions of an *e*ATRP, *i.e.*, in H_2O + 10% OEOMA (v/v) + 0.1 M Et_4NBr and the measured $E_{1/2}$ values are included in Table 4.1 (column 6). These values were measured in unbuffered solutions with neutral to slightly acidic pH; they should be compared with the values measured at pH 5-6 (Table 4.1, column 4). Both OEOMA and Br^- are expected to affect $E_{1/2}$ and the combined effects of these species is a positive shift of 80-90 mV for TPMA and PMDETA and a slight negative shift for Me_6TREN.

4.1.2 Stability constants of copper-amine complexes

The redox potentials of $[Cu^{II}L]^{2+}/[Cu^{I}L]^{+}$ are negatively shifted by about 0.3 V with respect to $E^{\ominus}_{Cu^{2+}/Cu^{+}}$ (-0.11 V vs. SCE),[9] indicating that the ligands induce more stabilization for the higher oxidation state of the metal. The relative stability of the complexes, that is, the ratio of the stability constants, can be calculated from the redox potentials according to eq. 4.8, which has been derived on the basis of a thermochemical cycle based on the relevant redox and complexation reactions:

$$E^{\ominus}_{[Cu^{II}L]^{2+}/[Cu^{I}L]^{+}} = E^{\ominus}_{Cu^{2+}/Cu^{+}} + \frac{RT}{F}\ln\frac{\beta^{I}}{\beta^{II}} \tag{4.8}$$

where R is the universal gas constant, F is the Faraday constant and β^{II} and β^{I} are the stability constants of $[Cu^{II}L]^{2+}$ and $[Cu^{I}L]^{+}$, respectively. The stability constants of Cu^{II} complexes have been previously reported. These values, together with the measured standard reduction potentials of $[Cu^{II}L]^{2+}$ and the known $E^{\ominus}_{Cu^{2+}/Cu^{+}}$ value of -0.11 V vs. SCE, were used to calculate β^{I}. The results are reported in Table 4.1, last column. The data show that both Cu^{I} and Cu^{II} form very stable binary complexes with amine ligands. The stability constants for both oxidation states of Cu depend on the type of amine (aromatic vs. aliphatic) and the number of donor atoms present in the ligand. The aromatic amine TPMA shows higher β values than the aliphatic amines PMDETA and Me_6TREN. The stability constants of the aliphatic amines increase by about 3 orders of magnitude on changing from the tridentate ligand, PMDETA, to the tetradentate one, Me_6TREN. A similar trend was previously reported in acetonitrile.[10]

4.1.3 Binding constants of X^- and OH^- with copper-amine complexes

One of the biggest limits of aqueous ATRP is the instability of ternary $[X\text{-}Cu^{II}L]^{+}$ deactivators, which may easily dissociate (reaction 4.9) or form inactive complexes with the hydroxide ion, $[HO\text{-}Cu^{II}L]^{+}$ (reaction 4.7). Such side reactions are also represented in the upper part of Scheme 4.1.

$$[Cu^{II}L]^{2+} + X^{-} \rightleftharpoons [X\text{-}Cu^{II}L]^{+} \tag{4.9}$$

$$[X\text{-}Cu^{II}L] + OH^{-} \rightleftharpoons [HO\text{-}Cu^{II}L]^{+} + X^{-} \tag{4.7}$$

The stability of Cu^{II} complexes can usually be directly assessed by spectrophotometric titrations. However, the absorbance spectra of halogenated complexes $[X\text{-}Cu^{II}L]^{+}$ (X = Cl, Br) were very similar to those of $[Cu^{II}L]^{2+}$, which precluded direct spectrophotometric

titration of $[Cu^{II}L]^{2+}$ with X^- to determine K_X. Hence, an indirect method based on the competition between X^- and N_3^- for Cu^{II} was adopted.[11] Addition of NaN_3 to a solution of $[Cu^{II}L]^{2+}$ results in the formation of a nitride-copper complex ($[N_3\text{-}Cu^{II}L]^+$) with a characteristic absorption band at *ca.* 380 nm (Figure 4.3).

$$[Cu^{II}L]^{2+} + N_3^- \rightleftharpoons [N_3\text{-}Cu^{II}L]^+ \tag{4.10}$$

Considering equilibrium 4.10, the mass balance and Lambert-Beer law, leads to the following relationship (detailed derivation in Appendix B):

$$\frac{1}{C^*_{Az} - \frac{A}{\varepsilon l}} = K_{Az}\frac{C^*_{Cu^{II}}\varepsilon l}{A} - K_{Az} \tag{4.11}$$

where A is absorbance, ε the molar absorptivity, l the optical path length, K_{Az} the azide binding constant and the starred parameters denote the total concentrations of the sub-script species, N_3^- and Cu^{II}, in solution.

A plot of $1/(C^*_{Az} - A/\varepsilon l)$ vs. $C^*_{Cu}\varepsilon l/A$ gives a straight line with an intercept and slope equal to $-K_{Az}$ and K_{Az}, respectively. An example of spectrophotometric titration of $[Cu^{II}L]^{2+}$ with N_3^-, together with plots of $1/(C^*_{Az} - A/\varepsilon l)$ vs. $C^*_{Cu}\varepsilon l/A$ for all complexes, is reported in Figure 4.3. Regression analysis of each set of data gave similar values of slope and intercept (absolute value). However, the uncertainty of the intercept was always significantly greater than that of the slope. Therefore, K_{Az} was only calculated from the slope and the results together with some characteristic spectrophotometric data of $[N_3\text{-}Cu^{II}L]^+$ are collected in Table 4.2. The molar absorptivity ε was determined from the limiting maximum absorbance of $[N_3\text{-}Cu^{II}L]^+$ observed during spectrophotometric titration of $[Cu^{II}L]^{2+}$ with N_3^-.

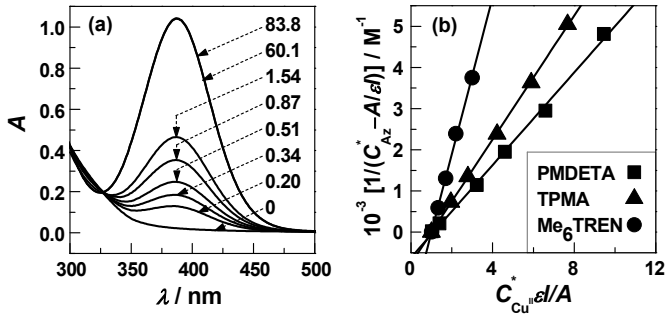

Figure 4.3. (a) UV-Vis spectra of 0.4 mM $[Cu^{II}TPMA]^{2+}$ in the presence of increasing amounts of NaN_3 (C^*_{Az} = 0 – 83.8 mM) at pH 6. (b) Experimental data with the best fit lines for all $[N_3\text{-}Cu^{II}L]^+$ complexes.

Table 4.2. Binding constants of azide, halide and hydroxide ions with $[Cu^{II}L]^{2+}$.[a]

L	λ_{max} (nm) [b]	ε ($M^{-1}cm^{-1}$) [b]	K^{II}_{Az} [c]	K^{II}_{Cl} [c]	K^{II}_{Br} [c]	K^{II}_{OH}
TPMA	387	2550	7.95×10^2	9.04	8.05	7.08×10^5
Me_6TREN	388	2938	1.93×10^3	12.6	4.26	5.0×10^5 [d]
			(1.73×10^3)[d]		(*4.4*)[d]	
PMDETA	371	2485	5.53×10^2	3.70	0.84	1.4×10^5 [e]

[a]Uncertainty on $K \leq 5\%$; ionic strength 0.1 M Et_4NBF_4; $T = 25 \pm 2$ °C. [b]Wavelength (λ) of maximum absorbance and extinction coefficient (ε) of $[N_3\text{-}Cu^{II}L]^+$. [c]pH 6. [d]From reference 11. [e]From reference 6.

In the presence of both azide and halide ions, formation of $[X\text{-}Cu^{II}L]^+$ (eq. 4.12) should be considered to be in competition with reaction 4.10.

$$[Cu^{II}L]^{2+} + X^- \rightleftharpoons [X\text{-}Cu^{II}L]^+ \tag{4.12}$$

Taking into account both reactions 4.12 and 4.10, and mass balances leads to the following equation (see Appendix B):

$$\frac{C^*_{X^-}}{C^*_{Az} - \frac{A}{\varepsilon l}} = \frac{K_{Az}}{K_X}\left(\frac{C^*_{Cu^{II}}\varepsilon l}{A} - \frac{1}{K_{Az}\left(C^*_{Az} - A/\varepsilon l\right)}\right) - \frac{K_{Az}}{K_X} \tag{4.13}$$

where K_X is the halidophilicity constant and $C^*_{X^-}$ is the total halide ion concentration. Eq. 4.13 can be rewritten in a more compact form:

$$y = \frac{K_{Az}}{K_X}x - \frac{K_{Az}}{K_X} \tag{4.14}$$

where $y = C^*_{X^-}/(C^*_{Az} - A/\varepsilon l)$ and $x = (C^*_{Cu^{II}}\varepsilon l/A) - 1/K_{Az}(C^*_{Az} - A/\varepsilon l)$.

A plot of y vs. x should give a straight line with slope K_{Az}/K_X and intercept $-K_{Az}/K_X$. An example of the application of this approach is reported in Figure 4.4 for the association of $[Cu^{II}PMDETA]^{2+}$ with Br^-. Similar results were obtained for all other reactions of $[Cu^{II}L]^{2+}$ with X^- and the association constants, calculated from the slope, are reported in Table 4.2.

Table 4.2 also reports the binding constants, K_{OH}, of OH^- with Cu^{II} complexes. In the case of TPMA, K_{OH} was measured using the same approach described for the determination of K_X, whereas the binding constants for Cu^{II} complexes of Me_6TREN and PMDETA were taken from the literature. To determine K_{OH}, a buffered solution of 4×10^{-4} M

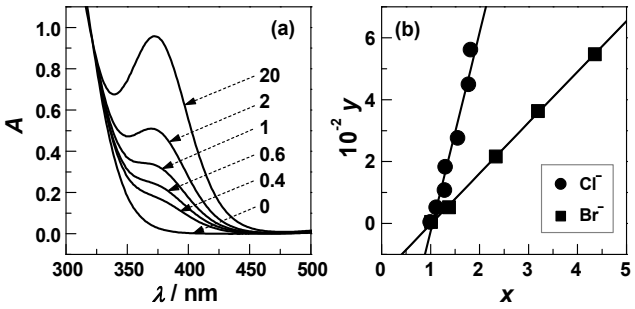

Figure 4.4. (a) UV-Vis spectra of 0.4 mM $[Cu^{II}PMDETA]^{2+}$ + 0.096 M Et_4NBr in the presence of different amounts of NaN_3 (C_{Az} = 0 – 20 mM) at pH 6. (b) Linear plots of the data (according to eq. 4.14) with the best fit lines.

$[Cu^{II}TPMA]^{2+}$, pH 9.06, with a fixed ionic strength (0.1 M Et_4NBF_4) was titrated with NaN_3. At pH 9.06, copper is almost exclusively present as $[HO\text{-}Cu^{II}TPMA]^+$, so during titration, substitution of OH^- by N_3^- occurs, producing $[N_3\text{-}Cu^{II}TPMA]^+$. Measuring the concentration of the azide complex from its absorbance at 380 nm and fitting the data to eq. 4.14 yields the value of K_{OH} reported in Table 4.2. This value is in good agreement with the K_{OH} values previously reported for the other two copper-amine complexes, and all of them are about 4 orders of magnitude greater than K_X.[6,11] This means that under basic conditions Cu^{II} will be predominantly present as $[HO\text{-}Cu^{II}L]^+$ rather than $[X\text{-}Cu^{II}L]^+$ with dramatic consequences for control over polymer growth due to the lack of deactivator. Therefore, basic conditions should be avoided in order to attain an efficient and well-controlled aqueous ATRP.

The halidophilicity of $[Cu^{I}TPMA]^+$ complexes was evaluated with equation 4.15, derived from a thermochemical cycle involving $[Cu^{II}L]^{2+}$ and $[X\text{-}Cu^{II}L]^+$ reduction, and formation of the ternary complexes $[X\text{-}Cu^{II}L]^+$ and $[X\text{-}Cu^{I}L]$. Eq. 4.15 relates the ratio of the association constants with the standard reduction potentials:

$$E^{\ominus}_{[X\text{-}Cu^{II}L]^+/[X\text{-}Cu^{I}L]} = E^{\ominus}_{[Cu^{II}L]^{2+}/[Cu^{I}L]^+} + \frac{RT}{F}\ln\frac{K_X^{I}}{K_X^{II}} \qquad (4.15)$$

where K_X^{II} and K_X^{I} are the association constants of X^- with $[Cu^{II}L]^{2+}$ and $[Cu^{I}L]^+$, respectively. Using the $E^{\ominus}_{[X\text{-}Cu^{II}L]^+/[X\text{-}Cu^{I}L]}$ values measured for the ternary $[X\text{-}Cu^{II}TPMA]^+$ complexes (Table 4.1) and the K_X^{II} values reported in Table 4.2, gave K_X^{I} = 31 ± 5 and 155 ± 25 for the association of $[Cu^{I}TPMA]^+$ with Cl^- and Br^-, respectively. Comparison of K_{Cl}^{II} with K_{Br}^{II} on one hand and K_{Cl}^{I} with K_{Br}^{I} on the other hand, indicates that the affinity of

the metal for the halide ions is inverted in the two oxidation states: $[Cu^{II}TPMA]^{2+}$ binds slightly better with Cl^- than Br^-, whereas the opposite is true for $[Cu^{I}TPMA]^{+}$. This peculiar trend, and the general greater affinity of Cu^I for halide ions, have already been reported for free copper ions in water.[12]

Typically, in aqueous ATRP experiments with regeneration of the active catalyst, the overall concentration of Cu^{II} hardly exceeds 5×10^{-4} M. According to the K_X values reported in Table 4.2, the fraction of Cu^{II} present as $[X\text{-}Cu^{II}L]^+$ in a solution containing 5×10^{-4} M $Cu^{II}X_2$ and 5×10^{-4} M amine ligand should be less than 2%. Figure 4.5 shows distribution diagrams of ternary systems Cu/L/X, with $C^*_{Cu^{II}} = C^*_L = 5\times10^{-4}$ M and variable concentration of X^-. It is clear that for all systems a large excess of X^- is required to obtain deactivator concentrations high enough to guarantee efficient deactivation of $P_n^\bullet$.

The low halidophilicity constants in water have severe consequences on the deactivation process, which requires the presence of a sufficient amount of a stable halide complex, $[X\text{-}Cu^{II}L]^+$, that can rapidly react with the propagating radicals. A large excess of halide ions in the solution significantly improves control.[13]

It has been shown that the real activator in ATRP is a tetracoordinate Cu^I species possessing a free coordination site on the metal center for the incoming halogen atom in the atom transfer (or inner-sphere electron transfer) activation step.[14] Therefore, the effect of the halide ions on the activation step is to decrease its rate by binding to $[Cu^IL]^+$ and hence subtracting some activator from the ATRP equilibrium. In addition, the presence of excess X^- shifts the equilibrium of reaction 4.12 in favor of $[X\text{-}Cu^{II}L]^+$, thus increasing the concentration of the deactivator. The combined overall effect on the polymerizing system is a decrease of the propagating radical concentration, which is beneficial for obtaining a well-controlled polymerization.

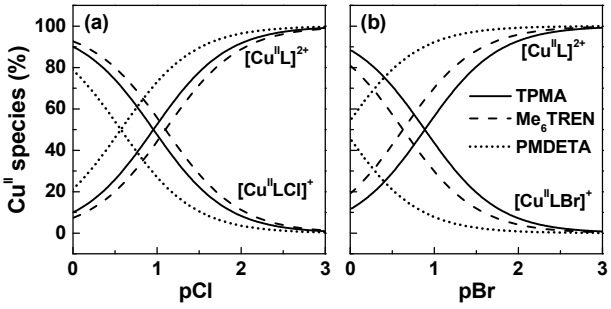

Figure 4.5. Distribution diagrams of Cu^{II} in water + 0.1 M Et_4NBF_4 in the presence of amine ligand, L, and halide ion, X^-: $C^*_{CuII} = C^*_L = 5\times10^{-4}$ M; $pX = -\log C_{X^-}$.

4.2 Defining the limits of control of aqueous *e*ATRP

To examine the effect of the previously described parameters and define guidelines for a controlled aqueous ATRP, the electrochemically mediated polymerization of OEOMA (molecular weight, M_w = 500) was studied in a catalytic system composed of $[Cu^{II}L]^{2+}$/HEBiB 1:2 in H_2O + 10% OEOMA (v/v). Initially, the catalyst was present only as $[Cu^{II}L]^{2+}$ (or $[Cu^{II}L]^{2+}$ + $[X\text{-}Cu^{II}L]^{+}$) and polymerization was triggered by application of a potential (E_{app}) equal to, or more negative than, the onset potential of Cu^{II} reduction. As already seen, $[Cu^{II}L]^{2+}$ exhibits a reversible peak couple in cyclic voltammetry (CV). When the initiator HEBiB is added, the CV response drastically changes: the cathodic peak greatly increases, while the anodic one decreases, clearly indicating that the Cu^{I} species generated at the electrode reacts with the initiator (Figure 4.6). All electrolysis experiments were therefore carried out at an applied potential inside the reduction wave of $[Cu^{II}L]^{2+}$. In the following sections, the effect of various parameters such as E_{app}, halide ion concentration, and pH is reported with the aim of defining the optimal values of each parameter.

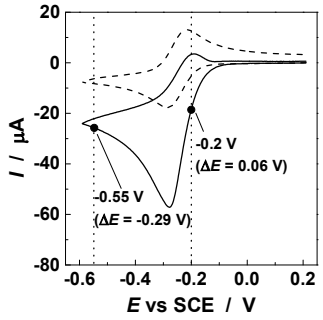

Figure 4.6. Cyclic voltammograms of 1 mM $[Cu^{II}TPMA]^{2+}$ in H_2O + 10% OEOMA (v/v) + 0.1 M Et_4NBF_4, recorded at v = 0.2 V s^{-1}, in the absence (dashed line) and presence (solid line) of 2 mM HEBiB; the two dots on the CV correspond to the E_{app} values used in the polymerization experiments. $\Delta E = E_{app} - E_{1/2}$.

4.2.1 Effect of E_{app} and Br^- concentration

In the first series of experiments, with $[Cu^{II}TPMA]^{2+}$ as the catalyst, the effects of both applied potential and excess bromide ions were studied (Table 4.3). Electrogeneration of the active catalyst was carried out under potentiostatic conditions, whereby the magnitude of E_{app} can be chosen to control the Cu^{II} to Cu^{I} ratio at the electrode surface. It depends on $\Delta E = E_{app} - E_{1/2}$ and is dictated by the Nernst equation. Considering only binary complexes, for simplicity, the Cu^{II} to Cu^{I} ratio can be expressed as:

$$E_{app} = E_{1/2} + \frac{RT}{nF}\ln\frac{C_{[Cu^{II}L]^{2+}}}{C_{[Cu^{I}L]^{+}}} \quad (4.16)$$

In a first experiment at E_{app} = -0.55 V (Table 4.3, entry 1), 71% conversion was achieved within 30 min. The process was very fast, but the control was not exceptionally good ($Đ$ = 1.48). At E_{app} = -0.20 V ($E_{app} - E_{1/2}$ = 0.06 V), the $C_{[Cu^{II}L]^{2+}}/C_{[Cu^{I}L]^{+}}$ at the electrode is ~ 10. A continuous regeneration of a small quantity of $[Cu^{I}L]^{+}$ is achieved, and consequently the concentration of R$^{\bullet}$ is remarkably lower. Therefore, this applied potential decreased the rate of the radical-radical termination reactions and hence enhanced the average life-time of the propagating polymer chains. Under these conditions (Table 4.3, entry 2), active polymer chains lived roughly 5 times longer than in the previous experiment, resulting in higher conversion and polymers with a much better dispersity.

Table 4.3. Electrochemically mediated aqueous ATRP of OEOMA at 25 °C with $[Cu^{II}TPMA]^{2+}$.[a]

En.	Electrolyte	pH	$E_{1/2}$[b] (V)	E_{app}[b] (V)	ΔE[c] (V)	t (h)	Q (C)	Conv. (%)	$M_{n,th}$	$M_{n,app}$	M_w/M_n
1	Et_4NBF_4	5-6	-0.26	-0.55	-0.29	0.5	4.8	71	38000	115000	1.48
2	Et_4NBF_4	5-6	-0.26	-0.20	0.06	2.5	1.9	96	52000	67000	1.24
3	Et_4NBr	5-6	-0.26	-0.55	-0.29	1.2	6.0	74	40000	55000	1.30
4	Et_4NBr	5-6	-0.26	-0.20	0.06	4	3.1	95	51000	63000	1.17

[a]All experiments were carried out in H_2O + OEOMA (10%, v/v) in the presence of 0.1 M electrolyte and 1 mM $[Cu^{II}TPMA]^{2+}$; $C_{OEOMA}/C_{HEBiB}/C_{[Cu^{II}TPMA]2+}$ = 216:2:1. [b]vs. SCE. [c]$\Delta E = E_{app} - E_{1/2}$.

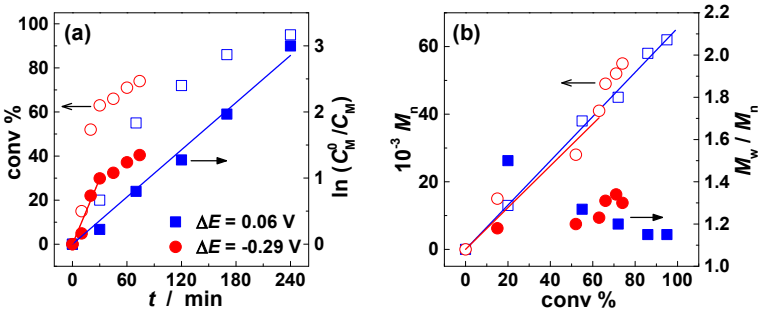

Figure 4.7. Effect of E_{app} on *e*ATRP of OEOMA (10%, v/v) in H_2O + 0.1 M Et_4NBr + 1 mM $[Cu^{II}TPMA]^{2+}$ at 25 °C; $C_{OEOMA}/C_{HEBiB}/C_{[Cu^{II}TPMA]^{2+}}$ = 216:2:1: $E_{app} - E_{1/2}$ = -0.29 V (●); $E_{app} - E_{1/2}$ = 0.06 V (■). (a) Conversion and first-order kinetic plot; (b) evolution of molecular weight and molecular weight distribution with conversion.

Another way to improve control of the process is to add an excess of bromide ions to the solution. This affects both the concentration of the activator and deactivator: $[Cu^{I}L]^{+}$ is partially converted to inactive $[X\text{-}Cu^{I}L]$, while $[X\text{-}Cu^{II}L]^{+}$ is preserved. For example, in the case of TPMA, addition of 0.1 M Br^{-} results in at least 40% of Cu^{II} present as the deactivator$[Br\text{-}Cu^{II}L]^{+}$, whereas about 94% of Cu^{I} is converted to $[Br\text{-}Cu^{I}L]$. Both factors favor deactivation over activation, thereby increasing the polymerization control. Using $E_{app} - E_{1/2}$ = -0.29 V with 0.1 M Et_4NBr (Table 4.3, entry 3), results in a significant improvement of control as compared to the first run (entry 1). However, a comparison of these first three experiments indicates that the effect of adding an excess of Br^{-} is less pronounced than the effect of changing E_{app} to a more positive potential. It is also clear that a well-controlled reaction can be obtained when these two synergistic effects, excess Br^{-} and $E_{app} > E_{1/2}$, are appropriately combined. This is well illustrated in Figure 4.7 and Table 4.3, entry 4, when $E_{app} - E_{1/2}$ = 0.06 V and 0.1 M Br^{-} were used.

4.2.2 Effect of pH

The polymerization experiments discussed so far were conducted in a slightly acidic environment (pH 5-6), due to a dissociation of the catalyst itself, which acts as a weak acid (see Table 4.1 for pK_a). Under these conditions, only a small amount of Cu^{II} is present as $[HO\text{-}Cu^{II}TPMA]^{+}$ and, as shown in Table 4.3, this does not represent a serious problem for the deactivation reaction and the overall molecular weight control. In a second series of experiments, the role of pH on electrochemically mediated ATRP was investigated (Table 4.3). Since both the standard reduction potential of the complex and its catalytic activity change with pH, it was necessary to adjust the applied potential for each experiment. E_{app} was chosen based on the voltammetric response of $[Cu^{II}TPMA]^{2+}$ in the presence of HEBiB, in order to obtain a roughly fixed catalytic current, Figure 4.8b.

The voltammetric analysis of the system described in the previous sections indicated that the reaction could be hampered at either extremely high or low pH, due to the formation of inactive $[HO\text{-}Cu^{II}TPMA]^{+}$ and $[HO\text{-}Cu^{I}TPMA]$ at high pH, and protonation of the ligand with partial dissociation of the catalyst at low pH. These predictions were confirmed by the CV curves reported in Figure 4.8b. The remarkable catalytic current enhancement observed at pH 5.5 decreases significantly both at higher and lower pH. The *e*ATRP experiments confirmed the same trend. As the pH was increased above the pK_a value of $[Cu^{II}TPMA]^{2+}$ (pK_a = 7.4), a decrease of efficiency in terms both of degree of

Table 4.3. Electrochemically mediated aqueous ATRP of OEOMA at 25 °C with $[Cu^{II}TPMA]^{2+}$ at different pH values.[a]

	pH	$E_{1/2}$[b] (V)	E_{app}[b] (V)	ΔE[c] (V)	$C_{Cu^I}/C_{Cu^{II}}$[d]	t (h)	Q (C)	Conv. (%)	$M_{n,th}$	$M_{n,app}$	M_w/M_n
1	11	-0.41	-0.35	0.06	0.1	1.6	1.6	78	42000	89000	1.50
2	8.5	-0.31	-0.26	0.06	0.1	4	2.3	80	43000	118000	1.20
3	5.5	-0.26	-0.20	0.06	0.1	4	3.1	95	51000	63000	1.17
4	2.5	-0.20	-0.18	0.02	0.5	4	1.7	98	53000	47000	1.15
5	1.5	-0.12[e]	-0.18	-0.04	2	4	4.5	>99	54000	47000	1.19
6	0.5	-	-0.18	-	-	4	1.5	0	-	-	-

[a]All experiments were carried out in H_2O + OEOMA (10%, v/v) in the presence of 0.1 M Et_4NBF_4 and 1 mM $[Cu^{II}TPMA]^{2+}$; $C_{OEOMA}/C_{HEBiB}/C_{[Cu^{II}TPMA]^{2+}}$ = 216:2:1. [b]vs. SCE. [c]$\Delta E = E_{app} - E_{1/2}$. [d]According to eq. 4.16. [e]At pH 1.5, cyclic voltammetry shows an irreversible peak; $E_{1/2}$ was roughly estimated by the anodic shift of the reduction peak of $[Cu^{II}TPMA]^{2+}$.

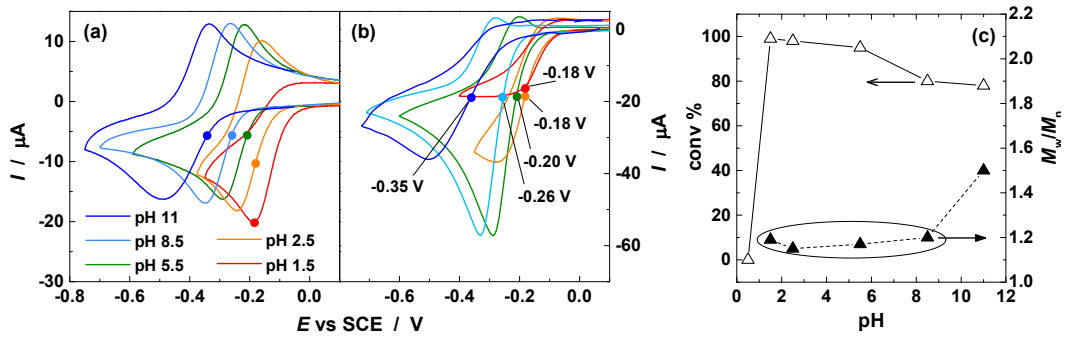

Figure 4.8. Cyclic voltammetry of 1 mM $[Cu^{II}TPMA]^{2+}$ (a) in the absence and (b) in the presence of 2 mM HEBiB in 10% OEOMA (v/v) in H_2O + 0.1 M Et_4NBF_4 at various pH values, υ = 0.2 V s^{-1}; the dots on the CV curves correspond to the E_{app} values used in the polymerization experiments. (c) Conversion (△) and molecular weight dispersity (▲) of the *e*ATRP experiments as a function of pH. A reasonable pH interval of stability of the catalyst is highlighted inside the circle.

conversion and dispersity was observed (Table 4.3, entries 1-2 and Figure 4.8c). The catalytic efficiency of $[Cu^{II}TPMA]^{2+}$ was better preserved at low pH than at high pH. In spite of the decrease in catalytic current below pH 5.5, $[Cu^{II}TPMA]^{2+}$ produced perfectly controlled polymers with quantitative conversion down to pH 1.5 (Table 4.3, entries 3-5, Figure 4.8). However, complete dissociation of the catalyst occurred in strongly acidic conditions, pH 0.5, resulting in no detectable polymerization within 4 h of reaction.

4.2.3 ATRP with other ligands

A third series of experiments involved the investigation of catalytic systems based on $[Cu^{II}Me_6TREN]^{2+}$ and $[Cu^{II}PMDETA]^{2+}$. The electrolyses were performed in H_2O + 10 % OEOMA (v/v) containing Et_4NBr as background electrolyte and the results are summarized in Table 4.4. In the case of Me_6TREN, experiments under typical working conditions (0.1 M Br^-, $E_{app} - E_{1/2} = 0.06$ V, $C_{[Cu^{II}L]^{2+}}/C_{[Cu^{I}L]^{+}} \approx 10$ at the electrode) did not give satisfactory results within a pH range from 6 to 9 (entries 1-2). High conversion could be achieved after 6 h of electrolysis, but the dispersity of the polymer (> 1.8) indicated poor control. This is probably due to the relatively high K_{ATRP} and high concentration of propagating radicals in the system $[Cu^{I}Me_6TREN]^{+}$/HEBiB. To mitigate this effect, E_{app} was positively shifted to $E_{app} - E_{1/2} = 0.12$ V to impose $C_{[Cu^{II}L]^{2+}}/C_{[Cu^{I}L]^{+}} \approx 100$ at the electrode surface. This increased the degree of control by decreasing the rate of activation, while enhancing the rate of deactivation. As shown in Table 4.4 (entry 3) and Figure 4.9, shifting E_{app} to more positive potentials gives the expected result: a well-controlled polymerization with > 99% conversion.

Table 4.4. Electrochemically mediated aqueous ATRP of OEOMA at 25 °C with $[Cu^{II}Me_6TREN]^{2+}$ and $[Cu^{II}PMDETA]^{2+}$.[a]

En.	Ligand	pH	$E_{1/2}$[b] (V)	E_{app}[b] (V)	ΔE[c] (V)	t (h)	Q (C)	Conv. (%)	$M_{n,th}$	$M_{n,app}$	M_w/M_n
1	Me_6TREN	9.0	-0.50	-0.44	0.06	6	3.5	97	53000	144000	1.81
2	Me_6TREN	6-7	-0.42	-0.36	0.06	6	1.7	83	45000	110000	1.80
3	Me_6TREN	6-7	-0.42	-0.30	0.12	2.5	2.2	>99	54000	58000	1.28
4	PMDETA	10	-0.29	-0.23	0.06	2	1.9	>99	54000	73000	1.50
5	PMDETA	7-8	-0.29	-0.23	0.06	2	2.1	>99	54000	59000	1.32
6	PMDETA	6.3	-0.26	-0.20	0.06	2	1.8	>99	54000	56000	1.30
7	PMDETA	5.2	-0.26	-0.20	0.06	2	2.4	90	49000	97000	1.45
8	PMDETA	4.3	-0.06[d]	-0.00	0.06	2	2.0	0	-	-	-
9	PMDETA[e]	7-8	-0.26	-0.23	0.06	2	3.0	>99	54000	54000	1.23

[a]All experiments were carried out in H_2O + OEOMA (10%, v/v) containing, unless otherwise stated, 0.1 M Et_4NBr used as background electrolyte; $C_{OEOMA}/C_{HEBiB}/C_{[Cu^{II}TPMA]2+} = 216:2:1$; 2 mM HEBiB. [b]vs. SCE. [c]$\Delta E = E_{app} - E_{1/2}$. [d]At pH 4.3 cyclic voltammetry shows an irreversible peak; $E_{1/2}$ was roughly estimated by the anodic shift of the reduction peak of $[Cu^{II}PMDETA]^{2+}$. [e]$[Et_4NBr] = 0.3$ M.

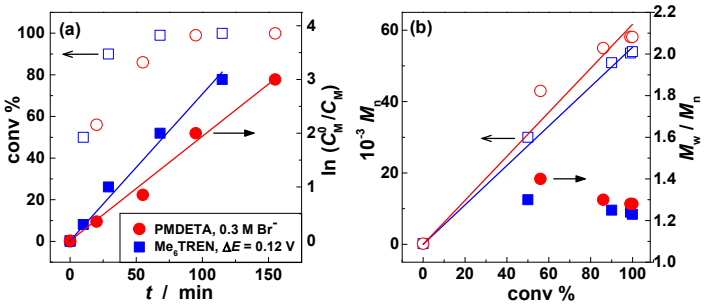

Figure 4.9. *e*ATRP of OEOMA performed at 25 °C in H_2O + OEOMA (10%, v/v), using the catalytic systems $[Cu^{II}Me_6TREN]^{2+}$ + 0.1 M Et_4NBr at $E_{app} - E_{1/2}$ = 0.12 V (■) and $[Cu^{II}$-MDETA$]^{2+}$ + 0.3 M Et_4NBr at $E_{app} - E_{1/2}$ = 0.06 V (●): (a) conversion and first-order kinetic plot; (b) evolution of molecular weight and molecular weight distribution with conversion.

Conversely, when $[Cu^{II}PMDETA]^{2+}$ was used as catalyst, the process produced quite well-controlled polymers and resulted in total conversion of the monomer within 2 h. However, due to the higher basicity of PMDETA and the lower stability constants of Cu complexes of PMDETA, with respect to complexes of both TPMA and Me_6TREN, the pH range of stability of $[Cu^{I}PMDETA]^{+}$ is much narrower than that of $[Cu^{I}TPMA]^{+}$ (Table 4.4, entries 4-7). This is particularly evident under acidic conditions in which $[Cu^{I}$-TPMA$]^{+}$ is an efficient catalyst down to pH 1.5, while $[Cu^{I}PMDETA]^{+}$ loses catalytic activity when pH is below 5.

As shown in Table 4.4 (entries 4-7) $M_w/M_n \geq 1.30$ was observed for Cu/PMDETA, even in the presence of 0.1 M Br^-. This is because $[Br\text{-}Cu^{II}PMDETA]^{+}$ is not very stable with K_{Br} = 0.81. Therefore, to further decrease M_w/M_n, a synthesis with 0.3 M Et_4NBr was performed, to increase roughly three times the concentration of the deactivator $[Br\text{-}Cu^{II}PMDETA]^{+}$. This resulted in an improvement in polymer control in terms both of M_w/M_n and molecular weight, which perfectly matched the theoretical value, without appreciably sacrificing the reaction rate (Table 4.4, entry 9 and red circles in Figure 4.9).

4.2.4 Effect of type of halide ion (Cl, Br)

Effect of switching the supporting electrolyte from Et_4NBr to Et_4NCl was investigated, and results are reported in Table 4.5. In the presence of high Cl^- concentration, halogen exchange from the starting HEBiB initiator is achieved in the first stage of the reaction;[15] in other words, chains grew with a C-Cl chain end. The absence of bromine atoms is desirable for certain biological applications. Polymerizations in the presence of Et_4NCl were slightly slower but better controlled when using TPMA or Me_6TREN as ligand.

ATRP with C-Cl chain ends is characterized by significantly lower ATRP equilibrium constants with respect to C-Br, due to the higher C-Cl bond strength.[16] The effect is a lower radical concentration, which accounts for the observed lower rate and better control.

Table 4.5. Electrochemically mediated aqueous ATRP of OEOMA at 25 °C with different halide ions as supporting electrolytes.[a]

	Ligand	X	pH	$E_{1/2}$[b] (V)	E_{app}[b] (V)	ΔE[c] (V)	t (h)	Q (C)	Conv. (%)	$M_{n,th}$	$M_{n,app}$	M_w/M_n
1	TPMA	Br	5-6	-0.26	-0.20	0.06	4	3.1	95	51000	63000	1.17
2		Cl	5-6	-0.29	-0.23	0.06	4	1.8	94	51000	54000	1.11
3	Me_6TREN	Br	6-7	-0.42	-0.30	0.12	2.5	2.2	>99	54000	58000	1.28
4		Cl	6-7	-0.44	-0.32	0.12	3	2.6	>99	54000	64000	1.26

[a]All experiments were carried out in H_2O + OEOMA (10%, v/v) containing 0.1 M Et_4NX used as background electrolyte; $C_{OEOMA}/C_{HEBiB}/C_{[Cu^{II}TPMA]2+}$ = 216:2:1; 2 mM HEBiB. [b]vs. SCE. [c]$\Delta E = E_{app} - E_{1/2}$.

Table 4.6. Electrochemically mediated aqueous ATRP of OEOA at 25 °C with $[CuTPMA]^{2+}$.[a]

En.	C_{Cl^-} (M)	pH	$E_{1/2}$[b] (V)	E_{app}[b] (V)	ΔE[c] (V)	t (h)	Conv. (%)	$M_{n,th}$	$M_{n,app}$	M_w/M_n
1	0	5-6	-0.18	-0.55	-0.37	3	57	84000	98000	1.47
2	0	5-6	-0.18	-0.18	0	5	38	68000	65900	1.24
3	0.1	5-6	-0.22	-0.22	0	8	48	26500	27700	1.23
4	0.1	5-6	-0.22	-0.16	0.06	8	28	15800	17100	1.08

[a]All experiments were carried out in H_2O + OEOA (10%, v/v) containing Et_4NCl used as background electrolyte; $C_{OEOA}/C_{HEBiB}/C_{[Cu^{II}TPMA]2+}$ = 228:2:1; 2 mM HEBiB. [b]vs. SCE. [c]$\Delta E = E_{app} - E_{1/2}$.

4.2.5 Effect of nature of the monomer

Besides the chain end functionality, the nature of the monomer has profound implications on ATRP equilibrium constant. In particular, K_{ATRP} is much lower for acrylates than methacrylates, due to the lower stability of a secondary radical than a tertiary one.[16] For this reason, polymerization of oligo(ethyleneoxide) methylether acrylate (OEOA) was significantly slower than polymerization of OEOMA, and only moderate conversion was

observed after several hours (Table 4.6). Modulating E_{app} had similar results in the polymerization of both OEOA and OEOMA, with control improving with more positive E_{app} (entries 1-2). Addition of Et_4NCl supporting electrolyte provided polymers with lower dispersities, but significantly slowed reaction rates, because of formation of the inactive $[Cl\text{-}Cu^{I}L]^{+}$ species (entries 3-4).[14]

4.2.6 Rate of polymerization as a function of pH

The overall rate, R_p, of polymerization in a controlled ATRP is given by:[17]

$$R_p = k_p^{app} C_M = k_p K_{ATRP} \left(\frac{C_{P_nX} C_{[Cu^{I}L]^{+}} C_M}{C_{[X\text{-}Cu^{II}L]^{+}}} \right) \quad (4.17)$$

where k_p is the propagation rate constant of the radicals and C_{PnX} is the concentration of the growing chains. k_p^{app} is the apparent rate constant of polymerization, which can be determined from the slope of the linear plot of $\ln([M]_0/[M])$ vs. time. The role of pH on the polymerization rate was investigated for $[Cu^{II}TPMA]^{2+}$ and $[Cu^{II}PMDETA]^{2+}$ and Figure 4.10 shows the dependence of k_p^{app} on pH. The two catalyst systems show a similar dependence of k_p^{app} on pH. The polymerization rate increases, in a relatively strong alkaline environment (pH ≥ 10), probably because the deactivator $[Br\text{-}Cu^{II}L]^{+}$ is completely absent as it is replaced by the inactive $[HO\text{-}Cu^{II}L]^{+}$ complex. This is reflected in both an increase of k_p^{app} and a decrease in polymerization control.

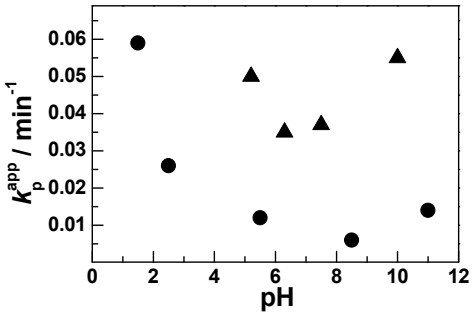

Figure 4.10. Dependence on pH of k_p^{app} measured for the polymerization of OEOMA, catalyzed by (●) $[Cu^{II}TPMA]^{2+}$ and (▲) $[Cu^{II}PMDETA]^{2+}$.

At low pH, despite the sharp decrease in the catalytic activity of the complex (lower currents in Figure 4.8b), there is an increase in the polymerization rates. Table 4.3 shows that a relatively more negative potential was applied at acidic pH (< 2.5), which imposed a higher $C_{Cu^{I}}/C_{Cu^{II}}$ ratio, and hence accounted for the increased k_p^{app}, according to eq. 4.17. It is noteworthy, however, that in the case of $[Cu^{II}TPMA]^{2+}$, despite a significant increase

in k_p^{app} at low pH, control over polymer growth was not compromised (high conversion and low M_w/M_n).

At similar pH and $E_{app} - E_{1/2}$, $[Cu^{II}TPMA]^{2+}$ provided lower k_p^{app} and better control (M_w/M_n = 1.2-1.15 vs. ≥ 1.3) than $[Cu^{II}PMDETA]^{2+}$. This may be rationalized by a significantly higher K_X for $[Cu^{II}TPMA]^{2+}$, which results in a higher deactivator ($[Br\text{-}Cu^{II}L]^+$) concentration and consequently higher deactivation rate. The increase in deactivation rate can explain both the decrease in k_p^{app} and the superior control over polymer growth.

4.2.7 Conditions of good control in aqueous *e*ATRP

A thorough examination of all the factors that can explain the peculiar reactivity of ATRP catalysts in water was carried out, with particular attention directed to understanding the limits of control. This study allowed the determination of a pH range where copper catalysts are stable: the range of catalyst stability is limited by ligand protonation at low pH and formation of hydroxy complexes at high pH. Evaluation of halidophilicity constants shows that Cu^I has higher affinity for halide ions than Cu^{II} and that, in general, the deactivator complexes $[X\text{-}Cu^{II}L]^+$ readily dissociate. An excess of halide ions in solution affects both activator and deactivator concentration. $[Cu^IL]^+$ is partially converted to inactive $[X\text{-}Cu^IL]$, while $[X\text{-}Cu^{II}L]^+$ is preserved; both factors favor deactivation over activation, thus increasing the chances of gaining control over molecular weight distribution.

Overall, the results obtained in this study allow some guidelines to be set for the efficient aqueous ATRP of OEOMA. In general, the catalyst must exhibit sufficiently low

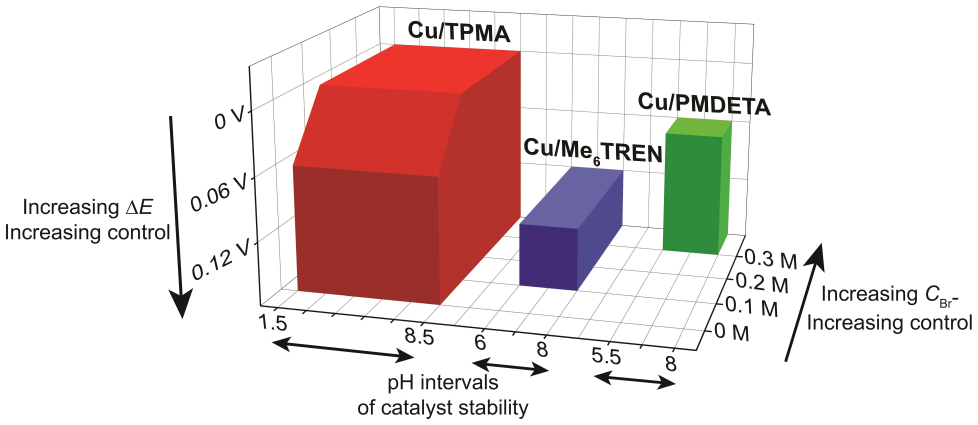

Figure 4.11. Schematic representation of the optimal conditions for a well-controlled aqueous *e*ATRP. Controlled polymerizations (M_w/M_n < 1.3 and M_n in good agreement with theoretical values) were found for the experimental conditions that are inside the colored zones.

K_{ATRP} and k_{disp}, and high K_X. Figure 4.11 displays the necessary conditions to achieve a well-controlled electrochemically mediated polymerization for each of the three investigated complexes; experimental conditions should be inside the colored zones. It is immediately clear that Cu/TPMA is the best and most versatile catalyst in water: it is characterized by adequately low K_{ATRP}, high K_X, and a greater tolerance to acidic media (pH down to 1.5). For each complex, control is possible within a well-defined pH range. Moreover, for the best control over polymer growth, $\Delta E = E_{app} - E_{1/2} \geq 0$ and a sizeable excess of halide ions must be used. It must be stressed that ΔE cannot be increased without any limit because E_{app} should also be near the reduction potential of Cu^{II}.

Contrary to what was believed until now, ATRP of OEOMA can be controlled under strongly acidic conditions, while high pH should be avoided. This series of experiments opened a new avenue for the polymerization of acidic monomers, a class of building blocks that was considered to be problematic, or even impossible, to be polymerized by ATRP (see the next chapter).

References

(1) Pintauer, T.; Reinöhl, U.; Feth, M.; Bertagnolli, H.; Matyjaszewski, K. *Eur. J. Inorg. Chem.* **2003**, *2003*, 2082−2094.

(2) Golub, G.; Cohen, H.; Paoletti, P.; Bencini, A.; Messori, L.; Bertini, I.; Meyerstein, D. *J. Am. Chem. Soc.* **1995**, *117*, 8353−8361.

(3) Anderegg, G.; Gramlich, V. *Helv. Chim. Acta* **1994**, *77*, 685− 690.

(4) Ambundo, E. A.; Deydier, M.; Grall, A. J.; Aguera-Vega, N.; Dressel, L. T.; Cooper, T. H.; Heeg, M. J.; Ochrymowycz, L. A.; Rorabacher, D. B. *Inorg. Chem.* **1999**, *38*, 4233−4242.

(5) Fantin, M.; Isse, A. A.; Gennaro, A.; Matyjaszewski, K. *Macromolecules* **2015**, *48*, 6862–6875.

(6) Navon, N.; Golub, G.; Cohen, H.; Paoletti, P.; Bencini, A.; Valtancoli, B.; Meyerstein, D. *Inorg. Chem.* **1999**, *38*, 3484−3488.

(7) Mincheva, R.; Paneva, D.; Mespouille, L.; Manolova, N.; Rashkov, I.; Dubois, P. *J. Polym. Sci., Part A: Polym. Chem.* **2009**, 47, 1108−1119

(8) (a) Ashford, E. J.; Naldi, V.; O'Dell, R.; Billingham, N. C.; Armes, S. P. Chem. Commun. **1999**, *14*, 1285−1286. (b) Jain, P.; Dai, J.; Baker, G. L.; Bruening, M. L. *Macromolecules* **2008**, *41*, 8413−8417.

(9) Bernardo, M. M.; Heeg, M. J.; Schroeder, R. R.; Ochrymowycz, L. A.; Rorabacher, D. B. *Inorg. Chem.* **1992**, *31*, 191−198.

(10) Bortolamei, N.; Isse, A. A.; Di Marco, V. B.; Gennaro, A.; Matyjaszewski, K. *Macromolecules* **2010**, *43*, 9257−9267.

(11) Golub, G.; Lashaz, A.; Cohen, H.; Paoletti, P.; Bencini, A.; Valtancoli, B.; Meyerstein, D. *Inorg. Chim. Acta* **1997**, *255*, 111−115.

(12) Martell, A. E.; Smith, R. N. Critically selected stability constants of metal complexes database, Version 2.0; Texas A&M University: College Station, TX, USA, **1995.**

(13) Bortolamei, N.; Isse, A. A.; Magenau, A. J. D.; Gennaro, A.; Matyjaszewski, K. *Angew. Chem. Int. Ed.* **2011**, *123*, 11593−11596.

(14) De Paoli, P.; Isse, A. A.; Bortolamei, N.; Gennaro, A. *Chem. Commun*. **2011**, *47*, 3580−3582.

(15) Peng, C. H.; Kong, J.; Seeliger, F.; Matyjaszewski, K. *Macromolecules* **2011**, *44*, 7546–7557.

(16) Tang, W.; Kwak, Y.; Braunecker, W.; Tsarevsky, N. V.; Coote, M. L.; Matyjaszewski, K. *J. Am. Chem. Soc.* **2008**, *130* (32), 10702–10713.

(17) Matyjaszewski, K. *Macromolecules* **2012**, *45*, 4015−4039.

Chapter 5

Aqueous ATRP of Acidic Monomers

One of the advantages of ATRP is the tolerance towards a large array of monomers, except those without radical stabilizing substituents and acidic monomers. For the latter case, several reasons were hypothesized for this lack of success, including ligand protonation at low pH,[1,2] competitive complexation of the carboxylate moieties to copper,[1] or displacement of the halide anion from the Cu^{II} deactivating complex.[2] The controlled synthesis of (co)polymers containing carboxylic acid groups, like methacrylic acid (MAA), can lead to a plethora of applications. Such polymers are hydrophilic, often pH responsive, and generally well biocompatible. They have also unique complexing properties. Thus, ATRP of MAA is highly desirable for various applications.

Unfortunately, until now ATRP allowed to synthetize only well-controlled (M_w/M_n < 1.5) random copolymers with a quite low (≤ 20%) MAA content. They were prepared either by SARA ATRP[3] or photoinduced ATRP catalyzed by 10-phenyl phenothiazine[4] or iridium complexes.[5] For the synthesis of well-defined (meth)acrylic acid (MAA or AA) homopolymers, ATRP of protected monomers in organic solvents has been employed. Usually, tert-butyl methacrylate is polymerized in an organic solvent, and then deprotected and purified.[6]

Armes and coworkers polymerized the sodium salt of MAA, obtained by titration of the monomer with NaOH to pH 9. Despite obtaining good control by ATRP, their synthesis required high concentration of the catalyst $CuBr_2$/bipyridine (> 10,000 ppm, calculated as the mole ratio of copper catalyst to monomer, $(n_{Cu}/n_M)\times10^6$), high temperature (90 °C), and long reaction times (up to 21 h). The polymerization was limited to low molecular weights due to the build-up of anionic charge density on the polymer backbone.[7]

Although both RAFT[8] and NMP[9] can be used for the direct polymerization of AA and MAA, the synthesis of controlled acidic polymers is still a challenge for ATRP. The

direct polymerization of MAA in its acidic (non-ionized) form presents several advantages: (*i*) the propagation rate constant, k_p, of MAA is 10 times higher than that of sodium methacrylate;[10] (*ii*) polymerization is not inhibited by the build-up of polyanionic charge on the polymer backbone;[7] (*iii*) carboxylic acids are weaker nucleophiles and weaker complexing agents than carboxylates (they may not compete for copper ions with ATRP amine ligands or halide ions); (*iv*) polymerization does not require neutralization/titration of the monomer.

***e*ATRP of MAA under typical aqueous conditions.** It was shown in the previous chapter that electrochemically mediated ATRP of 10% v/v OEOMA in water provided excellent control under acidic conditions. In particular, with $[Br\text{-}Cu^{II}TPMA]^+$ as catalyst at pH 2.5, 98% conversion was achieved within 4 h in a well-controlled process yielding polymers with M_w/M_n = 1.15 (Table 4.4). Therefore, considering that a 10% v/v solution of MAA has pH ~2.3, an *e*ATRP of this monomer was performed, replicating the experimental conditions that were successful for OEOMA (Table 5.1, entry 1). Unfortunately, only 7% of MAA was converted after 60 minutes, when the reaction completely stopped. Such a dramatic difference demonstrated that it was impossible to extrapolate to MAA the experimental settings that worked well for OEOMA.

Scheme 5.1. Structures of the investigated initiators and ligands.

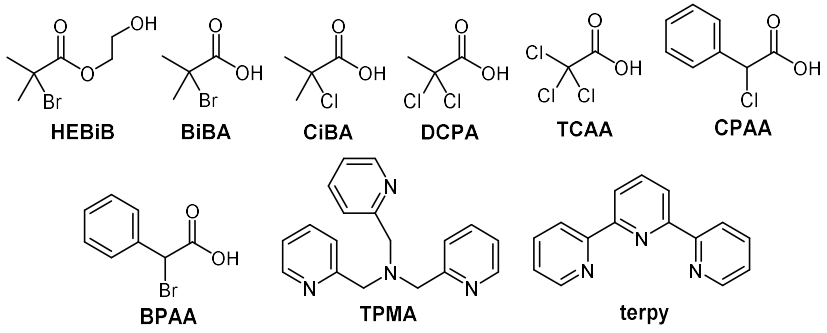

Developing a successful, well-controlled ATRP of MAA requires understanding first the reasons leading to the difficulties in controlling, or even obtaining, the polymerization. To this end, the ATRP system composed of the catalyst $Cu^{II}X_2$/TPMA and the initiator 2-hydroxyethyl bromoisobutyrate (HEBiB) or 2-bromoisobutyric acid (BiBA) was investigated in 10% MAA in water. The ligand TPMA was selected because it was already used in acidic environments.[2] In addition, besides forming a copper complex with

a very high stability constant and sufficient halidophilicity, it suppresses Cu^{I} disproportionation.

5.1 Investigation of the catalytic system

Stability of catalyst and initiator. Cyclic voltammetry (CV) of $[Cu^{II}TPMA]^{2+}$ in 10% v/v MAA in water + 0.1 M NaBr exhibits a reversible peak couple, with $E^{\ominus}$ = -0.20 V vs. SCE (solid line in Figure 5.1a). $E^{\ominus}$ was obtained as the midpoint between the cathodic, E_{pc}, and anodic, E_{pa}, peak potentials, $(E_{pc} + E_{pa})/2 = E_{1/2} \approx E^{\ominus}$. For comparison, $E^{\ominus}$ of $[Cu^{II}TPMA]^{2+}$ in 10% OEOMA in water + 0.1 M Et_4NBr is -0.26 V vs. SCE (Table 4.1). This difference in the redox potentials (0.06 V) suggests that the complex is a slightly less active and weaker reducing agent in the presence of MAA than in the presence of OEOMA, but is still a suitable catalyst. To check the stability of $[Cu^{II}TPMA]^{+}$ during electrolysis, the typical conditions of a polymerization experiment were simulated by keeping a cell with all components needed for *e*ATRP under intense stirring for 2 h and then a CV was recorded. The shape of the voltammetric curve of $[Cu^{II}TPMA]^{2+}$ was unchanged (dashed line in Figure 5.1a). Since no other peak appeared in the CV, the initial complex did not dissociate, or, in other words, MAA does not compete with TPMA for Cu^{2+} ions.

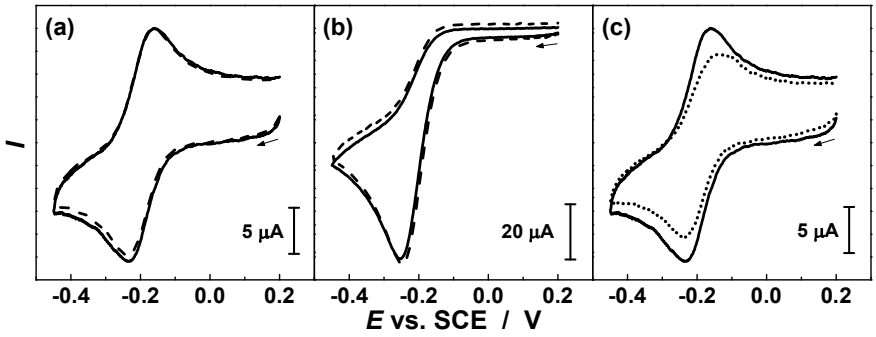

Figure 5.1. CV of 10^{-3} M $[Cu^{II}TPMA]^{2+}$ in 10% v/v MAA in water + 0.1 M NaBr (a) in the absence and (b) in the presence of 5×10^{-3} HEBiB. CV were recorded immediately after addition of the reagents (solid line), after two hour of stirring (dashed line). (c) CV of 10^{-3} M $[Cu^{II}TPMA]^{2+}$ in 10% v/v MAA in water + 0.1 M NaBr in the absence of HEBiB (solid line), and in the presence of HEBiB after application of E_{app} = -0.18 V vs. SCE for 2.5 h, which triggered the polymerization of MAA oligomers (dotted line).

A similar situation was observed in the presence of the initiator HEBiB (Figure 5.1b). As expected, in this case, the CV was irreversible, confirming the catalytic behavior of the system. According to the catalytic cycle in Scheme 5.2, the electrogenerated $[Cu^{I}L]^{+}$

quickly disappears by reaction with the initiator, RX. This reaction regenerates Cu^{II} complexes, which are subsequently further reduced at the electrode, causing the increased cathodic current (I_{pc}). As in the previous case, the voltammetric pattern was essentially unchanged after two hours of stirring in the presence of MAA. This indicated that the initiator was stable and did not undergo hydrolysis, while its catalytic activity remained unchanged.

Scheme 5.2. Catalytic cycle involving heterogeneous electron transfer to Cu^{II}.

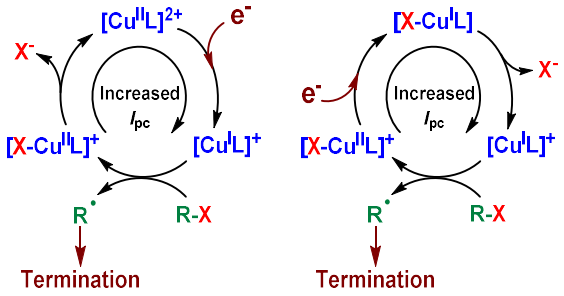

In the presence of PMAA oligomers, obtained from the *e*ATRP of MAA under standard aqueous conditions (7% of MAA conversion), a signal corresponding to the original $[Cu^{II}TPMA]^{2+}$ was observed (Figure 5.1c). This proved that the complex was stable also in the presence of PMAA, which could act as a stronger polydentate ligand, using multiple carboxylic groups to bind Cu ions. On the other hand, the absence of any catalytic current implied the absence of active C-Br bonds.

Halide ions have remarkably lower association constants with $[Cu^{II}TPMA]^{2+}$ in pure water as compared to organic solvents (reaction 5.1, equilibrium constant, $K_X < 13$, Table 4.2).

$$[Cu^{II}TPMA]^{2+} + X^- \overset{K_X}{\rightleftharpoons} [X\text{-}Cu^{II}TPMA]^+ \qquad (5.1)$$

The equilibrium constant of reaction 5.1, for X = Cl, was determined by spectrophotometric titration in 20% v/v MAA in water at 0.1 M ionic strength (Figure 5.2). The obtained value, $K_{Cl} = 38$, was higher than the value in pure water. This result showed that the monomer did not compete with the halide ions; conversely, MAA acted as an organic solvent, reducing the polarity of the environment and facilitating the formation of the ternary $[X\text{-}Cu^{II}TPMA]^+$ deactivator complex. A similar behavior was observed when MeOH was added to water.[11]

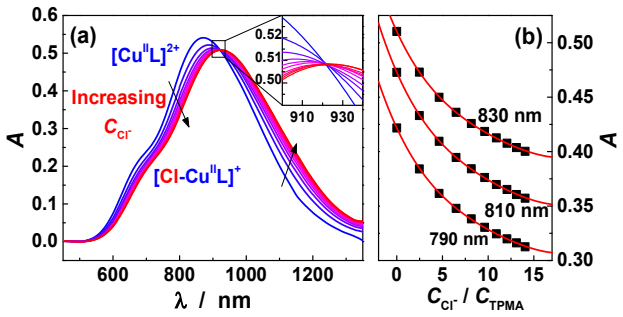

Figure 5.2. (a) Vis-NIR spectra of 3×10^{-3} M $[Cu^{II}TPMA]^{2+}$ solutions at 25 °C in 20% v/v MAA in water + 0.1 M Et_4NBF_4, $V_0 = 2$ mL, $C_0 = 3\times10^{-3}$ M; step additions of a 20% v/v MAA aqueous solution containing 3×10^{-3} M $[Cu^{II}TPMA]^{2+}$ and 9.98×10^{-2} M Et_4NCl. (b) Absorbance values at three selected wavelengths and best-fit curves.

Evaluation of the role of radical-radical termination. Having proved the stability of both catalyst and initiator, the stability of the growing polymer was then studied. Excessive radical-radical termination could be the cause of low conversion and lack of control. Electrochemically mediated ATRP allows a clear insight into radical chain-termination reactions: Scheme 5.2 shows that one $[X\text{-}Cu^{II}L]^+$ should accumulate in solution for each terminated radical. To allow the further activation of C-Br bonds, Cu^{II} species must be reduced back to Cu^{I} at the working electrode. Therefore, each termination event is accompanied by the consecutive mono-electronic reduction of a Cu^{II} complex, with the consumption of one elementary charge. By recording the total consumed charge during an *e*ATRP experiment, the number of active chains lost by radical-radical termination could be evaluated by equation 2 (chronoamperometry curve used for the determination of the consumed charge is reported in Figure 5.3). Total charge Q is the sum of two contributions: the initial reduction of Cu^{II} species to Cu^{I}, $Q_{Cu^{II}/L}$, and the reduction of Cu^{II} species accumulated after radical-radical termination reactions, Q_R.

$$Q = Q_{Cu^{II}/L} + Q_R = \left(n_{Cu^{II}/L} + n_R\right)F \tag{5.2}$$

where $n_{Cu^{II}/L}$ is the number of moles of Cu^{II} species initially converted to Cu^{I}, n_R is the number of moles of chain terminated by radical-radical reactions, and F is the Faraday constant. $n_{Cu^{II}/L}$ was estimated by using the Nernst equation; the Cu^{II} to Cu^{I} ratio can be expressed as:

$$E_{app} = E_{1/2} + \frac{RT}{F} \ln \frac{C_{Cu^{II}/L}}{C_{Cu^{I}/L}} \quad (3)$$

where R is the gas constant. At $E_{app} = E_{1/2}$ = -0.20 V, the $C_{Cu^{II}/L} / C_{Cu^{I}/L}$ at the electrode is ~1, therefore half of the Cu^{II} species are converted to Cu^{I}. This corresponds to $n_{Cu^{II}/L}$ = 5.9×10^{-6} mol and $Q_{Cu^{II}/L}$ = 0.57 C. Using the determined Q = 1.6 C, it follows that n_R = 1.1×10^{-5} mol. The number of growing chains is equal to the number of moles of initiator, n_{RX} = 1.2×10^{-4} mol. It follows that the fraction of radical-radical terminated chains, n_R/n_{RX}, is only 9% of the total number of chains. Such a value is compatible with a controlled radical polymerization.[12] Therefore, the chain end functionality was not lost mainly through radical-radical termination, but rather through a different pathway.

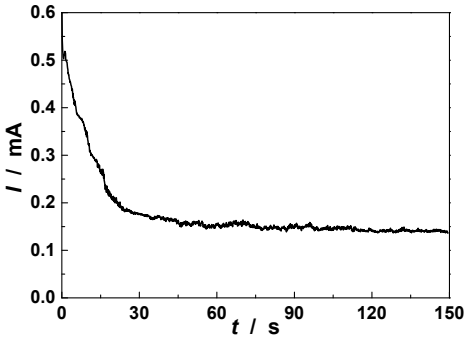

Figure 5.3. Chronoamperometry recorded during the *e*ATRP of 10% v/v MAA in water + 0.1 M NaBr at E_{app} = -0.18 V vs. SCE. Conditions: C_{MAA}:C_{HEBiB}:$C_{Cu(OTf)_2}$:C_{TPMA} = 200:1:0.1:0.1.

Analysis of the chain end structure. To analyze the chain end via NMR spectroscopy, a synthesis with a low degree of polymerization (DP) PMAA was carried out by SARA ATRP ($C_M : C_{RX} : C_{Cu(OTf)_2} : C_{TPMA} : C_{NaBr}$ = 10:1:0.0001:0.03:5 in 5% v/v MAA in D_2O, total V = 5 mL, 10 cm Cu wire with diameter d = 1 mm, RX = α-bromoisobutyric acid). The ^{1}H-NMR and 2D-Heteronuclear Multiple Bond Coherence (HMBC) spectrum of the products (Figure 5.4) showed the presence of a lactone (structure **A** in Scheme 5.3). First, the broad signals in the proton spectrum, centered at δ(^{1}H) = 1.05 and 1.95 ppm, were assigned to the protons 3 and 4, respectively, of the bulk polymer chain (structure **B**). In structure **A**, protons 3a and 3b have different chemical shifts (δ(^{1}H) = 2.60 and 2.21) and show J coupling, representing an AB system, typical of a cyclic structure (AB quartet, 2H, J_{AB} = 13.9 Hz). Relevant chemical shift associations are reported in Figure 3. The HMBC spectrum shows that protons 3a and 3b correlate (being at a distance of 2-3 bonds)

to carbons 1, 2, 3, 4, 5, 7 and 8. Protons 7 correlate to carbons 3, 4 and 8. The peak of carbon 4, $\delta(^{13}C) = 82.3$, was unambiguously assigned to the lactone quaternary carbon. This is in fair agreement with the ^{13}C NMR spectrum of γ-valerolactone (carbon 4 of structure **C**, $\delta(13C) = 77.3$),[13] which has molecular structure similar to that of **A**. Scheme 5.3 also displays a set of chain end configurations (structures **D** and **E**) typical of a polymer obtained by ATRP. Such structures are not compatible with a peak at $\delta(^{13}C) = 82.3$ ppm. Carbon 2 of the active chain end (Structure **D**) should have a chemical shift in the interval $55 < \delta(^{13}C) < 70$,[14] in agreement with the spectrum of α-bromoisobutyric acid (BiBA).[13] Conversely, radical-radical termination (by disproportionation) would produce tertiary carbon atoms as chain end with $\delta(^{13}C) < 50$, (carbon 2 in structure **E**).

Scheme 5.3. Cyclization reaction, chain end lactone and PMAA chain ends, R = H or oligomer chain.

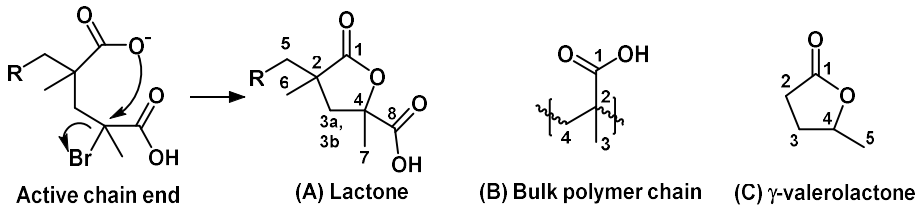

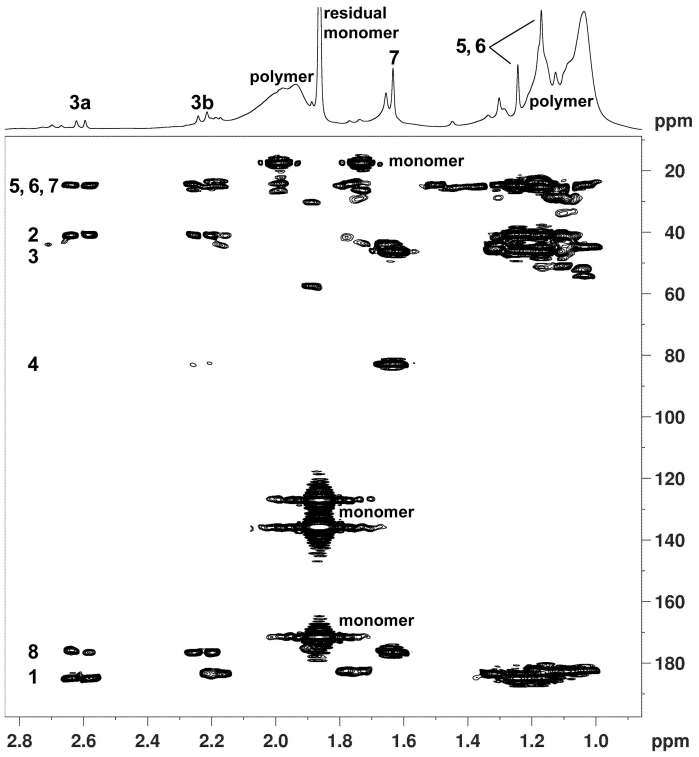

Figure 5.4. HMBC of the products of a SARA ATRP of MAA with target DP = 10, in D_2O. Relevant atoms are labeled in agreement with structure **A** in Scheme 4 (with R = H).

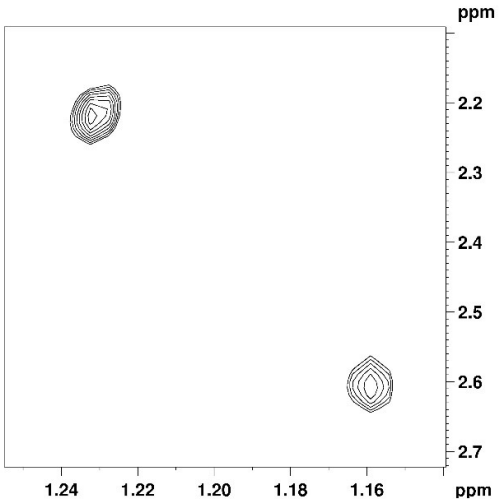

Figure 5.5. Detail of ROESY spectrum of the SARA ATRP mixture.

Additionally, connectivity in the ROESY spectrum (Figure 5.5) suggested the presence of a lactone. The two doublets at $\delta = 2.60$ and $\delta = 2.21$ (f1 axis), were attributed to the two protons in position 3 in structure **A**, for their shape and their coupling constant $^{3}J(H,H) = 13.9$ Hz. In the ROESY spectrum, they correlate (therefore they are "close" in space, below 4 Å) to the singlets at $\delta(^{1}H) = 1.16$ [$\delta(^{13}C) = 24.6$] and $\delta(^{1}H) = 1.24$ [$\delta(^{13}C = 24.7)$], respectively. From their shape and chemical shift, the two singlets were attributed to C5 and C6 (with R = H). Each of the two methylene protons in 3 is "close" only to the protons of one methyl (C5 or C6). This situation is possible only in a well-defined cyclic structure (lactone, **A**) and not in an open structure (**B** or **C**). In an open structure, the rotation around sigma bonds would put both methylene protons close to both methyl groups (C5 and C6), resulting in cross ROESY correlations.

FT-IR of the dried polymerization mixture was consistent with the presence of a lactone (Figure 5.6). The shoulder at $\nu = 1770$ cm^{-1} was assigned to the stretching of the lactone carbonyl.

A close inspection of the NMR data showed several slightly different AX systems, indicating the presence of multiple slightly different lactone structures. These signals were associated to lactones at the chain end of polymers with different lengths. In any case, the most relevant signals were associated to structure **A**, with R = H. This indicated that the majority of the cyclization occurred immediately after the first monomer addition to the initiator BiBA, and that most of the polymerization was prevented from the beginning of the reaction.

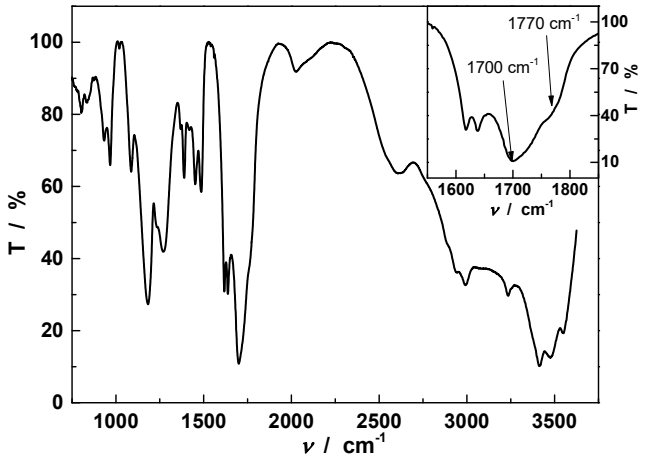

Figure 5.6. FT-IR of the dried polymerization mixture. The shoulder at 1770 cm^{-1} was associated to the lactone carbonyl stretching. Inset: close up of the carbonyl-stretching region of the spectrum.

Once the main cause of termination was identified, three solutions were applied to reduce the effect of this S_N-type reaction. As will be discussed in the next sections, first, the Br chain end was switched to a Cl chain end. Then, the pH was lowered to reduce the concentration of carboxylate anions. Finally, conditions were selected to accelerate the ATRP synthesis, in order to diminish the extent of the cyclization side reaction.

5.2 Electrochemically mediated ATRP of MAA

5.2.1 Effect of halide ions

ATRP in water is performed with a relatively high concentration (0.1–0.3 M) of halide ions to prevent the dissociation of the ternary deactivator complex $[X\text{-}Cu^{II}L]^+$. When switching from 0.1 M NaBr to 0.1 M NaCl as supporting electrolyte, a remarkable improvement in the *e*ATRP of MAA was observed, with conversion that increased from 7% to 43% (Table 5.1). A further increase in conversion (65%) was obtained with 0.3 M NaCl. The lifetime of growing chains was increased, so that polymerization could proceed for longer time (from less than 1 h to about 3 h). After this time, the reaction stopped, suggesting the loss of chain end functionality.

Chloride anions are worse leaving groups than bromide ones, therefore they are displaced less effectively from the chain end. With high Cl^- concentration, halogen exchange from the starting HEBiB initiator was achieved in the first stage of the reaction;[15] in other words, chains grew with a C-Cl chain end. Changing the halide ions and their concentration can also affect other important ATRP parameters, such as $[X\text{-}Cu^{II}L]^+$ association

constant and ATRP equilibrium constants (see Figure 2.2). Nevertheless, this dramatic improvement in conversion can be attributed mostly to the better stability of the C-Cl chain end functionality.

The positive results obtained on moving from NaBr to NaCl supporting electrolyte prompted to test NaF. However, only a small conversion was observed (Table 5.1, entry 4). The use of alkyl fluorides as ATRP initiators is still challenging, even in aqueous environment.

Table 5.1. *e*ATRP of 10 % v/v MAA in water at E_{app} = -0.18 V vs. SCE and T = 25 °C.[a]

Entry	Supporting electrolyte	t (h)	Q (C)	Conv. (%)	k_p^{app} (min^{-1})	$M_{n,th}$	$M_{n,app}$	I_{eff}[b]	M_w/M_n
1	0.1 M NaBr	3	1.6	7	0.0007	1300	-	-	-
2	0.1 M NaCl	3	3.2	43	0.0042	8000	15.6	0.53	2.5
3	0.3 M NaCl	3	1.7	65	0.0070	13500	16.3	0.82	2.2
4	0.03 M NaF + 0.1 M $NaClO_4$	3	5.9	3	0.0001	800	-	-	-

[a] Measured pH = 2.2. Conditions: $C_M : C_{RX} : C_{Cu(OTf)_2} : C_{TPMA}$ = 200:1:0.1:0.1. $C_{Cu^{2+}} = 5.9\times10^{-4}$ M.
[b] Initiation efficiency $I_{eff} = M_{n,th}/M_{n,app}$.

5.2.2 Effect of pH

As already seen in the previous chapter, cyclic voltammetry in Figure 5.7a confirmed that thermodynamic and electrochemical properties of the catalyst change drastically with pH. $E^{\ominus}$ of the complex in 10% MAA in water + 0.3 M NaCl changed from -0.20 V vs. SCE at pH 2.2, to -0.06 V vs. SCE at pH 0.9. Moreover, the CV recorded at pH 0.9 was almost completely irreversible. In this case $E^{\ominus}$ was estimated as $(E_{pc} + E_{pc/2})/2$, the midpoint between the peak potential, E_{pc}, and the half-peak potential, $E_{pc/2}$ (the potential at half-peak current). [16] This is a very rough estimate as the effect of any chemical reaction following electron transfer to Cu^{II} was not taken into account. In fact, the irreversibility of the voltammetric response could be caused by $[Cu^{I}L]^+$ protonation and consequent dissociation, occurring during the timescale of the CV experiment (seconds). $[Cu^{I}L]^+$ stability constant is significantly lower than that of $[Cu^{II}L]^{2+}$ (in pure water, $\log \beta^{I} = 13.6$, $\log \beta^{II} = 17.59$, Table 4.1). Nevertheless, $[Cu^{I}L]^+$ activated the C-X bond faster than it dissociated, owing to the extremely high activation rate constant of Cu^{I} amine complexes in water (Table 3.2).

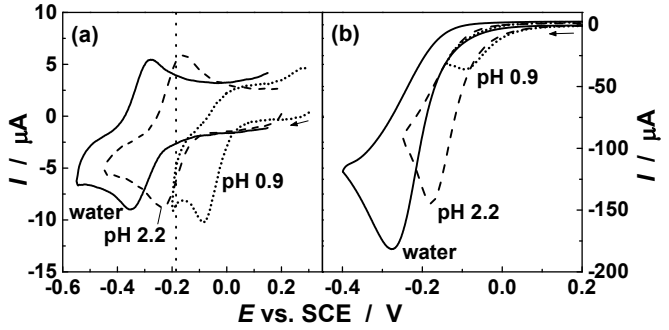

Figure 5.7. Cyclic voltammetry of 5.9×10^{-4} M $[Cu^{II}TPMA]^{2+}$ in pure water (solid line), 10% v/v MAA in water (dashed line), and 10% v/v MAA in water + 0.126 M HCl (dotted line). CVs were recorded in the absence (a) and presence (b) of 5.9×10^{-4} M α-bromophenylacetic acid. NaCl was added to have a total C_{Cl^-} = 0.3 M, T = 25 °C; measured pH values are labeled on the curves. The dashed line represents E_{app} = -0.18 V vs.SCE (vertical dotted line).

Linear correlations between K_{ATRP} and $E^{\Theta}_{[Cu^{II}L]^{2+}/[Cu^{I}L]^{+}}$ have been experimentally observed.[17] On the basis of these correlations, it can be estimated that a 0.14 V drop in the reduction potential of the complex (from pH 2.2 to 0.9) is accompanied by a decrease in K_{ATRP} of 2 to 3 orders of magnitude. Therefore, the activity of the complex at pH 0.9 is expected to be similar to that in polar organic solvents (e. g. DMSO or DMF, where K_{ATRP} is 2 and 3 orders of magnitude smaller than in water, respectively[17c]). A lower K_{ATRP} leads to lower radical concentration, which could be beneficial, since problems in controlling aqueous ATRP are linked to a too high radical concentration.

Figure 5.7b confirms the predicted large decrease of $[Cu^{II}TPMA]^{2+}$ catalytic activity when switching from water to acidic environments. In the presence of α-bromophenylacetic acid (BPAA), the cathodic current drastically dropped when MAA, or MAA + HCl, were added to water. Nevertheless, in the most unfavorable conditions, *i.e.*, at pH 0.9, a cathodic current of 35 µA was recorded. This value is more 3 times greater than I_{pc} of the catalyst alone (compare the red traces in Figure 5.6), clearly indicating that, even at pH 0.9, Cu^{I} could still activate the C-X bonds.

Lowering the pH by addition of HCl had a strong effect on the electrochemical ATRPs (Table 5.2, entries 1-7), in particular, allowing to drastically reduce the extent of the chain end cyclization reaction. In the series of reactions reported in Table 5.2, decreasing the pH from 2.2 (the pH of 10% v/v MAA in water) to 0.9 allowed to increase conversion to 96%, while dispersity decreased from 2.18 to 1.49. Good linearity of the

first-order kinetic plot (Figure 5.7) and good agreement between experimental and theoretical molecular weights proved the occurrence of a controlled polymerization. Figure 5.8 shows conversions and molecular-weight distributions as a function of pH. Both parameters rapidly improved while lowering pH, the best results being observed around pH 0.9. In fact, further decreasing pH to 0.6 caused a slower polymerization without any decrease in molecular-weight dispersity. The kinetic plot in Figure 5.8b for the experiment at pH 0.9 indicates that the polymerization slightly slowed down after 2–3 hours, possibly due to some radical-radical termination or cyclization of the chain end. However, this happened only when conversion was >90%.

In a solution of 10% v/v MAA in water, with pH = 2.2, 5.3×10^{-3} M (0.45%) of MAA is present in its ionized form, as carboxylate anions. Lowering pH allowed to decrease the concentration of carboxylate, which is a stronger nucleophile than the carboxylic acid, and to decrease the negative impact of the lactone formation at the chain end. Another possibility is that Cu^{I} complexes catalyze not only the desired ATRP process, but also the chain end cyclization. In this scenario, decreasing pH significantly altered the reactivity of the Cu^{I} complex, which may be less efficient in catalyzing the cyclization side reaction.

Table 5.2. *e*ATRP of 10% v/v MAA in water at different pH and T = 25 °C.[a]

	pH	E_{app} (V vs. SCE)	t (h)	Q (C)	Conv. (%)	k_p^{app} (min^{-1})	$M_{n,th}$	$M_{n,app}$	I_{eff}	M_w/M_n
1[b]	2.2[c]	-0.18	3	1.7	66	0.007	13600	16300	0.83	2.18
2[b]	1.4	-0.18	3	3.4	82	0.010	14300	20100	0.71	1.88
3	1.4	-0.18	3	3.0	83	0.011	14500	21800	0.67	1.72
4	1.1	-0.18	5	4.6	97	0.013	16900	21300	0.79	1.54
5	0.9	-0.18	4	4.7	96	0.015	16800	21800	0.77	1.49
6	0.6	-0.18	4	3.4	90	0.011	15800	19900	0.79	1.50
7	0.9	-0.10	4	2.3	74	0.006	15900	38000	0.34	1.43
8[d]	0.9	-0.18	4	3.2	96	0.014	16800	18000	0.93	1.42
9[e]	0.9	-0.18	4	3.2	86	0.012	14900	19900	0.75	1.45

[a] pH was set by addition of HCl; NaCl was added to have a constant total 0.3 M C_{Cl^-}. Conditions: $C_M : C_{RX} : C_{CuCl_2} : C_{TPMA} : C_{NaCl}$ = 200:1:0.1:0.1:29. $C_{Cu^{2+}}$ = 5.9×10^{-4} M. [b] HEBiB was used as initiator. [c] pH of 10% v/v MAA in water. [d] $C_{CuCl_2} : C_{TPMA}$ = 0.1:0.4. [e] terpy used as ligand.

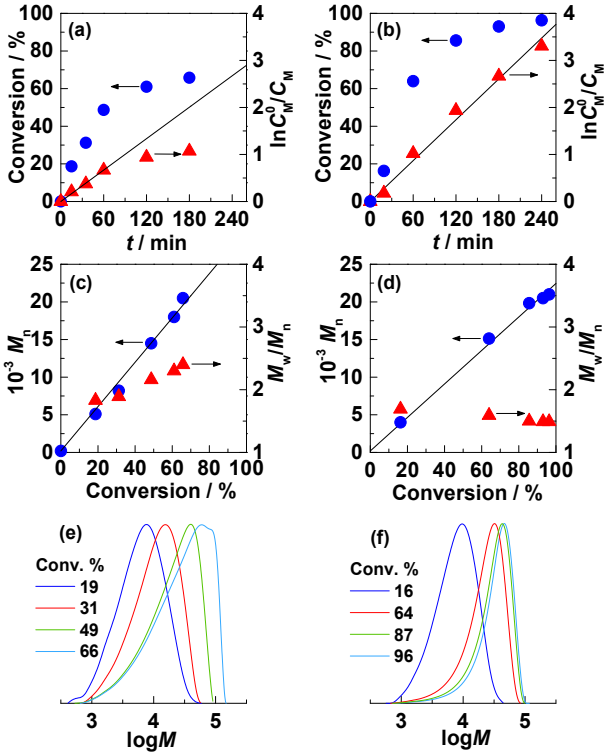

Figure 5.8. First-order kinetic plots (a, b), evolution of molecular weight and molecular-weight distribution (c, d), and GPC traces (e, f) as a function of conversion for *e*ATRP of 10% v/v MAA in H_2O at E_{app} = -0.18 V vs. SCE at pH 2.2 (a, c, e) or at pH 0.9 (b, d, f); NaCl was added to have a total 0.3 M C_{Cl^-}. Conditions: $C_M : C_{RX} : C_{CuCl_2} : C_{TPMA}$ = 200:1:0.1:0.1, $C_{Cu^{2+}}$ = 5.9×10^{-4} M, T = 25 °C.

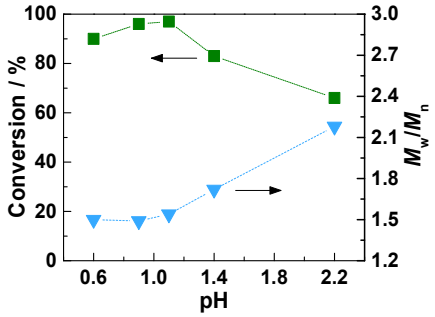

Figure 5.9. Conversion (■) and molecular weight dispersity (▼) of *e*ATRP experiments as a function of pH.

Below pH 1.4, the initiator 2-bromoisobutyric acid (BiBA) was used instead of HEBiB. BiBA is an activated tertiary bromide that better mimics the PMAA chain end. Two experiments performed at pH 1.4 showed that BiBA performed similarly, or slightly better, than HEBiB in terms of control over molecular weights and dispersity (Table 5.2, entries 2-3).

TPMA was not the only ligand able to polymerize MAA in such acidic conditions: *e*ATRP catalyzed by $[Cu^{II}terpy]^{2+}$ (terpy = 2,2';6',2''-terpyridine) at pH 0.9 produced overall similar results (Table 5.2, entry 9). This confirmed the peculiar stability of aromatic amine ligands in acidic environments, compared to aliphatic amine ligands. For example, *N,N,N',N'',N''*-pentamethyldiethylenetriamine (PMDETA) was unable to provide controlled polymers below pH 5.

5.2.3 Modulating polymerization rates

Modulating E_{app} is an easy way to modify the overall rate of *e*ATRP reactions. For example, when $E_{app} - E_{1/2} \approx$ -0.12 V the reaction rate reached its maximum value in 50% v/v BA in DMF.[18] This rate limit is dictated by the mass transport of reagents to and from the electrode surface.

In the *e*ATRP of MAA at pH 0.9, $E_{app} - E_{1/2}$ = (-0.18 + 0.06) V = -0.12 V, therefore Cu^{II} reduction was limited by mass transport and polymerization was proceeding with the highest possible rate. Consequently, the contribution of lactone formation to chain termination was minimized. An experiment was performed at $E_{app} - E_{1/2}$ = -0.04 V (Table 5.2, entry 7), where the reaction rate was not limited by the mass transport. The synthesis was 2.5 times slower, with M_n values not matching the theoretical ones. Nevertheless, molecular-weight distribution (1.43) was slightly lower than eATRP at $E_{app} - E_{1/2}$ = -0.12 V.

Using an excess of ligand was more efficient than E_{app} modulation to reduce dispersity. A TPMA to copper ratio of 4/1 provided better control, both in terms of initiation efficiency and dispersity, with respect to a 1/1 ratio (Table 5.2, entries 5 and 8). Therefore, L/Cu ratio of 4/1 was used in all the succeeding experiments. Another aqueous acidic system, ARGET ATRP of OEOMA promoted by ascorbic acid feeding, showed the same behavior.[19]

A modification of Cu/TPMA structure could cause the shift in the complex standard reduction potential from pure water to pH 0.9 (Figure 5.7). At acidic pH partial protonation of the ligand may occur, which can result in the dissociation of one or more arms of the tetradentate TPMA ligand. Excess TPMA can assist complex formation by binding to vacant coordination sites.

5.2.4 Confirming the "livingness" of the synthesis by using an electrochemical switch

Repetitively stepping E_{app} from –0.2 V to +0.8 V vs. SCE created an electrochemical switch that allowed to activate or deactivate the polymerization *in situ*. The negative potential favors formation of Cu^{I} at the electrode and hence triggers an active state, whereas

the positive potential favors the quick oxidation of Cu^{I} to Cu^{II} and leads to a dormant state (Figure 2.3a). In the first 20 minutes of the experiment, no potential was applied and as a result no monomer conversion occurred (Figure 5.9a). Upon switching the potential to -0.2 V vs. SCE, 22% monomer conversion was observed after ~10 min, at which point the potential was switched to +0.8 V vs. SCE. Once this potential change occurred, Cu^{I} was quickly oxidized and the polymerization halted, achieving negligible monomer conversion over the following 20 min.

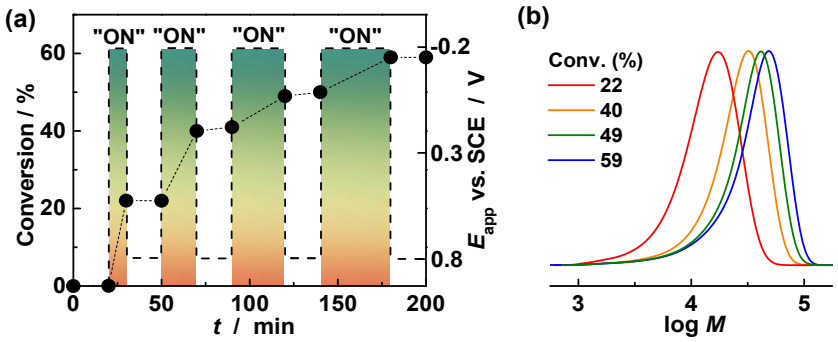

Figure 5.10. (a) Conversion (solid circles) and applied potential (dashed line) with respect to time. (b) Evolution of molecular weight with monomer conversion, after each step at E_{app} = -0.2 V vs. SCE; measured by gel permeation chromatography. Conditions: $C_M : C_{RX} : C_{CuCl_2} : C_{TPMA} : C_{NaCl}$ = 200:1:0.1:0.4:29, T = 25 °C. pH 0.9 was set by addition of HCl.

This electrochemical switch cycle was then repeated for three additional cycles, resulting in an increased monomer conversion to 40, 49, and then to 59% during active periods. Throughout the cycling process, clear shifts to higher molecular weight were observed by GPC (Figure 5.9b) without any detectable lower molecular weight fraction.This behavior is characteristic of a living polymerization: efficient reinitiation of chain ends resulted from preservation of chain end functionality.

5.2.5 High molecular weight PMAA

Syntheses of high molecular weight PMAA were carried out by lowering the initiator concentration. The selected experimental conditions (Table 5.3) allowed to easily obtain polymers with tunable and high M_n: Figure 5.11 shows that molecular weights increased fairly linearly with conversion and that final M_n closely matched the theoretical value (with $M_w/M_n \leq 1.42$). When targeting DP 2000, a polymer with DP > 1000 and M_w/M_n = 1.33 was synthetized in 3 h.

Table 5.3. *e*ATRP of 10% v/v MAA in water targeting different DP, at pH 0.9 and *T* = 25 °C.[a]

	Target DP	*t* (h)	*Q* (C)	Conversion (%)	k_p^{app} (min^{-1})	$M_{n,th}$	$M_{n,app}$	I_{eff}	M_w/M_n
1	200	4	3.2	96	0.014	16800	18000	0.93	1.42
2	500	3	5.9	87	0.010	37600	36500	1.03	1.37
3	1000	3	4.2	66	0.06	57900	60000	0.97	1.33
4	2000	3	3.4	53	0.05	91400	87600	1.04	1.33

[a] pH was set by addition of HCl; NaCl was added to have a constant total 0.3 M C_{Cl^-}. E_{app} = -0.18 V vs. SCE. Conditions: $C_M : C_{CuCl_2} : C_{TPMA} : C_{NaCl} = 200:0.1:0.4:29$. $C_{Cu^{2+}} = 5.9\times10^{-4}$ M. C_{BiBA} was changed to target DP from 200 to 2000.

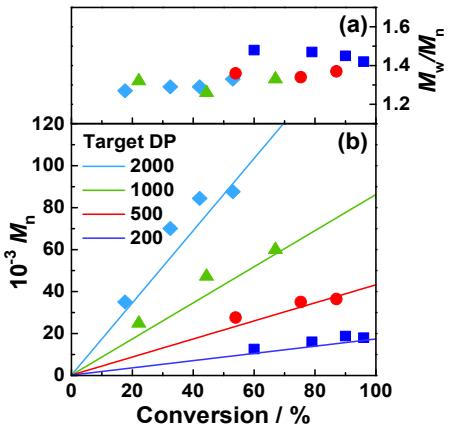

Figure 5.11. Evolution of molecular-weight distributions (a) and molecular weights (b) as a function of conversion for *e*ATRP of 10% v/v MAA in H_2O at E_{app} = -0.18 V vs. SCE at pH 0.9. Conditions: $C_M : C_{CuCl_2} : C_{TPMA} : C_{NaCl} = 200:0.1:0.4:29$. $C_{Cu^{2+}} = 5.9\times10^{-4}$ M. C_{BiBA} was changed to target DP from 200 to 2000. The solid lines represent theoretical M_n.

5.2.6 Different initiators and polymer architectures

Besides BiBA, several other simple and inexpensive organic acids were used as initiators for the synthesis of PMAA (Table 5.4).

Chloroisobutyric acid (CiBA), perfectly matched the chain end and allowed to completely avoid the presence of Br. Unfortunately, CiBA was a slow and inefficient initiator. Figure 5.12 shows that when CiBA was used in place of BiBA, polymerization was much slower and molecular weights diverged from the theoretical values. Isobutyrates were reported to be poor initiators for the synthesis of polymethacrylates, due to penultimate effect.[20] Nevertheless, final M_w/M_n = 1.34 was good, pointing out that polymerization was

well-controlled, but initiation efficiency was very low because activation of P_n-Cl was faster than activation of CiBA. This problem was circumvented when using the more active bromo-initiator, BiBA.

The initiator α-chlorophenylacetic acid (CPAA) was tested to increase initiation efficiency (CPAA structure is similar to that of the extremely active ethyl α-chlorophenylacetate.[21] In this case, M_n closely matched the theoretical value, confirming the simultaneous initiation of all chains. However, the produced polymer had broader dispersity (Table 5.4, entries 1-2).

Table 5.4. *e*ATRP of 10% v/v MAA in water with various initiators, at pH 0.9 and T = 25 °C.[a]

	Initiator	t (h)	Q (C)	Conv. (%)	k_p^{app} (min^{-1})	$M_{n,th}\times10^{-3}$	$M_{n,app}\times10^{-3}$	I_{eff}	M_w/M_n
1	CiBA	4	2.2	67	0.005	11.8	53.8	0.22	1.34
2	CPAA	4	4.1	94	0.012	16.4	17.4	0.95	1.64
3	DCPA	4	5.2	98	0.017	17.1	20.5	0.83	1.37
4	TCAA	4	6.4	99	0.020	17.0	17.6	0.98	1.38
5[b]	TCAA	3	5.8	95	0.017	49.2	42.9	1.15	1.32
6[c]	TCAA	4	5.3	97	0.016	17.0	18.0	0.94	1.41
7[d]	TCAA	4	5.8	98	0.016	17.0	17.5	0.97	1.46

[a] pH was set by addition of HCl; NaCl was added to have a total 0.3 M C_{Cl^-}. E_{app} = -0.18 V vs. SCE. Conditions: $C_M : C_{RX} : C_{CuCl_2} : C_{TPMA} : C_{NaCl}$ = 200:1:0.1:0.4:29. $C_{Cu^{2+}} = 5.9\times10^{-4}$ M. [b] $C_M : C_{TCAA}$ = 200:0.333 (target DP = 600). [c] $C_{CuCl_2} : C_{TPMA}$ = 0.1:0.2. [d] $C_{CuCl_2} : C_{TPMA}$ = 0.1:0.1.

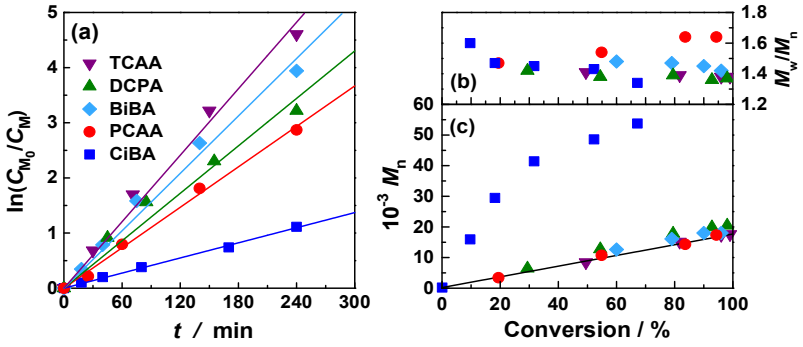

Figure 5.12. (a) First-order kinetic plots and (b) evolution of molecular-weight distributions and (c) molecular weights as a function of conversion for *e*ATRP of 10% v/v MAA in H_2O at E_{app} = -0.18 V vs. SCE at pH 0.9; NaCl was added to have a total 0.3 M C_{Cl^-}; conditions: $C_M : C_{RX} : C_{CuCl_2} : C_{TPMA} : C_{NaCl}$ = 200:1:0.1:0.4:29, T = 25 °C. Polymerization initiators are listed in legend. The black solid line represents theoretical M_n.

Scheme 5.4. From left to right, DCPA initiator and PMAA with degree of polymerization 1 and 2.

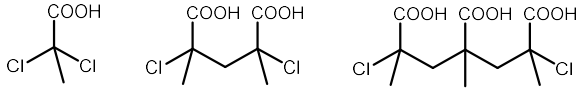

Polychlorinated initiators were used to produce different polymer architectures. 2,2-dichlropropionic acid (DCPA) generated two chains per initiator molecule, producing therefore telechelic polymers. Symmetry of the growing chain guarantees the generation of telechelic polymers: the dormant species are perfectly symmetrical and must consequently grow from both sides (Scheme 5.4).

Trichloroacetic acid (TCAA) allowed to quickly produce polymers with high conversion and low dispersity. As observed when using BiBA as initiator, control improved for higher L/Cu ratios, up to a ratio of 4/1 (Table 5.4). In this case, the growing polymer is not exactly symmetrical and the activation of all three C-Cl bonds of TCAA may be impeded by steric repulsion. Nevertheless, several considerations and experimental evidences suggest that all three C-Cl bonds in TCAA are reactive, therefore allowing the synthesis of well-defined three-arm star polymers. (*i*) Initiator activity increases with the number of halogen atoms, therefore TCAA is more active than both DCPA and BiBA.[14] (*ii*) After activation of the first two C-Cl bonds in TCAA, the remaining C-Cl bond is predicted to be significantly more active than the chain end because is subjected twice to the penultimate effect.[20] (*iii*) Figure 5.12a, Table 5.4 and Table 5.5 show that, in both *e*ATRP and SARA-ATRP, the apparent rate of polymerization, k_p^{app} sharply increased

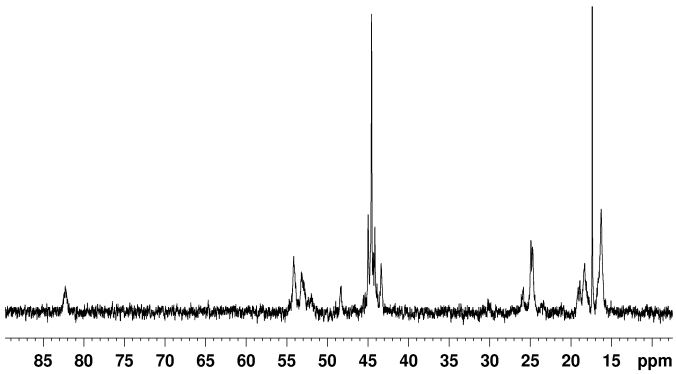

Figure 5.13. ^{13}C NMR of the polymerization mixture, obtained with TCAA initiator. Conditions: $C_M : C_{RX} : C_{Cu(OTf)_2} : C_{TPMA} : C_{NaCl} : C_{HCl}$ = 20:1:0.0001: 0.03:3:2, in 10% v/v MAA in D_2O, total V = 5 mL, 10 cm Cu wire with diameter d = 1 mm).

with the number of halogen atoms in the initiator (BiBA (1 halogen atom) < DCPA (2) < TCAA(3)). In other words, DCPA and TCAA behave as if the concentration of active halogen atoms was two or three times higher, respectively, than in the case of BiBA. (*iv*) A SARA ATRP targeting DP 20 was carried out for relatively long times (2 h), allowing all chains to terminate (conditions: $C_M : C_{RX} : C_{Cu(OTf)_2} : C_{TPMA} : C_{NaCl} : C_{HCl}$ = 20:1:0.0001:0.03:3:2, in 10% v/v MAA in D_2O, total V = 5 mL, 10 cm Cu wire with diameter d = 1 mm). ^{13}C NMR of the polymerization mixture (Figure 5.13) did not show any peak in the range typical of C-Cl bonds, $55 < \delta(^{13}C) < 70$.[14] This indicates that all three chlorine atoms of TCAA reacted with $[Cu^{I}L]^{+}$.

5.2.7 SARA ATRP

With the aim of testing a different ATRP method, a series of experiments was conducted (re)generating the active Cu^{I} complex through comproportionation, in the presence of a Cu wire (SARA ATRP). Cu^0 was both a reducing agent of Cu^{II} and a supplemental activator of the C-X bond. SARA ATRP setup is simpler than *e*ATRP, which requires electrochemical instrumentation. It has to be considered that water typically promotes fast disproportionation, not comproportionation, of Cu^{I}. However, both the presence of a high C_{X^-} and the higher reduction potential of the catalyst favor the fast comproportionation of Cu^0 and Cu^{II} species.

Table 5.5. SARA ATRP of 10% v/v MAA in water with various initiators, at pH 0.9 and T = 25 °C.[a]

En.	Initiator	t (h)	Conv. (%)	k_p^{app} (min^{-1})	$M_{n,th}\times10^{-3}$	$M_{n,app}\times10^{-3}$	I_{eff}	M_w/M_n
1	BiBA	1.7	79	0.017	14.9	19.5	0.76	1.44
2	DCPA	2.5	96	0.023	16.8	23.7	0.71	1.25
3	TCAA	1.2	94	0.043	16.3	18.9	0.87	1.33

[a] pH was set by addition of HCl. Conditions: $C_M : C_{RX} : C_{CuCl_2} : C_{TPMA} : C_{NaCl}$ = 200:1:0.01:0.3:29; 10 cm Cu wire (d = 1 mm). Total V = 5 mL.

Copper wire (10 cm, d = 1 mm) was able to promote a fast and sufficiently controlled ATRP of 10% v/v MAA in water with three different initiators (Table 5.5). With the initiators DCPA and TCAA, good levels of control over molecular-weight distributions ($M_w/M_n \leq 1.33$) were observed. SARA ATRPs were faster than the corresponding *e*ATRPs, and reached high to very high conversions in only about two hours. Agreement

between experimental and theoretical M_n values was satisfactory. This result proved that synthesis of PMAA in acidic conditions is flexible and versatile, because similar successful results were obtained using different low-ppm polymerization methods (*e*ATRP and SARA-ATRP).

5.3 Electrochemically mediated ATRP of acrylic acid

Electrochemical polymerization with NaCl supporting electrolyte under acidic conditions was successfully applied to acrylic acid (AA), by using the bifunctional DCPA initiator (Table 5.6). In this case, no HCl was added, but the polymerization rate was lower because of lower activity of the secondary C-Cl chain end of AA, compared to the tertiary chain end of MAA. To increase reaction rate, relatively negative E_{app} = -0.30 V vs. SCE was applied. In addition, a larger electrode area was used (15 cm^2 for AA vs. 6 cm^2 for MAA polymerization). Put together, these two expedients led to a reasonable reaction time (4-5 h), but considerably increased the charge consumption (>10 C), mainly because of a concurrent H^+ reduction.

Table 5.6. *e*ATRP of 10% v/v AA in water with different C_{NaCl}, T = 25 °C.[a]

En.	RX	C_{RX}/C_{Cl}-	E_{app} (V vs. SCE)	t (h)	Q (C)	Conv (%)	k_p^{app} (h^{-1})	$M_{n,th}$	$M_{n,app}$	I_{eff}	$Đ$
1	DCPA	1/12	-0.30	5	16.2	55	0.15	7000	13000	0.54	1.50
2	DCPA	1/4	-0.30	5	14.6	80	0.31	10200	15700	0.65	1.43
3	DCPA	1/1.2[b]	-0.30	4	10.2	91	0.57	11500	20300	0.57	1.45

[a] measured pH was 2.0. Conditions: $C_M : C_{DCPA} : C_{CuCl_2} : C_{TPMA}$ = 175:1:0.1:0.4; C_{Cu} = 8.3×10^{-4} M; geometrical electrode area 15 cm^2. [b] 0.09 M Et_4NBF_4 was added.

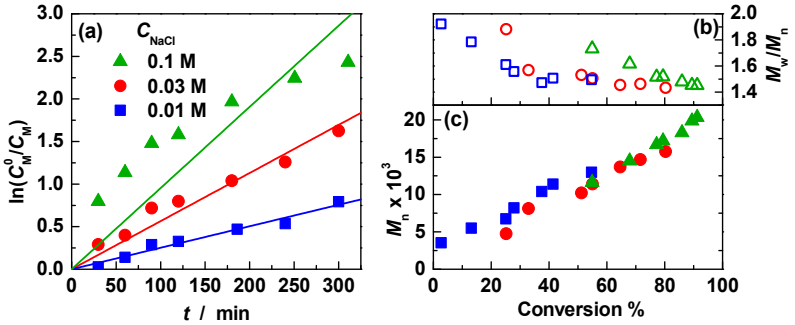

Figure 5.14. (a) First-order kinetic plots and (b) evolution of molecular-weight distributions and (c) molecular weights as a function of conversion for *e*ATRP of 10% v/v AA in H_2O at E_{app} = -0.30 V vs. SCE at pH 0.9, with different NaCl concentrations.; conditions: $C_M : C_{DCPA} : C_{CuCl_2} : C_{TPMA}$ = 175:1:0.1:0.4, T = 25 °C.

The effect of NaCl concentration was investigated (Table 5.6, entries 1-3). A clear increase in polymerization rate was observed with decreasing C_{Cl^-}, because of decreasing formation of the inactive [Cl-Cu^{I}L] species. A 0.03 M NaCl concentration provided better control in terms of narrow dispersity, molecular weight close to the theoretical value, and linear kinetics of monomer consumption (Figure 5.14).

5.4 Conclusions

To understand why ATRP of acidic monomers is problematic, the catalytic system composed of the complex Cu/TPMA and the initiator HEBiB was investigated in aqueous methacrylic acid (MAA). Simple electrochemical methods (cyclic voltammetry) and spectroscopic techniques (vis-NIR titration) confirmed the stability of both the copper complex and initiator in the presence of MAA and PMAA. Analysis of the consumed charge during *e*ATRP electrolysis proved that radical-radical termination did not stop the polymerization. Detailed 2D NMR of the chain end showed that early termination of the growing polymers was caused by an intramolecular cyclization reaction with the terminal halogen as leaving group.

Once the main cause of termination was determined, three approaches allowed to exceptionally increase conversion and improve control over PMAA growth: *(i)* using Cl as chain end halogen, *(ii)* lowering the pH to 0.9, *(iii)* increasing the polymerization rate. MAA was polymerized by relatively low ppm (500 ppm) copper ATRP with adequate control over molecular weight dispersity ($M_w/M_n < 1.5$) and M_n in very good agreement with theoretical values. Both *e*ATRP and SARA ATRP could efficiently control the reaction, which proceeded with fast kinetics at ambient temperature (up to 99% conversion in 4 h), and required inexpensive and relatively non-toxic reagents (NaCl, diluted HCl and water). The living and controlled nature of the process was demonstrated by linear first-order kinetics, linear increase in polymer molecular weight with monomer conversion, and the possibility to completely reactivate the polymerization by stepping the applied potential.

A variety of simple and inexpensive carboxylic acids were used as initiators. Bromoisobutyric acid (BiBA), 2,2-dichloropropionic acid (DCPA) and trichloroacetic acid (TCAA) were found to be excellent initiators, yielding linear, telechelic and three-arm stars PMAA, respectively. The bifunctional DCPA initiator was also successfully applied to the electrochemically mediated ATRP of acrylic acid.

RAFT polymerization is currently the most often used technique for the controlled polymerization of methacrylic acid. In comparison to the obtained results, RAFT is characterized by somewhat superior livingness and control over molecular-weight dispersity ($Đ < 1.3$ vs. ≤ 1.4). On the other hand, ATRP proceeded at significantly lower temperature (25 °C vs. $\geq$ 60 °C) and required commercially available reagents, while most of RAFT chain transfer agents must be synthetized. Overall, the successful direct synthesis of an acidic polymer allowed to overcome one of the biggest limitations of ATRP, and proved that water is an excellent solvent for the atom transfer radical polymerization of polar monomers.

References

(1) Mori, H.; Müller, A. H. E. *Prog. Polym. Sci.* **2003**, *28*, 1403–1439.

(2) Fantin, M.; Isse, A. A.; Gennaro, A.; Matyjaszewski, K *Marcomolecules* **2015**, *48*, 6862-6875.

(3) Fleischmann, S.; Percec, V. *J. Polym. Sci. Part A Polym. Chem.* **2010**, *48*, 4884–4888.

(4) Treat, N. J.; Fors, B. P.; Kramer, J. W.; Christianson, M.; Chiu, C. Y.; Alaniz, J. R. De; Hawker, C. J. *ACS Macro Lett.* **2014**, *136*, 580–584.

(5) Fors, B. P.; Hawker, C. J. *Angew. Chem., Int. Ed.* **2012**, *51*, 8850–8853.

(6) Burguière, C.; Pascual, S.; Bui, C.; Vairon, J. P.; Charleux, B.; Davis, K. a.; Matyjaszewski, K.; Bétremieux, I. *Macromolecules* **2001**, *34*, 4439–4450.

(7) Ashford, E. J.; Naldi, V.; O'Dell, R.; Billingham, N. C.; Armes, S. P. *Chem. Commun.* **1999**, *14*, 1285–1286.

(8) (a) Chiefari, J.; Chong, Y. K.; Ercole, F.; Krstina, J.; Jeffery, J.; Le, T. P. T.; Mayadunne, R. T. A.; Meijs, G. F.; Moad, C. L.; Moad, G.; Rizzardo, E.; Thang, S. H. *Macromolecules* **1998**, *31*, 5559–5562. (b) Chaduc, I.; Lansalot, M.; D'Agosto, F.; Charleux, B. *Macromolecules* **2012**, *45*, 1241–1247.

(9) Couvreur, L.; Lefay, C.; Belleney, J.; Charleux, B.; Guerret, O.; Magnet, S. *Macromolecules* **2003**, *36*, 8260–8267.

(10) (a) Lacík, I.; Beuermann, S.; Buback, M. *Macromol. Chem. Phys.* **2004**, *205*, 1080-1087. (b) Lacík, I.; Učňova, L.; Kukučková, S.; Buback, M.; Hesse, P.; Beuermann, S. *Macromolecules* **2009**, *42* , 7753-7761.

(11) Tsarevsky, N. V.; Pintauer, T.; Matyjaszewski, K. *Macromolecules* **2004**, *37*, 9768–9778.

(12) Matyjaszewski, K. *Macromolecules* **2012**, *45*, 4015–4039. Actually, the fraction of radical-radical terminated chain is ≤ 9%, because charge *Q* determined from chronoamperometry can be overestimated because of reduction of oxygen, impurities or reduction of water to hydrogen.

(13) *Spectral Database for Organic Compounds (SDBS)*; ^{13}C NMR spectrum; SDBS No.: 2408; http://sdbs.db.aist.go.jp/sdbs/cgi-bin/direct_frame_disp.cgi?sdbsno=2408 (accessed December 25, 2015).

(14) Destarac, M.; Matyjaszewski, K.; Boutevin, B. *Macromol. Chem. Phys.* **2000**, *201*, 265–272.

(15) Peng, C. H.; Kong, J.; Seeliger, F.; Matyjaszewski, K. *Macromolecules* **2011**, *44*, 7546–7557.

(16) Bard, A. J.; Faulkner, L. R. *Electrochemical Methods: Fundamentals and Applications*, 2nd Ed.; Wiley: New York, NY, USA, 2001, p. 231.

(17) (a) Qiu, J.; Matyjaszewski, K.; Thouin, L.; Amatore, C. *Macromol. Chem. Phys.* **2000**, *201*, 1625−1631. (b) Matyjaszewski, K.; Goebelt, B.; Paik, H. J.; Horwitz, C. P. *Macromolecules*

2001, *34*, 430−440. (c) Braunecker, W. A.; Tsarevsky, N. V.; Gennaro, A.; Matyjaszewski, K. *Macromolecules* **2009**, *42* , 6348–6360.

(18) Magenau, A. J. D.; Bortolamei, N.; Frick, E.; Park, S.; Gennaro, A.; Matyjaszewski, K. *Macromolecules* **2013**, *46*, 4346-4353.

(19) Simakova, A.; Averick, S. E.; Konkolewicz, D.; Matyjaszewski, K. *Macromolecules* **2012**, *45*, 6371-6379.

(20) Lin, C. Y.; Coote, M. L.; Petit, A.; Richard, P.; Poli, R.; Matyjaszewski, K. *Macromolecules* **2007**, *40*, 5985–5994.

(21) Tang, W.; Kwak, Y.; Braunecker, W.; Tsarevsky, N. V.; Coote, M. L.; Matyjaszewski, K. *J. Am. Chem. Soc.* **2008**, *130*, 10702−10713.

Chapter 6

Role of the Cathodic Material in Aqueous *e*ATRP

One of the drawbacks of electrochemically mediated ATRP, in its current state of development, is the requirement that both the working and counter electrodes are made of platinum, a noble, expensive, rare and non-functionalizable metal. In *e*ATRP, the working electrode (WE) acts only as a source of electrons for the reduction of the deactivating $[X\text{-}Cu^{II}L]^+$ species to the active $[Cu^{I}L]^+$ complex. Since the WE is not directly involved in the polymerization process, Pt can be replaced with any other material able to offer a working potential window wide enough for the reduction of all Cu^{II} species to be achieved without interference from other reduction/oxidation processes. As a proof of concept of the viability of efficient *e*ATRP without Pt electrodes, controlled polymerizations of 10% (v/v) OEOMA in water, catalyzed by Cu/TPMA, were investigated employing different cathodic materials such as glassy carbon, graphite, gold, nickel, nickel-chromium, stainless steel, and titanium. Potential side reactions in water, such as electrode oxidation/corrosion, release of metals in solution and direct Cu^{II} reduction by the metal electrodes, were taken into account.

6.1 Evaluation of working electrode properties

Voltammetric behavior of the electrodes in the polymerization medium. Electrode materials were tested to check their compatibility with the polymerization environment. In particular, a good electrode material should not undergo oxidation or corrosion at the applied potential during *e*ATRP. Figure 6.1 shows linear sweep voltammetry of all tested electrodes in a typical polymerization medium (OEOMA/HEBiB/TPMA/Et_4NBr = 216/2/1/1/100, $C_{Cu} = 10^{-3}$ M, V_{tot} = 15 mL, T = 25 °C). Each electrode material was initially polished with 1000, 2500, 4000 grit sandpapers, and then with 3, 1 and 0.25 μm diamond pastes (with ultrasonic rinsing between each step). Before each experiment, cleaning with the diamond pastes was repeated. As shown in the figure the onset potential

of the anodic discharge limit strongly depends on the nature of the electrode material. The observed anodic current is due to oxidation of the electrode itself, except in the case of Pt, Au and carbon-based electrodes, which do not easily undergo oxidation. The anodic wave on these electrodes is attributed to oxidation of the electrolyte. Whatever the nature of the oxidation process, the anodic wave is indicative of the stability of the system towards oxidation and defines the working potential window offered by each electrode material. The onset potential of the anodic wave at each electrode in Figure 6.1 should be compared to the typical applied potential (E_{app}) during *e*ATRP. E_{app} in aqueous media is typically ~ -0.2 V vs. SCE, a value slightly more positive than $E_{1/2}$ of the copper complex. Such E_{app} allowed performing fast polymerization of OEOMA with good control on molecular weights (Chapter 4). Figure 6.1 shows that, in correspondence of typical E_{app} (vertical dotted line in Fig. 6.1), Fe is quickly oxidized and therefore is not suitable for *e*ATRP in aqueous systems. Cu is only slowly oxidized, while all other electrodes are stable. A passivating oxide layer protects the non-noble metals Ni, NiCr, Ti and 304 stainless steel (304SS).

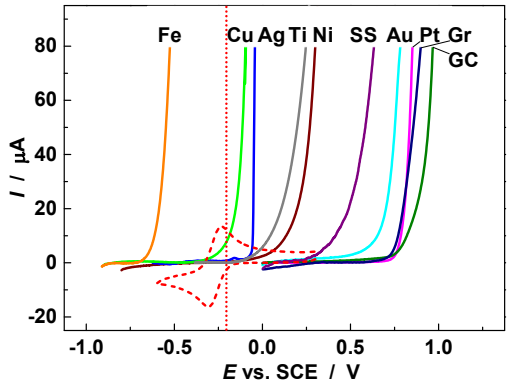

Figure 6.1. Linear sweep voltammetry at v = 0.2 V s^{-1} recorded on various working electrodes, labeled on the curves, in 10% v/v OEOMA in water + 0.1 M Et_4NBr (solid lines). Electrode area = 0.03 - 0.1 cm^2. Cyclic voltammetry of 10^{-3} M $[Cu^{II}TPMA]^{2+}$ in the same solvent (red dashed line). Typical E_{app} of aqueous *e*ATRP (-0.2 V vs. SCE, vertical red dotted line). T = 25 °C. Gr = graphite, GC = glassy carbon.

Blank tests: ARGET ATRP catalyzed by zerovalent metals. Blank tests were carried out to determine if the metal electrodes could reduce $[Cu^{II}L]^{2+}$ to the active $[Cu^{I}L]^{+}$ and start the ATRP reaction without any applied potential, according to the so-called ARGET ATRP procedure.[1] Conditions were: OEOMA/HEBiB/$Cu(OTf)_2$/TPMA/Et_4NBr = 216/2/1/1/100, C_{Cu} = 10^{-3} M, V_{tot} = 15 mL, T = 25 °C, in the presence of a polished metal.

All metals were tested, except Fe that was considered not suitable because of its very low oxidation potential. For all tested metals, except Cu, very limited monomer conversion (≤ 5%) was observed after 4 h. Therefore, they could be used in *e*ATRP without significant interference of reactions involving the WE material. Conversely, Cu wire was able to effectively start the polymerization, by the formation of $[Cu^{I}L]^{+}$ through comproportionation with Cu^{II} species (this process is called SARA ATRP).[2] Usually, SARA ATRP reactions are conducted in the presence of excess amine ligand, to push the comproportionation equilibrium (eq. 6.1) toward Cu^{I} formation.[3] In this case, the reaction was carried out in the absence of excess amine ligand ($C_{Cu} = C_{TPMA}$), so that comproportionation through reaction 6.1 was impeded. Nevertheless, Br^{-} could also act as ligand[4] and promote the comproportionation reactions in eqs. 6.2 and 6.3.

$$Cu^{0} + [Cu^{II}L]^{2+} + L \rightleftharpoons 2[Cu^{I}L]^{+} \quad (6.1)$$

$$Cu^{0} + [Cu^{II}L]^{2+} + 2Br^{-} \rightleftharpoons [Cu^{I}L]^{+} + Cu^{I}Br_{2}^{-} \quad (6.2)$$

$$Cu^{0} + [Br\text{-}Cu^{II}L]^{2+} + Br^{-} \rightleftharpoons [Cu^{I}L]^{+} + Cu^{I}Br_{2}^{-} \quad (6.3)$$

The polymerization in the presence of Cu wire was fast and well-controlled, reaching 96% conversion with a dispersity around 1.2 (entry 9 in Table 6.1). This result pointed out that a Cu electrode cannot be used in *e*ATRP without also triggering a SARA ATRP reaction. On the other hand, this proved that SARA ATRP can be carried out in the absence of excess amine ligand, exploiting the presence of bromide anions as Cu^{I} ligands. This is a substantial improvement of SARA ATRP, since amine ligands usually are by far the most expensive reagent of ATRP reactions.

6.2 Potentiostatic *e*ATRP

*e*ATRP experiments were carried out with all tested metals as working electrodes, except Fe and Cu (Table 6.1). E_{app} was chosen from cyclic voltammetry (CV) of the copper complex (Figure 6.2a).[5] On a 3-mm diameter GC disk (routinely used for CV analysis) as well as on bulky electrodes (used for the bulk electrolysis), CV of $[Cu^{II}TPMA]^{2+}$ presents a quasi-reversible peak couple, with $\Delta E_p = E_{pc} - E_{pa} = 0.072$ V and 0.109 V respectively. A similar behavior was observed on noble metal electrodes, Pt and Au (both small disks and bulky electrodes). Therefore, in these cases the same fixed potential (potentiostatic condition, $E_{app} = -0.2$ V vs. SCE) was applied during the polymerization.

On graphite, silver and other non-noble metals, the voltammetric response of the catalyst was electrochemically much less reversible, with $\Delta E_p > 0.250$ V. The thin layer of non-conductive oxides present on the surface of non-noble metals increases the distance at which electron transfer can occur, thus reducing the heterogeneous electron transfer rate.[6] Figure 6.2b shows cyclic voltammograms of $[Cu^{II}TPMA]^{2+}$ recorded on bulky GC and Ni electrodes. Electron transfer to $[Cu^{II}TPMA]^{2+}$ is much faster on GC than on Ni and this is reflected on cyclic voltammetry of the system both in the absence and presence of the initiator HEBiB. When there is no initiator, the effect of the reduced rate of electron transfer is manifested as a large separation between the cathodic and anodic peaks, whereas in the presence of initiator, the effect is a shift of the catalytic reduction wave to more negative potentials. To take into account the less reversible behavior of Cu^{II} reduction on non-noble metals, silver and graphite, E_{app} was chosen to obtain roughly the same cathodic current (in the presence of 2 mM HEBiB) observed on the GC electrode. This is shown in Figure 6.2b for the Ni electrode. Table 6.1 reports E_{app} values and results of the electrochemical polymerizations under potentiostatic conditions of 10% v/v OEOMA in water for each WE.

Pt, Au and GC could efficiently reduce $[Cu^{II}TPMA]^{2+}$ to the active $[Cu^{I}TPMA]^{+}$, triggering a fast and well-controlled polymerization of OEOMA (Figure 6.3). Polymer M_n was close to the theoretical values and dispersity was narrow. As expected, the reaction rate increased with increasing electrode area. Mechanical cleaning of the working electrodes was important: when an unpolished, new GC plate was used, the current dropped to ~ 0 A after few minutes and no polymer was produced.

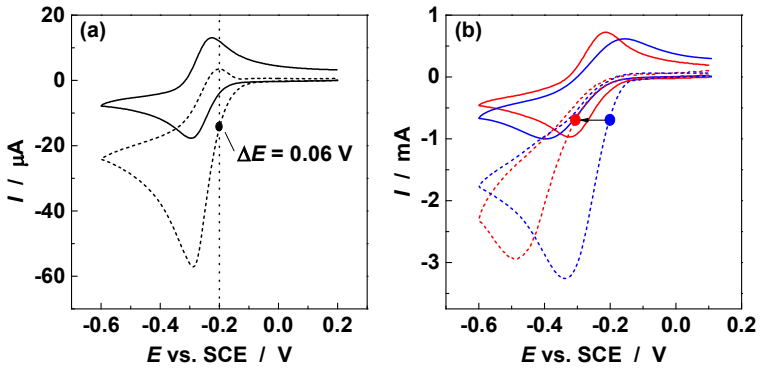

Figure 6.2. Cyclic voltammetry of 10^{-3} M $[Cu^{II}TPMA]^{2+}$ in 10% v/v OEOMA in water + 0.1 M Et_4NBr on a GC disk electrode (a) or on bulky GC (b, red lines) and Ni (b, blue lines) electrodes. The CVs were recorded in the absence (solid lines) and presence (dashed lines) of 2×10^{-3} M HEBiB.

Table 6.1. Potentiostatic *e*ATRP of 10% v/v OEOMA in H_2O with different WE.[a]

	WE	A[b] (cm^2)	E_{app}[c]	t (h)	Q (C)	Conv (%)[c]	$M_{n,th}$	$M_{n,app}$	$k_p^{app} \times 10^2$ (min^{-1})[d]	$Đ$	I_{eff}[e] (%)
1	Pt	6	-0.20	4	3.2	95	51500	62000	1.28	1.17	0.83
2	Au	5	-0.20	4	3.8	89	48200	62000	0.90	1.25	0.78
3	GC	4	-0.20	5.5	2.0	92	50100	63600	0.75	1.15	0.79
4	Ti	5	-0.20	6	0.2	56	30500	53800	0.15	1.17	0.57
5	Ni	9	-0.32	1.5	3.4	87	46200	58200	0.02	1.56	0.79
6	NiCr	5	-0.32	5.5	0.6	64	35300	63900	0.22	1.08	0.55
7	304SS	5	-0.32	6	3.2	90	48600	137100	0.68	1.76	0.35
8	Ag	4	-0.32	2	0.4	6	-	-	-	-	-
9	Gr	4	-0.32	2	0.4	8	-	-	-	-	-
10	Cu	6	-[f]	4	-	96	52100	49700	1.50	1.18	1.05

[a] Polymerization conditions: OEOMA/HEBiB/$Cu(OTf)_2$/TPMA/Et_4NBr = 216/2/1/1/100, C_{Cu} = 10^{-3} M, V_{tot} = 15 mL, T = 25 °C. [b] Estimated electrode geometric surface area. [c] V vs. SCE. [d] The slope of the linear plot of $\ln(C_M^0/C_M)$ vs. time. [e] $M_{n,th}/M_{n,app}$ ratio. [f] SARA ATRP conditions: OEOMA/HEBiB/$Cu(OTf)_2$/TPMA/Et_4NBr = 216/2/1/1/100, C_{Cu} = 10^{-3} M, V_{tot} = 15 mL, T = 25 °C.

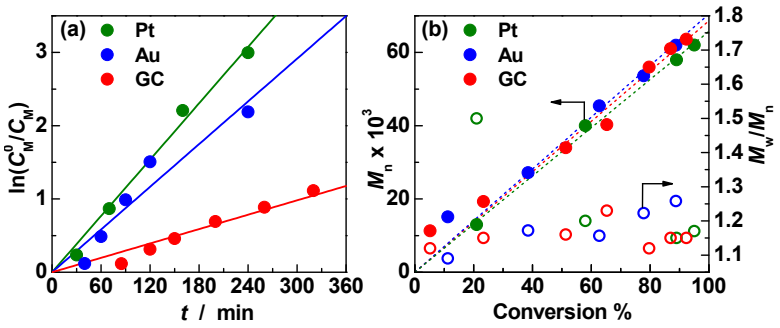

Figure 6.3. Potentiostatic *e*ATRP of OEOMA 10% v/v in H_2O, (a) monomer consumption versus time, and (b) molecular weight increment and change in dispersity with conversion. Other conditions: OEOMA/HEBiB/$Cu(OTf)_2$/TPMA/Et_4NBr = 216/2/1/1/100, C_{Cu} = 10^{-3} M, V_{tot} = 15 mL, T = 25 °C.

All non-noble metals could also trigger OEOMA polymerization. When WE = Ti or NiCr, the dispersity of POEOMA was very narrow, but an induction period of *ca.* 2 hours was observed, during which no polymerization occurred. Conversion after 6 h reached only 56% with Ti and 64% (after 5.5 h) with NiCr, and the polymerization rates were about one order of magnitude lower than with Pt working electrode. Moreover, the initi-

ator efficiency, which accounts for the number of chains effectively started by RX initiator molecules, was only about 0.5. It is possible that generated radicals interacted with the electrode metal instead of propagating by addition to the monomer.

When WE = Ni or 304SS, chronoamperometry curves recorded during *e*ATRP showed increasing current in the first ~20 minutes of electrolysis, instead of the typically observed decrease in current due to $[Cu^{II}L]^{2+}$ consumption (Figure 6.4a). A possible explanation for this unusual behavior is that initially the oxide layers are consumed by reduction at the applied potential, which significantly modifies the surface properties of the electrode (e.g. by "activation", increase of surface roughness, *etc.*). A faster electron transfer may take into account for the observed increase in the current. Because of the high current, the polymerization was very fast, but poorly controlled.

Silver and graphite could not effectively trigger a controlled polymerization; less than 10% monomer conversion was observed after 2 hours. Deposition of a layer of polymer/oligomer on the graphite surface occurred during electrolysis.

Overall, these results pointed out that most of the tested electrode materials could reduce selectively Cu^{II} species and trigger the polymerization under potentiostatic conditions (fixed E_{app}). When non-noble metals were used as WE, control over reaction parameters was difficult, and slow reaction rates or uncontrolled polymerization were observed. These problems could be solved by reducing Cu^{II} under galvanostatic conditions (fixed current), as explained in the next section.

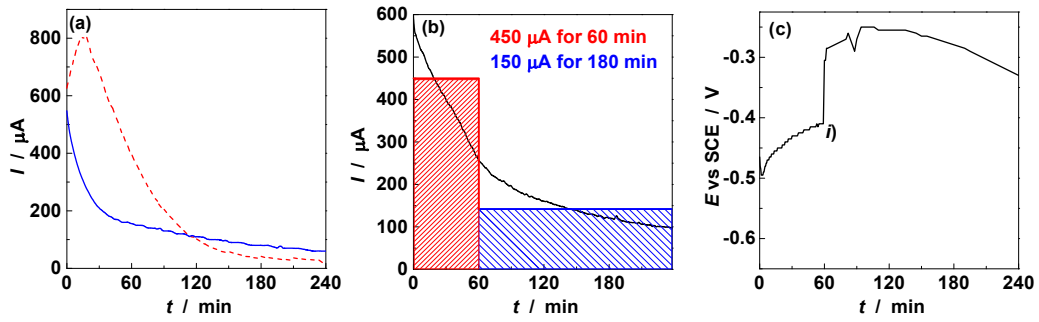

Figure 6.4. (a) Chronoamperometry recorded during *e*ATRP of OEOMA 10% v/v in H_2O, using Pt at -0.2 V vs. SCE (blue solid line) or Ni at -0.32 V vs. SCE (red dashed line) as working electrode. (b) Splitting of the Pt chronoamperometry curve in two galvanostatic steps. (c) Chronopotentiometry recorded during a galvanostatic *e*ATRP of OEOMA 10% v/v in H_2O at a Ni working electrode: at point i) the initial current of -0.45 mA was changed to -0.15 mA. Other *e*ATRP conditions: OEOMA/HEBiB/$Cu(OTf)_2$/TPMA/Et_4NBr = 216/2/1/1/100, $C_{Cu} = 10^{-3}$ M, V_{tot} = 15 mL, T = 25 °C.

6.3 Galvanostatic *e*ATRP

Switching from potentiostatic (fixed potential) to galvanostatic (fixed current) experiments solved several problems: *i*) it was not necessary to choose E_{app} through a preliminary cyclic voltammetry experiment; *ii*) electrolysis was less susceptible to changes in electrode surface properties, *iii*) the syntheses were less influenced by WE area. Moreover, in comparison to a potentiostatic system, a galvanostatic electrolysis process requires a much simpler two-electrode system and can be performed with a current generator (instead of a three-electrode system and a potentiostat). On the other hand, galvanostatic experiments required careful selection of the applied current (or current steps). This was done by using the chronoamperometry response obtained during a well-controlled *e*ATRP with Pt working electrode (Figure 6.4b). The curve was split in two parts, an initial one at higher current, to allow the initial quick reduction of Cu^{II} to Cu^{I}, and a second one at lower current, to slowly regenerate Cu^{I} by reduction of any $[X\text{-}Cu^{II}L]^{+}$ arising from radical-radical termination reactions. Figure 6.4c shows a chronopotentiometry recorded during a galvanostatic experiment with a Ni working electrode. The working potential (*E*) initially became less negative, but, after a certain time, a turning point beyond which *E* shifted back toward the negative direction was observed. A similar behavior was observed also for 304SS. These findings are in line with the unusual trends of the current previously observed during controlled-potential electrolysis at both electrodes. In the initial stages of electrolysis, under both potentiostatic and galvanostatic conditions, reduction of the surface oxide films takes place, resulting in activation of the electrode. Since a more active electrode surface requires smaller overpotential to maintain the fixed applied current, the working potential shifts to less negative values. Once the surface has been fully activated, the concentration overpotential arising from consumption of $[Cu^{II}TPMA]^{2+}$ becomes more important and the potential shifts to more negative values.

Galvanostatic *e*ATRP with Ag as working electrode showed excellent results (Table 6.2, entry 1). Conversion of 90% was reached in 3 hours, with good control over molecular weights and dispersities.

For the other metals (Ni, NiCr, 304SS), galvanostatic conditions provided higher conversions (Table 6.2), but broad dispersities and low initiator efficiency. Moreover, induction periods were observed (see as example the 1-2 h induction period in Figure 6.5a,c, WE = NiCr). A successful approach to avoid these problems is presented in the next section.

Table 6.2 Galvanostatic *e*ATRP of 10% v/v OEOMA in H_2O with different WE.[a]

	WE	t (h)	Q (C)	Conv (%)	$M_{n,th}$	$M_{n,app}$	$k_p^{app} \times 10^{2}$ [b] (min^{-1})	$Đ$	I_{eff} [c] (%)
1	Ag	3	2.7	90	48.5	59.7	1.01	1.32	0.81
2	Ni	4	3.2	83	45.2	91.8	0.84	1.29	0.48
3	NiCr	5	3.8	93	50.7	86.8	1.02	1.16	0.58
4	304SS	4	3.2	79	42.7	130	0.50	1.18	0.33

[a] Polymerization conditions: OEOMA/HEBiB/$Cu(OTf)_2$/TPMA/Et_4NBr = 216/2/1/1/100, C_{Cu} = 10^{-3} M, V_{tot} = 15 mL, T = 25 °C. Current steps: 0.45, 0.15 mA for 1, 3 h. [b] The slope of the linear plot of $\ln(C_{M_0}/C_M)$ vs. time. [c] Ratio $M_{n,th}$ / $M_{n,app}$.

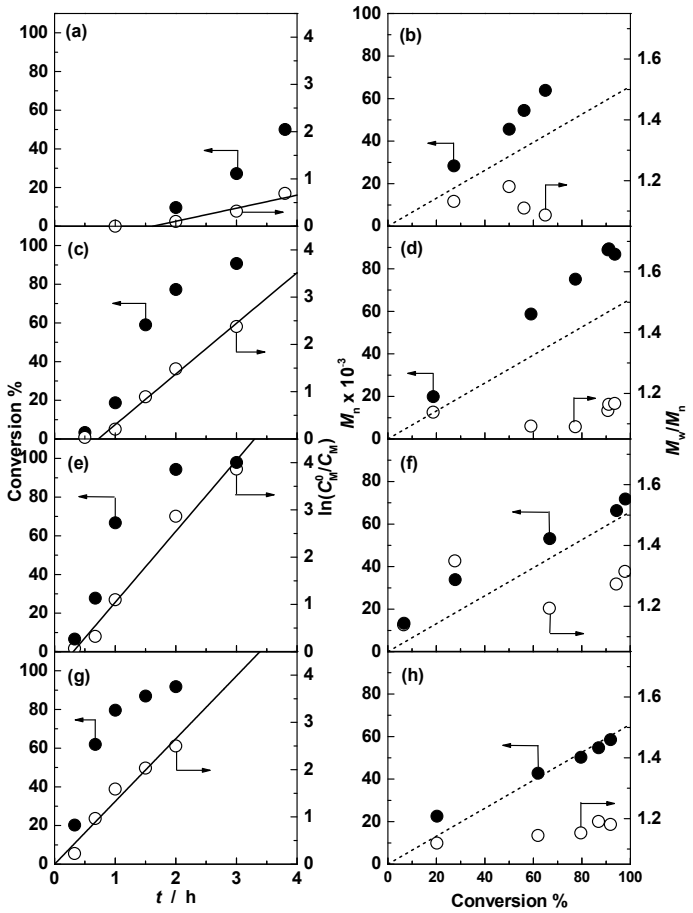

Figure 6.5. First-order kinetic plots (a, c, e, g) and evolution of molecular weight and molecular-weight distribution (b, d, f, h) for the *e*ATRP of OEOMA 10% v in H_2O, WE = NiCr. (a, b) Potentiostatic conditions, E_{app} = -0.320 V vs. SCE. (c, d) Galvanostatic conditions with 2 current steps (0.45, 0.15 mA for 60, 240 min). (e, f) Galvanostatic conditions with 2 current steps (0.45, 0.15 mA for 35, 215 min; pre-electrolysis: 0.45 mA for 25 min). (g, h) Galvanostatic conditions 4 current steps (0.52, 0.35, 0.2, 0.12 mA for 8, 45, 60, 130 min; pre-electrolysis: 0.52 mA for 22 min). Conditions: OEOMA/HEBiB/$Cu(OTf)_2$/TPMA/Et_4NBr = 216/2/1/1/100, C_{Cu} = 10^{-3} M, V_{tot} = 15 mL, T = 25 °C.

6.3.1 Galvanostatic *e*ATRP with pre-electrolysis of Cu^{II}

In general, *e*ATRP with metal electrodes showed long induction periods after which polymerization starts but often with low initiator efficiency (*i.e.* a significant portion of the initiator RX was consumed, without reacting with the monomer, in the initial part of the electrolysis). This suggested that, at the beginning of the experiment, side reactions may occur between the working metal electrode and RX (or radicals generated from RX reduction). A well-controlled ATRP started only after a certain period of time (1-3 h), when a significant quantity of Cu^{II} was reduced to Cu^{I}. It should be noted that many reactions in competition with ATRP can occur in the presence of transition metals, for example organometallic mediated polymerization and other reactions involving direct interaction between radical and the metal center.[7] Our approach to solve this problem was to produce in solution a significant amount of the active complex $[Cu^{I}L]^{+}$ before adding the initiator. In this way, the initiator would be immediately involved in the ATRP equilibrium, and side reactions occurring with the transition metal would be minimized. Moreover, starting with a large quantity of the active complex, the initiator will be quickly converted to growing radicals, increasing the likelihood of complete initiation.

Experimentally, $[Cu^{II}TPMA]^{2+}$ was reduced in the absence of initiator HEBiB, which was added from a degassed stock solution after 25 minutes (Table 6.3). The consumed charge corresponded to the reduction of 47% of Cu^{II} to Cu^{I}. Polymerization conducted with pre-electrolysis of Cu^{II} did not show an induction period. Additionally, significantly better linear kinetics and molecular weights much closer to theoretical values were observed (see as example Figure 6.5f, WE = NiCr). The reactions were fast, with conversion > 90% in 3 to 4 h. Figure 6.6a shows an example of chronopotentiometry recorded during a two-step galvanostatic *e*ATRP with WE = 304SS.

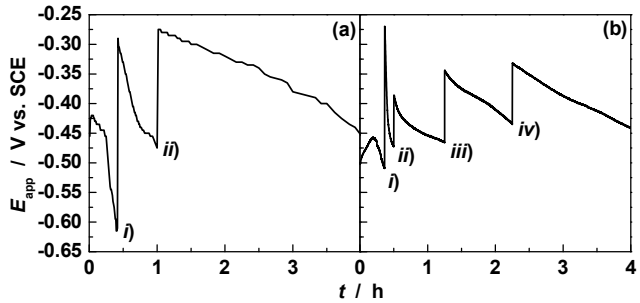

Figure 6.6. (a) Chronopotentiometry at 304SS working electrode: *i*) initiator was added (25 min pre-electrolysis, I = 0.45 mA); *ii*) current was changed (0.45, 0.15 mA for 35, 180 min). (b) Chronopotentiometry at Ti working electrode: *i*) initiator was added (22 min pre-electrolysis, I = 0.52 mA); *ii*), *iii*) and *iv*) current was changed (0.52, 0.35, 0.2, 0.12 mA for 8, 45, 60, 130 min).

Table 6.3. Galvanostatic *e*ATRP of 10% v/v OEOMA in H_2O, with pre-electrolysis.[a]

	Current Steps	WE	t (h)	Q (C)	Conv (%)	$M_{n,th}$	$M_{n,app}$	$k_p^{app} \times 10^{2}$ [b] (min^{-1})	$Đ$	I_{eff} [c] (%)
1	2	Ti	4[d]	2.97	92	50100	68000	1.26	1.32	0.76
2	2	NiCr	3	2.0	98	53100	71700	2.14	1.31	0.74
3	2	304SS	3.5	2.3	96	51800	64800	1.41	1.26	0.80
4	4	NiCr	2	2.0	92	49800	58500	2.21	1.18	0.85
5	4	304SS	1.5	1.6	98	53100	67700	4.18	1.25	0.78
6[e]	4	NiCr	1.5	1.6	92	49800	76100	2.79	1.21	0.65
7[g]	4	304SS	2	2.0	89	48300	92500	1.52	1.39	0.52

[a] Polymerization conditions: OEOMA/HEBiB/$Cu(OTf)_2$/TPMA/Et_4NBr = 216/2/1/1/100, C_{Cu} = 10^{-3} M, V_{tot} = 15 mL, T = 25 °C. 2 current steps (0.45, 0.15 mA for 35, 215 min; pre-electrolysis: 0.45 mA for 25 min) or 4 current steps(0.52, 0.35, 0.2, 0.12 mA for 8, 45, 60, 130 min; pre-electrolysis: 0.52 mA for 22 min). [b] The slope of the linear plot of $\ln(C_{M_0}/C_M)$ vs. time. [c] Ratio $M_{n,th}$ / $M_{n,app}$. [d] Pre electrolysis for 10 min. [e]Al as counter electrode, directly immersed in the polymerization medium.

It was recently shown that increasing the number of current steps in galvanostatic *e*ATRP helped improving the control over the polymerizations.[8] Current steps were chosen emulating the chronoamperometry obtained with a Pt working electrode, as shown in Figure 6.4b for the two-step process. Entries 4-6 of Table 3 show that, when the number of current steps was raised from 2 to 4, polymerization rates were greatly enhanced and dispersities diminished (for NiCr and 304SS electrodes). Figure 6.6b shows an example of a four-step chronopotentiometry recorded with WE = 304SS. In this case, variation of the working potential is significantly lower than in the two-step electrolysis. This allowed avoiding undesired reactions occurring at very negative potentials, which could decrease both polymerization rate and control (*i.e.* Cu^0 deposition on the electrode or excessive generation of Cu^I species). Figure 6.5 shows kinetic plots, molecular weight, and dispersity trends of *e*ATRP of 10% OEOMA in water with WE = NiCr, under the following operative conditions (top to bottom): potentiostatic, two-step galvanostatic, two-step galvanostatic with pre-electrolysis of Cu^{II}, four-step galvanostatic with pre-electrolysis of Cu^{II}.

6.3.2 Simplified *e*ATRP with sacrificial Al counter electrode

Park et al. recently reported the use of a sacrificial anode in electrochemically mediated ATRP, thus avoiding the necessity of a separated compartment for the counter electrode.[8]

An Al wire, directly immersed in the polymerization media, was used as counter electrode. In this case, a twofold excess of ligand with respect to C_{Cu} was needed to complex Al^{3+} ions released from CE oxidation. Otherwise, Al^{3+} can compete with copper for the amine ligand, reducing the effective concentration of active catalyst species.[9] Results of galvanostatic *e*ATRP with WE = NiCr or 304SS and CE = Al are reported in Table 6.3, entries 6, 7. With respect to *e*ATRP with separated anodic/cathodic compartments, control was slightly worse, but still satisfactory. Moreover, both polymerization rate and conversion were high.

Analysis of polymerization mixtures and electrode surfaces. ICP-MS analysis of the polymerization mixtures showed that only small to negligible amounts of potentially harmful metals were released from the electrodes. NiCr electrode released 4×10^{-6} M of Cr ions (as Cr^{3+}), Ni released 1.4×10^{-4} M of Ni ions, and 304SS released 8.6×10^{-4} M of Fe ions. Interestingly, high reaction rates were constantly observed with WE = 304SS. This suggested that the relatively large amount Fe ions released from 304SS was did not compete with Cu ions for the ligand TPMA.

Scanning electrode microscopy of Ti and NiCr electrodes did not show any significant modification in the surface morphology during the *e*ATRP process (Figure 6.7). In particular, no signs of corrosion or pitting were observed. This was in agreement with the

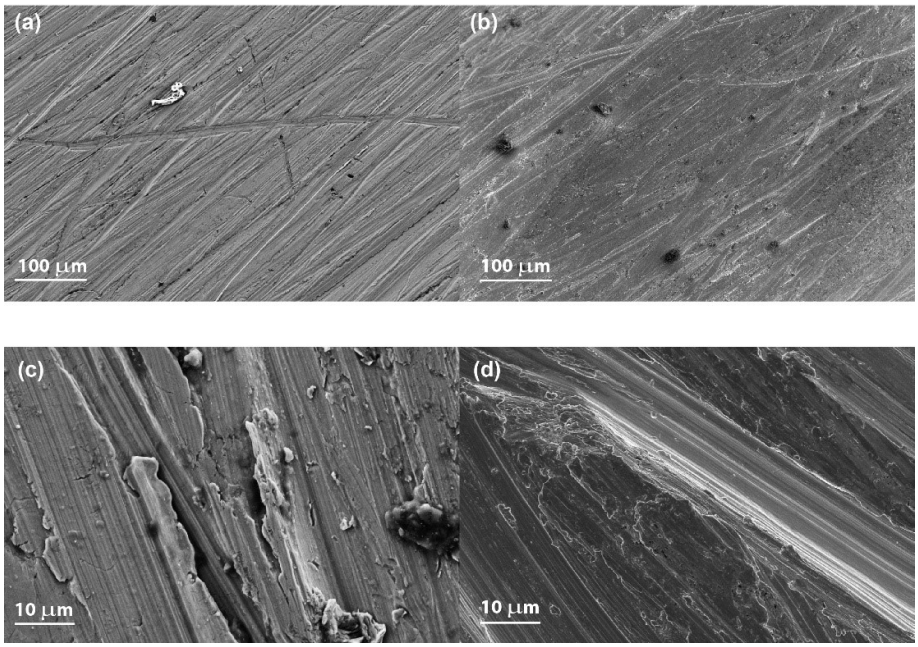

Figure 6.5. Scanning electron microspy images of 304SS (a, b) and Ti (c, d) electrode surfaces. Images were taken before (a, c) and after *e*ATRP of 10% OEOMA in water (b,d).

ICP-MS data, which indicated only a small release of ions from the metal electrodes. These results point out that the tested WE can be used without substantial contamination of the polymerization mixture, avoiding the need of complex purification procedures. Moreover, the negligible modification or corrosion of the surface suggests that the same WE material can be reused several times without the need of long and complex mechanical activation.

6.4 Conclusions

*e*ATRP of OEOMA in water was successfully conducted by using various noble and non-noble cathodic materials, with fast kinetics, high conversions (> 90%) and good control over molecular weights and molecular-weights distributions. Noble metals and glassy carbon could work under potentiostatic (fixed applied potential) conditions. Non-noble metals provided better performances under galvanostatic (fixed current) conditions and pre-electrolysis to produce the active Cu^{I} complex before addition of the initiator. The polymerizations did not require the use of organic solvents or expensive/rare materials as working electrode. Moreover, setup was simplified by directly introducing an Al counter electrode in the reaction mixture, without separation of cathodic and anodic compartments. Further simplification was achieved by using a two-electrode system under galvanostatic conditions, which does not require the use of expensive electrochemical instrumentation.

Overall, these results are a substantial simplification and economization of the *e*ATRP setup, which can make this technique significantly more attractive in both academia and industry. We believe that the introduced improvements are a necessary step toward the scale-up and commercialization of this powerful polymerization technique.

References

(1) (a) Jakubowski, W.; Matyjaszewski, K. *Angew. Chem., Int. Ed.* **2006**, *45*, 4482−4486. (b) Kwak, Y.; Matyjaszewski, K. *Polym. Int.* **2009**, *58*, 242−247. (c) Dong, H.; Matyjaszewski, K. *Macromolecules* **2008**, *41*, 6868−6870. (c) Zhang, Y.; Wang, Y.; Matyjaszewski, K. *Macromolecules* **2011**, 44, 683−685.

(2) (a) Matyjaszewski, K.; Tsarevsky, N. V.; Braunecker, W. A.; Dong, H.; Huang, J.; Jakubowski, W.; Kwak, Y.; Nicolay, R.; Tang, W.; Yoon, J. A. *Macromolecules* **2007**, *40*, 7795−7806. (b) Percec, V.; Guliashvili, T.; Ladislaw, J. S.; Wistrand, A.; Stjerndahl, A.; Sienkowska, M. J.; Monteiro, M. J.; Sahoo, S. *J. Am. Chem. Soc.* **2006**, *128*, 14156−14165. (c) Guliashvili, T.; Mendonca, P. V.; Serra, A. C.; Popov, A. V.; Coelho, J. F. J. *Chem.−Eur. J*. **2012**, *18*, 4607−4612. (d) Zhang, Y.; Wang, Y.; Matyjaszewski, K. *Macromolecules* **2011**, *44*, 683−685. (e) Hornby, B. D.; West, A. G.; Tom, J. C.; Waterson, C.; Harrisson, S.; Perrier, S. *Macromol. Rapid Commun*. **2010**, *31*, 1276−1280. (f) Matyjaszewski, K.; Coca, S.; Gaynor, S. G.; Wei, M.; Woodworth, B. E. *Macromolecules* **1997**, *30*, 7348−7350.

(3) Konkolewicz, D.; Krys, P.; Go, J. R.; Mendonça, P. V.; Zhong, M.; Wang, Y.; Gennaro, A.; Isse, A. A.; Fantin, M.; Matyjaszewski, K. *Macromolecules* **2014**, *47*, 560–570.

(4) Bortolamei, N. PhD Thesis, University of Padova, 2012.

(5) Bortolamei, N.; Isse, A. A.; Magenau, A. J. D.; Gennaro, A.; Matyjaszewski, K. *Angew. Chem. Int. Ed.* **2011**, *50*, 11391–11394.

(6) Bard, A. J.; Faulkner, R. L. Electrochemical methods, 2nd ed., John Wiley & Sons, New York, 2001.

(7) Poli, R. *Eur. J. Inorg. Chem.* **2011**, *2011*, 1513–1530.

(8) Park, S.; Chmielarz, P.; Gennaro, A.; Matyjaszewski, K. *Angew. Chem. Int. Ed.*, **2015**, *54*, 2388-2392.

(9) Lorandi, F.; Fantin, M.; Isse, A. A.; Gennaro, A. *Manuscript in preparation*.

Chapter 7

Mechanism of Metal-Free ATRP

Photoredox catalysis recently emerged as a powerful tool in both organic synthesis and polymerization. Generally, photoredox catalysts behave as strong oxidants and/or reductants upon irradiation, but they are poor oxidants and reductants in the ground state. Therefore, photoredox reactions can be precisely controlled by light.

A photoinduced ATRP was successfully catalyzed by *fac*-[Ir(ppy)$_3$] (**1**, ppy = 2-pyridylphenyl, in Figure 7.1).[1] Upon irradiation with visible light, excited *fac*-[Ir(ppy)$_3$]* (**1***), a very strong reductant, $E^{\circ}_{1^+/1^*}$ = - 1.73 V vs. SCE, can reduce an alkyl bromide to generate an Ir^{IV} complex and an organic radical which initiates polymerization. The Ir^{IV} complex is a strong oxidant ($E^{\circ}_{1^+/1}$ = 0.77 V vs. SCE in CH_3CN), which can react with the propagating radical to provide the ground state catalyst **1** and polymer chain with a bromine at a chain end. Well-defined poly(methyl methacrylate) (PMMA, M_n = 22,900, M_w/M_n = 1.25) was obtained using low ppm amounts of **1** under visible light irradiation. A metal-free ATRP process was subsequently developed by using 10-phenylphenothiazine (**2**, Ph-PTZ, in Figure 7.1) as an organic-based photoredox catalyst to synthesize well-defined polymethacrylates and polyacrylonitrile.[2] Analogous to **1**, Ph-PTZ **2** is also excited to form a very strong reductant Ph-PTZ* ($E^{\circ}_{2^+/2^*}$ = - 2.10 V vs. SCE in CH_3CN). The oxidized radical cation Ph-PTZ$^{\bullet+}$, formed upon reaction of Ph-PTZ* with the alkyl

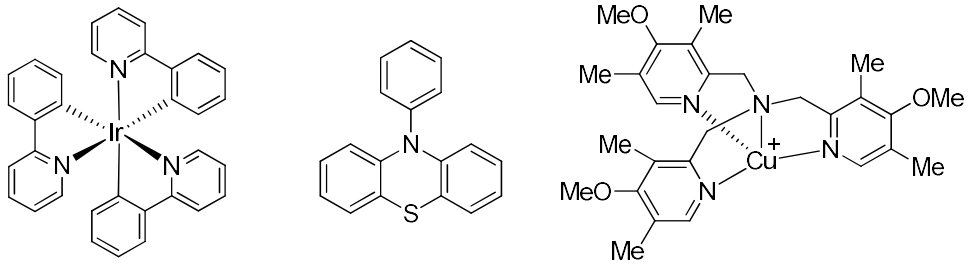

Figure 7.1. Structures of photoredox catalysts **1**, **2** and a traditional Cu-based ATRP catalyst **3**.

halide, is a strong oxidant ($E^{o}_{2^{+}/2}$ = 0.68 V vs. SCE in CH_3CN), able to deactivate the propagating alkyl radicals, generate a ω-halide polymer chain and regenerate the ground state catalyst **2**.

While it was proved that activation in Cu-based ATRP occurs *via* inner sphere electron transfer (ISET) only,[3] it is likely that photoinduced ATRP catalyzed by **1** or **2** occurs *via* an outer sphere electron transfer (OSET). The ISET process occurs via a Cu-X-R transition state that drastically lowers the activation energy. *fac*-[Ir(ppy)$_3$] **1** is a coordinatively saturated metal complex, therefore it cannot form any additional bond with the metal center, and thus RX reduction most likely takes place *via* an OSET. Similarly, the activator in metal-free ATRP is an aromatic organic molecule that is not likely to react strongly with X^-. In addition, there is a significant difference between the redox properties of Cu-based and photoredox catalysts. The most active Cu-based ATRP catalyst reported so far is $[Cu^{I}(TPMA^{*3})]^+$ (**3**, $TPMA^{*3}$ = tris((4-methoxy-3,5-dimethylpyridin-2-yl)methyl)-amine)) which has E^{o} = -0.18 V vs. SCE.[4] Compared to these values, both **1*** and **2*** have much more negative redox potentials (Figure 7.1), indicating much greater reactivity in the reduction of alkyl halides. They are so active that they can participate in OSET processes.

The mechanism of the deactivation process also plays an important role in controlling an ATRP reaction. In atom transfer radical addition (ATRA) reactions by photoredox catalysts such as **1**, it was proposed that $R^{\bullet}$ is first oxidized to a carbocation,[5] which subsequently traps a nucleophilic halide anion to yield the product. However, in the polymerization of methyl methacrylate (MMA) and acrylonitrile (AN), the derived carbocations should be unstable and would be involved in side reactions with residual water or elimination to form short oligomers rather than polymers. No such products were observed in photoinduced metal-free ATRP, indicating that the deactivation step might not involve a carbocation as a key intermediate.

This chapter presents a detailed mechanistic study on photoinduced metal-free ATRP. Structure-reactivity relationships were established, using cyclic voltammetry (CV) and spectroscopic techniques. Kinetic analysis of both activation and deactivation steps, according to Marcus theory and further developments,[6] elucidated the following questions: 1) Does the activation step follow ISET or OSET mechanism? 2) What is the mechanism of the deactivation process during the controlled polymerization? 3) What are the key intermediates in these reactions? 4) How does this photoinduced metal-free ATRP system compare to classic Cu-catalyzed ATRP?

7.1 Polymerization reactions

Polymerization of MMA with Ph-PTZ 2. The results of photoinduced metal-free ATRP of MMA with Ph-PTZ **2** under different conditions, in dimethylacetamide (DMA), under different light intensities, and in the presence of different ATRP initiators, are summarized in Table 7.1. The standard polymerization under conditions: $[MMA]_0:[EBPA]_0:[\mathbf{2}]_0$ = 100:1:0.1, MMA/DMA = 1/1 (v/v), (EBPA: ethyl α-bromophenylacetate), at room temperature with irradiation at 365 nm (2.1 mW/cm^2) reached 16% conversion of MMA after 4 h, yielding PMMA with M_n = 2070, and M_w/M_n = 1.50 (Table 7.1, entry 1) which is close to the theoretical value $M_{n,th}$ (predicted for a transfer-less process with a quantitative initiation). Polymerizations with stronger light intensity source (4.9 mW/cm^2 at 365 nm) were faster, reaching 45 % conversion after 4 h (entry 2).

With ethyl α-bromoisobutyrate (EBiB) as ATRP initiator instead of EBPA, the M_n = 3840 of PMMA was higher than $M_{n,th}$ with broader distribution (M_w/M_n = 1.79, entry 3). Indeed, activation of EBiB in ATRP is slower than activation of PMMA-Br, due to penultimate unit effect.[7] The polymerization using ethyl α-chlorophenylacetate (ECPA) was not controlled at all, resulting in 55% conversion after 4 h with the formation of a polymer with bimodal distribution M_n = 16000, M_w/M_n = 3.44, (entry 4), indicating that a chloride-based initiator was not suitable in this photoinduced metal-free system.

Table 7.1. Selected results of metal-free ATRP of MMA under different conditions.[a]

Entry	Conditions	Irradiation (mW/cm^2)	Conv.[b]	$M_{n,th}$[c]	$M_{n,GPC}$[c]	M_w/M_n[d]
1	[MMA]:[EBPA]:[**2**] = 100:1:0.1	2.1	16%	1,800	2,070	1.50
2	[MMA]:[EBPA]:[**2**] = 100:1:0.1	4.9	45%	4,700	5,440	1.44
3	[MMA]:[EBiB]:[**2**] = 100:1:0.1	2.1	20%	2,200	3,840	1.79
4	[MMA]:[ECPA]:[**2**] = 100:1:0.1	4.9	55%	5,700	16,000	3.44
5	[MMA]:[EBPA]:[**2**] = 100:1:0	2.1	27%	2,900	28,700	2.25
6	[MMA]:[ECPA]:[**2**] = 100:1:0	4.9	15%	1,700	17,900	2.02
7	[MMA]:[ECPA]:[**2**]:[n-Bu_4NBr] = 100:1:0.1:1	4.9	79%	8,100	10,800	2.47

[a] Reaction conditions: MMA/DMA = 1/1 (v/v), under room temperature irradiation at 2.1 mW/cm^2 or 4.9 mW/cm^2, 365 nm. [b] Determined by ^{1}H NMR. [c] Calculated on the basis of conversion obtained by ^{1}H NMR (i.e. $M_{n,th} = M_{EBPA} + 100 \times \text{conversion} \times M_{MMA}$). [d] Determined by GPC in THF, based on linear PMMA as calibration standards.

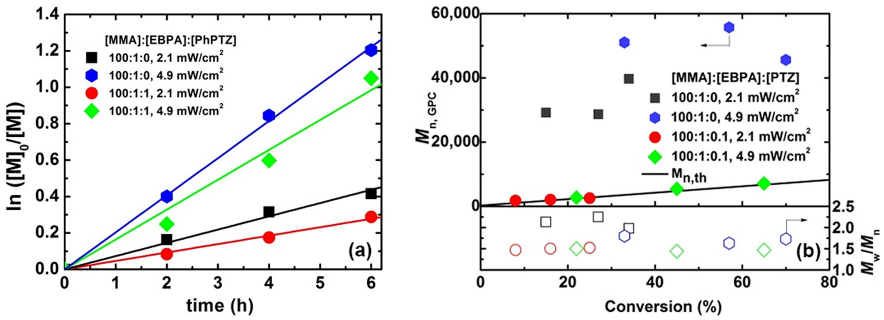

Figure 7.2. (a) Semilogarithmic kinetic plots of polymerization of MMA with or without **2**; (b) Number-average molecular weight (M_n, filled symbols), and dispersity (M_w/M_n, open symbols) versus conversion.

Background reactions. The activation step should involve the reaction between excited state of metal-free photoredox catalyst and alkyl bromide. Nevertheless, under strong irradiation, radicals could also be formed by homolytic cleavage of the C-Br bond in the initiator EBPA or in the polymer-Br chain end. Polymerizations of MMA were conducted with EBPA both in the absence and presence of Ph-PTZ **2** under the following conditions: $[MMA]_0:[EBPA]_0:[\mathbf{2}]_0$ = 100:1:0 or 100:1:0.1, MMA/DMA = 1/1 (v/v), and irradiation with 365 nm at 2.1 or 4.9 mW/cm^2. Polymerization of MMA without **2** provided PMMA with much higher M_n than the theoretical value and M_w/M_n values as high as 2.2 (Table 7.1, entry 7 and Figure 7.2b), suggesting an uncontrolled free radical polymerization. These reactions also provide a clear indication that a radical could be formed from EBPA under irradiation.

The rates of polymerization with **2** under both irradiation intensities were slower than the one without **2** (Figure 7.2a), indicating that the concentration of radicals was decreased and a radical deactivation process was involved in the presence of **2**. The metal-free ATRP of MMA with **2** gave PMMA with predictable M_n, growing with conversion and low dispersity, suggesting that the process is well controlled (Table 7.1, entries 1 and 2).

Similarly, the background reaction for polymerization of MMA with ECPA in the absence of **2** reached only 15% conversion after 4 h of irradiation with 365 nm at 4.9 mW/cm^2, providing PMMA with M_n = 17900, and M_w/M_n = 2.02 (entry 6, Table 7.1). However, the same reaction with **2** was much faster (entry 6 vs. 4, Table 7.1, 15% vs. 55% conversion at 4 h), though with the same poor control, indicating that the Ph-PTZ-catalyzed system is efficient to activate alkyl chloride but inefficient to deactivate the propagating radicals.

Salt effects. Similarly as metal-catalyzed ATRP, one possible deactivation mechanism is the transfer of a halogen atom from the radical cation-anion ion pair $Cat^{\bullet+}X^-$ (X = Br or Cl) formed in the activation step to the propagating radical (eq. 7.1-7.2).

$$\text{ACTIVATION} \qquad Cat^* + RX \longrightarrow Cat^{\bullet+}X^- + R^\bullet \qquad (7.1)$$

$$\text{DEACTIVATION} \qquad Cat^{\bullet+}X^- + R^\bullet \longrightarrow Cat + RX \qquad (7.2)$$

In a polar solvent such as DMA, the ion pair $Cat^{\bullet+}X^-$ would dissociate to the free radical cation ($Cat^{\bullet+}$) and a halide anion (Br^- or Cl^-) and could reach an equilibrium state. Therefore, if deactivation occurs according to eq. 7.2, the overall rate of polymerization and control over molecular weight distribution would be strongly influenced by the dissociation equilibrium $Cat^{\bullet+}X^- = Cat^{\bullet+} + X^-$, which can be shifted to the left if a large excess of halide ions is added. Additionally, it must be noted that halide anions, whether linked to $Cat^{\bullet+}$ or free in solution, are a fundamental reagent of the deactivation step, for the production of halogen-capped dormant chains. Therefore, excess tetra-*n*-butylammonium bromide (*n*-Bu_4NBr) was added to improve deactivation in the polymerization of MMA when using Ph-PTZ **2** as a catalyst. However, the polymerization of MMA with added *n*-Bu_4NBr under reaction conditions $[MMA]_0:[EBPA]_0:[\mathbf{2}]_0:[n\text{-}Bu_4NBr]_0$= 100:1:0.1:x, x = 0.2, 1 or 2, 50% DMA, irradiation with 365 nm, did not give any observable difference in polymerization rates and dispersities.

On the other hand, when an excess *n*-Bu_4NBr was added to the reaction using ECPA, the M_n (10,800) of obtained PMMA was close to the theoretical value ($M_{n,th}$ = 8,100), although the dispersity was still high (M_w/M_n = 2.47, entry 7, Table 7.1). The polymerization with ECPA and *n*-Bu_4NBr showed better deactivation of the growing chains, indicating that deactivation was more efficient in the presence of bromide ions.

Polymerization with different catalysts. The set of compounds shown in Figure 7.3 was chosen to study the effect of key structural features on their properties and reactivity. Compounds **2** and **4-6** are *N*-aryl phenothiazine derivatives, **7** and **8** contain a naphtalene ring in different positions. **8** and **9** are simpler, commercially available phenothiazine derivatives. 9-Phenylcarbazole **11** and thianthrene **12** were selected due to the structural similarity to phenothiazine, and compounds **13** and **14** were selected due to similar photosensitivities (HOMO-LUMO gap).[8]

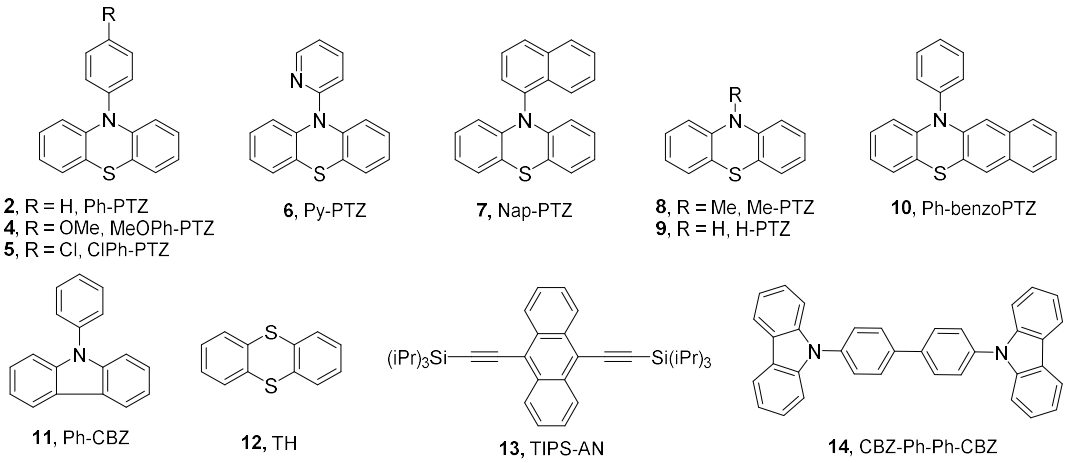

Figure 7.3. Structures of catalysts studied in metal-free ATRP.

All catalysts were investigated for photoinduced metal-free ATRP of MMA with EBPA as initiator under standard conditions and the results are summarized in Figure 7.4. The reaction conditions were $[MMA]_0:[EBPA]_0:[Cat]_0 = 100:1:0.1$, in MMA/DMA = 1/1 (v/v), at room temperature with irradiation of 365 nm at 2.1 mW/cm^2. The reactions with all phenothiazine-based compounds, **2** and **4-10,** were all slower than the background reaction, indicating that some deactivation was involved. Overall, the polymerization results allowed us to divide the investigated compounds into three categories according to their performance. (*i*) The metal-free ATRP with all N-aryl phenothiazines **2**, **4-7** and benzo[*b*]phenothiazine **10** provided well-defined PMMA with predetermined M_n and dispersities $Đ$ = 1.4-1.5. (*ii*) Catalysts **8** (Me-PTZ) and **9** (H-PTZ) only provided limited control. The obtained M_n were close to the theoretical values at low conversion of MMA (<30 %), but they became significantly higher at higher conversion. This observation indicates that both **8** and **9** decomposed during the later stage of the reaction and could not deactivate the radicals (**9** decomposed faster and showed poorer control from the beginning of the polymerization). (*iii*) The polymerizations with **11-14** provided faster reactions than the background reaction, indicating that these catalysts efficiently activated the C-Br bond but could not deactivate the propagating radical efficiently. This is further supported by the evidence that the M_n of synthesized PMMA using these catalysts was always much higher than theoretical M_n (Figure 7.4b).

Since the background reaction using EBPA as initiator was a fast process, it was not possible to determine whether all catalysts were involved in the activation step. Therefore, EBiB was used as initiator rather than EBPA under metal-free ATRP conditions. All the

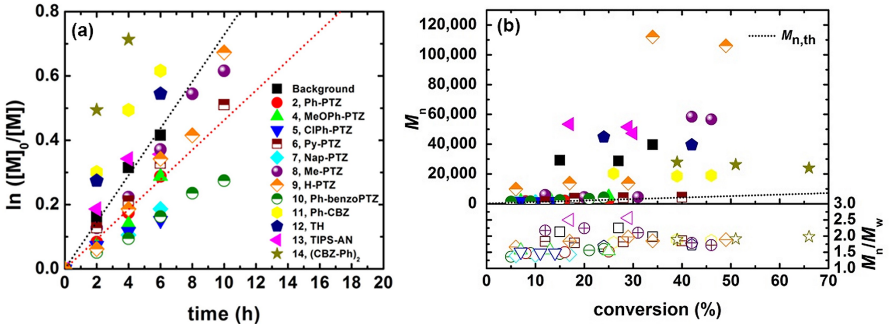

Figure 7.4. (a) Semilogarithmic kinetic plots for the polymerization of MMA with catalysts shown in Figure 7.3, conditions: $[MMA]_0$:$[EBPA]_0$:$[Cat]_0$ = 100:1:0.1, in MMA/DMA = 1/1 (v/v), at room temperature with irradiation of 365 nm (2.1 mW/cm^2); red dotted line: linear fit for standard polymerization with **2**, black dotted line: linear fit for background polymerization; (b) number-average molecular weight (M_n, filled symbols), and dispersity (M_w/M_n, open symbols) versus conversion.

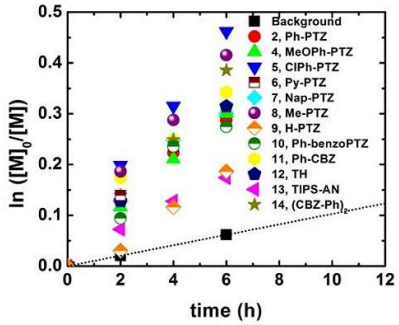

Figure 7.5. Semilogarithmic kinetic plots for the polymerization of MMA with catalysts shown in Figure 7.3, conditions: $[MMA]_0$:$[EBiB]_0$:$[Cat]_0$ = 100:1:0.1, in MMA/DMA = 1/1 (v/v), at room temperature with irradiation of 365 nm (2.1 mW/cm^2); black dotted line: linear fit for background polymerization.

polymerizations with any of the catalysts shown in Figure 7.3 were faster than the background reaction using only EBiB, strongly indicating that all the catalysts efficiently photoactivated alkyl halides (Figure 7.5).

7.2 Electrochemical characterization of the catalysts

Cyclic voltammetry (CV) was used to measure the oxidation potentials of the catalysts and to assess the stability of their radical cations ($Cat^{\bullet+}$). All CVs were recorded in DMA in the presence of 0.1 M Et_4NClO_4 and some examples are reported in Figure 7.6. Comprehensive results about electrochemical properties and catalytic activity of the catalyst are reported in Table 7.2. Within the electrochemical potential window of the solvent, all

compounds, except **13**, could be oxidized to form a radical cation (Cat = $Cat^{\bullet+}$ + e^-). The reversibility of the voltammetric pattern is a direct indication of the stability of the radical cations. All substituted phenothiazines (**2**, **4-8**, **10**) showed a reversible oxidation wave (Figure 7.6a), indicating that the electrogenerated radical cation was a stable species. The CV of unsubstituted phenothiazine **9** had limited chemical reversibility: the radical cation quickly decomposed to form a product that was reduced at a lower potential (Figure 7.6b). From cyclic voltammetry conducted at different scan rates (Figure 7.6c), a lifetime in the order of 10 s was estimated for the radical cation $\mathbf{9}^{\bullet+}$ (in the CV conducted at 0.02 V s^{-1} roughly half of $\mathbf{9}^{\bullet+}$ has decomposed; at this slow scan rate, the reverse scan reached the cathodic peak potential *ca* 8 s after the potential was inverted). Also **12** showed a similar behavior with a faster decay rate, with a lifetime < 5 ms. Other tested carbazole derivatives (**11** and **14**) exhibited an irreversible oxidation peak, indicating that their specific radical cations were not stable in DMA.

A stable radical cation is necessary for the efficient deactivation of the growing radicals, thus only the compounds with a reversible redox behavior should efficiently control the polymerization. The experimental results confirmed this conclusion, as effective deactivation was observed only for compounds with reversible redox properties. Moreover,

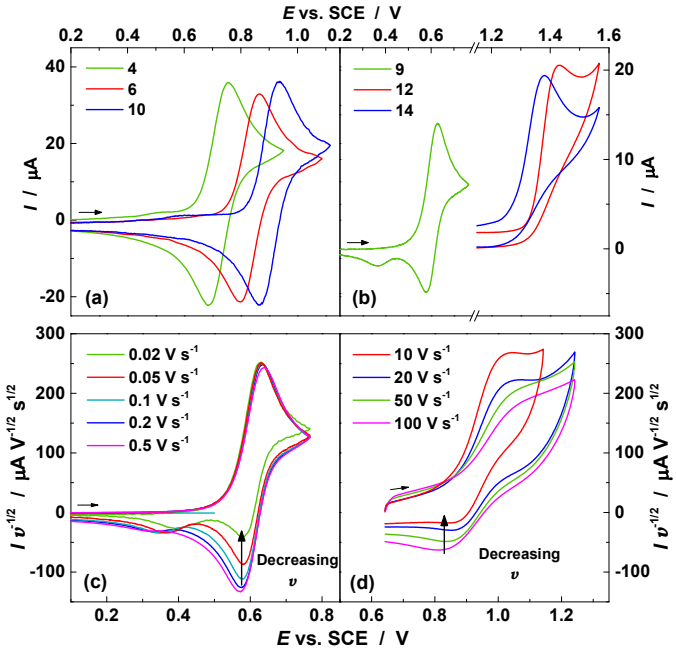

Figure 7.6. Selected cyclic voltammograms for compounds characterized by (a) reversible and (b) partially reversible or irreversible oxidation, $C = 2\times10^{-3}$ M, in DMA + 0.1 M Et_4NClO_4 at 25 °C. (a) $\upsilon = 0.2$ V s^{-1}; (b) $\upsilon = 0.05$ V s^{-1}. Cyclic voltammetry of 2×10^{-3} M (a) **9** and (b) **12** at various scan rates (current intensity was normalized by $\upsilon^{-1/2}$).

CV analysis confirmed the limited stability of $\mathbf{9}^{\bullet+}$, which indeed could efficiently deactivate the growing radicals only at the beginning of the experiment, since a fraction of $\mathbf{9}^{\bullet+}$ decomposed by side reactions leading to the progressive consumption of the catalyst. Therefore, cyclic voltammetry was a reliable technique that allowed a rapid screening of the analyzed photoactive molecules as candidates for radical deactivation and control of photoATRP experiments. CV experiments also demonstrated that stable radical cations $Cat^{\bullet+}$ should be involved in the deactivation reaction mechanism.

For the compounds exhibiting a reversible redox behavior, the oxidation potential of the catalyst in the excited state ($E^{\ominus}_{Cat^{\bullet+}/Cat^*}$) could be estimated from the excitation energy of the photocatalysts (E_{hv}), according to the following equation:[9]

Table 7.2. Characterizations and reactivities of catalysts studied in metal-free ATRP.

Catalyst	$E^{\ominus}_{Cat^{\bullet+}/Cat}$ (V vs. SCE)	λ_{max} (nm)[a]	$E^{\ominus}_{Cat^{\bullet+}/Cat^*}$ (V vs. SCE)[b]	Lifetime τ_0 (ns)	CV reversibility	Act[c]	Deact[d]
2, Ph-PTZ	0.815[e]	445	-1.97	4.5	+	+	+
4, MeOPh-	0.797	445	-1.99	6.0	+	+	+
5, ClPh-PTZ	0.830	445	-1.96	3.0	+	+	+
6, Py-PTZ	0.903	510	-1.53	7.4	+	+	+
7, Nap-PTZ	0.833	405	-2.23	7.6	+	+	+
8, Me-PTZ	0.826	445	-1.97	2.3	+	+	+/–
9, H-PTZ	0.606	450	-2.15	2.1	+/–	+	+/–
9, Ph-ben-	0.902	440	-1.92	12.9	+	+	+
11, Ph-CBZ	1.423[f]	365	-2.03	4.7	–	+	–
12, TH	1.393[g]	445	-1.36	4.9	–	+	–
13, TIPS-AN	>1.5[h]	445	-	2.1	–	+	–
14, $(CBZ\text{-}Ph\text{-})_2$	1.392[f]	410	-	3.4	–	+	–

[a] Obtained from ref. 10. [b]From eq. 7.3.[c] Activation based on whether polymerization was faster than the background reaction with EBiB as ATRP initiator (cf. Figure 7.5). [d] Deactivation evaluation based on whether $M_{n,GPC}$ was close to $M_{n,th}$ (cf. Figure 7.4). [e] For comparison, values in CH_3CN are $E^{\ominus}_{\mathbf{2}^{\bullet+}/\mathbf{2}}$ = 0.68 V vs. SCE and $E^{\ominus}_{\mathbf{2}^{\bullet+}/\mathbf{2}^*}$ = -2.10 V vs. SCE.[2b] [f] Potential of the anodic peak at υ = 0.2 V s^{-1}. [g] $E^{\ominus}_{Cat^{\bullet+}/Cat}$ was estimated at high scan rates (υ > 10 V s^{-1}), where partial reversibility in CV could be achieved (Figure 7.6c-d). [h] No oxidation wave was observed inside the potential range of DMA.

$$E^{\ominus}_{\mathrm{Cat}^{\bullet+}/\mathrm{Cat}^{*}} = E^{\ominus}_{\mathrm{Cat}^{\bullet+}/\mathrm{Cat}} - E_{h\nu} = E^{\ominus}_{\mathrm{Cat}^{\bullet+}/\mathrm{Cat}} - \frac{hc}{\lambda_{\max}} \tag{7.3}$$

where h is the Planck constant, c is the speed of light, $E^{\ominus}_{\mathrm{Cat}^{\bullet+}/\mathrm{Cat}}$ is the standard reduction potential of $\mathrm{Cat}^{\bullet+}$ in the ground state and λ_{max} is the wavelength of maximum emission intensity of the excited state (obtained from ref. 10). $E^{\ominus}_{\mathrm{Cat}^{\bullet+}/\mathrm{Cat}}$ was obtained from cyclic voltammetry as the half sum of anodic and cathodic peak potentials, $E^{\ominus}_{\mathrm{Cat}^{\bullet+}/\mathrm{Cat}} \approx E_{1/2} = (E_{\mathrm{pa}} + E_{\mathrm{pc}})/2$.

7.3 Kinetic analysis of metal-free ATRP activation

The strongly negative values for $E^{\ominus}_{\mathrm{Cat}^{\bullet+}/\mathrm{Cat}^{*}}$ suggested the viability of an OSET (eq. 7.4). This reaction involves a concerted dissociative electron transfer (DET) to RX, as consolidated in the literature for the reductive cleavage of alkyl halides.[11] Therefore, assessment of ET kinetics cannot be made by a straightforward application of the well-known Marcus theory for electron-transfer processes. A modified model of Marcus theory, developed by Savéant, is available and is currently used to analyze the dynamics of DET processes.[6b-d]

$$\mathrm{Cat} + \mathrm{RX} \xrightarrow{k_{\mathrm{act}}} \mathrm{Cat}^{\bullet+} + \mathrm{R}^{\bullet} + \mathrm{X}^{-} \tag{7.4}$$

According to the DET theory, a quadratic activation-driving force relationship similar to that of Marcus theory of OSET exists also for DET processes (eq. 7.5).

$$\Delta G^{\ddagger} = \Delta G_0^{\ddagger}\left(1 + \frac{\Delta_r G^{\ominus}}{4\Delta G_0^{\ddagger}}\right)^2 \tag{7.5}$$

where $\Delta G_0^{\ddagger}$ is the intrinsic barrier of the reaction, i.e. the activation free energy when $\Delta_r G^{\ominus} = 0$. The intrinsic barrier is given by $\Delta G_0^{\ddagger} = \left(\lambda_o + D_{\mathrm{RX}}\right)/4$, where λ_o is the solvent reorganization energy and D_{RX} is the R-X bond energy. The principal difference between OSET and DET is that the intrinsic barrier of the latter mainly comes from the energy of the breaking bond. When the two fragments of DET, $\mathrm{R}^{\bullet}$ and X^{-}, are able to give rise to ion-dipole interactions in the solvent cage, the dynamics of ET is significantly affected and eq. 7.5 does not correctly predict the activation free energy. The "sticky" model of DET takes into account formation of the ion-dipole adduct by introducing an interaction energy, D_p, into eq. 7.5:

$$\Delta G^{\ddagger} = \Delta G_0^{\ddagger}\left(1+\frac{\Delta_r G^{\circ\prime} - D_P}{4\Delta G_0^{\ddagger}}\right)^2 \tag{7.6}$$

Although D_p is of electrostatic nature and is often very small,[37d] it decreases significantly the intrinsic barrier, now given by $\Delta G_0^{\ddagger} = [\lambda_o + (D_{RX}^{1/2} - D_p^{1/2})^2]/4$, resulting in enhanced rate of electron transfer.

Eq. 7.6 was used to calculate $\Delta G^{\ddagger}$ of reaction 7.4 for a series of catalysts and alkyl halide initiators. The activation free energy was then used to calculate the activation rate constant, k_{act}, according to eq. 7.7:

$$k_{ET} = k_{act} = Z\,\exp\left(-\frac{\Delta G^{\ddagger}}{RT}\right) \tag{7.7}$$

where Z is the pre-exponential factor. The results are presented in Table 7.3, whereas details of the calculations as well as all parameters used in eqs. 7.6 and 7.7 are reported in Appendix C. In the examined cases, Cat can be an organic molecule in the excited state (*e.g.* **2***), the same organic molecule in the ground state (**2**), or the excited state metal complex **1***. RX is either the initiator α-bromophenylacetate (EBPA) or methyl 2-bromoisobutyrate (MBiB), which mimics the PMMA growing chain end. The driving force for the photoinduced electron transfer ($\Delta_r G^{\circ\prime}$) is estimated from the standard potentials of the redox couples of the donor ($E^{\circ\prime}_{Cat^{\bullet+}/Cat}$) and acceptor ($E^{\circ\prime}_{RX/R^{\bullet}+X^-}$), and the energy to excite the catalyst, E_{hv}, by using the Weller equation:[12]

$$\Delta_r G^{\circ\prime} = F\left(E^{\circ\prime}_{Cat^{\bullet+}/Cat} - E^{\circ\prime}_{RX/R^{\bullet}+X^-} - E_{hv}\right) - \frac{N_A e^2}{4\pi\varepsilon_0\varepsilon r} \tag{7.8}$$

where N_A is the Avogadro constant, e is the elementary charge, ε_0 is the permittivity of vacuum and ε the relative permittivity of the solvent at 25 °C. The last term is the Columbic energy experienced by the radical ion pair at distance r.

Unfortunately, not all the data required for estimating the frequency factor Z, $\Delta G_0^{\ddagger}$ and D_P in DMA are available; therefore, it was assumed that the thermodynamic data for RX reduction and bond dissociation were similar in DMF and in DMA. Also, the "sticky" interaction energy between methyl isobutyrate radical (MiB$^{\bullet}$) and Br^- is unknown in DMA, but this interaction, for activated alkyl bromides, like MBiB, is always small in polar solvents like DMF and CH_3CN (0.24–0.50 kcal mol^{-1}).[13] Radical–anion interactions

depend on the dielectric constant, which are very similar for CH_3CN, DMF and DMA. Therefore, we considered that this contribution to the activation energy should be similar to the one reported for the methyl propionate radical (MP•) and Br^- in CH_3CN (0.24 kcal mol^{-1}).

All excited catalysts show high reactivity towards RX reduction, with k_{act} values in the 10^6-10^{10} $M^{-1}s^{-1}$ range. For the DET reaction between EBPA and **2***, $k_{act} = 7.0\times10^9$ M^{-1} s^{-1} was experimentally determined in DMA,[10] whereas the calculated value is 2.0×10^{10} M^{-1} s^{-1}. Considering that a series of approximations had been forcefully introduced into the calculation, the agreement between experiment and theory can be considered satisfactory. Therefore, unlike transition-metal catalyzed ATRP, which involves activation *via* an atom transfer (or ISET) mechanism, activation in photoinduced ATRP follows a concerted dissociative electron transfer mechanism (an OSET mechanism).

Table 7.3. Activation rate constants and relevant thermodynamic parameters for reaction 7.4 in DMA.[a]

Donor	RX	$E^{\ominus}_{Cat^{\bullet+}/Cat^*}$	$E^{\ominus}_{RX/R^{\bullet}+X^-}$ [b]	$\Delta_r G^{\ominus}$	$\Delta G_0^{\ddagger}$	$\Delta G^{\ddagger}$	k_{act}	φ_{act} [c]
1*, Ir(ppy)3*	MBiB	-1.73[d]	-0.52	-28.9	16.4	5.1	5.8×10^7	0.4
2*, Ph-PTZ*	MBiB	-1.97	-0.52	-34.6	16.5	3.7	5.8×10^8	1.3×10^{-3}
2*, Ph-PTZ*	EBPA	-1.97	-0.22[e]	-41.5	15.3	1.6	2.0×10^{10}	4.6×10^{-2}
2*, Ph-PTZ*	MCiB	-1.97	-0.76	-29.1	19.2	7.2	1.5×10^6	3.5×10^{-6}
2, Ph-PTZ	MBiB	0.82[f]	-0.52	29.6	16.5	34.5	1.0×10^{-14}	-
8*, Me-PTZ*	MBiB	-1.96	-0.52	-34.4	16.6	3.8	4.3×10^8	5.0×10^{-4}
11*, Ph-CBZ*	MBiB	-1.91	-0.52	-33.3	15.5	4.0	3.3×10^8	7.7×10^{-4}

[a] Potentials in V vs. SCE; energies in kcal mol^{-1} [b] In DMF.[14] [c] Calculated from eq. 7.9 or 7.10. $C_{RX} = 5\cdot10^{-2}$ M; τ_0 from Table 7.2; Φ_F was determined to be roughly constant and on average 0.01 for a large set of phenothiazine derivatives,[15] therefore $\Phi_F = 0.01$ was used for **2***, **8*** and **11***; Φ_F = 0.40 for **1***.[41] [c] In CH_3CN.[20g] [e] in DMF, calculated as in Ref. 14, using thermodynamic data from Ref. 3 [f] $E^{\ominus}_{Cat^{\bullet+}/Cat}$.

All the analyzed phenothiazine derivatives have redox properties that are relatively similar to each other. Table 7.3 shows that **2*** (Ph-PTZ*) and **8*** (Me-PTZ*) should react with MBiB with similar high rate constants (5.8×10^8 and 4.3×10^8 $M^{-1}s^{-1}$, respectively). Such values are higher than k_{act} for extremely active Cu-based ATRP systems (*e.g.* activation of tertiary RBr initiators by $[Cu^{I}Me_6TREN]^+$ in water, see chapter 3, or DMSO,

see ref. 16), and are typical of fast polymerizations that are often difficult to control. Nevertheless, these values cannot be directly compared to the k_{act} of a traditional ATRP, because reactions that occur from an excited state are usually less than 100% efficient. ATRP activation by Cat* must compete with all decay pathways (radiative and non-radiative) that can bring the molecules back to their ground state. The quantum yield for a first-order reaction from a given excited state is:[17]

$$\varphi = \frac{k'}{k' + k_0}\Phi_F \cong \frac{k'}{k_0}\Phi_F \cong k'\tau_0\Phi_F \tag{7.9}$$

where k' is the rate constant of the first-order reaction that occurs from the excited state, Φ_F is the quantum efficiency for the formation of the excited state, k_0 is the rate constant of radiative decay, and $\tau_0 = 1/k_0$ is the lifetime of the excited state. ATRP activation can be considered a pseudo-first-order reaction, with rate constant k', if we take into account that the polymerization is living and that therefore RX concentration is roughly constant during the reaction ($k' = k_{act}[RX]$). Therefore, eq. 7.9 can be written as

$$\varphi_{act} = k_{act}[RX]\tau_0\Phi_F \tag{7.10}$$

Quantum yields for metal-free ATRP activation are reported in Table 7.3. For example, with $\varphi_{act} = 1.3\times10^{-3}$, only 1 out of *ca.* 10^3 molecules of **2*** survives for a sufficiently long time in the excited state to be able to activate MBiB. In other words, even if **2*** is able to react with MBiB with a rate constant of 5.8×10^8 M s^{-1}, the actual rate of activation is significantly decreased by the low lifetime τ_0 of the excited state and the fluorescence quantum efficiency Φ_F. Since the rate of activation is also the rate of formation of the deactivator, these parameters affect also the deactivation steps. In particular, deactivation can occur only if the rate of activation by Cat* is higher than the background reaction, which is the case for all analyzed compounds, as shown in Figure 7.5.

A further insight into the efficiency of activation (eqs. 7.9 and 7.10) can indicate why the photoinduced ATRP of MMA required only 50-100 ppm of **1**,[2a] but 1000 ppm of **2**. When comparing **1*** with **2***, one has to consider that the former has both longer lifetime (1900 vs. 4.5 ns) and higher quantum efficiency (0.40 vs. 0.01). As shown in Table 7.3, **1*** can activate the RX bond much more efficiently than **2***. Therefore, a much higher portion of the Ir complex will be part of the activation/deactivation process, while under the same conditions most of **2*** will quickly decay back to the ground state, thereby being unable to participate in any activation/deactivation process.

The standard reduction potential of PMMA$^{\bullet}$ is expected to be similar to (or only slightly more negative than) that of MiB$^{\bullet}$, -0.70 V vs. SCE.[18] Moreover, the activation energy of this reaction is low, because the reduction of the radicals does not require the scission of any bond. As a result, radicals can be quickly reduced to carbanions by Cat*, with a diffusion-controlled rate constant. However, in a controlled ATRP process, like that under investigation, the concentration of R$^{\bullet}$ is very small, and hardly ever exceeds 10^{-6} M. Therefore, the rate of radical reduction, which is proportional to both Cat* and R$^{\bullet}$ concentrations, is essentially too slow to compete with other radical reactions such as propagation and deactivation back to the dormant state. The preserved chain end functionality is high, as confirmed by several successful chain extension tests.[2]

From Table 7.3, it is clear that the standard potential of the **2**$^{\bullet+}$**/2** couple in the ground state is too positive to effectively reduce RX and generate radicals. Therefore, the reaction cannot proceed in the absence of light. When the light source is switched off, activation stops almost instantly because of the very fast decay of Cat* to its ground state.

7.4 Kinetic analysis of metal-free ATRP deactivation

Deactivation mechanisms. DFT calculations showed that in DMA both the catalyst radical cation **2**$^{\bullet+}$ and the ion pair complex **2**$^{\bullet+}$**Br**$^{-}$ exist in equilibrium, with $\Delta_r G$ = 0.2 kcal mol^{-1}: [10]

$$\mathbf{2}^{\bullet+} + \mathrm{Br}^{-} \underset{}{\overset{\Delta_r G}{\rightleftharpoons}} \mathbf{2}^{\bullet+}\mathbf{Br}^{-} \qquad (7.11)$$

Five possible deactivation mechanisms of MiB$^{\bullet}$ with **2**$^{\bullet+}$ or with **2**$^{\bullet+}$**Br**$^{-}$ were evaluated (Scheme 7.1): (a) inner-sphere electron transfer (ISET) mechanism through a concerted Br atom transfer from **2**$^{\bullet+}$**Br**$^{-}$ to MiB$^{\bullet}$ *via* transition state **TS1**; (b) dissociative electron transfer (DET) from MiB$^{\bullet}$ to **2**$^{\bullet+}$**Br**$^{-}$ to form MiB^{+}, **2** and **Br**$^{-}$, followed by recombination of MiB^{+} and Br^{-} to generate MBiB; (c) outer-sphere electron transfer (OSET-I) from MiB$^{\bullet}$ to **2**$^{\bullet+}$**Br**$^{-}$ to form an anionic **2** **Br**$^{-}$ complex and MiB^{+}, followed by dissociation to the catalyst **2** and **Br**$^{-}$, and counteriaons recombination; (d) outer-sphere electron transfer from MiB$^{\bullet}$ to the dissociated radical cation **2**$^{\bullet+}$ (OSET-II); and (e) associative electron transfer from **2**$^{\bullet+}$ to MiB$^{\bullet}$ and **Br**$^{-}$ to form the ground-state catalyst **2** and MBiB, involving a termolecular encounter (AET-ter).

ISET and AET-ter pathways produce RX without the formation of any intermediate, while all other ET pathways (DET, OSET-I, and OSET-II) generate the R^{+} cation, which then rapidly recombines with the halide anion to form RX. All reaction free energies

Scheme 7.1. Possible deactivation mechanisms in photoinduced metal-free ATRP.

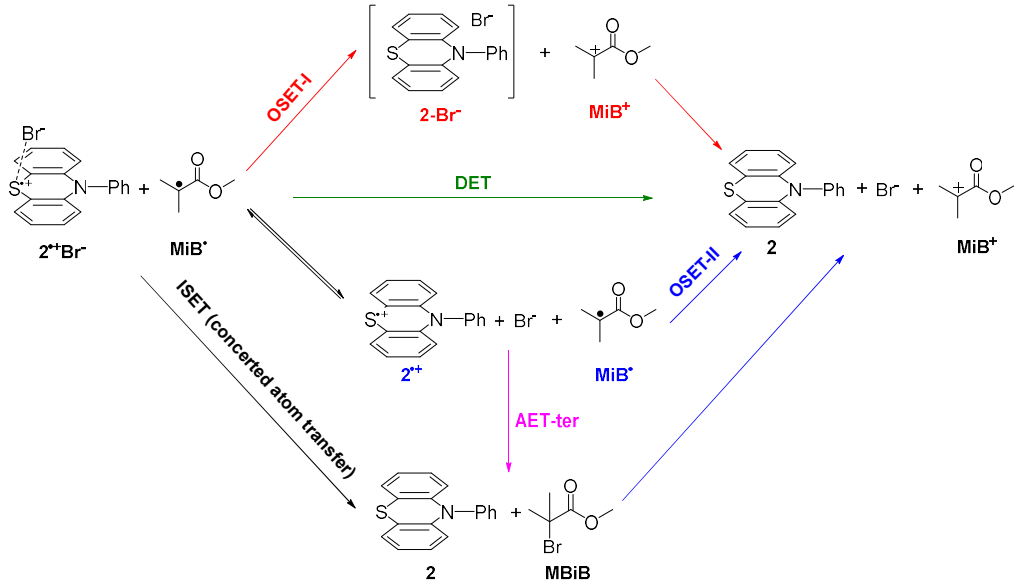

($\Delta_r G^e$) and the energy of the transition state for the concerted Br atom transfer (ISET) were obtained from DFT optimizations.[10] The barriers for the outer-sphere electron transfer pathways (OSET-I, OSET-II) were calculated using the Marcus theory, whereas the activation free energy of the DET pathway was calculated by eq. 7.6. The AET-ter pathway (eq. 7.12) is the exact reverse process of DET of the activation step with the catalyst at the ground state (eq. 7.4).[19]

$$Cat^{\bullet+} + R^{\bullet} + X^{-} \xrightarrow{k_{AET\text{-}ter}} Cat + RX \qquad (7.12)$$

Since the intrinsic barrier is defined as the activation free energy at zero driving force, reactions 7.4 and 7.12 have the same $\Delta G_0^{\ddagger}$ value. $\Delta G_0^{\ddagger}$ and $\Delta G^{\ddagger}$ were already calculated for Ph-PTZ + MBiB (Table 7.3). Nevertheless, in this case $\Delta G^{\ddagger}$ was recalculated using DFT data for a better comparison of this reaction route with the other reaction pathways, for which only DFT data were available.[10] Detailed calculations on the determination of $\Delta G_0^{\ddagger}$ and $\Delta G^{\ddagger}$ for each pathway are reported in Appendix C. $\Delta G^{\ddagger}$ was obtained using either eq. 7.5 or 7.6. The computed reaction energy profiles of the five pathways are summarized in Figure 7.7 and Table 7.4.

Activation energy for deactivation pathways. The ISET pathway requires 10.5 kcal/mol of activation free energy with respect to the ion pair complex $\mathbf{2}^{\bullet+}\mathbf{Br}^{-}$. Among the other four outer-sphere electron transfer pathways, AET-ter pathway involving $\mathbf{2}^{\bullet+}$, MiB$^{\bullet}$ and Br^{-} to form **2** and MBiB has the lowest activation energy, 3.9 kcal/mol. The electron trans-

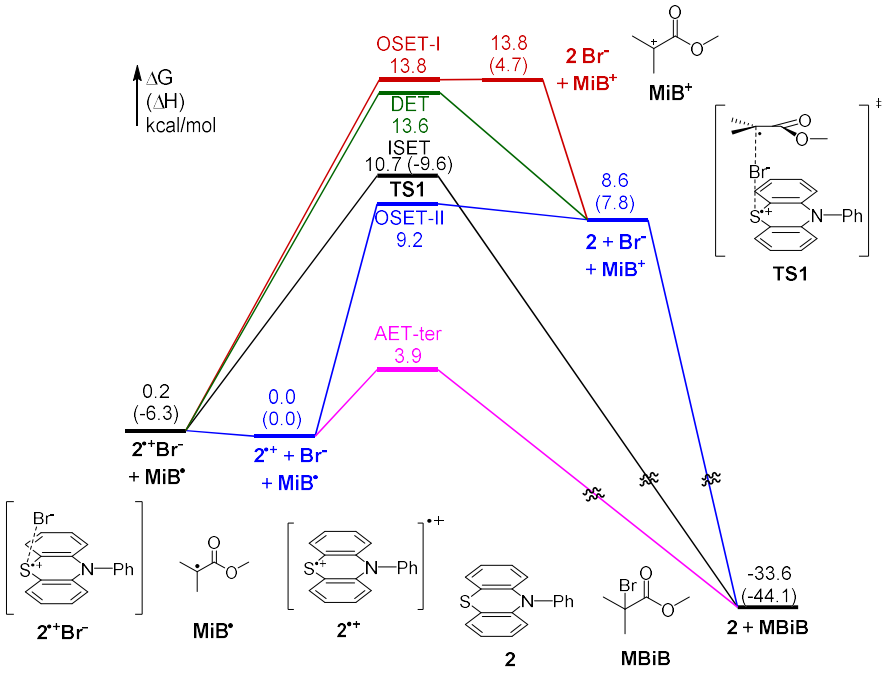

Figure 7.7. Reaction energy profiles for the reaction of **2**$^{\bullet+}$**Br**$^{-}$ with MiB$^{\bullet}$. Magenta: associative electron transfer involving a termolecular encounter (AET-ter). Black: inner-sphere electron transfer (ISET) (*i.e.* concerted atom transfer); Green: dissociative electron transfer from MiB$^{\bullet}$ to **2**$^{\bullet+}$**Br**$^{-}$ (DET); Red: stepwise outer-sphere electron transfer from MiB$^{\bullet}$ to **2**$^{\bullet+}$**Br**$^{-}$ to form **2** **Br**$^{-}$ (OSET-I); Blue: outer-sphere electron transfer from MiB$^{\bullet}$ to the dissociated radical cation **2**$^{\bullet+}$ (OSET-II). Reaction free energies and energy of **TS1** were obtained through DFT calculations.[10]

fer from MiB$^{\bullet}$ to the dissociated radical cation **2**$^{\bullet+}$ (OSET-II) requires 9.2 kcal/mol of activation free energy, which is close to the activation energy of ISET pathway (10.5 kcal/mol). The other two reaction pathways, OSET-I and DET, have higher barriers of 13.6 and 13.4 kcal/mol, respectively.

These calculations suggest AET-ter to be the most favored pathway. Additionally, some experimental observations are in contrast with OSET-I, OSET-II and DET. First, the reaction of **2** with ECPA (alkyl chloride) was not as controlled as the reaction between **2** and EBPA (alkyl bromide). The effects of the halide (better control with RBr than RCl) rule out the possibility of OSET-II, which should not be affected by the nature of X^{-}. Also, the lack of oligomer formation during the polymerization provides further evidence against the formation of MiB^{+}, thus ruling out not only OSET-II pathway but also DET and OSET-I pathways.

The effects of halides on the barriers of ISET and all other four deactivation pathways were then explored. When MCiB is used in place of MBiB as the initiator in the reaction

Table 7.4. Activation energy for deactivation pathways $\Delta G^{\ddagger}$ ($\Delta H^{\ddagger}$) in kcal mol^{-1}.

Entry	Catalyst	Initiator	Deactivation pathway				
			ISET[a]	AET-ter[b]	DET[a]	OSET-I[a]	OSET-II[b]
1	**2**, Ph-PTZ	MBiB	10.5 (−3.3)	3.9	13.4	13.6	9.2
2	**2**, Ph-PTZ	MCiB	12.5 (−2.4)	6.1	16.5	11.2	9.2

[a] Activation energies with respect to the ion pair complex $\mathbf{Cat}^{\bullet+}\mathbf{X}^{-}$; [b] Activation energies with respect to separated ions $\mathbf{Cat}^{\bullet+}$ and $\mathbf{X}^{-}$.

with catalyst **2** (entry 2, Table 7.4), the barriers of the ISET, AET-ter and DET pathways increase, whereas that of OSET-I decreases. As expected, the halide has no effect on the barrier of the OSET-II pathway. While the most preferred pathway with MCiB is still AET-ter, the activation free energy is 2.2 kcal/mol higher than the reaction with MBiB.

In summary, the computed activation energies indicate that the AET-ter pathway is preferred in the deactivation process. The poor control of polymerization of MMA with alkyl chloride as ATRP initiator provides a further support for the AET-ter deactivation mechanism. With **2** as catalyst, $\Delta G^{\ddagger}$ of AET-ter increases by 2.2 kcal/mol when Cl^{-} is used in place of Br^{-}. This will result in a considerable lowering of the deactivation rate, which might not be able to outrun radical-radical termination reactions (see next section).

7.4.1 Comparison of rates of deactivation pathways

In a controlled radical polymerization, the deactivation reaction should be faster than radical-radical termination to maintain the living character. Therefore, the rate constants and reaction rates for different deactivation pathways were calculated for catalyst **2***, and the results are summarized in Table 7.5. The rate of radical termination could be obtained from $R_t = k_t[R^{\bullet}]^2$, where k_t is the rate constant of radical-radical termination and $[R^{\bullet}]$ is the concentration of the propagating radical. $[R^{\bullet}] \approx 4.6 \times 10^{-8}$ M could be estimated from $k_p^{app} = k_p[R^{\bullet}]$, where the propagation rate constant, $k_p = 10^3$ M^{-1} s^{-1} [20]and k_p^{app}, the apparent rate constant of propagation, was obtained from the polymerization of MMA with **2** under 4.9 mW/cm^2 irradiation (Figure 7.2a).

For a termolecular reaction pathway AET-ter, the frequency factor Z_{ter} is calculated following Tolman's approach:[21]

$$Z_{ter} = N_A^2 8\pi^2 \left(\frac{2RT}{\pi}\right)^{1/2} \left[\left(\frac{m_A + m_B}{m_A m_B}\right)^{1/2} + \left(\frac{m_B + m_C}{m_B m_C}\right)^{1/2}\right] d_{A\leftrightarrow B}^2 d_{B\leftrightarrow C}^2 \delta \qquad (7.13)$$

where A, B and C are the three species involved in the reaction, d is the distance between the centers of the spheres equivalent to the subscript particles, and δ is the distance between the first two spheres when hit by the third. Usually δ is taken to be between 0.3 Å[19] and 1 Å.[21c] The smaller value of 0.3 Å was used to avoid overestimating Z_{TER}. The hard sphere diameters of the species involved in the reaction were estimated from their computed volumes or taken from the literature (see detailed calculations in Appendix C). Then, using $\Delta G^{\ddagger}_{AET\text{-}ter} = 3.9$ kcal mol^{-1} (Table 7.4), the rate constant was calculated from eq. 7.14 as $k_{AET\text{-}ter} = 4.6\times10^{7}$ M^{-2} s^{-1}. This deactivation rate constant is slightly higher than k_{deact} in typical Cu-based ATRP (chapter 3 and ref. 22).

$$k_{AET\text{-}ter} = Z_{ter} e^{\frac{-\Delta G^{\ddagger}_{AET\text{-}ter}}{RT}} \tag{7.14}$$

The rate of termolecular deactivation is given by:

$$R_{AET\text{-}ter} = k_{AET\text{-}ter}[2^{\bullet+}][Br^{-}][R^{\bullet}] \tag{7.15}$$

However, both $\mathbf{2}^{\bullet+}$ and Br^{-} concentration need to be estimated. Considering around 10% of termination, [Br^{-}] should be *ca.* 5×10^{-3} M. Moreover, current intensity of Br^{-} oxidation in the CV registered during a metal-free ATRP confirmed that around 5–10×10^{-3} M of Br^{-} was generated after a few hours (Figure 7.8). The radical cation $\mathbf{2}^{\bullet+}$ could not be directly detected during the electrochemical measurements, and it slowly decomposed by the reaction with Br^{-}.[23] Therefore, a low value of 5×10^{-4} M was chosen for the concentration of $\mathbf{2}^{\bullet+}$. Using these concentrations together with [$R^{\bullet}$] ≈ 4.6×10^{-8} M gives $R_{AET\text{-}ter} = 5.3\times10^{-6}$ M s^{-1}.

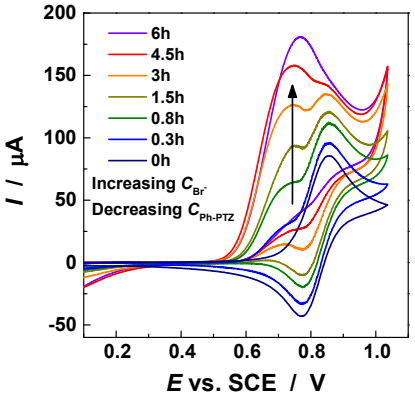

Figure 7.8. Cyclic voltammetry during photo-mediated experiment. Initial [**2**] = 5.9×10^{-3} M.

Table 7.5. Rate constants and rates of proposed deactivation pathways.

Reaction		Rate law	k (M^{-1} s^{-1})	R (M s^{-1})	R/R_t
Termination	$2R^{\bullet} \rightarrow R\text{-}R$	$R_t = k_t[R^{\bullet}]^2$	10^7	2.1×10^{-8}	1
AET,ter	$\mathbf{2}^{\bullet+} + R^{\bullet} + Br^- \rightarrow RBr + \mathbf{2}$	$R_{AET\text{-}ter} = k_{AET\text{-}ter}[\mathbf{2}^{\bullet+}][Br^-][R^{\bullet}]$	3.4×10^7	3.9×10^{-6}	1.9×10^2
	$\mathbf{2}^{\bullet+} + R^{\bullet} + Cl^- \rightarrow RCl + \mathbf{2}$	$R_{AET\text{-}ter} = k_{AET\text{-}ter}[\mathbf{2}^{\bullet+}][Cl^-][R^{\bullet}]$	7.8×10^5	$<9.0\times10^{-8}$	<4.3
ISET	$\mathbf{2}^{\bullet+}\mathbf{Br}^- + R^{\bullet} \rightarrow RBr + \mathbf{2}$	$R_{ISET} = k_{ISET}[\mathbf{2}^{\bullet+}\mathbf{Br}^-][R^{\bullet}]$	6.1×10^3	5.0×10^{-10}	2.4×10^{-2}
OSET-II	$\mathbf{2}^{\bullet+} + R^{\bullet} \rightarrow R^+ + \mathbf{2}$	$R_{OSET\text{-}II} = k_{OSET\text{-}II}[\mathbf{2}^{\bullet+}][R^{\bullet}]$	3.5×10^3	7.7×10^{-8}	3.7
DET	$\mathbf{2}^{\bullet+}\mathbf{Br}^- + R^{\bullet} \rightarrow \mathbf{2} + Br^- +$	$R_{DET} = k_{DET}[\mathbf{2}^{\bullet+}\mathbf{Br}^-][R^{\bullet}]$	45	3.7×10^{-12}	1.8×10^{-4}
OSET-I	$\widetilde{\mathbf{2}}^{\bullet+}\mathbf{Br}^- + R^{\bullet} \rightarrow \mathbf{2}\text{-}\mathbf{Br}^- + R^+$	$R_{OSET\text{-}I} = k_{OSET\text{-}I}[\mathbf{2}^{\bullet+}\mathbf{Br}^-][R^{\bullet}]$	32.4	$<2.7\times10^{-12}$	$<1.3\times10^{-4}$

[a] Unit: M^{-2} s^{-1}. [b] Activation of MCiB is much slower than activation of MBiB, $k_{act,MCiB}/k_{act,MBiB} = 2.6\times10^{-3}$. This implies that $[\mathbf{2}^{\bullet+}]$ is much smaller with MCiB than with MBiB. For the same reason $[Cl^-] < [Br^-]$. Therefore, $R_{AET\text{-}ter}$ and $R_{AET\text{-}ter}/R_t$ are overestimated.

A similar approach was used to calculate the rate constants and rates of all other deactivation pathways (see Appendix C for the detailed calculations). Although the concentration of $\mathbf{2}^{\bullet+}$ has a high uncertainty, the ratio of deactivation rates is independent of $[\mathbf{2}^{\bullet+}]$ and $[\mathbf{R}^{\bullet}]$. To single out the effective deactivation pathway, the rate of all deactivation reactions must be first compared to R_t and then to each other. R/R_t values calculated for all deactivation pathways are reported in Table 7.5 (last column). ISET, DET and OSET-I are to be discarded as possible deactivation pathways as they are at least 2 orders of magnitude slower than termination. The rate of OSET-II is comparable with R_t, but clearly this deactivation pathway cannot provide good control. This leaves AET-ter, which is more than 2 orders of magnitude faster than radical-radical termination when RBr is used as initiator or bromide ions are added, as the only possible deactivation pathway.

The same conclusion is reached if $R_{AET\text{-}ter}$ is calculated on the basis of experimental data. In this case, using $\Delta G^{\ddagger} = 29.6$ kcal mol^{-1} (Table 7.3) gives $\Delta G^{\ddagger}_{AET\text{-}ter} = 5.0$ kcal/mol. It follows that $k_{AET\text{-}ter} = 5.8\times10^6$ M^{-2} s^{-1}, $R_{AET\text{-}ter} = 6.8\times10^{-7}$ M s^{-1} and $R_{AET\text{-}ter}/R_t = 32$. It is clear that AET-ter is the fastest deactivation pathway and, in particular, at least one order of magnitude faster than all other deactivation reactions. When RCl is used as initiator, AET-ter is only four times faster than termination, which explains why control is lost with a chloride as polymerization initiator (ECPA).

Scheme 7.2. Proposed overall mechanism for photoinduced metal-free ATRP.

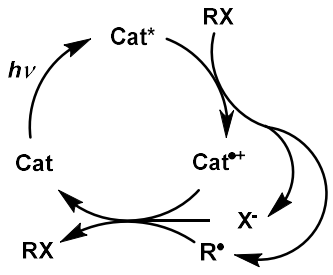

Overall Mechanism. A possible overall mechanism was constructed in Scheme 7.2 by combining all the information from experimental data and calculations based on electron transfer theories (Marcus and further developments). After Ph-PTZ **2** is excited to the excited state **2***, a dissociative electron transfer occurs from **2*** to the conventional ATRP initiator (alkyl bromide, MBiB), forming the alkyl radical required to initiate the polymerization. In this process, **2** is oxidized to the radical cation, $\mathbf{2}^{\bullet+}$, which exists in equilibrium with $2^{\bullet+}Br^-$. The associative electron transfer (AET-ter) from $2^{\bullet+}$ to the propagating radical and bromide anion finishes the catalytic cycle to regenerate ground-state catalyst 2 and polymer chain with bromine as chain-end fidelity.

7.5 Conclusions

The mechanism of photoinduced metal-free ATRP was investigated via a combination of different types of investigation involving polymerization, kinetics, cyclic voltammetry, and dissociative electron transfer theories. A controlled radical polymerization needs to meet two criteria: fast initiation/activation and efficient deactivation. All selected catalysts are involved in the activation process, and generate alkyl radicals upon irradiation, but not all are efficient deactivators. All phenothiazine derivatives participate in the deactivation process; however, only *N*-aryl phenothiazine derivatives are stable enough to survive until the later stages of the polymerization. Alkyl chlorides could not be successfully used as ATRP initiators and provide an uncontrolled radical polymerization.

Photoinduced metal-free ATRP provides a fascinating avenue to synthesize well-defined polymers in the absence of residual transition metals. For the analyzed phenothiazine-based photocatalysts, activation involves a dissociative electron transfer to RX. Activation rate constants are higher than for classic Cu-based ATRP systems. However, due to a short lifetime of the excited states, activation of RX is quite slow and

relatively large amounts of catalyst should be used. Comparison of all reasonable deactivation pathways showed that the most favored reaction route is the termolecular reaction of $2^{\bullet+}$, $R^{\bullet}$ and Br^{-}. Similarly to activation reaction, deactivation rate constants are at least as high as that reported for copper complexes, but in this case the rate is severely reduced by the low likelihood of three-center encounters. Therefore, precise control over macromolecular architecture by metal-free ATRP appears to be limited by the establishment of a fairly slow activation/deactivation process.

In order to obtain a well-controlled metal-free ATRP, the catalyst should efficiently absorb photons, and therefore must be excited at the proper wavelength. In addition, photoexcitation should produce a strongly reducing excited state ($E^{\Theta}_{Cat^{\bullet+}/Cat^{*}} \approx$ -2 V vs. SCE), with a sufficiently long lifetime ($\tau_0 \geq 5$ ns) and high quantum efficiency ($\Phi_F \geq 0.01$) to ensure efficient activation of the R-X bond. The generated radical cation should also be stable (lifetime >> 10 s) and have a high reduction potential ($E^{\Theta}_{Cat^{\bullet+}/Cat} \approx 0.8$ V vs. SCE) to ensure the quick oxidative trapping of $R^{\bullet}$ and Br^{-}.

References

(1) Fors, B. P.; Hawker, C. J. *Angew. Chem. Int. Ed.* **2012**, *51*, 8850–8853.

(2) (a)Treat, N. J.; Sprafke, H.; Kramer, J. W.; Clark, P. G.; Barton, B. E.; Read de Alaniz, J.; Fors, B. P.; Hawker, C. J. *J. Am. Chem. Soc.* **2014**, *136*, 16096-16101. (b) Pan, X.; Lamson, M.; Yan, J.; Matyjaszewski, K. *ACS Macro Lett.* **2015**, *4*, 192-196.

(3) Lin, C. Y.; Coote, M. L.; Gennaro, A.; Matyjaszewski, K. *J. Am. Chem. Soc.* **2008**, *130*, 12762-12774.

(4) Kaur, A.; Ribelli, T. G.; Schröder, K.; Matyjaszewski, K.; Pintauer, T. *Inorg. Chem.* **2015**, *54*, 1474-1486.

(5) Wallentin, C.-J.; Nguyen, J. D.; Finkbeiner, P.; Stephenson, C. R. J. *J. Am. Chem. Soc*. **2012**, *134*, 8875-8884.

(6) (a) Marcus, R. A. *J. Chem. Phys.* **1956**, *24*, 966-978; (b) Pause, L.; Robert, M.; Savéant, J.-M. *J. Am. Chem. Soc*. **2000**, *122*, 9829-9835; (c) Savéant, J. M. *J. Am. Chem. Soc.* **1987**, *109*, 6788-6795; (d) Savéant, J. M. *J. Am. Chem. Soc*. **1992**, *114*, 10595-10602.

(7) Lin, C. Y.; Coote, M. L.; Petit, A.; Richard, P.; Poli, R.; Matyjaszewski, K. *Macromolecules* **2007**, 40, 5985-5994.

(8) (a) Tehfe, M.-A.; Lalevée, J.; Morlet-Savary, F.; Graff, B.; Blanchard, N.; Fouassier, J.-P. *ACS Macro Lett*. **2012**, *1*, 198-203; (b) Kolosov, D.; Adamovich, V.; Djurovich, P.; Thompson, M. E.; Adachi, C. *J. Am. Chem. Soc.* **2002**, *124*, 9945-9954.

(9) Kalyanasundaram, K. *Coord. Chem. Rev.* **1982**, *46*, 159-244.

(10) Pan, X.; Fang, C.; Fantin, M.; Malhotra, N.; Young So, W; Peteanu, L. A.; Isse, A. A.; Gennaro, A.; Liu, P.; Matyjaszewski, K., *J. Am. Chem. Soc.* DOI: 10.1021/jacs.5b13455. Published Online: January 28, 2016. http://pubs.jacs.org.

(11) (a) Isse, A. A.; Sandonà, G.; Durante, C.; Gennaro, A. *Electrochim. Acta* **2009**, *54*, 3235-3243; (b) Costentin, C.; Robert, M.; Savéant, J.-M. *J. Am. Chem. Soc*. **2003**, *125*, 10729-10739; (c) Isse, A. A.; Gennaro, A. *J. Phys. Chem. A* **2004**, *108*, 4180-4186; (d) Cardinale, A.; Isse, A. A.; Gennaro, A.; Robert, M.; Savéant, J.-M. *J. Am. Chem. Soc*. **2002**, *124*, 13533-13539; (e) Andrieux, C. P.; Le Gorande, A.; Savéant, J. M. *J. Am. Chem. Soc*. **1992**, *114*, 6892-6904; (f) Andrieux, C. P.; Gallardo, I.; Savéant, J. M.; Su, K. B. *J. Am. Chem. Soc*. **1986**, *108*, 638-647.

(12) Rehm, D.; Weller, A. *Isr. J. Chem*. **1970**, *8*, 259-271.

(13) Isse, A. A.; Bortolamei, N.; De Paoli, P.; Gennaro, A. *Electrochim. Acta* **2013**, *110*, 655-662.

(14) Isse, A. A.; Lin, C. Y.; Coote, M. L.; Gennaro, A. *J. Phys. Chem. B* **2011**, *115*, 678-684.

(15) Saucin, M.; Van de Vorst, A. *Radiat. Environ. Biophys.* **1980**, *17*, 159-168.

(16) Lorandi, F.; Fantin, M.; Isse, A. A.; Gennaro, A. *Polymer* **2015**, *72*, 238-245.

(17) Turro, N. J., Modern Molecular Photochemistry **1978**, University Science Books, Herndon, VA, USA.

(18) Bortolamei, N.; Isse, A. A.; Gennaro, A. *Electrochim. Acta* **2010**, *55*, 8312-8318.

(19) Savéant, J.-M. J. *Electroanal. Chem*. **2000**, *485*, 86-88.

(20) Matyjaszewski, K. *Macromolecules* **2012**, *45* (10), 4015–4039.

(21) (a) R.C. Tolman, Statistical Mechanics, Chemical Catalog Co, New York, **1927**, p. 247. (b) J.R. Partington, An Advanced Treatise on Physical Chemistry, vol. 1, Longmans, London, **1967**, p. 292. (c) J.W. Moore, R.N. Pearson, Kinetics and Mechanism, vol. 131, Wiley, New York, **1981**, p. 130.

(22) (a) Matyjaszewski, K.; Paik, H.-j.; Zhou, P.; Diamanti, S. J. *Macromolecules* **2001**, *34*, 5125-5131; b) Tang, W.; Kwak, Y.; Braunecker, W.; Tsarevsky, N. V.; Coote, M. L.; Matyjaszewski, K. *J. Am. Chem. Soc*. **2008**, *130*, 10702-10713; c) Zerk, T. J.; Bernhardt, P. V. *Inorg. Chem*. **2014**, *53*, 11351-11353.

(23) Shine, H. J.; Silber, J. J.; Bussey, R. J.; Okuyama, T. *J. Org. Chem*. **1972**, *37*, 2691-2697.

Conclusions and Future Perspectives

ATRP in water has peculiar differences with respect to the same reaction in traditional organic solvents. It is characterized by extreme reactivity of the active $[Cu^{I}L]^{+}$ catalyst and low stability of the tertiary deactivator $[X\text{-}Cu^{II}L]^{+}$. Controlled electrochemically mediated ATRP is possible by modulating the rate of (re)generation of the active $[Cu^{I}L]^{+}$ complex and hence the ratio between Cu^{I} and Cu^{II} concentrations during polymerization. In the case of methacrylic monomers, successful results can be achieved by applying potentials slightly more positive than $E^{\ominus}$ of the catalyst. Also, a large excess of halide ions should be added to the system, which increases $C_{[X\text{-}Cu^{II}L]^{+}}$ and decreases $C_{[Cu^{I}L]^{+}}$. pH should be appropriately selected: efficacy of the catalyst is limited by formation of inactive $[HO\text{-}Cu^{II}L]^{+}$ at high pH, and by protonation of the ligand at low pH. Pyridinic ligands (*e.g.* TPMA) are stable down to pH 1, while aliphatic amine ligands (*e.g.* Me_6TREN) are stable only at pH ≥ 5.

In order to study the peculiar reactivity of $[Cu^{I}L]^{+}$ in water, electrochemical techniques based on direct monitoring of Cu^{I} species or on the generation of transient reactive species near the electrode were used to accurately determine ATRP activation rate constants both in water and organic solvents. Electrochemical techniques proved to be powerful, enabling determination of a very broad range of k_{act} values ($10^{-4} < k_{act} < 10^{8}$ M^{-1} s^{-1}). In water, the reactivity of $[Cu^{I}L]^{+}$ decreases 10-100 times in the presence of typical monomer concentrations (10-20%). In general, k_{act} strongly depends on K_{ATRP} both in water and in organic solvents, whereas k_{deact} is roughly constant in CH_3CN but slightly increases with increasing K_{ATRP} in water. Good linear correlations of k_{act} with K_{ATRP} and bond dissociation free energy of the initiator were observed for several catalysts and extensive series of alkyl halide initiators including both chlorides and bromides. This sets the basis for easy prediction of the reactivity of $[Cu^{I}L]^{+}$/RX initiation systems.

Investigation of the ATRP catalytic system in the ionic liquid 1-butyl-3-methylimidazolium trifluoromethanesulfonate showed that this solvent is similar to conventional organic solvents, in terms of speciation of the catalyst, redox potentials of the catalytic complex, reactivity of $[Cu^{I}L]^{+}$, and stability of $[X\text{-}Cu^{II}L]^{+}$.

ATRP of acid monomers (acrylic and methacrylic acid) is hampered by a side reaction involving the active chain end (an intramolecular cyclization with the terminal halide atom as leaving group). Conducting the reaction with the more stable C-Cl end functionality and lowering pH allowed us to obtain controlled polymers with linear, telechelic and three-arm star architectures. A relatively negative E_{app} was necessary to compensate for the lower activity of $[Cu^{I}TPMA]^{+}$ in the acidic environment. Fast, controlled reactions up to high degree of polymerization were obtained by regenerating the Cu^{I} species by either electric current (*e*ATRP) or comproportionation with a copper wire (SARA ATRP).

*e*ATRP conventional setup–which requires expensive, rare and non-functionalizable platinum working and counter electrodes–was expanded by using carbon materials and inexpensive metals and alloys, which are appealing for the successful scale-up commercialization of the electrochemical process. Methacrylic monomers were polymerized in water with satisfactory control by using a simple two-electrode setup (without Pt) under galvanostatic conditions (fixed current). A sacrificial Al counter electrode allowed avoiding separation of anodic and cathodic compartments.

The mechanism of metal-free ATRP differs from traditional, Cu-based ATRP. Activation of the C-X bond by excited state phenyl-phenothiazine is characterized by an extremely high rate constant, but the reaction rate is severely reduced by the low quantum efficiency and lifetime of the excited species. The most likely deactivation pathway involves the simultaneous three-center encounter of a halide ion, a radical and the deactivator (phenothiazonium radical cation). Although the low likelihood of this termolecular reaction somehow hinders deactivation, the rate of the deactivation reaction is fast enough to warrant satisfactory control over molecular weight distribution. The development of new metal-free catalysts should take into account that the ideal photoactive molecule is characterized by high absorption coefficient, elevated quantum efficiency, long excited state lifetime, very negative reduction potential of the excited state and positive reduction potential of the ground state. Moreover, it should not easily react with Br^{-}.

Thanks to the definition and quantification of the mechanism and potential side reactions of aqueous ATRP, water should no longer be considered a problematic solvent. On the basis of the results reported in this thesis, a more confident and reliable design of experimental conditions is now possible (*e.g.* Cu^{I} regeneration rate, pH, type and concentration of halide ions, nature of the ligand, *etc*.). New catalysts, initiating systems and

monomers should be tested, particularly those relevant for biological applications (such as grafting hydrophilic monomers from proteins, DNA, or nanogels).

The polymerization of acidic monomers, once considered one of the biggest limitations of ATRP, should be extended and applied to several systems in order to exploit the unique properties of acidic polymers (good complexing ability, charge, response to stimuli such as temperature, pH, and ionic strength).

Appendix A

Experimental Section

A.1 Chemicals

Copper. Copper(II) trifluoromethanesulfonate ($Cu(OTf)_2$, Alpha Aesar, 98%), copper(II) chloride (Sigma-Aldrich, 99%), copper(II) bromide (Sigma-Aldrich, 99%), 2,2';6',2"-terpyridine (terpy, Alfa Aesar, 97%), and tetrakis(acetonitrile)copper(I) tetrafluoroborate ($Cu^I(CH_3CN)_4BF_4$, Sigma-Aldrich, 97%) were used without further purification. Stock solutions of copper(I) in CH_3CN were standardized by spectrophotometric analysis using 2,9-dimethyl-1,10-phenantroline as a specific ligand, as described in the literature.[1] Copper wire was activated with 3:1 v/v MeOH/aqueous HCl, rinsed with MeOH and dried under N_2.

Amine ligands. tris(2-pyridylmethyl)amine (TPMA, ATRP Solutions, 98%), tris[2-(dimethylamino)ethyl]amine (Me_6TREN, Alfa Aesar 99+%) and N,N,N′,N″,N″-pentamethyldiethylenetriamine (PMDETA, Sigma-Aldrich, 98%) were used as received.

Initiators. α -chloroisobutyric acid was synthetized according to a published procedure.[2] α-chlrophenylacetic acid (CPAA, 97%) was purchased from Combi-Blocks and used as received. All other initiators were purchased from Sigma-Aldrich or Alfa-Aesar with good purity and used without further purification.

Supporting electrolytes and other salts. Tetraethylammonium chloride (Et_4NCl, Sigma-Aldrich, 99%), tetraethylammonium bromide (Et_4NBr, Sigma-Aldrich, 99%) and tetraethylammonium tetrafluoroborate (Et_4NBF_4, Alfa Aesar, 99%) were purified by recrystallization from dichloromethane-acetone-hexane (2/2/1, v/v), ethanol-diethyl ether (1/2, v/v) and ethanol, respectively. They were then dried under vacuum for at least 48 h and stored over P_2O_5. Sodium chloride (Fisher Scientific, 99.0%) and sodium bromide (Fisher Scientific, 99.0%) were used as received.

Monomers. Oligo(ethyleneoxide) methyl ether acrylate (OEOA, Sigma-Aldrich, average M_w 480) and oligo(ethyleneoxide) methyl ether methacrylate (OEOMA, Sigma-Aldrich, average M_w 500) were passed through a column filled with basic alumina to remove polymerization inhibitors. *N*-isopropylacrylamide (NiPAM, Sigma-Aldrich, 97%) was recrystallized from *n*-hexane. Methacrylic acid (MAA, Sigma-Aldrich, 99%) and acrylic

acid (AA, Sigma-Aldrich, 99%) were distilled through a 10 cm Vigreux column to remove the polymerization inhibitors. Copper turnings were added in the distillation flask and, only for AA distillation, copper wire was inserted in the bottom of the Vigreux column.

Buffers. When necessary, pH was adjusted to the desired values with buffers prepared from the tertiary amines, diethylpiperazine, (DEPP), tetraethyl ethylenediamine (TEEN), and tetraethyl methylenediamine, (TEMN), all from Alfa Aesar with good purity (98%). These amines are sterically hindered and are not able to form complexes with hydrated metal ions in aqueous solutions (the formation of precipitates was observed only after days).[3] Sodium hydrogen phosphate (Fisher Scientific, 99%) was used as received.

Other chemicals. Metal-free ATRP photocatalysts were synthetized as described in reference 4. Deionized water was further purified by double distillation or by a Barnstead Nanopure system (Thermo Scientific). Sodium azide (NaN_3, Sigma-Aldrich, 99%), 37% HCl aqueous solution (Fisher Scientific, ACS grade) were all used without purification.

A.2 Instrumentation

Cyclic Voltammetry (CV). CVs were performed either by an Autolab PGSTAT30 potentiostat (Eco-Chimie, Utrecht, The Netherlands) interfaced to a PC running GPES 4.9 software, or a PARC 173 potentiostat, equipped with a function generator PARC 175 and a digital oscilloscope Le Croy Waverunner LT322. The experiments were carried out in a three electrode cell with a glassy carbon disc working electrode (3 mm diameter, Metrohm) and a Pt counter electrode. In aqueous solutions, the reference electrode was saturated calomel electrode (SCE, Schott Gerade), whereas Ag|AgI|0.1 M n-Bu_4NI in DMF was used as reference electrode in non-aqueous solutions. The latter was calibrated after each experiment against the ferrocenium/ferrocene couple (Fc^+/Fc), which allowed conversion of all potentials to the aqueous saturated calomel electrode (SCE) scale by using $E^{e}_{Fc^+/Fc}$ = 0.527 V vs. SCE in DMA. Chronoamperometry experiments were performed using a rotating disc electrode (RDE) with a glassy carbon tip of 3 mm diameter (Autolab, Eco-Chimie). Prior to each experiment, the working electrode surface was cleaned by polishing with 0.25-μm diamond paste, followed by ultrasonic rinsing in ethanol for 5 min. Digital simulation of voltammetric responses was performed with DigiSim 3.03 (Bioanalytical Systems, Inc.).

UV-Vis absorbance spectra. Absorbance spectra were acquired with a UV-Vis Cary-5 spectrometer, in a 1.00 cm quartz optical cell. Working solutions were prepared from a

stock solution of the examined complex at a buffered pH and a constant ionic strength of 0.1 M.

NMR. NMR was used to measure monomer conversion and $M_{n,th}$ during polymerization reactions ($M_n = M_{RX} + (C_M/C_{RX})M_M \times$conversion). The signal of Et_4NBF_4, Et_4NBr or solvent was used as internal standard to determine monomer conversion using a Bruker 300 MHz instrument.

Gel Permeation Chromoatography (GPC). GPC was used to measure relative M_w, M_w/M_n, of the polymer samples. OEOMA samples were filtered over neutral alumina, $MgSO_4$ and 200 nm PTFE filters prior to injection. Analysis was carried out at 70 °C on two Agilent PLgel 5 μm MIXED-C, 300 × 7.5 mm columns, connected in series; the mobile phase was a mixture of DMF + 1% v/v acetic acid + 1% v/v trimethylamine. Calibration was performed with PMMA standards. PMAA and PAA samples were filtered with a 200 nm PTFE or PES filter. Analysis was performed using a Waters RI detector and PSS columns with a calibration based on sodium methacrylate standards (PSS) in 0.1 M Na_2HPO_4 as mobile phase, at 30 °C.

A.3 General procedures

Ionic liquid purification. 20 mL of [BMIm][OTf] were mixed with 80 mL of bidistilled water and the solution was titrated with aqueous KOH, until pH = 7. Water was removed through a rotating evaporator. The neutralized ionic liquid was dissolved in 40 mL of CH_2Cl_2 and the organic fraction was extracted 5 times, under vigorous stirring, with 30 mL of bidistilled water. The aqueous fractions were combined and evaporated at a rotavap and then dried at 100 °C for 12 h under vacuum. Purified [BMIm][OTf] was stored under Ar.

General procedure for the determination of K_X. A stock solution containing 0.5 mM $Cu(OTf)_2$, 1 mM amine ligand, 0.12 M Et_4NX (X = Cl, Br) and 2.5 mM TEEN was prepared and then the pH was adjusted to 6 by addition of $HClO_4$. 4 mL aliquots of this solution were placed into several 5 mL volumetric flasks, and a different amount of concentrated NaN_3 was added to each flask, then the flask was filled with distilled water. UV-Vis spectra of these solutions were recorded using a 1.00 cm cuvette.

General eATRP procedure. A seven-necked, thermostated electrochemical cell was used for the polymerizations. In a typical experiment with $[Cu^{II}TPMA]^{2+}$ as catalyst, 0.315 g of Et_4NBr (1.50 mmol), 12.7 mL H_2O, 1.5 mL OEOMA (1.62 g, 3.24 mmol), 0.73 mL of a 20.5 mM $Cu^{II}(OTf)_2$ stock solution (1.50 μmol Cu) and 0.73 mL of 21.5 mM TPMA

stock solution were added to the cell. 4.35 μL of HEBiB (3.00 μmol) was added to this mixture. The cell was equipped with a Pt gauze working electrode (surface area ~ 6 cm^2), a saturated calomel reference electrode (SCE) and a Pt plate counter electrode. The counter electrode was separated from the cathodic compartment by a glass frit and a methylcellulose gel saturated with Et_4NBF_4. The solution was thermostated at 25 °C and degassed with Ar for at least 15 min, then the reaction was performed under vigorous stirring (~2 cm stirring bar at ~1000 rpm), by applying the appropriate potential to the working electrode. Cyclic voltammetry measurements were taken on a glassy carbon or Pt disc working electrode (area ~ 0.07 cm^2) before and after the polymerization. A similar setup was used in *e*ATRP experiments with different cathode materials.

General SARA ATRP procedure. 0.050 g of NaCl (8.56×10^{-4} mol), 0.5 mL of MAA (0.508 g, 5.9×10^{-3} mol), 2.6 mg TPMA (9.0×10^{-6} mol), 0.051 mL of a 0.05 M $CuCl_2$ stock solution (3.0×10^{-6} mol Cu), 0.295 mL of a 0.100 M BiBA solution (2.95×10^{-5} mol), and 0.65 mL of a 1.2 M HCl solution (6.3×10^{-4} mol) were added to 3.75 mL of H_2O. The solution was degassed for at least 30 minutes and then transferred to a previously degassed and sealed flask containing 10 cm Cu wire with diameter d = 1 mm.

General metal-free ATRP procedure. Methyl methacrylate (2.1 mL, 20 mmol, 100 equiv), 0.035 mL of ethyl α-bromophenylacetate (EBPA, 48.6 mg, 0.2 mmol, 1 equiv), 5.5 mg of Ph-PTZ (**2**, 0.02 mmol, 0.1 equiv), and 2.1 mL of DMA were added into a 10 mL Schlenk flask. The flask was tightly sealed and oxygen was removed by three cycles of freeze-pump-thaw. All the photoinduced ATRPs were conducted with one of two photoreactors: a 2.1 mW/cm^2 SHANY® UV (http://www.shanycosmetics.com/) or a 4.9 mW/cm^2 MelodySusie® UV (http://www.melodysusie.com/).

Samples were periodically withdrawn from the reaction mixtures and analyzed by GPC and ^{1}H NMR.

Refereces

(1) Gahler, A. R. *Anal. Chem.* **1954**, *26*, 577–579.

(2) Kundiger, D. G.; Ikenberry, E. A.; Ovist, E. B. W.; Peterson, J. G.; Dick, C. R. *J. Am. Chem. Soc.* **1960**, *82*, 2953–2956.

(3) Yu, Q.; Kandegedara, A.; Xu, Y.; Rorabacher, D. B. *Anal. Biochem.* **1997**, *253*, 50–56.

(4) Pan, X.; Fang, C.; Fantin, M.; Malhotra, N.; Young So, W; Peteanu, L. A.; Isse, A. A.; Gennaro, A.; Liu, P.; Matyjaszewski, K., *Submitted Manuscript.*

Appendix B

Derivation of Formulas for K_X Determination

As NaN_3 is added to a $[Cu^{II}L]^{2+}$ solution, the following equilibrium is established:

$$[Cu^{II}L]^{2+} + N_3^- \rightleftharpoons [N_3\text{-}Cu^{II}L]^+ \qquad K_{N_3} = \frac{C_{[N_3\text{-}Cu^{II}L]^+}}{C_{[Cu^{II}L]^{2+}} C_{N_3^-}} \tag{B.1}$$

Mass balance for Cu^{II} is

$$C_{[Cu^{II}L]^{2+}} = C^*_{Cu^{II}} - C_{[N_3\text{-}Cu^{II}L]^+} \tag{B.2}$$

where $C^*_{Cu^{II}}$ is the total Cu^{II} concentration present in solution. Considering this mass balance and rearranging eq. B.1, the following relation is obtained

$$\frac{1}{C_{N_3^-}} = K_{N_3} \frac{C^*_{Cu^{II}}}{C_{[N_3\text{-}Cu^{II}L]^+}} - K_{N_3} \tag{B.3}$$

$[Cu^{II}L(N_3)]^+$ concentration is obtained by spectrophotometry, and therefore can be expressed through the Lambert-Beer law as $C = A/\varepsilon l$, where A is absorbance, ε is the extinction coefficient of $[N_3\text{-}Cu^{II}L]^+$ and l is optical path length. Replacing $C_{[N_3\text{-}Cu^{II}L]^{2+}}$ with $A/\varepsilon l$ and considering the following mass balance:

$$C_{N_3^-} = C^*_{N_3^-} - C_{[Cu^{II}L(N_3)]^+} \tag{B.4}$$

lead to the following equation:

$$\frac{1}{C^*_{N_3^-} - A/\varepsilon l} = K_{N_3} \frac{C^*_{Cu^{II}} \varepsilon l}{A} - K_{N_3} \tag{B.5}$$

where $C^*_{N_3^-}$ is the total concentration of azide ion. A plot of the left member of eq. B.5 vs. $1/A$ gives a straight line with intercept $-K_{N_3}$ and slope $K_{N_3} C^*_{Cu^{II}} \varepsilon l$. K_{N_3} can be obtained directly from the intercept and also from the slope, as

$$K_{N_3} = \frac{\text{slope}}{C^*_{Cu^{II}} \varepsilon l}$$

K_{N_3} values obtained from both intercept and slope were always in good agreement, therefore the average of the two values was reported in Table 4.2.

When a second complexing anion (X^-) is introduced into the system, the following equilibrium must be taken into account

$$[Cu^{II}L]^{2+} + X^- \rightleftarrows [X\text{-}Cu^{II}L]^+ \qquad K_{N_3} = \frac{C_{[X\text{-}Cu^{II}L]^{2+}}}{C_{[Cu^{II}L]^{2+}} C_{X^-}} \tag{B.6}$$

Matching $C_{[Cu^{II}L]^{2+}}$ from eq. B.1 and B.6, and considering the new mass balance

$$C_{[X\text{-}Cu^{II}L]^+} = C^*_{Cu^{II}} - (C_{[Cu^{II}L]^{2+}} + C_{[X\text{-}Cu^{II}L]^+}) \tag{B.7}$$

the following equation is obtained

$$\frac{C^*_{X^-}}{C^*_{N_3^-} - A/\varepsilon l} = \frac{K_{N_3}}{K_X}\left(\frac{C^*_{Cu^{II}}\varepsilon l}{A} - \frac{1}{K_{N_3}(C^*_{N_3^-} - A/\varepsilon l)}\right) - \frac{K_{N_3}}{K_X} \tag{B.8}$$

where $C^*_{X^-}$ is the total concentration of the second complexing ion. Variation of X^- concentration was always negligible because in the experimental conditions

- when X^- was a halide ion, $C^*_{X^-} > 200\ C^*_{Cu^{II}}$, therefore C_{X^-} variations are negligible and $C_{X^-} \approx C^*_{X^-}$.
- when X^- was the hydroxide ion, pH was buffered.

Eq. B.8 can be written in a more compact form as

$$y = \frac{K_{N_3}}{K_X}x - \frac{K_{N_3}}{K_X} \tag{B.9}$$

where $y = \frac{C^*_{X^-}}{C^*_{N_3^-} - A/\varepsilon l}$ and $x = \frac{C^*_{Cu^{II}}\varepsilon l}{A} - \frac{1}{K_{N_3}(C^*_{N_3^-} - A/\varepsilon l)}$. A plot of x vs y gives a straight line with slope K_{N_3}/K_X and intercept $-K_{N_3}/K_X$. Again, K_X is calculated as the average between the value obtained from the slope and that obtained from the intercept.

Appendix C

Detailed Calculations on Metal-Free ATRP Activation and Deactivation

C.1. Kinetic analysis of photoinduced ATRP activation

The reduction of MBiB by a series of electron donors (catalyst, Cat) was studied at 25 °C.

$$\mathrm{Cat} + \mathrm{RX} \xrightarrow{k_{act}} \mathrm{Cat}^{\bullet+} + \mathrm{R}^{\bullet} + \mathrm{X}^{-} \qquad \text{(C.1)}$$

This reaction is an outer sphere electron transfer (OSET) from a donor (Cat) to an acceptor (RX), which undergoes a concerted bond breakage. It is a special case of outer sphere electron transfer, and it is known as dissociative electron transfer (DET).

In the following description of kinetic analysis all equations refer to the general activation reaction (C.1), but the numerical calculations will be illustrated taking the reaction of the catalyst Ph-PTZ* (**2***) with MBiB as an example. According to the sticky model of dissociative electron transfer theory,[1] the rate constant of reaction C.1 can be calculated by

$$k_{act} = Z \exp\left(-\frac{\Delta G^{\ddagger}}{RT}\right) \qquad \text{(C.2)}$$

$$\Delta G^{\ddagger} = \Delta G_0^{\ddagger}\left(1 + \frac{\Delta_r G^{\circ} - D_p}{4\Delta G_0^{\ddagger}}\right) \qquad \text{(C.3)}$$

$$\Delta G_0^{\ddagger} = \frac{\left(\sqrt{D_{RX}} - \sqrt{D_p}\right) + \lambda_o}{4} \qquad \text{(C.4)}$$

where $\Delta_r G^{\circ}$ is the reaction free energy, $\Delta G_0^{\ddagger}$ is the intrinsic barrier (*i.e.* the activation free energy when $\Delta_r G^{\circ} = 0$) of reaction C.1, λ_o is the solvent reorganization energy, D_{RX} is the R–X bond dissociation energy and D_p is the interaction energy between R$^{\bullet}$ and X^{-} in the solvent cage.

For activated alkyl bromides like MBiB, D_p is always small in polar solvents like DMF and CH_3CN, e.g. 0.24 – 0.50 kcal mol^{-1}.[2] The radical–anion interactions depend on the

dielectric constant, which has very similar values for CH_3CN, DMF and DMA. The interaction energy between the methyl isobutyrate radical (MiB•) and X^- in DMA is not known. We used the value reported for the methyl propionate radical and X^- in CH_3CN (0.24 and 0.69 kcal mol^{-1} for Br^- and Cl^-, respectively). The relevant thermodynamic, kinetic and geometric parameters used in the calculations are listed in Table C.1.

Table C.1. Thermodynamic, kinetic and geometric parameters for the homogenous electron transfer to RX.

Cat	RX	r_{Cat}	r_{RX}	r^a	λ_o	D_{RX}	$E^{\ominus}_{RX/R^{\bullet}+X^-}$ [b]	D_P
		Å	Å	Å	kcal mol^{-1}	kcal mol^{-1}	V vs. SCE	kcal mol^{-1}
1*, $Ir(ppy)_3$*	MBiB	5.31[c]	3.42	2.80	14.21	58.7	-0.52	0.24
2*, Ph-PTZ*	MBiB	4.49	3.42	2.80	14.53	58.7	-0.52	0.24
2*, Ph-PTZ*	EBPA	4.49	3.64	2.86	14.24	53.9	-0.22	0.24
2*, Ph-PTZ*	MCiB	4.49	3.47	2.68	15.07	75.7	-0.76	0.69
2, Ph-PTZ	MBiB	4.21	3.42	2.80	14.71	58.7	-0.52	0.24
8*, Me-PTZ*	MBiB	3.94	3.42	2.80	14.94	58.7	-0.52	0.24
11*, Ph-CBZ	MBiB	4.37	3.42	2.80	14.60	58.7	-0.52	0.24

Effective radius of DET products ($R^{\bullet}+X^-$) calculated as $r = (2r_{RX} - r_X)r_X / r_{RX}$. [b]Standard potential of the redox reaction $RX + e^- \longrightarrow R^{\bullet} + X^-$. [b]Calculated from crystallographic data.

$\Delta_r G^{\ominus}$ of reaction C.1 was calculated from the standard potentials of the donor and acceptor redox couples in the ground state, $E^{\ominus}_{Cat^{\bullet+}/Cat}$ and $E^{\ominus}_{RX/R^{\bullet},X^-}$, and the energy of the excited reactant, $E_{h\nu}$, using the Weller equation:[3]

$$\Delta_r G^{\ominus} = F\left(E^{\ominus}_{Cat^{\bullet+}/Cat} - E^{\ominus}_{RX/R^{\bullet}+X^-} - E_{h\nu}\right) - \frac{N_A e^2}{4\pi\varepsilon_0\varepsilon r} \qquad (C.5)$$

$$\Delta_r G^{\ominus} = 96485\,\mathrm{C\,mol^{-1}}(0.815 + 0.52 - 2.787)\mathrm{V} - \frac{6.022\times10^{23}\,\mathrm{mol^{-1}}(1.602\times10^{-19}\,\mathrm{C})^2}{4\times3.1416\times8.854\times10^{-12}\,\mathrm{J^{-1}C^2m^{-1}}\times37.78\times(4.49+3.42)\times10^{-10}\,\mathrm{m}}$$
$$= -144.7\,\mathrm{kJ\,mol^{-1}} = -34.59\,\mathrm{kcal\,mol^{-1}}$$

where e is the elementary charge, ε_0 is the permittivity of vacuum and ε the relative permittivity of the solvent at 25 °C.[4] The last term is the Coulombic energy experienced by the ions $Cat^{\bullet+}$ and X^- at a distance r (the distance was approximated to the sum of the radii of the two hitting molecules $r = r_{Cat^*} + r_{RX}$). The radii were obtained from the computed

volume of the molecules, based on an isoelectron density surface of 0.001 electrons/Bohr^3 using the DFT-optimized structures (see below for further details on the DFT optimizations).

$E^{\ominus}_{\mathrm{Cat}^{\bullet+}/\mathrm{Cat}}$ and E_{hv} were experimentally determined in DMA (Table 7.2). Values of $E^{\ominus}_{\mathrm{RX/R}^{\bullet}+\mathrm{X}^-}$ for MBiB and MCiB were taken from the literature,[5] whereas $E^{\ominus}_{\mathrm{RX/R}^{\bullet}+\mathrm{X}^-}$ of EBPA was calculated from published thermodynamic data[6] as described previously, using the following equation:[5]

$$E^{\ominus}_{\mathrm{RX/R}^{\bullet}+\mathrm{X}^-} = \frac{1}{F}\left(-\mathrm{BDE} + T\Delta_{\mathrm{BD}}S^{\ominus}_{(\mathrm{g})} - \Delta G^{\ominus}_{\mathrm{s}}(\mathrm{R}^{\bullet}) - \Delta G^{\ominus}_{\mathrm{s}}(\mathrm{X}^{\bullet}) + \Delta G^{\ominus}_{\mathrm{s}}(\mathrm{RX})\right) + E^{\ominus}_{\mathrm{X}^{\bullet}/\mathrm{X}^-} \qquad \text{(C.7)}$$

where BDE and $\Delta_{\mathrm{BD}}S^{\ominus}_{(\mathrm{g})}$ are the bond dissociation enthalpy and entropy in gas phase, and $\Delta G^{\ominus}_{\mathrm{s}}$ is the Gibbs free energy of solvation in DMF. Eq. C.7 can be written as

$$\begin{aligned} E^{\ominus}_{\mathrm{RX/R}^{\bullet}+\mathrm{X}^-} &= \frac{1}{F}\left(-\mathrm{BDE} + T\Delta_{\mathrm{BD}}S^{\ominus}_{(\mathrm{g})} - \Delta\Delta G^{\ominus}_{\mathrm{s}}\right) + E^{\ominus}_{\mathrm{X}^{\bullet}/\mathrm{X}^-} \\ &= \frac{1}{96485\ \mathrm{J\ mol^{-1}\ V^{-1}}}\left(-228781 + 34016 + 4728\right)\mathrm{J\ mol^{-1}} + 1.75\ \mathrm{V} = -0.22\ \mathrm{V} \end{aligned} \qquad \text{(C.8)}$$

where $\Delta\Delta G^{\ominus}_{\mathrm{s}} = \Delta G^{\ominus}_{\mathrm{s}}(\mathrm{R}^{\bullet}) - \Delta G^{\ominus}_{\mathrm{s}}(\mathrm{X}^{\bullet}) + \Delta G^{\ominus}_{\mathrm{s}}(\mathrm{RX})$.

The intrinsic barrier $\Delta G^{\ddagger}_0$ of reaction C.1 was calculated as

$$\Delta G^{\ddagger}_0 = \frac{\left(\sqrt{D_{\mathrm{RX}}} - \sqrt{D_{\mathrm{p}}}\right)^2 + \lambda_{\mathrm{o}}}{4} = \frac{\left(\sqrt{58.7} - \sqrt{0.24}\right)^2 + 14.53}{4}\ \mathrm{kcal\ mol^{-1}} = 16.49\ \mathrm{kcal\ mol^{-1}}$$

where D_{RX} is RX bond energy, obtained through DFT calculation.

The solvent reorganization energy λ_{o} was determined by using an empirical equation obtained on the basis of an extensive set of experimental data:[7]

$$\lambda_{\mathrm{o}} = 95\left(\frac{1}{2r_{\mathrm{Cat}}} + \frac{1}{2r} - \frac{1}{r_{\mathrm{Cat}} + r}\right)\mathrm{kcal\ mol^{-1}} = 14.53\ \mathrm{kcal\ mol^{-1}} \qquad \text{(C.9)}$$

where r is the effective radius of RX, which was calculated from the equation $r = (2r_{\mathrm{RX}} - r_{\mathrm{X}})r_{\mathrm{X}}/r_{\mathrm{RX}}$,[8] using $r_{\mathrm{Br}} = 1.96$ Å, $r_{\mathrm{Cl}} = 1.81$ Å[9] together with the r_{Cat} and r_{RX} values reported in Table C.1.

k_{act} estimate

The rate constant of reaction C.1 can be calculated as follows:

$$k_{\text{act,DET}} = Z \exp\left(-\frac{\Delta G^{\ddagger}}{RT}\right) \tag{C.2}$$

$$Z = N_{\text{A}}\sqrt{\frac{8\pi RT}{\mu}}\left(r_{\text{Cat}} + r_{\text{RX}}\right)^2$$

In the case Cat = Ph-PTZ* (**2***) (M = 275.38 g mol^{-1}) and RX = MBiB (M = 181.03 g mol^{-1}), μ = 109.22 g mol^{-1} and Z = 2.85 10^{11} M^{-1} s^{-1}.

Using D_P = 0.24 kcal mol^{-1} for Br$^-$ and 0.69 kcal mol^{-1} for Cl$^-$, and calculating λ_o from eq. C.9, $\Delta G_0^{\ddagger}$ was computed for all Cat/RX couples. The activation free energy of reaction C.1 was then calculated through eq. C.3. Finally, eq. C.2 provided k_{act}. The results of all calculations are presented in Table 7.3.

C.2. Examples of calculations of activation energies for deactivation pathways for Ph-PTZ

Five possibilities were considered for the deactivation process: (a) inner-sphere electron transfer (ISET) mechanism; (b) dissociative electron transfer (DET); (c) outer-sphere electron transfer between Cat$^{\bullet+}$X$^-$ and R$^\bullet$ (OSET-I), followed by addition of X$^-$ to R$^+$; (d) outer-sphere electron transfer between Cat$^{\bullet+}$ and R$^\bullet$ (OSET-II), followed by recombination of R$^+$ and X$^-$; (e) the termolecular associative electron transfer (AET-ter). Geometric and thermodynamic parameters for the three catalysts **2**, **8** and **11** and for the initiators MBiB and MCiB are provided in Table C.2. Detailed calculations are here reported for the **2** + MBiB catalytic system, while results for all investigated systems are presented in Table 7.5.

Table C.2. Parameters used for the determination of energy barriers for the deactivation pathways.

Catalyst Complex	D_{RX} (kcal mol^{-1})	Radius (Å)			$\Delta_r G^e$ (kcal mol^{-1})		
		MiB$^\bullet$	Cat$^{\bullet+}$-X$^-$	Cat$^{\bullet+}$	OSET-I	OSET-II	DET
2$^{\bullet+}$**Br**$^-$	20.9	3.0	4.6	4.1	13.6	8.7	8.4
2$^{\bullet+}$**Cl**$^-$	36.0	3.0	4.5	4.1	11.0	8.7	7.5

AET-ter deactivation

The exact reverse process of metal-free ATRP activation, which is a dissociative electron transfer (DET), is an associative electron transfer involving a termolecular encounter (AET-ter):

$$\mathbf{2} + \mathrm{RX} \underset{k_{\text{AET-ter}}}{\overset{k_{\text{act}}}{\rightleftharpoons}} \mathbf{2}^{\bullet+} + \mathrm{X}^{-} + \mathrm{R}^{\bullet}$$

The activation free energy of the termolecular deactivation ($\Delta G^{\ddagger}_{\text{AET-ter}}$) is

$$\Delta G^{\ddagger}_{\text{AET-ter}} = \Delta G^{\ddagger}_{0}\left(1 - \frac{\Delta G^{\ominus} + D_{\text{p}}}{4\Delta G^{\ddagger}_{0}}\right)^{2}$$

In the case RX = MBiB with **2** as the photocatalyst, $\Delta G^{\ddagger}_{0} = 16.5\ \text{kcal mol}^{-1}$ and the DFT-calculated reaction free energy is $\Delta_{\text{r}}G^{\ominus} = 33.6$ kcal mol^{-1}. In addition, $D_{\text{p}} = 0.24$ kcal mol^{-1}. Therefore, calculation of the activation free energy gives $\Delta G^{\ddagger}_{\text{AET-ter}} = 3.9\ \text{kcal mol}^{-1}$ as reported in Figure 7.7.

When instead $\Delta_{\text{r}}G^{\ominus} = 29.6$ kcal mol^{-1}, obtained from experimental data, was used together with the above $\Delta G^{\ddagger}_{0}$ and D_{p} values, a slight increase of $\Delta G^{\ddagger}_{\text{AET-ter}}$ to 5.0 kcal mol^{-1} was observed.

OSET-II deactivation

$$\mathbf{2}^{\bullet+} + \mathrm{R}^{\bullet} \rightleftharpoons \mathbf{2} + \mathrm{R}^{+}$$

In this case, no bond is being broken or formed during electron transfer, therefore:

$$\Delta G^{\ddagger}_{\text{OSET-II}} = \Delta G^{\ddagger}_{0}\left(1 + \frac{\Delta_{\text{r}}G^{\ominus}}{4\Delta G^{\ddagger}_{0}}\right)^{2}$$

$\Delta_{\text{r}}G^{\ominus} = 8.6$ kcal mol^{-1} from DFT optimizations and $\Delta G^{\ddagger}_{0} = \left(\lambda_{\text{i}} + \lambda_{\text{o}}\right)/4$. The inner reorganization energy, λ_{i}, is fairly negligible for phenothiazines. This was observed by comparing the experimental barrier and the solvent reorganization energy of a series of phenothiazines (H-PTZ, Me-PTZ,[10] Bz-PTZ[11]). The rate constant of self-exchange, k_{ex}, is reported for a series of phenothiazines. The intrinsic barrier calculated is equal to $\lambda_{\text{o}}/4$ within the experimental error, indicating that these compounds do not undergo appreciable internal rearrangement upon ET. Therefore, λ_{i} can be fairly neglected. It is also likely that there are no significant structural changes on passing from $\mathrm{R}^{\bullet}$ to R^{+}, since both molecules have sp^2 hybridization. Therefore, neglecting λ_{i} contribution in the intrinsic barrier and calculating the solvent reorganization energy as follows:

$$\lambda_o = 95[(2r_{\mathbf{2}^{\bullet+}})^{-1} + (2r_{R\cdot})^{-1} - (r_{\mathbf{2}^{\bullet+}} + r_{R\cdot})^{-1}] = 95\left(\frac{1}{2\cdot 4.08} + \frac{1}{2\cdot 2.95} - \frac{1}{4.08+2.95}\right) = 14.23 \text{ kcal mol}^{-1}$$

lead to $\Delta G_0^{\ddagger} = 3.56 \text{ kcal mol}^{-1}$ and

$$\Delta G^{\ddagger}_{\text{OSET-II}} = \left(3.56 \text{ kcal mol}^{-1}\right)\left(1 + \frac{8.6}{4\times 3.56}\right)^2 = 9.16 \text{ kcal mol}^{-1}$$

OSET-I deactivation

$\mathbf{2}^{\bullet+}\text{Br}^{-}\text{-C} + \text{R}^{\bullet} \rightleftarrows \mathbf{2}\text{-Br}^{-}\text{-C} + \text{R}^{+}$

As in the case of OSET-II, Marcus theory of outer-sphere electron transfer can be applied to the OSET-I deactivation pathway:

$$\Delta G^{\ddagger}_{\text{OSET-I}} = \Delta G_0^{\ddagger}\left(1 + \frac{\Delta_r G^{\ominus}}{4\Delta G_0^{\ddagger}}\right)^2$$

$\Delta_r G^{\ominus} = 13.6$ kcal mol^{-1} from DFT optimizations and, neglecting λ_i as in the case of OSET-II mechanism, gives $\Delta G_0^{\ddagger} = 3.47 \text{ kcal mol}^{-1}$ with λ_o given by

$$\lambda_o = 95[(2r_{\text{Cat}})^{-1} + (2r_{R\cdot})^{-1} - (r_{\text{Cat}} + r_{R\cdot})^{-1}] = 95\left(\frac{1}{2\cdot 4.56} + \frac{1}{2\cdot 2.95} - \frac{1}{4.56+2.95}\right) = 13.87 \text{ kcal mol}^{-1}$$

With these values $\Delta G^{\ddagger}_{\text{OSET-I}}$ is calculated as

$$\Delta G^{\ddagger}_{\text{OSET-I}} = \left(3.47 \text{ kcal mol}^{-1}\right)\left(1 + \frac{13.66}{4\times 3.47}\right)^2 = 13.6 \text{ kcal mol}^{-1}$$

DET deactivation

$\mathbf{2}^{\bullet+}\text{Br}^{-}\text{-C} + \text{R}^{\bullet} \rightarrow \mathbf{2} + \text{Br}^{-} + \text{R}^{+}$

Sticky interaction does not occur here, because there is no interaction between Br^- and a radical. The Gibbs free energy of activation is therefore given by

$$\Delta G^{\ddagger}_{\text{DET}} = \Delta G_0^{\ddagger}\left(1 + \frac{\Delta_r G^{\ominus}}{4\Delta G_0^{\ddagger}}\right)^2$$

$\Delta_r G^{\ominus} = 8.4$ kcal mol^{-1} from DFT optimizations, whereas $\Delta G_0^{\ddagger}$ for a dissociative electron transfer can be calculated from the bond dissociation energy and solvent reorganization energy:

$$\Delta G_0^{\ddagger} = \frac{D_{\mathbf{2}^{\bullet+}\mathbf{Br}^-} + \lambda_o}{4}$$

Using the computed $D_{\mathbf{2}^{\bullet+}\mathbf{Br}^-}$ value of 20.9 kcal mol^{-1} and λ_o calculated as

$$\lambda_o = 95[(2r_{Cat})^{-1} + (2r_{R^\bullet})^{-1} - (r_{Cat} + r_{R^\bullet})^{-1}] = 95\left(\frac{1}{2\cdot 4.56} + \frac{1}{2\cdot 2.95} - \frac{1}{4.56+2.95}\right) = 13.87 \text{ kcal mol}^{-1}$$

leads to

$$\Delta G_{DET}^{\ddagger} = \left(8.69 \text{ kcal mol}^{-1}\right)\left(1 + \frac{8.4}{4\times 8.69}\right)^2 = 13.42 \text{ kcal mol}^{-1}$$

C.3. Calculation of deactivation rates of the different pathways for Ph-PTZ

Rate of radical termination

The rate of radical termination was estimated from

$$R_t = k_t[R^\bullet]^2 = \left(10^7 \text{ M}^{-1}\text{ s}^{-1}\right)\left(4.62\times 10^{-8} \text{ M}\right)^2 = 2.1\times 10^{-8} \text{ M s}^{-1}$$

[R$^\bullet$] was calculated from $k_p^{app} = k_p[R^\bullet]$, using $k_p = 10^3$ M^{-1}s^{-1} and a value of k_p^{app} of 4.62×10^{-5} s^{-1}, determined for photoinduced ATRP, with **2** as catalyst and MBiB as initiator, under 4.9 mW/cm^2 irradiation (Figure 7.2). We then compared this termination rate to the deactivation rate, considering that, in a controlled process, deactivation must be faster than radical termination.

Rate of termolecular AET deactivation pathway (AET-ter)

As already seen, the exact reverse process of metal-free ATRP activation is the termolecular AET deactivation reaction.

$$\mathbf{2}^{\bullet+} + X^- + R^\bullet \xrightarrow{k_{AET\text{-}ter}} \mathbf{2} + RX$$

In the literature, the rate of termolecular reactions was often considered to be very slow because of the low likelihood of a three-center simultaneous encounter. Nevertheless, in rare cases the exact calculation was carried out.

The frequency factor Z_{ter} for a termolecular reaction can be calculated following Tolman's approach:[12]

$$Z_{ter} = N_A^2 8\pi^2 \left(\frac{2RT}{\pi}\right)^{1/2}\left[\left(\frac{m_A + m_B}{m_A m_B}\right)^{1/2} + \left(\frac{m_B + m_C}{m_B m_C}\right)^{1/2}\right] d_{A\leftrightarrow B}^2 d_{B\leftrightarrow C}^2 \delta = 2.6\times 10^{10} \text{ M}^{-2}\text{ s}^{-1}$$

where A, B and C are the three species involved in the reaction. *d* is the center-to-center distance between the subscript particles. δ is the distance between the two first spheres when hit by the third. Usually δ is taken to be between 0.3 Å[13] and 1 Å.[14] The lower limit value, 0.3 Å, was used.

If we define A = **2**, B = Br^- and C =$R^\bullet$, then m_A = 0.27537 kg mol^{-1}, m_B = 0.0799 kg mol^{-1}, m_C = 0.101 kg mol^{-1}. r_A = 4.08 Å; r_B = 1.96 Å; and r_C = 2.95 Å. With these values, Z_{ter} = 2.6×10^{10} $M^{-2}s^{-1}$ was obtained. Using $\Delta G^{\ddagger}_{\text{AET-ter}} = 3.9\,\text{kcal mol}^{-1}$, the deactivation rate constant was then calculated as

$$k_{\text{AET-ter}} = Z_{\text{ter}} e^{\frac{-\Delta G^{\ddagger}_{\text{AET-ter}}}{RT}} = \left(2.6\times10^{10}\ \text{M}^{-2}\ \text{s}^{-1}\right) e^{\left(\frac{-3940\,\text{cal mol}^{-1}}{1.987\text{cal mol}^{-1}\text{K}^{-1}\times298.15\,\text{K}}\right)} = 3.4\times10^{7}\ \text{M}^{-2}\ \text{s}^{-1}$$

The rate of the termolecular deactivation reaction is

$$R_{\text{AET-ter}} = k_{\text{AET-ter}}[2^{\bullet+}][\text{Br}^-][\text{R}^\bullet]$$

Therefore, estimates for both $[2^{\bullet+}]$ and $[Br^-]$ are needed. Considering around 10% of termination, $[Br^-]$ should be *ca* 5×10^{-3} M. Moreover, the CV registered during a metal-free ATRP showed an oxidation current compatible with the presence of around 5×10^{-3} M Br^-, generated after a few hours of polymerization (Figure 7.8).

$\mathbf{2}^{\bullet+}$ was not detected during the electrochemical measurements. Moreover, it is known that this cation slowly disappears by reaction with Br^-.[15] Therefore 5×10^{-4} M was chosen as a reasonable estimate of $[2^{\bullet+}]$.

On the basis of these estimates it is finally possible to calculate the termolecular deactivation rate as

$$R_{\text{AET-ter}} = k_{\text{AET-ter}}[2^{\bullet+}][\text{Br}^-][\text{R}^\bullet] = 3.9\times10^{-6}\ \text{M s}^{-1}$$

$k_{\text{AET-ter}}$ and $R_{\text{AET-ter}}$ were also calculated on the basis of the value of $\Delta G^{\ddagger}_{\text{AET-ter}}$ of 5.0 kcal mol^{-1} derived from the experimental data. Using the same values of Z, $[\mathbf{2}^{\bullet+}]$, $[R^\bullet]$ and $[Br^-]$ used in the previous case gives

$$k_{\text{AET-ter}} = Z_{\text{ter}} e^{\frac{-\Delta G^{\ddagger}_{\text{AET-ter}}}{RT}} = \left(2.6\times10^{10}\ \text{M}^{-2}\ \text{s}^{-1}\right) e^{\left(\frac{-5000\,\text{cal mol}^{-1}}{1.987\text{cal mol}^{-1}\text{K}^{-1}\times298.15\,\text{K}}\right)} = 5.8\times10^{6}\ \text{M}^{-2}\ \text{s}^{-1}$$

$$R_{\text{AET-ter}} = k_{\text{AET-ter}}[2^{\bullet+}][\text{Br}^-][\text{R}^\bullet] = 6.8\times10^{-7}\ \text{M s}^{-1}$$

Rate of ISET deactivation pathway

The rate of the bimolecular deactivation reaction

2$^{\bullet+}$Br^{-}-C + R$^{\bullet}$ → RBr + **2**

is given by

$$R_{\mathrm{ISET}} = k_{\mathrm{ISET}}[\mathbf{2}^{\bullet+}\,\mathrm{Br}^{-}\text{-C}][\mathrm{R}^{\bullet}]$$

where **2**$^{\bullet+}$Br^{-}-C is the ion pair adduct with covalent bond.

The deactivation rate constant, k_{ISET}, was calculated from the computed activation free energy ($\Delta G^{\neq}_{\mathrm{ISET}}$ = 10.5 kcal mol^{-1}) and the bimolecular collision frequency given by:

$$Z = N_{\mathrm{A}}\sqrt{\frac{8\pi RT}{\mu}}\left(r_{\mathbf{2}^{\bullet+}\mathbf{Br}^{-}} + r_{\mathrm{R}^{\bullet}}\right)$$

The reduced mass μ of the reagents 2$^{\bullet+}$Br^{-} and MiB$^{\bullet}$ is 0.07858 kg mol^{-1}, whereas their respective radii are 4.56×10^{-10} m and 2.95×10^{-10} m. Thus, Z = 3.02×10^{11} M^{-1}s^{-1}. Using this value together with $\Delta G^{\ddagger}_{\mathrm{ISET}} = 10.5\,\mathrm{kcal\,mol^{-1}}$ gives

$$k_{\mathrm{ISET}} = Ze^{\frac{-\Delta G^{\ddagger}_{\mathrm{ISET}}}{RT}} = \left(3.02\times10^{11}\ \mathrm{M^{-1}\,s^{-1}}\right)e^{\left(\frac{-10500\,\mathrm{cal\,mol^{-1}}}{1.987\mathrm{cal\,mol^{-1}K^{-1}}\times298.15\,\mathrm{K}}\right)} = 6.1\times10^{3}\ \mathrm{M^{-1}\,s^{-1}}$$

2$^{\bullet+}$Br^{-}-C must be formed by the association of **2**$^{\bullet+}$ with Br^{-}. Therefore, its concentration can be obtained from the equilibrium constant of the reaction

2$^{\bullet+}$ + Br^{-} = **2**$^{\bullet+}$Br^{-}-C

$\Delta_{\mathrm{r}}G^{\ominus}$ of this reaction is 0.2 kcal mol^{-1}, which allowed the calculation of the formation equilibrium constant of **2**$^{\bullet+}$**Br**$^{-}$**-C**:

$$K_{\mathrm{f},\mathbf{2}^{\bullet+}\mathbf{Br}^{-}\text{-}\mathbf{C}} = e^{\frac{-\Delta G^{\ominus}}{RT}} = e^{\left(\frac{-200\,\mathrm{cal\,mol^{-1}}}{1.987\mathrm{cal\,mol^{-1}K^{-1}}\times298.15\,\mathrm{K}}\right)} = 0.71$$

As in the case of the AET termolecular deactivation [**2**$^{\bullet+}$] = 5×10^{-4} M and [Br^{-}] = 5×10^{-3} M can be used. Inserting these concentration values into the expression

$$K_{\mathrm{f},\mathbf{2}^{\bullet+}\mathbf{Br}^{-}} = \frac{[\mathbf{2}^{\bullet+}\,\mathbf{Br}^{-}\text{-C}]}{[\mathbf{2}^{\bullet+}][\mathrm{Br}^{-}]}$$

provides a very low equilibrium concentration of 1.8×10^{-6} M for **2**$^{\bullet+}$**Br**$^{-}$**-C**.

Therefore, the rate of deactivation was estimated as

$$R_{\mathrm{ISET}} = k_{\mathrm{ISET}}[\mathbf{2}^{\bullet+}\,\mathbf{Br}^{-}\text{-}\mathbf{C}][\mathrm{R}^{\bullet}] = 5.0\times10^{-10}\ \mathrm{M\,s^{-1}}$$

This is unreasonably low as a deactivation rate, being more than two orders of magnitude lower than the rate of radical-radical termination.

Rate of OSET-II deactivation pathway

This reaction pathway involves two consecutive reactions

$$\mathbf{2}^{\bullet+} + \mathrm{R}^{\bullet} \underset{k_{\mathrm{b,OSET\text{-}II}}}{\overset{k_{\mathrm{OSET\text{-}II}}}{\rightleftharpoons}} \mathrm{R}^{+} + \mathbf{2}$$

$$\mathrm{R}^{+} + \mathrm{Br}^{-} \rightarrow \mathrm{RBr}$$

From the activation free energy of 9.16 kcal mol^{-1}, it is possible to calculate the rate constant for the bimolecular deactivation reaction, $k_{\mathrm{OSET\text{-}II}}$. The collision frequency Z was calculated using a reduced mass μ of 0.07387 kg mol^{-1} for $\mathbf{2}^{\bullet+}$ and MiB$^{\bullet}$ and $r_{\mathbf{2}^{\bullet+}}$ = 4.08×10^{-10} m and $r_{\mathrm{R}^{\bullet}}$ = 2.95×10^{-10} m.

$$Z = N_{\mathrm{A}}\sqrt{\frac{8\pi RT}{\mu}}\left(r_{\mathbf{2}^{\bullet+}} + r_{\mathrm{R}^{\bullet}}\right) = 2.73\times10^{11}\ \mathrm{M^{-1}s^{-1}}$$

The rate constant is

$$k_{\mathrm{OSET\text{-}II}} = Ze^{\frac{-\Delta G^{\ddagger}_{\mathrm{OSET\text{-}II}}}{RT}} = \left(2.73.10^{11}\ \mathrm{M^{-1}\ s^{-1}}\right)e^{\left(\frac{-9160\ \mathrm{cal\ mol^{-1}}}{1.987\mathrm{cal\ mol^{-1}K^{-1}}\times298.15\ \mathrm{K}}\right)} = 5.3\times10^{4}\ \mathrm{M^{-1}\ s^{-1}}$$

To calculate the overall rate of the OSET reaction, also the reverse reaction, *i. e.* the back electron transfer between R^{+} and **2** in the solvent cage, which is likely to be very fast, must be considered. The rate constant of the back electron transfer, $k_{\mathrm{b,OSET\text{-}II}}$, was calculated from $k_{\mathrm{OSET\text{-}II}}$ and the equilibrium constant of the reaction, $K_{\mathrm{OSET\text{-}II}}$, derived from the reaction Gibbs free energy:

$$K_{\mathrm{OSET\text{-}II}} = \frac{k_{\mathrm{OSET\text{-}II}}}{k_{\mathrm{b,OSET\text{-}II}}} = e^{\frac{-\Delta_{\mathrm{r}}G^{\mathrm{e}}}{RT}} = e^{\left(\frac{-8600\ \mathrm{cal\ mol^{-1}}}{1.987\mathrm{cal\ mol^{-1}K^{-1}}\times298.15\ \mathrm{K}}\right)} = 4.96\times10^{-7}$$

It follows that

$$k_{\mathrm{b,OSET\text{-}II}} = \frac{k_{\mathrm{OSET\text{-}II}}}{K_{\mathrm{OSET\text{-}II}}} = \frac{5.26\times10^{4}\ \mathrm{M^{-1}s^{-1}}}{4.96\times10^{-7}} = 1.06\times10^{11}\ \mathrm{M^{-1}s^{-1}}$$

which confirms that the reaction between R^{+} and **2** is extremely fast.

The carbocation R^{+} is also expected to react at a diffusion-controlled rate with Br^{-} to generate RBr:

$$R^+ + Br^- \xrightarrow{k_{diff}} RBr$$

k_{diff} for a bimolecular reaction can be estimated from the viscosity η of the solvent[16] (for DMA, η = 9.27×10^{-4} Pa s):

$$k_{diff} = \frac{8RT}{3\eta} = 7.13\times10^{9}\ M^{-1}s^{-1}$$

The reaction of R^+ with Br^- is about 15 times slower than the back electron transfer between **2** and R^+. Therefore, the steady-state approximation can be applied to the intermediate R^+, which is consumed by fast reactions with both **2** and Br^-:

$$\frac{d[R^+]}{dt} = k_{OSET-II}[\mathbf{2}^{\bullet+}][R^\bullet] - k_{b,OSET-II}[R^+][\mathbf{2}] - k_{diff}[R^+][Br^-] = 0$$

$$[R^+] = \frac{k_{OSET-II}[\mathbf{2}^{\bullet+}][R^\bullet]}{k_{b,OSET-II}[\mathbf{2}] + k_{diff}[Br^-]}$$

It is now possible to calculate the overall rate of OSET-II deactivation pathway. The reaction rate can be conveniently defined as the rate of formation of RBr:

$$R_{OSET-II} = \frac{d[RBr]}{dt} = k_{diff}[R^+][Br^-] = k_{diff}[Br^-]\frac{k_{OSET-II}[\mathbf{2}^{\bullet+}][R^\bullet]}{k_{b,OSET-II}[\mathbf{2}] + k_{diff}[Br^-]}$$

Using [**2**$^{\bullet+}$] = 5×10^{-4} M, [R$^\bullet$] = 4.62×10^{-8} M and [Br$^-$] = 5×10^{-3} M, together with previously estimated values of k_{OSET}, $k_{b,OSET}$ and k_{diff} gives $R_{OSET-II}$ = 7.6×10^{-8} M s^{-1}.

Rate of OSET-I deactivation pathway

Deactivation through OSET-I occurs according to the following sequence of reactions:

2$^{\bullet+}$$Br^-$ + R$^\bullet$ ⇄ **2**-Br^- + R^+

2-Br^- → **2** + Br^-

R^+ + Br^- → RBr

Both decomposition of **2-Br$^-$** and combination of R^+ with Br^- are much faster than electron transfer from **2**$^{\bullet+}$**Br$^-$** to R$^\bullet$, which is considered to the rate-determining step of the whole sequence. The overall rate of the deactivation pathway is assumed to be equal to the rate of the electron transfer and is calculated as follows:

$$Z = N_A\sqrt{\frac{8\pi RT}{\mu}}\left(r_{\mathbf{2}^{\bullet+}\mathbf{Br}^-} + r_{R^\bullet}\right) = 3.02\times10^{11}\ M^{-1}s^{-1}$$

for μ = 0.07872 kg mol^{-1}, $r_{\mathbf{2}^{\bullet+}\mathbf{Br}^-\text{-}\mathbf{C}}$ = 4.56×10^{-10} m and $r_{R^\bullet}$ = 2.95×10^{-10} m.

$$k_{\text{OSET-I}} = Ze^{\frac{-\Delta G^{\ddagger}_{\text{OSET-I}}}{RT}} = \left(3.02\times10^{11}\ \text{M}^{-1}\ \text{s}^{-1}\right)e^{\left(\frac{-13600\ \text{cal mol}^{-1}}{1.987\text{cal mol}^{-1}\text{K}^{-1}\times298.15\ \text{K}}\right)} = 32.4\ \text{M}^{-1}\ \text{s}^{-1}$$

$$R_{\text{OSET-I}} = k_{\text{OSET-I}}[\mathbf{2}^{\bullet+}\mathbf{Br}^{-}\text{-}\mathbf{C}][\text{R}^{\bullet}] = 2.69\times10^{-12}\ \text{M s}^{-1}$$

with $[\text{R}^{\bullet}] = 4.62\times10^{-8}$ M and $[\mathbf{2}^{\bullet+}\mathbf{Br}^{-}\text{-C}] = K_{\text{f},\mathbf{2}^{\bullet+}\mathbf{Br}^{-}}[\mathbf{2}^{\bullet+}][\text{Br}^{-}] = 1.8\times10^{-6}$ M .

Rate of DET deactivation pathway

The rate of the deactivation through dissociative electron transfer was calculated as previously described after estimating Z and $\Delta G^{\ddagger}$. The relevant reactions are

$\mathbf{2}^{\bullet+}\mathbf{Br}^{-}\text{-}\mathbf{C} + \text{R}^{\bullet} \rightarrow \mathbf{2} + \text{Br}^{-} + \text{R}^{+}$

$\text{R}^{+} + \text{Br}^{-} \rightarrow \text{RBr}$

and the rate-determining step is the DET reaction. As in the case of OSET-I, $\mu = 0.07872$ kg mol^{-1}, $r_{\mathbf{2}^{\bullet+}\mathbf{Br}^{-}\text{-}\mathbf{C}} = 4.56\times10^{-10}$ m and $r_{\text{R}^{\bullet}} = 2.95\times10^{-10}$ m, therefore $Z = 3.02\times10^{11}$ M^{-1}s^{-1}. The rate constant and the deactivation rate are

$$k_{\text{DET}} = Ze^{\frac{-\Delta G^{\ddagger}_{\text{DET}}}{RT}} = \left(3.02\times10^{11}\ \text{M}^{-1}\ \text{s}^{-1}\right)e^{\left(\frac{-13420\ \text{cal mol}^{-1}}{1.987\text{cal mol}^{-1}\text{K}^{-1}\times298.15\ \text{K}}\right)} = 45\ \text{M}^{-1}\ \text{s}^{-1}$$

$$R_{\text{DET}} = k_{\text{DET}}[\mathbf{2}^{\bullet+}\mathbf{Br}^{-}\text{-}\mathbf{C}][\text{R}^{\bullet}] = 3.7\times10^{-12}\ \text{M}^{-1}\ \text{s}^{-1}$$

References

(1) (a) Saveant, J. M. *J. Am. Chem. Soc.* **1987,** *109*, 6788-6795. (b) Cardinale, A.; Isse, A. A.; Gennaro, A.; Robert, M.; Savéant, J.-M. *J. Am. Chem. Soc.* **2002,** *124*, 13533-13539. (c) Pause, L.; Robert, M.; Savéant, J.-M. *J. Am. Chem. Soc.* **2000,** *122*, 9829-9835. (d) Pause, L.; Robert, M.; Savéant, J.-M. *J. Am. Chem. Soc.* **2001,** *123*, 4886-4895.

(2) Isse, A.A.; Bortolamei, N.; De Paoli, P.; Gennaro, A. Electrochim. Acta, 2013, 110, 655-662.

(3) Rehm, D.; Weller, A. *Isr. J. Chem.* **1970,** *8*, 259-271.

(4) Riddick, J. A.; Bunger, W. B.; Sakano, T. K. Organic Solvents: Physical Properties and Methods of Purification, 4th Edition **1986**, Series Editor: Arnold Weissberger. New York, NY, U.S.A. Wiley-Interscience.

(5) Isse, A. A.;Lin, C. Y.; Coote, M. L.; Gennaro, A. *J. Phys. Chem. B* **2011,** *115*, 678-684.

(6) Lin, C. Y.; Coote, M. L.; Gennaro, A.;Matyjaszewski, K. *J. Am. Chem. Soc.* **2008,** 130, 12762–12774.

(7) (a) Kojima, H.; Bard, A. J. *J. Am. Chem. Soc.* **1975,** *97*, 6317-6324. (b) Donkers, R. L.; Maran, F.; Wayner, D. D. M.; Workentin, M. S. *J. Am. Chem. Soc.* **1999,** *121*, 7239-7248.

(8) Saveant, J. M. *J. Am. Chem. Soc.* **1992,** *114*, 10595-10602.

(9) D. R. Lide, ed., CRC Handbook of Chemistry and Physics 87th ed. **2006**, Taylor and Francis, Boca Raton, Florida, US.

(10) Kowert, B. A.; Marcoux, L.; Bard, A. J. *J. Am. Chem. Soc.* **1972,** *94*, 5538-5550.

(11) Youcheng, W. L. *Sci China Chem.* **1999,** 42, 138-144.

(12) (a) R.C. Tolman, Statistical Mechanics, Chemical Catalog Co, New York, **1927**, p. 247. (b) J.R. Partington, An Advanced Treatise on Physical Chemistry, vol. 1, Longmans, London, **1967**, p. 292. (c) J.W. Moore, R.N. Pearson, Kinetics and Mechanism, vol. 131, Wiley, New York, **1981**, p. 130.

(13) Savéant, J.-M. *J. Electroanal. Chem.* **2000,** *485*, 86-88.

(14) J.W. Moore, R.N. Pearson, Kinetics and Mechanism, vol. 131, Wiley, New York, 1981, p. 130.

(15) Shine, H. J.; Silber, J. J.; Bussey, R. J.; Okuyama, T. *J. Org. Chem.* **1972,** *37*, 2691-2697.

(16) Laidler, K. J. *Chemical Kinetics*, 3rd ed., Harper & Row, Publishers Inc., **1987**, p. 216.

Appendix D

Publications

Articles

- Konkolewicz, D.; Krys, P.; Góis, J.R.; Mendonça, P.V.; Zhong, M.; Wang, Y.; Gennaro, A.; Isse, A.A.; **Fantin, M.**; Matyjaszewski, K. Aqueous RDRP in the Presence of Cu^0: The Exceptional Activity of Cu^I Confirms the SARA ATRP Mechanism, *Macromolecules* **2014**, *47*, 560-570.
- Lorandi, F.; **Fantin, M.**; Isse, A. A.; Gennaro, A. RDRP in the Presence of Cu^0: The Fate of Cu^I Proves the Inconsistency of SET-LRP Mechanism, *Polymer* **2015**, *72*, 238-245.
- **Fantin, M.**; Isse, A. A.; Gennaro, A.; Matyjaszewski, K. Understanding the Fundamentals of Aqueous ATRP and Defining Conditions for Better Control, *Macromolecules* **2015**, *48*, 6862-6875.
- Pan, X.; Fang, C.; **Fantin, M.**; Malhotra, N.; Young So, W; Peteanu, L. A.; Isse, A. A.; Gennaro, A.; Liu, P.; Matyjaszewski, K. Mechanism of Photoinduced Metal-Free Atom Transfer Radical Polymerization: Experimental and Computational Studies, *J. Am. Chem. Soc.* **2016**, DOI: 10.1021/jacs.5b13455.

Conferences

- **Fantin, M.**; Isse, A. A.; Gennaro, A. Atom Transfer Radical Polymerization in water: peculiarities and limits of control, *GEI 2013 Giornate dell'Elettrochimica Italiana*, September 22 – 27, **2013** Pavia, Italy.
- Konkolewicz, D.; Simakova, A.; Averick, S. E.; Magenau, A. J. D.; Krys, P.; Gois, J. R.; Mendonca, P.; Fantin, M.; Isse, A. A.; Gennaro, A.; Matyjaszewski, K. Aqueous Atom Transfer Radical Polymerization: From Challenges to Solutions and Bioconjugates, *248th ACS National Meeting and Exposition,* August 10-14, **2014**, San Francisco, CA, USA.

- Lorandi, F.; **Fantin. M.**; Abdirisak, A.A.; Gennaro, A. Fundamental Aspects of Aqueous Atom Transfer Radical Polymerization, *XXV Congresso Nazionale della Società Chimica Italiana*, September 7–12, **2014** Rende (CS), Italy.

- Lorandi, F.; **Fantin. M.**; Abdirisak, A.A.; Gennaro, A. Fast and Well-Controlled Atom Transfer Radical Polymerization in Water, *XXV Congresso Nazionale della Società Chimica Italiana*, September 7–12, **2014** Rende (CS), Italy.

- **Fantin. M.;** Abdirisak, A.A.; Gennaro, A. Atom Transfer Radical Polymerization in the Presence of Metallic Copper: Is Activation Due to Cu^0 Or Cu^I?, *XXV Congresso Nazionale della Società Chimica Italiana*, September 7–12, **2014** Rende (CS), Italy.

- **Fantin M.**; Isse A. A.; Gennaro A. Controlling Aqueous Atom Transfer Radical Polymerization, *65th meeting of the International Society of Electrochemistry*, August 31 – September 5, **2014** Lausanne, Switzerland.

- Isse A. A.; Lorandi, F.; Fantin M.; Gennaro A. Role of Metallic Copper in Atom Transfer Radical Polymerization, *65th meeting of the International Society of Electrochemistry*, August 31 – September 5, **2014** Lausanne, Switzerland.

- Park, S.; Chiemlarz, P.; **Fantin. M.**; Matyjaszewski, K. Modulating Cu^I Generation through Electrochemistry, *CRP Consortium Meeting*, March 27–30, **2015** Pittsburgh, PA, United States.

- **Fantin, M.**; Isse, A. A.; Gennaro, A.; Matyjaszewski, K. Atom Transfer Radical Polymerization of Methacrylic Acid, *GEI 2015 Giornate dell'Elettrochimica Italiana*, September 20–24, **2015** Bertinoro (FC), Italy.

- De Bon, F.; Fantin, M.; Isse, A. A.; Gennaro, A. Electrochemically Mediated Atom Transfer Radical Polymerization in Ionic Liquids, *GEI 2015 Giornate dell'Elettrochimica Italiana*, September 20–24, **2015** Bertinoro (FC), Italy.

- **Fantin, M.**; Isse, A. A.; Pan, X.; Malhotra, N.; Matyjaszewski, K., Gennaro, A. Photoinduced Metal-Free Atom Transfer Radical Polymerization: Mechanism and Catalysts Screening, *GEI 2015 Giornate dell'Elettrochimica Italiana*, September 20–24, **2015** Bertinoro (FC), Italy.

- Fantin, M.; Isse, A. A.; Gennaro, A. Electrochemical Determination of Activation Rate Constants in Atom Transfer Radical Polymerization, *GEI 2015 Giornate dell'Elettrochimica Italiana*, September 20–24, **2015** Bertinoro (FC), Italy.

- Lorandi, F.; Fantin, M.; Isse, A. A.; Gennaro, A. Electrochemically Mediated Atom Transfer Radical Polymerization: Role of Cathodic Materials, *GEI 2015 Giornate dell'Elettrochimica Italiana*, September 20–24, **2015** Bertinoro (FC), Italy.

Fantin, M. is written in bold in oral or poster presentations done by the author.